Hussain Sarwar Khan

Advanced Predictive and AI-Based Converter Control Strategies for AC and DC Microgrids

ACTA WASAENSIA 580

University of Vaasa
VAASAN YLIOPISTO

ISBN 978-952-395-259-1 (print)
978-952-395-260-7 (online)

ISSN 0355-2667 (Acta Wasaensia 580, print)
2323-9123 (Acta Wasaensia 580, online)

URN https://urn.fi/URN:ISBN:978-952-395-260-7

PunaMusta Oy, Joensuu, 2026.

ACADEMIC DISSERTATION

To be presented, with the permission of the Board of the School of Technology and Innovations of the University of Vaasa, for public examination on the 27th of March, 2026, at noon.

Article based dissertation, School of Technology and Innovations, Electrical Engineering

Author	Hussain Sarwar Khan https://orcid.org/0000-0003-1111-3046
Supervisors	Professor Kimmo Kauhaniemi University of Vaasa. School of Technology and Innovations, Electrical Engineering
	Professor Hannu Laaksonen University of Vaasa. School of Technology and Innovations, Electrical Engineering.
Custos	Professor Kimmo Kauhaniemi University of Vaasa. School of Technology and Innovations, Electrical Engineering
Reviewers	Prof. Dr. Saad Mekhilef (IEEE Fellow) Swinburne University of Technology Australia. School of Engineering
	Prof. Dr. Sergio Vazquez (IEEE Fellow) Universidad de Sevilla. School of Engineering, Electronics Engineering Department
Opponent	Professor Marko Hinkkanen Aalto University. School of Electrical Engineering, Department of Electrical and Automation

Tiivistelmä

Invertteripohjaisten hajautettujen energiaresurssien lisääntynyt hyödyntäminen tuo mukanaan merkittäviä haasteita sähkövoimajärjestelmän toimintaan ja stabiiliuteen. Erityisesti haasteita aiheuttavat matala inertia, epälineaariset kuormat sekä rajoitettu vikavirran syöttö. Perinteisiä lineaarisia säätimiä käytetään laajasti, mutta niillä on luontaisia puutteita, kuten hidas transienttivaste, heikko häiriöiden sietokyky ja rajoittunut kyky käsitellä epälineaarisuuksia tai parametriepävarmuuksia. Näiden rajoitusten ratkaisemiseksi tässä väitöskirjassa kehitetään ja validoidaan edistyneitä ennakoivia ja tekoälypohjaisia säätöstrategioita sekä vaihto- (AC) että tasasähkö (DC) mikroverkoille.

Ensiksi väitöskirjassa esitellään parannettu mallipohjainen ennakoiva säätö, FCS–MPC, invertteripohjaisille hajautetuille energiaresursseille. Kaksitavoitteinen kustannusfunktio mahdollistaa samanaikaisesti lähtöjännitteen säätämisen ja vikavirran rajoittamisen symmetrisissä vikatilanteissa. Kahden askeleen ennustemenetelmä mahdollistaa pienemmän kytkentätaajuuden, paremman vakiotilan tarkkuuden ja paremman robustisuuden parametrimuutoksia vastaan. Lisäksi toteutetaan ennakoiva hierarkkinen säätöarkkitehtuuri. Ehdotetun menetelmän stabiilius osoitetaan Lyapunovin analyysin avulla, ja perinteisiä menetelmiä parempi suorituskyky vahvistetaan MATLAB/Simulink-simulaatioilla sekä FPGA-in-the-loop-testauksella.

Toiseksi väitöskirja edistää tekoälypohjaista säätöä tasajännitteisissä mikrosähköverkoissa. Keinotekoinen neuroverkkoon (ANN) perustuva jännitteenohjain kehitetään FCS–MPC:n tuottaman aineiston avulla, mikä mahdollistaa nopean transienttivasteen ja robustin säädön epälineaarisilla vakio-tehokuormilla. Lisäksi ehdotetaan vähennettyyn anturimäärään perustuva ANN-säätö, joka käyttää vain jännitemittauksia, tarjoten kustannustehokkaan ja skaalautuvan ratkaisun käytännön toteutukseen. Molemmat lähestymistavat validoidaan reaaliaikaisilla laitteistosilmukkatesteillä (HIL-testeillä), jotka osoittavat luotettavan jännitteen säädön usean solmupisteen DC-verkoissa.

Kaiken kaikkiaan tämä väitöskirja tarjoaa perustan ennakoiville ja tekoälypohjaisille säätimille, jotka parantavat mikroverkkojen luotettavuutta, tehokkuutta ja skaalautuvuutta. Yhdistämällä teoreettisen mallinnuksen, reaaliaikaisen validoinnin ja avoimen tutkimuskäytännön työ tarjoaa polun kohti resilienttiä ja vähähiilistä tulevaisuuden invertteripohjaista sähkövoimajärjestelmää.

Avainsanat: hajautetut energiaresurssit, mikroverkot, robusti konvertterin säätö, mallipohjainen ja hierarkkinen ennakoiva ohjaus, keinotekoinen neuroverkko, laitteistosilmukkasimulaatio

Abstract

The increasing penetration of inverter-based distributed energy resources (DERs) is reshaping modern power systems. However, it also introduces major challenges to their operation and stability. In particular, the stability of modern power systems is affected by low inertia, nonlinear load characteristics and limited fault current contribution. Conventional linear controllers are widely used, but have inherent shortcomings, including slow transient response, poor disturbance rejection and an inability to effectively handle nonlinearities or parametric uncertainties. To address these limitations, this dissertation develops and validates advanced predictive and artificial intelligence (AI)-based control strategies for AC and DC islanded microgrids operating at low-voltage levels. First, this dissertation introduces an improved finite control set model predictive control (FCS–MPC) strategy for inverter-based DERs in AC microgrid. A dual-objective cost function is proposed to simultaneously regulate the output voltage and limit the fault current under symmetrical fault conditions. A two-step-ahead prediction method achieves reduced switching frequency, improved steady-state accuracy and robustness against parametric variations. Furthermore, a predictive hierarchical control architecture was implemented. The stability of the proposed scheme is formally established through Lyapunov analysis, while validation through MATLAB/Simulink simulations and FPGA-in-the-loop (FIL) verifies superior performance compared to conventional techniques.

Second, this dissertation advances AI-based control in DC microgrids. An artificial neural network (ANN) voltage controller was developed using datasets generated by the FCS–MPC, which preserves both a fast transient response and robustness under nonlinear constant power loads. Additionally, a reduced-sensor ANN controller is proposed that relies solely on voltage measurements, providing a cost-effective and scalable solution for real-world implementation. Both approaches are validated through real-time hardware-in-the-loop (HIL) testing, demonstrating reliable voltage regulation in multibus DC microgrid environments.

Overall, this dissertation contributes a comprehensive framework of predictive and AI-based controllers that enhance the reliability, efficiency and scalability of islanded microgrids. By bridging theoretical modelling, real-time validation and open research practices, this work provides a pathway for a resilient, low-carbon power system in the future.

Keywords: Distributed energy resources, Microgrids, Robust converter control, Finite control set model predictive control, Hierarchical predictive control, Artificial neural networks, Hardware-in-the-loop validation.

ACKNOWLEDGEMENT

بِسْمِ للّٰاِ الرَّحْمٰنِ الرَّحِيم

In the name of ALLAH, the Most Gracious, the Most Merciful

اقْرَأْ بِاسْمِ رَبِّكَ الَّذِي خَلَقَ ۝ خَلَقَ الْإِنسَانَ مِنْ عَلَقٍ ۝ اقْرَأْ وَرَبُّكَ الْأَكْرَمُ ۝ الَّذِي عَلَّمَ بِالْقَلَمِ ۝ عَلَّمَ الْإِنسَانَ مَا لَمْ يَعْلَمْ

Read in the name of your Lord who created. Created man from a clot. Read, and your Lord is the Most Generous—Who taught by the pen—Taught man that which he not knew. (Qur'an 96:1–5)

اللَّهُمَّ صَلِّ وَسَلِّمْ عَلَى نَبِيِّنَا مُحَمَّد

May ALLAH's peace and blessings be upon our Prophet Muhammad (SAW)

First and foremost, I offer my deepest gratitude to ALLAH Almighty for granting me the strength, knowledge, patience, and perseverance to complete this doctoral journey. Through His boundless mercy and countless blessings, this accomplishment has been realized, and without His divine grace, it would not have come to fruition.

I am profoundly grateful to my supervisor, Professor Kimmo Kauhaniemi, whose unwavering guidance, scholarly insight, and continuous support have been instrumental throughout this research journey. I also extend my sincere appreciation to my second supervisor, Professor Hannu Laaksonen, for his constructive feedback and thoughtful review of thesis.

I am deeply thankful to pre-examiners, Prof. Saad Mekhilef and Prof. Sergio Vazquez, for their valuable feedback, critical insights, and scholarly contributions that enhanced the rigor and quality of this work. I would also like to forward special thanks to Prof. Marko Hinkkanen for his kind acceptance to act as an official opponent for public defence.

This PhD journey began with the wish and encouragement of my beloved father, Sardar Asad Ullah Khan (late). Though he departed from this world before witnessing the completion of this milestone, his vision, discipline, and unwavering belief in my potential remain the guiding force behind this achievement. May ALLAH grant him the highest rank in Jannah and eternal peace.

میرا طریق امیری نہیں فقیری ہے،
خودی نہ بیچ، غریبی میں نام پیدا کر۔

To my beloved mother, whose constant prayers have been my spiritual strength and protection, I owe more than words can convey. Her sacrifices, patience, and

unconditional love laid the foundation of my character and education. In moments of doubt and exhaustion, it was her prayers that sustained me and gave me renewed strength. May ALLAH grant her a long, healthy, and peaceful life filled with honor and continued blessings.

تربیت سے تیری میں انجم کا ہم قسمت ہوا،
گھر مرے اجداد کا سرمایۂ عزت ہوا۔

My heartfelt gratitude goes to my dear wife, whose understanding and steadfast support made this achievement possible. Particularly after my transition to industry in 2023, when I could dedicate only weekends to my PhD studies and struggled to maintain a proper work–life balance, her encouragement enabled me to fulfill family and professional responsibilities and academic commitments. Her companionship transformed all the challenges into fruitful doctoral endeavor.

Life chiseled me by going through ups and downs during the doctoral journey. I arrived in Finland to pursue doctoral studies, unaware of the profound transformations that would follow. The loss of my father was one of the most difficult trials of my life. So, surely with hardship comes ease (Ash-sharh:5). In 2025, I participated in Finland's municipal elections and was honored to be elected as a member of the city council—an arena I had never envisioned entering. Most joyously, in August 2025, I became the father of a beautiful daughter, whose arrival added new meaning, responsibility, and light to my life.

I extend my sincere appreciation to my lab mates, colleagues, and co-authors for their insightful discussions, collaborative efforts, and expertise that significantly strengthened this research and made the journey both enriching and enjoyable.

I remain thankful to my siblings (brother and sisters) and friends in Pakistan, particularly my elder brother Yasir Asad Khan, for their encouragement from afar. I sincerely appreciate my friends in Vaasa, whose companionship and support made life in a foreign land feel like home.

While this work represents years of dedicated effort, any errors or shortcomings remain solely my responsibility. I sincerely hope that this research contributes, even in a small way, to the global transition toward sustainable and carbon-neutral energy systems for generations to come.

May ALLAH accept this humble effort and make it beneficial for mankind. Ameen.

Vaasa, 15.02.2026
Hussain Khan

Contents

Figures

Tables

Abbreviations

AC	Alternating Current
AI	Artificial Intelligence
ANN	Artificial Neural Network
CCS–MPC	Continuous Control Set Model Predictive Control
CF	Cost Function
CHIL	Controller Hardware-in-the-Loop
CP	Constant Power
CPL	Constant Power Load
CUT	Controller Under Test
CZ	Constant Impedance
DER	Distributed Energy Resource
DG	Distributed Generator
ESS	Energy Storage System
EPS	Electric Power System
FCS–MPC	Finite Control Set Model Predictive Control
FCS–MPVC	Finite Control Set Model Predictive Voltage Control
FIL	FPGA-in-the-Loop
FPGA	Field Programmable Gate Array
HIL	Hardware-in-the-Loop
IEC	International Electrotechnical Commission
LV	Low Voltage
MG	Microgrid
MIL	Model-in-the-Loop
MIMO	Multi-Input Multi-Output
MPC	Model Predictive Control
OPAL–RT	Real-Time Digital Simulation Platform (OPAL–RT Technologies)
PCC	Point of Common Coupling
PD	Proportional Derivative
PEI	Power Electronic Interface
PI	Proportional Integral
PID	Proportional Integral Derivative

PR	Proportional Resonant
PWM	Pulse Width Modulation
QSL	Quasi-Stationary Line
RER	Renewable Energy Resources
RES	Renewable Energy Sources
SFC	State Feedback Control
SIL	Software-in-the-Loop
SMC	Sliding Mode Control
SVM	Space Vector Modulation
THD	Total Harmonic Distortion
VSC	Voltage Source Converter

Publications

I. **Khan, H. S.**, Kumar, J., & Kauhaniemi, K. (2021, November). Design and implementation of model predictive control for parallel distributed energy resources in islanded AC microgrids. In *2021 6th IEEE Workshop on the Electronic Grid* (*eGRID*) (pp. 01–07). IEEE. https://doi.org/10.1109/eGRID52793.2021.9662156 © 2021 IEEE.

II. **Khan, H. S**., Aamir, M., Kauhaniemi, K., Mumtaz, M., Hassan, M. W., & Ali, M. (2021, June). Improved finite control set model predictive control for distributed energy resources in islanded microgrids with fault-tolerance capability. *Engineering Science and Technology, an International Journal*, *24*(3), 694–705. https://doi.org/10.1016/j.jestch.2020.12.015 © 2021 by Authors. Published by Elsevier. CC BY licence.

III. **Khan, H. S.**, & Kauhaniemi, K. (2023, December). Design and FPGA-in-loop-based validation of predictive hierarchical control for islanded AC microgrids. *Engineering Science and Technology, an International Journal*, *48*, 101557. https://doi.org/10.1016/j.jestch.2023.101557 © 2023 by Authors. Published by Elsevier. CC BY licence.

IV. **Khan, H. S**., Mohamed, I. S., Kauhaniemi, K., & Liu, L. (2021, November). Artificial neural network-based voltage control of DC/DC converter for DC microgrid applications. In *2021 6th IEEE Workshop on the Electronic Grid* (*eGRID*) (pp. 1–6). IEEE. https://doi.org/10.1109/eGRID52793.2021.9662132 © 2021 IEEE.

V. **Khan, H. S.**, & Kauhaniemi, K. (2023, June). FPGA-validated advanced learning-based voltage control of DC/DC converter feeding CPL in DC microgrid applications. In *2023 IEEE 32nd International Symposium on Industrial Electronics* (*ISIE*) (pp. 1–6). IEEE. https://doi.org/10.1109/ISIE51358.2023.10228168 © 2021 IEEE.

VI. **Khan, H. S.**, & Kauhaniemi, K. (2025, January). Artificial intelligence-based reduced sensor voltage control strategy for DC microgrid applications. *IET Renewable Power Generation* https://doi.org/10.1049/rpg2.70072 © 2025 by Authors. Published by Wiley. CC BY licence.

Author's Contributions

Publication I: Hussain Sarwar Khan: Conceptualisation, Methodology, Simulation, Formal analysis, Writing – original draft; Jagdesh Kumar: Writing – review & editing, Investigation; Kimmo Kauhaniemi: Supervision, Writing – review & editing.

Publication II: Hussain Sarwar Khan: Conceptualisation, Methodology, Simulation, Formal analysis, Writing – original draft; Muhammad Aamir: Writing – review & editing, Supervision; Kimmo Kauhaniemi: Writing – review & editing; Mohsin Mumtaz: Resources; Muhammad Waqar Hassan: Visualisation; Muhammad Ali: Resources.

Publication III: Hussain Sarwar Khan: Conceptualisation, Methodology, Investigation, Software, Formal analysis and Writing – original draft; Kimmo Kauhaniemi: Fund Acquisition, Supervision, Modification for the final layout, Writing – review & editing.

Publication IV: Hussain Sarwar Khan: Conceptualisation, Data curation, Methodology, Simulation, Formal analysis, Writing – original draft; Ihab S. Mohamed: Conceptualisation, Formal analysis, Writing – review & editing; Kimmo Kauhaniemi: Writing – review editing, Supervision; Lantao Liu: Writing – review & editing.

Publication V: Hussain Sarwar Khan: Conceptualisation, Methodology, Data curation, Simulation, Formal analysis, Writing – original draft; Kimmo Kauhaniemi: Writing – review & editing, Supervision.

Publication VI: Hussain Sarwar Khan: Conceptualisation, Data curation, Methodology, Simulation, Formal analysis, Writing – original draft; Kimmo Kauhaniemi: Supervision, Writing – review & editing.

Other Relevant Publications

Khan, H. S., Fuad, K. S., Karimi, M., & Kauhaniemi, K. (2021, August). Fault current level analysis of future microgrids with high penetration level of power electronic-based generation. In 2021 IEEE 9th International Conference on Smart Energy Grid Engineering (SEGE) (pp. 48-53). IEEE.

Kumar, J., **Khan, H. S.**, & Kauhaniemi, K. (2021, July). Smart control of battery energy storage system in harbour area smart grid: A case study of vaasa harbour. In IEEE EUROCON 2021-19th International Conference on Smart Technologies (pp. 548-553). IEEE.

Bhatti, M. Z. A., Siddique, A., Aslam, W., Atiq, S., & **Khan, H. S.** (2023). Improved model predictive direct power control for parallel distributed generation in grid-tied microgrids, Energies, 16(3), 1441.

Khan, M. K., Kauhaniemi, K., & **Khan, H. S.** (2025). Optimizing smart inverter control for improved distribution network hosting capacity: A model predictive control approach. International Journal of Electrical Power & Energy Systems, 165, 110472.

Khan, H. S., Khan, M. K., & Kauhaniemi, K. (2025). Distributed Energy Resource Behavior During Faults: Navigating Voltage Ride-Through Compliance Within the Realm of EN 50549. IET Generation, Transmission & Distribution, 19(1), e70131.

Khan, H. S., Hafeez, S., Mubarak, M. F., & Shahzad, K. (2026). Developing Strategic Fit in Changing Business Dynamics: The Case of an Electric Vehicle Charging Infrastructure Manufacturer. In Electric Vehicle Supply Chain Management (pp. 292-311). Routledge.

1 INTRODUCTION

Fossil fuels have played a key role in the energy sector for centuries. Coal, gas and oil fuelled the industrial revolution and drove the global economy to rapid growth. However, energy production using fossil fuels causes environmental pollution and global warming and harms environmental enthalpy. In 2022, electricity and heat production were responsible for nearly 44% of global CO_2 emissions (CO_2 Emissions in 2022 – Analysis, 2023). The Paris Agreement, reached in 2015, is a global response to this concern. The aim of the agreement is to keep the global average temperature increase well below 2 degrees Celsius above preindustrial levels and to pursue efforts to limit it to 1.5 degrees Celsius by 2070 (Agreement, 2015).

However, power production using fossil fuels plays a key role in carbon emissions and wastes a large amount of energy. Between 40% and 70% of energy is lost in the form of heat, and an additional 2% and 4% of energy loss occurs during the transmission and distribution of electricity, leaving 33% available power overall at the consumer end for consumption, as depicted in Figure 1 ('Power Grid Efficiency – Sources of Grid Losses', 2022). Uncertainty in fuel prices, volatile markets and rapid growth in energy demand have motivated policymakers, industries and researchers to search for alternative, environmentally friendly, carbon-free and more efficient ways to meet the world's growing power demand.

Thanks to the rapid advancements and falling costs of renewable energy resources (RES), such as photovoltaic and wind technology, these are transforming the energy landscape (Roser, 2020). RES has opened up the possibility of decentralised generation and reduced reliance on fossil fuels. Furthermore, the rapid integration of renewable energy resources (RERs) into the power system on one front helps reduce carbon emissions, resulting in a development of sustainable future power system. However, the intermittency of RERs and decentralised generation presents new challenges, including voltage fluctuations and grid congestion, particularly in maintaining the stability and control of renewable-rich power systems (Bird et al., 2013). Advanced control methods are required to meet the need for stability. Subsequently, all these resources are connected to the power system through a power electronic interface (PEI). Therefore, the control of PEIs plays a major role in achieving the carbon-free electrical power systems of the future.

Inverter-based distributed energy resources can be integrated into different voltage levels, including medium-voltage (MV) and low-voltage (LV) networks. This makes the system more controllable and efficient than a traditional power system, where

power system operators have minimal control and less interference in the distribution system.

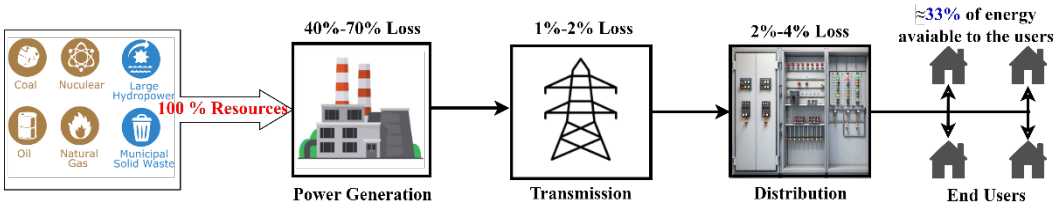

Figure 1. Energy losses in conventional power systems

Instead of individually controlled power converters, it is also possible to interface them with the main grid through microgrids (MGs), which is one of the special cases at the distribution level, to arrive at a modern power system.

MGs are among the most promising solutions for integrating renewable energy-based generation into traditional power systems. MGs are an innovative concept with a long history. The first power generation plant, which is also a special type of MG, was constructed in Manhattan by Edison in 1882. MGs constitute a cluster of generating units, loads, energy storage systems and effective control at the distribution level of the power system. MGs' structures have many advantages: independence, compatibility, flexibility, scalability, stability, economics and higher efficiency.

1.1 Problem Statement

The Energy and Climate Roadmap 2050, published by the Ministry of Employment and Economic Affairs of Finland in 2014, highlights the energy transition to zero carbon emissions, energy self-sufficiency and supply security. Finland is highly dependent on energy due to its cold climate, and its energy consumption per capita is high compared to global averages. However, its energy self-sufficiency is low. A viable solution for achieving energy self-sufficiency and efficiency is the extensive implementation of RERs, such as solar and wind. This transition has resulted in a surge of distributed energy resource (DER) units in distribution networks across the residential, commercial and industrial sectors. The use of solar, wind and other RERs in residential, commercial and large facility buildings has grown significantly in the last few years.

As the integration of DER units accelerates, the production of both AC and DC power has gained significance. Microgrids have emerged as a promising solution for integrating DERs at the distribution level in renewable-rich power systems. At the core of these microgrids are power electronic interfaces (PEIs). These devices

connect DER units to the grid, manage bidirectional energy flow and enable the flexible operation of both AC and DC networks. However, the integration of RERs introduces technical challenges. The intermittent nature of renewables complicates the maintenance of voltage and frequency stability, efficient power sharing among sources and the upholding of power quality in the presence of fluctuating loads (Bird et al., 2013, 2013; Eltigani & Masri, 2015). Microgrids must now handle fast-changing dynamics, nonlinearities and disturbances. Additionally, they are expected to provide a plug-and-play environment in which new DER units and loads can be added or removed with minimal disruption.

The control of PEIs, particularly for regulating converter current and voltage, has predominantly relied on linear controllers. Among these, proportional–integral (PI) (Rathnayake et al., 2021; Rocabert et al., 2012) and proportional–resonant (PR) (Ziouani et al., 2018) controllers have been widely used by industry due to their simplicity and effectiveness in stable conditions. However, in renewable-rich power systems, these controllers are not robust under rapid load variations, system nonlinearities and external disturbances due to their inability to track the sinusoidal reference with zero steady-state error, the tuning of gains, poor disturbance rejection capabilities and the inability to handle non-linearities. This can result in compromised voltage regulation, instability and reduced power quality, particularly during sudden changes or when managing diverse, demanding loads.

Advanced nonlinear control techniques have been introduced to address these challenges, including sliding mode control (SMC) (Mousavi et al., 2022) and deadbeat (DB) (Mattavelli, 2005; Buso et al., 2016) control approaches. Each approach offers certain advantages: SMC is robust to uncertainties, and DB provides a fast, dynamic response. However, the practical limitations of these approaches include chattering phenomena, complex mathematical modelling, high switching losses and significant computational burdens, especially in real-time, large-scale systems (Miveh et al., 2016).

The ongoing evolution of power systems, with even higher penetration of DERs and greater demands for flexibility and adaptability, necessitates more intelligent control solutions. Artificial intelligence (AI)-based controllers, particularly those employing artificial neural networks (ANNs), provide promising features. These include adaptability to system changes, the capacity to learn complex behaviours from data and reduced reliance on sensors. Such controllers are especially well suited for plug-and-play environments and complex microgrid operations.

Despite this progress, there remains a gap in the practical deployment and comparative evaluation of advanced nonlinear control techniques such as model predictive control (MPC) and AI-based control strategies for DER units in AC and DC

microgrids. Key questions remain about their effectiveness in maintaining voltage and frequency stability, ensuring efficient power sharing and delivering high power quality under real-world, fluctuating conditions.

This dissertation addresses these critical challenges by developing, implementing and rigorously evaluating advanced nonlinear and AI-driven control methods for DER units in AC and DC microgrids. This research aims to provide practical solutions for robust voltage and frequency regulation, efficient power sharing, power quality improvement and adaptability to rapidly changing, renewable-rich environments. Ultimately, this work seeks to enable the next generation of resilient and intelligent power systems.

1.2 Objectives

This PhD dissertation analyses how to mitigate and address the challenges introduced by the high penetration of RERs from the perspective of PEI control. Thus, the aim is:

- To develop robust and decentralised nonlinear control for distributed generation under diverse operating conditions.
- To design and evaluate hierarchical predictive control architectures for AC microgrids and to assess their real-time dynamic performance.
- To demonstrate that artificial neural network (ANN)-based control can be used for effective voltage regulation in DC microgrids with a high penetration of DER units.
- To design, develop and implement the AI-driven technique for DER units and to compare its performance against classical controllers under challenging modern power system scenarios.

1.3 Research Questions

The objectives of this dissertation are realised through the precise articulation of the research questions, which are subsequently addressed through relevant publications, as depicted by Figure 2. The research questions are outlined as follows:

- RQ1: How can decentralised nonlinear predictive control achieve reliable voltage regulation and power sharing in AC microgrids with diverse load conditions?

- RQ2: How can hierarchical predictive control strategies be designed and validated to ensure robust, decentralised voltage and frequency control in renewable rich power systems under varying load conditions and parametric uncertainties?

- RQ3: Can ANN-based control provide reliable voltage regulation in DC microgrids?

- RQ4: Can artificial intelligence-based control with reduced sensor requirements outperform conventional approaches (e.g. linear PI or MPC) for modern power system voltage regulation, particularly under challenging scenarios such as constant power loads?

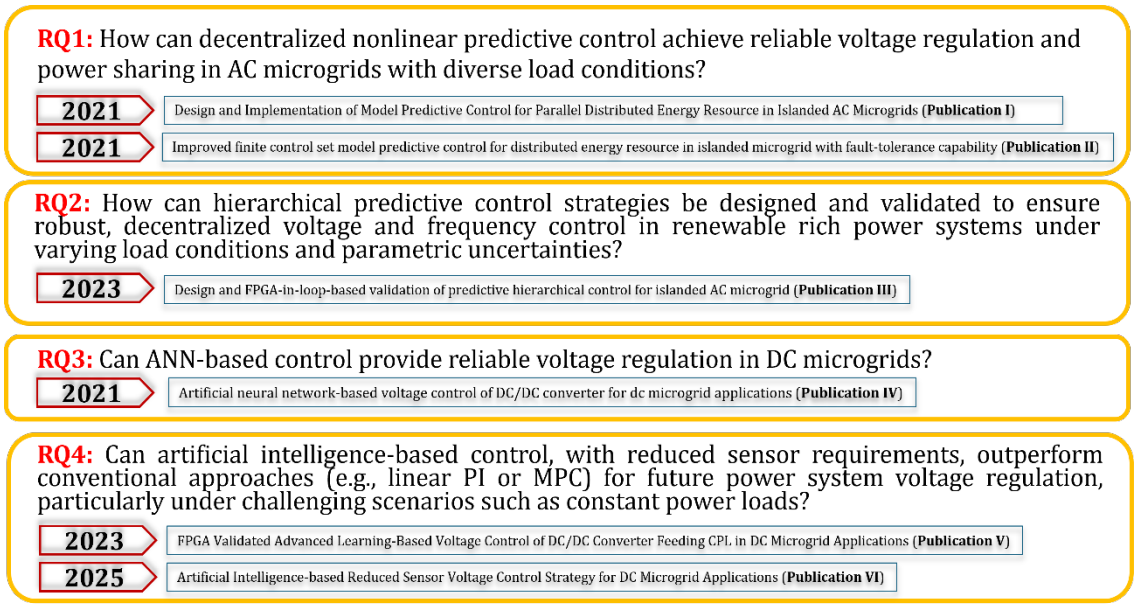

Figure 2. Outline of publications based on research questions

1.4 Scientific Contributions

This doctoral dissertation has made the following main scientific contributions:

- It develops and implements a hierarchical control structure for AC microgrids, integrating decentralised finite control set model predictive control (FCS–MPC). This strategy enhances power sharing and reduces total harmonic distortion (THD) in single-DG and multi-DG microgrids, even under parameter variations and with various loads, such as constant power (CP), constant impedance (CZ), constant current (CI) and industrial loads (Publications I–III).

- It presents a novel artificial intelligence (ANN)-based voltage control scheme for DER units (DC/DC boost converters), validated through FPGA-in-Loop. The scheme shows improved transient performance, computational efficiency and robustness, especially for DC microgrids with constant power loads and fewer sensing elements (Publications IV–VI).

- It provides rigorous mathematical proof of stability for the proposed control algorithms. This dissertation establishes Lyapunov-based stability for the FCS–MPC controllers applied to DC/AC converters and demonstrates the theoretical stability of ANN-based controllers for DC/DC converters, ensuring reliable operation across a wide range of scenarios (Publications III and VI).

- It validates the effectiveness and practicality of the control strategies developed using real-time simulation (OPAL–RT) and FPGA-in-the-loop setups. These experiments showcase the dynamic response, resilience and plug-and-play capabilities of control solutions in realistic future cases (Publications III, V and VI).

- It promotes transparency and collaboration in the field by sharing open-source repositories that include datasets, simulation models and board definition files on platforms such as GitHub. This approach enhances reproducibility and encourages further research within power systems and control communities (Publication III).

1.5 Outline of This Thesis

This dissertation is organised into two sections. The first section comprises six chapters that provide an overview and summary of the research conducted. The second section contains the appended original research articles. Figure 3 summarises the publications presented in chapters 3 and 4. A brief summary of each chapter is as follows:

Chapter 2 presents a brief literature review, establishing the theoretical framework for this dissertation.

Chapter 3 focuses on the development of improved finite control set model predictive control (FCS–MPC) strategies for AC microgrids.

Chapter 4 discusses AI-based control for DC microgrids, including ANN voltage controllers, such as a reduced-sensor scheme trained with MPC datasets validated through simulations and HIL experiments under challenging load conditions.

Chapter 5 presents the main findings and outlines future work regarding this research.

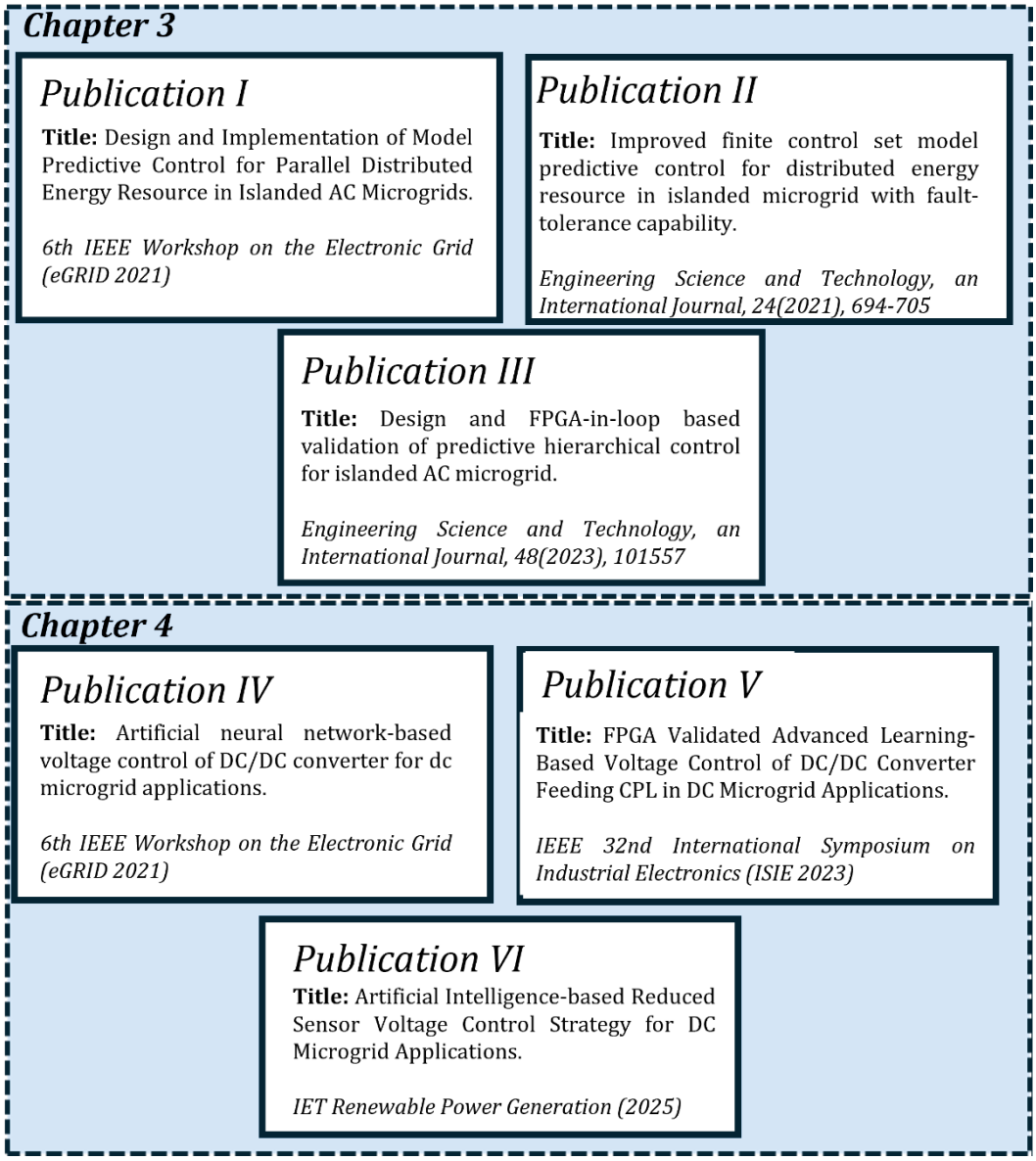

Figure 3. Publications I–VI related to chapters 3 and 4

1.6 Summary of Publications

This dissertation comprises six conference and journal articles, and the author of this thesis is the main and corresponding author of all these publications. Figure 4 illustrates the distribution of the author's publications across technology readiness levels and microgrid control layers.

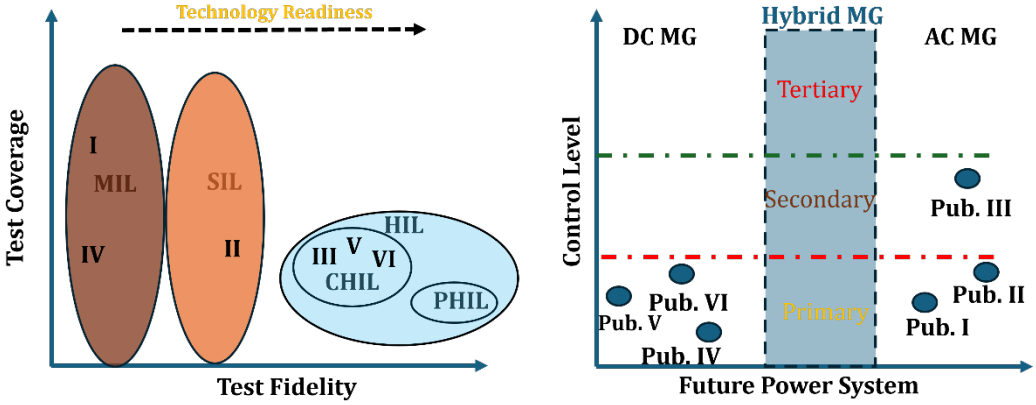

Figure 4. Overview of the author's publications mapped to different validation stages (MIL, SIL, CHIL, HIL and PHIL), their contributions across microgrid control levels (primary, secondary and tertiary) and technology readiness levels

Publication I: This publication presents a two-step-ahead FCS–MPC voltage control approach for DERs in autonomous power systems (microgrids). It analyses the performance of the given controller under steady-state, transient and uncertain load conditions. The major focus of this article is to study the controller's response under nonlinear loads. This approach eliminates the need for cascaded control loops, reducing system complexity while maintaining reliability. Conversely, the two-step horizon technique reduces the computation burden while maintaining the controller's performance.

Publication II: This publication presents an advanced control strategy for distributed energy resources in AC islanded microgrids, targeting an improved finite control set model predictive voltage control (FCS–MPVC). The research addresses the limitations of traditional linear controllers, such as slow transient response and poor disturbance rejection, by implementing a dual-objective cost function that simultaneously manages output voltage regulation and load current under fault conditions. The proposed control approach utilises the mathematical model of the system to anticipate state variables (current and voltage) for possible switching states at each sampling instant. A two-step horizon prediction was implemented to reduce the computational burden. Droop control is implemented for proper power sharing among DER units. MATLAB/Simulink simulations validate the controller's performance across operating conditions, such as three-phase faults, including linear, non-linear and unbalanced loads. The results demonstrated better performance with THD than with linear controllers. The dual objective effectively regulates and limits the fault current.

Publication III: The goal of this article is to develop a decentralised hierarchical nonlinear control strategy for DERs to improve transient stability, ensure proper power sharing among parallel DER units and maintain power quality under varying load conditions. At the primary control level, a reduced switching finite control set model predictive control (FCS–MPC) algorithm regulates voltage by predicting future voltage states over a two-step horizon and evaluating possible switching combinations via a predefined cost function. This approach selects the optimal switching action to minimise voltage error, thereby achieving a fast transient response. Additionally, a conventional droop control method is implemented on the outer layer of the primary control, which enables the sharing of active and reactive power between DERs, regardless of feeder impedance mismatches. A PI-based secondary control layer is employed to regulate voltage and frequency deviations that are neglected by the primary control. A key theoretical contribution of the paper involves the use of Lyapunov stability analysis to prove the stability of the proposed controller. Performance validation was performed through simulations in MATLAB/Simulink and FPGA-in-the-loop using a ZYBO Z7 (ZYNQ-7020) board. The results show that the controller response adheres to standards such as IEEE 519. Consequently, the system provides the effective regulation of voltage/frequency and robust power sharing under dynamic load scenarios. It demonstrates its suitability for autonomous modern power systems, where the MG is considered a special case. Furthermore, the open-source repository provides datasets and board definition files, encouraging further research and development. Additionally, the effects of various dynamic loads, such as commercial, residential and constant power, on the proposed controller were examined and evaluated.

Publication IV: The motivation of the article lies in addressing the limitations of traditional linear controllers (e.g. PI, PID) in handling non-linearities and parameter variations in DC microgrid applications. This article proposes an artificial neural network (ANN)-based voltage control strategy for a DC–DC step-up converter to overcome the limitations of conventional linear controllers, such as PI and PID. Initially, model predictive control (MPC) was used as a parent approach to develop the dataset. The obtained dataset was then used to train the ANN offline. Extensive MATLAB/Simulink simulations validate the effectiveness of the ANN compared to conventional PI and MPC controllers, demonstrating improved voltage regulation, transient response and robustness under varying load conditions. The main advantage of the proposed control scheme is that it has a lower computational burden than the parent technique, which is the MPC in this case.

Publication V: This paper addresses the challenge of voltage instability in modern power systems caused by constant power loads (CPLs) due to their negative impedance characteristics. Traditional linear and nonlinear control methods, such as

PI, sliding mode control (SMC) and model predictive control (MPC), have limitations, including an inability to handle non-linearities, high computational burden, sensitivity to parametric variations and instability under varying conditions. Therefore, this paper proposes an advanced artificial neural network (ANN)-based voltage control strategy for DC–DC converters. The ANN controller illustrates a superior transient response, robustness against load and input voltage variations, and less computational burden than conventional methods. Validation was performed using FPGA-in-the-loop (FIL) testing on the ZYBO Z7-7020 board, confirming its practical feasibility and effectiveness in mitigating the destabilising effects of CPLs in DC microgrids.

Publication VI: This paper examines the challenge of effective voltage regulation in modern power systems, with a focus on reducing the number of sensors while ensuring the system's reliability. A quasi-stationary line (QSL) modelling approach is employed to account for the uncertainties and disturbances within the system. A voltage control strategy based on artificial neural networks (ANNs) for DC–DC step-up converters is proposed, where the voltage error is designated as the input and the switching signal serves as the output feature. The trained ANN substitutes for model predictive voltage control (MPVC) to regulate distributed generators (DG) in a multibus DC microgrid. Real-time hardware-in-the-loop simulations using OPAL–RT 4510 confirm the efficacy of the controller, demonstrating better performance than conventional methods, such as proportional–integral (PI) and model predictive control (MPC), particularly in terms of transient response, reduced overshoot and robustness against load and voltage variations. Furthermore, the mathematical stability of the proposed control techniques was evaluated.

2 THEORETICAL BACKGROUND

One of the most significant paradigm shifts in conventional power systems is the integration of renewable energy, transitioning from centralised to decentralised power generation. This chapter focuses on a comprehensive, state-of-the-art literature review on controlling distributed energy resources and issues associated with RER penetration in microgrids.

This chapter will explore four key areas that shape today's evolving energy landscape: (1) the transition of traditional power systems towards renewable-rich power systems and their challenges, (2) microgrids' control hierarchies and their implementations, (3) DER unit control strategies and (4) methods for maintaining voltage stability in systems with a high share of distributed energy resources (DERs). By reviewing the existing literature on these topics, this chapter highlights significant knowledge gaps and lays the foundation for the contributions presented in this dissertation.

Importantly, the terms 'autonomous MG', 'islanded MG' and 'standalone MG' refer to the same concept. However, many researchers have used these terms in their studies.

2.1 Transition of Power Systems: From Conventional to Decentralised Grids

For nearly a century, conventional power systems have been centralised, with a unidirectional power flow from bulk generation, such as coal, natural gas and hydroelectric plants, to passive users through transmission and distribution networks. This system is based on established infrastructure and technologies, delivering efficient and high output from large centralised facilities. Kundur (2007) conducted a foundational analysis of the stability and control of these traditional systems. The generation in conventional power systems is based on synchronous generators, which provide natural stability due to their rotating mass and intrinsic resistance to changes in motion. The control architecture is based on a three-layer hierarchical system: primary frequency control, which responds within seconds (e.g. conventional droop control), secondary control that adjusts over minutes (e.g. automatic generation control) and tertiary control optimising operations over tens of minutes to hours (e.g. economic dispatch and unit commitment). This control architecture operates efficiently when the generation is controllable and predictable. Conversely, fluctuations in load demand introduce uncertainty and require improved management to enhance the robustness and reliability of the conventional power system. Conventional power systems depend on fossil fuels that are subject to resource depletion, and their centralised nature makes them vulnerable to a single

point of failure, potentially affecting a grid's stability. Additionally, greenhouse gas emissions are among the growing environmental concerns that require sustainable and climate-friendly energy generation alternatives.

Distributed energy resources (DERs), such as solar photovoltaic (PV) systems, wind turbines, biomass units and small hydroelectric installations, have emerged as viable and sustainable alternatives to conventional centralised power generation. Power generation through DER units is decentralised and enhances the reliability of energy. According to IEEE 1547–2018, DER is defined as follows: 'An electric generation and/or storage resource connected to the electric power system at a location closer to the customer than to the bulk power system' (*IEEE Standard for Interconnection and Interoperability of Distributed Energy Resources with Associated Electric Power Systems Interfaces*, 2018).

The Federal Energy Regulatory Commission (FERC) of United States offers a more detailed explanation:

> DERs are small-scale power generation or storage technologies (typically ranging from 1 kW to 10,000 kW) that can provide an alternative to or enhancement of the traditional electric power system. These resources can be located on a utility's distribution system, a subsystem of the distribution network or behind a customer meter. They may include electric storage, intermittent generation, distributed generation, demand response, energy efficiency, thermal storage or electric vehicles and their charging infrastructure. (*FERC Order No. 2222: Fact Sheet | Federal Energy Regulatory Commission*, n.d.)

DERs offer substantial environmental benefits, including significant reductions in greenhouse gas emissions, decreased transmission losses and the promotion of localised energy production. The decentralisation of energy systems enhances local energy autonomy, boosts grid resilience, improves reliability and reduces the vulnerability to large-scale outages.

However, the integration of DERs also introduces operational complexity. Traditional power systems rely on large generating units, each with well-defined control characteristics. In contrast, DER-based systems may involve thousands of smaller, diverse units, each with distinct response behaviours and control requirements. This shift complicates system management, coordination and reliability assurance. Moreover, incorporating DERs into existing power distribution networks presents several challenges, including economic, technical, regulatory and environmental obstacles, which are summarised in Table 1. However, recent studies have proposed effective solutions to address these barriers. To overcome technological limitations

and high capital costs, researchers have recommended hybridising renewables with combined cycle power plants, deploying advanced storage technologies such as hydrogen and thermal systems, and using AI for forecasting and dispatch optimisation (Ferdous & Barman, 2025; Z. Zhang, 2024).

Table 1. Key challenges in integrating RERs and their associated impacts on power systems (Garg & Tyagi, 2024; M. Y. A. Khan et al., 2025; Meegahapola et al., 2021; Olivares et al., 2014)

	Challenge	Impact
1.	Technological Limitations	High capital costs require advanced control approaches.
2.	Grid Infrastructure and Stability	Insufficient inertia resulting from few synchronous generators.
3.	Policy and Regulatory Framework	Incompatibility with the existing regulatory framework and old policy mechanisms.
4.	Economic and Financial Constraints	Financial challenges due to an uncertain return on investment and high capital costs.
5.	Environmental and Social Impacts	Land use conflicts and noise issues.
6.	Cybersecurity Risks	Increased risk of cyberattacks due to a multitude of remotely controlled DG nodes.
7.	Scalability and Grid Integration	Geographic and technological constraints limit the scalability and grid connections of RERs.
8.	Power Quality and Harmonics	Distortions caused by the widespread use of power electronic converters.
9.	Intermittency and Variability of RERs	Challenges in maintaining voltage and frequency stability under fluctuating generation.

Regarding grid infrastructure and stability, novel solutions include synthetic inertia, fast frequency response, improved inverter-based controls, fault-ride-through capabilities and distributed energy storage systems to buffer variability and enhance resilience (Rashid, 2024).

On the policy and regulatory front, financial incentives such as tax credits, feed-in tariffs, net-metering reforms and standardised interconnection frameworks have been shown to boost deployment, while innovative financial tools such as green bonds, concessional loans, crowdfunding and blockchain-enabled platforms can help overcome economic and financial barriers by attracting private capital and lowering investor risks (Moroz & Lyeonov, 2024; Sani et al., 2020). For environmental and

social challenges, circular economy practices, such as recycling and reusing battery materials, combined with sustainable land use planning, are critical for mitigating land conflicts and resource pressures (Ferdous & Barman, 2025).

In terms of cybersecurity, layered defence strategies involving encryption, intrusion detection, anomaly detection via AI and blockchain-enabled data integrity have been proposed to address the risks associated with the high penetration of remotely controlled distributed generators (Almasabi et al., 2024; Ekechukwu & Simpa, 2024; Gunduz & Das, 2020). To enhance scalability and grid integration, studies highlight the importance of coordinated transmission system operator–distribution system operator (TSO–DSO) scheduling, demand response programs, electric vehicle (EV) aggregation and diversified flexibility portfolios that include energy storage and demand-side management (Q. Li et al., 2024; Y. Wang et al., 2025) . For power quality and harmonics, practical solutions, such as advanced smart inverters, FACTS devices, multifunctional converters and distributed storage systems, have been validated in simulation and pilot projects to enhance harmonic compensation and maintain voltage stability (H. S. Khan et al., 2025; D. Wu et al., 2024).

Finally, the intermittency and variability of RERs are addressed through a combination of energy storage, demand response and operator coordination supported by stochastic optimisation and scenario-based scheduling, which help restore frequency and voltage stability while facilitating higher renewable penetration (Nguyen et al., 2021; Tang et al., 2022). These findings suggest that a multi-layered approach integrating advanced technologies, financial innovations, supportive policy frameworks and coordinated grid operation is necessary to ensure a reliable and sustainable transition towards renewable-based power systems.

2.2 Microgrid

The high penetration of RERs is necessary to achieve modern power system development with zero net carbon emissions. RERs generate DC power, which can lead to grid stability issues due to the variable and intermittent nature of RERs. Additionally, a bidirectional power flow requires new protection schemes, and the several DER units necessitate communication and advanced control to maintain a grid's stability. Additionally, due to fewer synchronous generators, voltage and frequency regulations have become more complex. To address this issue, MG has emerged as a solution for the successful integration of RERs and a fundamental building block for achieving a smart grid or future power system. Microgrids (MGs) are defined by various organisations, standards makers and researchers, each providing distinct perspectives on their characteristics and capabilities. IEEE 1547.4-

2011 addresses distributed resource island systems, which represent fundamental MG configurations. According to IEEE 1547.4-2011, 'distributed resource island systems' are defined as 'Parts of electric power systems (EPSs) that have distributed resources and load, have the ability to disconnect from and parallel with the EPS, include the local EPS and may include portions of the area EPS, and are intentional and planned' (*IEEE Guide for Design, Operation and Integration of Distributed Resource Island Systems with Electric Power Systems*, 2011).

The International Electrotechnical Commission (IEC) provides a complementary definition in IEC 62898-1, characterising an MG as follows:

> A group of interconnected loads and distributed energy resources with defined electrical boundaries that acts as a single controllable entity with respect to the network and can connect and disconnect from such network to enable it to operate in both connected and island modes. (IEC TS 62898-1, n.d.)

The U.S. Department of Energy (DOE) offers a similar perspective, defining an MG as follows:

> A group of interconnected loads and distributed energy resources within clearly defined electrical boundaries that acts as a single controllable entity with respect to the grid. A microgrid can connect and disconnect from the grid to enable it to operate in both grid-connected or island mode. (Ton & Smith, 2012)

The CIGRE C6.22 Working Group provides an operational perspective, defining MGs as follows:

> Electricity distribution systems containing loads and distributed energy resources (such as distributed generators, storage devices or controllable loads) that can be operated in a controlled, coordinated way either while connected to the main power network or while islanded. (Marnay et al., 2015)

From these definitions, it becomes evident that an MG fundamentally represents a cluster of generating units, loads and energy storage systems, all effectively controlled at the distribution level of the power system. The MG structure offers numerous advantages, including energy independence, grid compatibility, operational flexibility, system scalability, enhanced stability, economic benefits and increased efficiency.

MGs are typically classified into three primary categories based on their electrical configurations: AC, DC and hybrid. Operationally, MGs function in two modes: grid-

tied and islanded. The control architecture of microgrids is hierarchically organised into three control layers: primary, secondary and tertiary (Ahmethodzic & Music, 2021).

2.2.1 Microgrid Classifications

The MG taxonomy is established based on several technical and operational parameters: voltage level, generating capacity, load characteristics, control hierarchy, geographic location, grid interconnection methods and energy resource types, as demonstrated in Figure 5 (Babayomi, Li et al., 2025; Hirsch et al., 2018). This comprehensive classification system is essential because different microgrid types face distinct challenges and opportunities. For instance, voltage levels directly impact safety requirements and equipment costs, while generating capacity determines the potential for scalability. Understanding these taxonomic distinctions provides the foundation for analysing the three primary MG categories that follow, as each category exhibits different combinations of these parameters. As mentioned previously, an MG is divided into three main categories based on the distribution mode:

- **AC Microgrid:** This type of MG is based on AC distribution systems that reflect conventional grid infrastructure. A typical configuration of an AC MG is shown in Figure 6. The AC MG can operate in grid-tied and isolated modes. The primary advantage lies in its compatibility with an existing power system due to mature AC technologies and standardisation. It also enables bidirectional power flow between the utility grid and the prosumers, with the ability to integrate RERs efficiently. The core functionalities of the AC MG control framework are as follows:
    - Voltage and frequency regulation at the point of common coupling (PCC)
    - Accurate active and reactive power sharing among DER units
    - Grid synchronisation and mode transitions
    - Unit commitment and economic dispatch

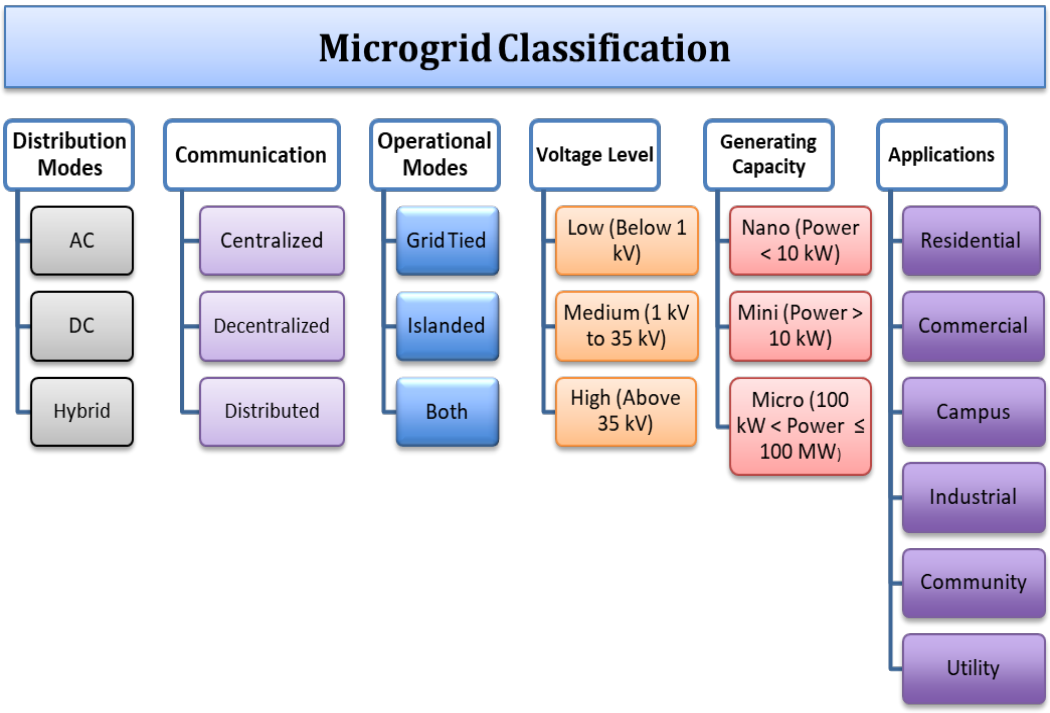

Figure 5. Microgrid classification framework illustrating primary taxonomic categories: distribution modes, communication structures, operational configurations, voltage classifications, capacity ranges and application sectors

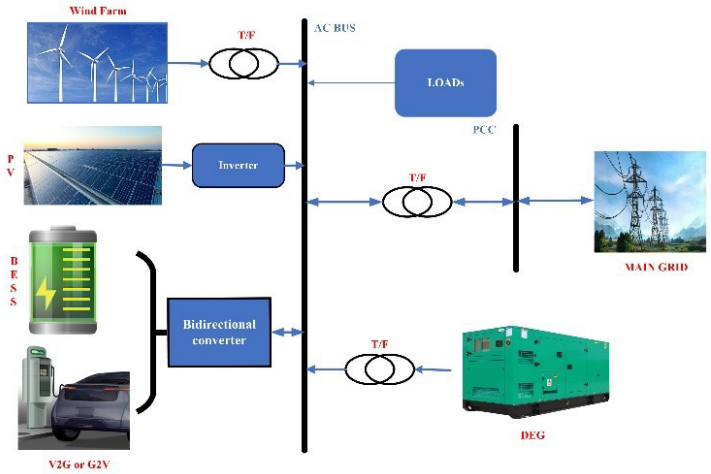

Figure 6. Typical configuration of an AC MG

- **DC Microgrid:** This type of MG is based on a DC bus infrastructure with the integration of RERs, since most renewables produce DC power. The DC MG has gained significant attention for its simplicity because it eliminates issues related to frequency, reactive power and harmonics. Additionally, the DC distribution system is simpler and more efficient than AC distribution networks. The typical configuration of a DC MG is presented in Figure 7. The primary responsibilities of the control system in a DC microgrid differ from those of AC microgrids in several key aspects. While AC microgrids must manage both voltage and frequency regulation, DC microgrids only require voltage control, since DC systems operate without frequency variations. Similarly, DC systems eliminate the need for reactive power management and the complexities of grid synchronisation inherent in AC systems. The core control functions for DC microgrids include the following:
    - The regulation of DC bus voltage
    - Accurate power sharing among distributed generators (DGs)
    - Coordination among distributed energy resources and energy storage systems (ESS)
    - Unit commitment and economic dispatch
    - Utilisation of DERs to their full potential

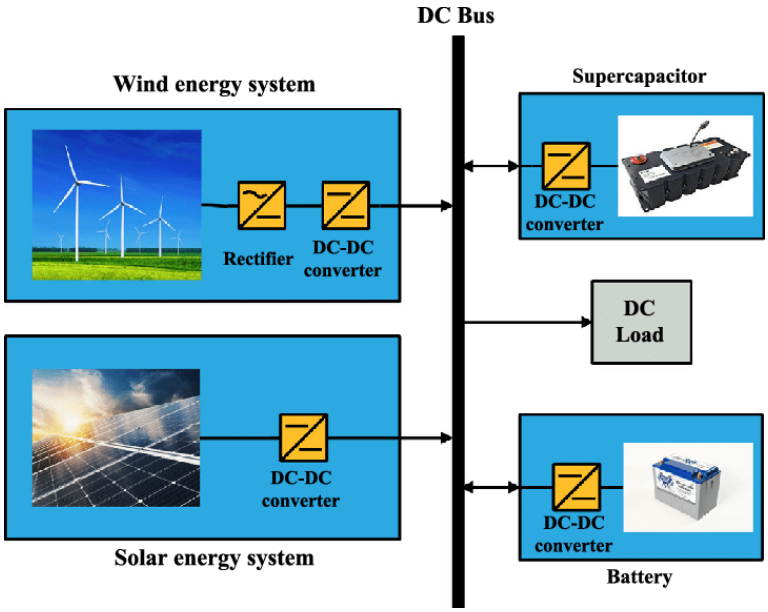

Figure 7. Typical configuration of a DC MG

- **Hybrid Microgrid:** This type of microgrid combines the benefits of both AC and DC systems, featuring a dual-bus architecture that interconnects AC and DC bus via an AC–DC bidirectional converter. This setup enables renewable DC sources, such as solar panels and battery energy storage, to connect directly to the DC bus while remaining compatible with traditional AC loads and grid connections through the AC bus. Interlinking converters handle power flow control between the AC and DC sides. These converters regulate voltage and can operate in various modes, including grid forming, grid following and voltage balancing. Hybrid microgrids offer greater flexibility and efficiency by reducing the number of conversion stages needed for each source and load while improving reliability through redundant power paths and the ability to supply critical DC and AC loads independently during partial system failures. These systems are increasingly utilised in modern applications, such as smart buildings, electric vehicle charging stations and renewable energy projects where both AC and DC elements are present. However, they require advanced control coordination and higher initial costs due to the need for a dual infrastructure. A hybrid MG is illustrated in Figure 8; however, a hybrid MG is outside the scope of this study.

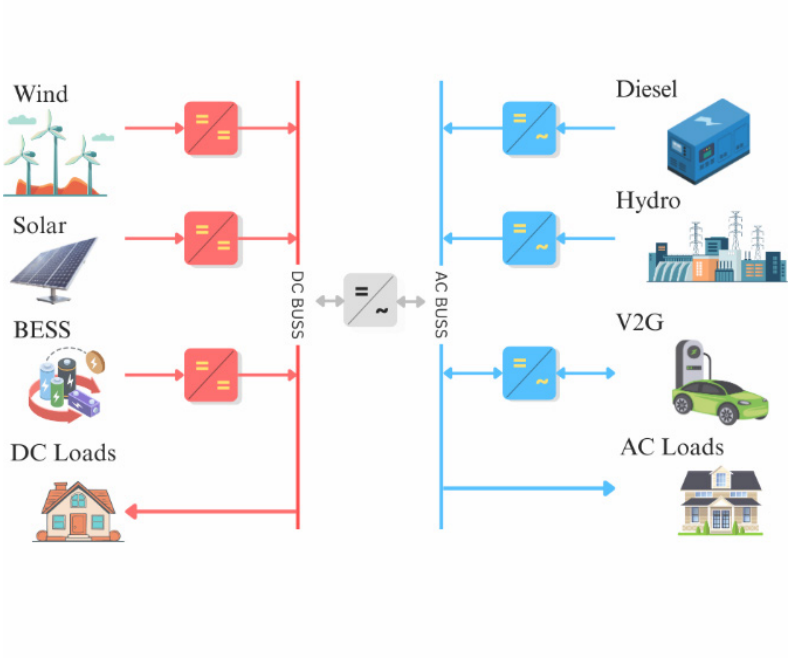

Figure 8. Block diagram of a hybrid MG

2.2.2 Control Architecture of MG

An MG is a promising solution for incorporating RERs and generating carbon-neutral electricity. Additionally, the control architecture of MGs evolves based on their type and operational modes. The hierarchical control concept for MGs is fundamentally based on the multi-level control structure of large conventional power systems. However, MG controllers are significantly more complex due to several factors, including the presence of power electronics-based distributed energy resources (DER) units, energy storage systems, islanding detection algorithms, cybersecurity issues, protection schemes and communication network configurations. Moreover, MG controls operate much faster than conventional power system controls, with response times ranging from microseconds to seconds, as depicted in Figure 9.

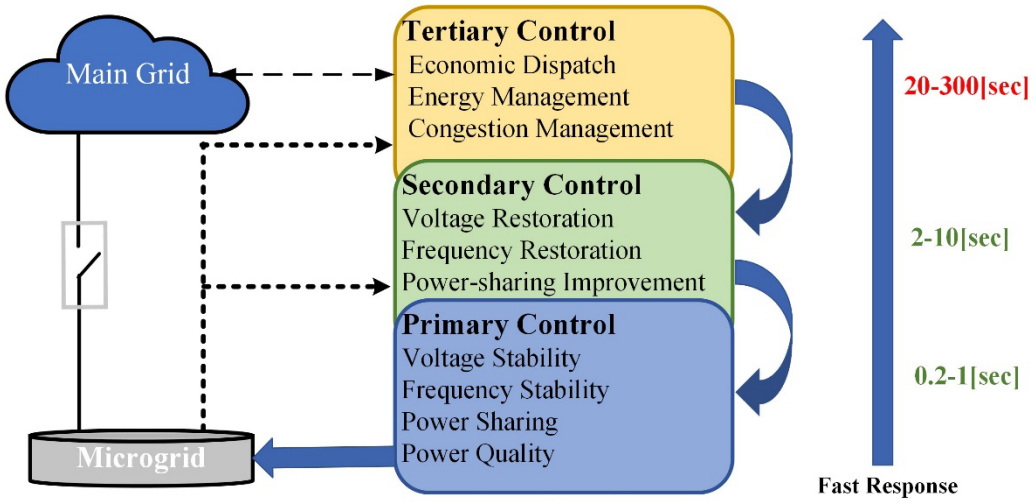

Figure 9. Hierarchical control structures and time scales (Publication III)

Given these complexities, it is essential to develop a comprehensive control framework that incorporates all the aforementioned challenges, as demonstrated in Figure 10. This theoretical control framework must be capable of handling the multifaceted nature of MG operations. The conventional hierarchical control structure for MGs comprises three control layers: primary, secondary and tertiary. Notably, many researchers divide the control structure into four levels: zero, primary, secondary and tertiary control layers (Guerrero et al., 2012; Palizban & Kauhaniemi, 2015; Shrivastava & Subudhi, 2020). However, in this thesis, we merge the zero-level and primary-level control layers as they are implemented at the same level, a practice also adopted by many studies (Beus et al., 2020; M. Y. A. Khan et al., 2025). The brief explanation of each control layer is as follows:

- **Primary Control:** This is the fastest control layer, implemented locally at DER units' terminals. It is further divided into two loops: the inner control

loop, which manages the voltage and the current based on system references and addresses power quality issues, and the outer loop, which handles accurate power sharing and frequency stabilisation at the power connection point. Usually, power-sharing techniques are applied in the outer loop. The outer loop responds more slowly than the inner loop (Katiraei et al., 2005; Lopes et al., 2006; Shrivastava & Subudhi, 2020).

- **Secondary Control:** The secondary control is at the second level of the control layer and is also known as the energy management system of the MG (Mehrizi-Sani & Iravani, 2010). It is responsible for restoring the voltage and frequency deviations caused by the primary control, changes in load or generation and the synchronisation of the MG with the electrical grid when switching between islanded and grid-connected modes. The secondary control is slower than the primary control and collects data on state variables from DGs, energy storage systems and loads. Subsequently, it sets new references for the current and the voltage for the primary control (Guerrero et al., 2010).

- **Tertiary Control**: The tertiary control is the highest level of the MG control. The tertiary control manages the efficient and optimised power flow between the MG and the electrical grid in grid-tied mode. This control layer was the slowest compared to the primary and secondary control layers. Additionally, economic and efficient optimisation is considered.

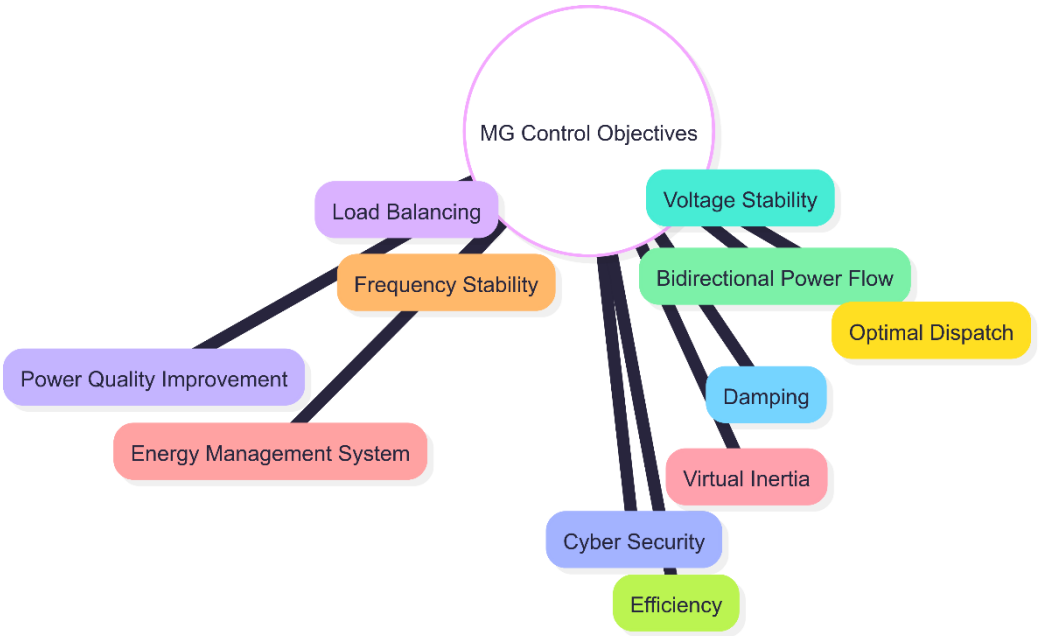

Figure 10. Key challenges and objectives of MG control systems

2.3 Control Techniques for DER Units in MG

As introduced in Section 2.2.2, MG control follows a hierarchical architecture consisting of primary, secondary and tertiary layers. Among these, the primary control layer, implemented locally at DER units through their power electronic interfaces (PEIs), is responsible for the fast regulation of current, voltage and power sharing. This section focuses on the control techniques applied at the primary level, which are fundamental for ensuring voltage and frequency stability, seamless mode transitions, reduced operational costs and the efficient mitigation of fluctuations and disturbances.

The hierarchical control of the microgrid manages the system's voltage, frequency and power sharing among the DERs in the MG, as illustrated in Figure 11 (Ahmethodzic & Music, 2021). Various control techniques have been proposed for controlling power electronics–based DGs. Most of these techniques rely on an outer- and inner-loop structure, also referred to as 'cascaded control'. The outer control loop typically employs droop control, while the inner control loop regulates voltage and current. Control approaches can be divided into many categories. However, in this dissertation, they are classified into five main categories: linear control, non-linear control, robust control, predictive control and intelligent control. Figure 12 presents a classification of control techniques found in the literature.

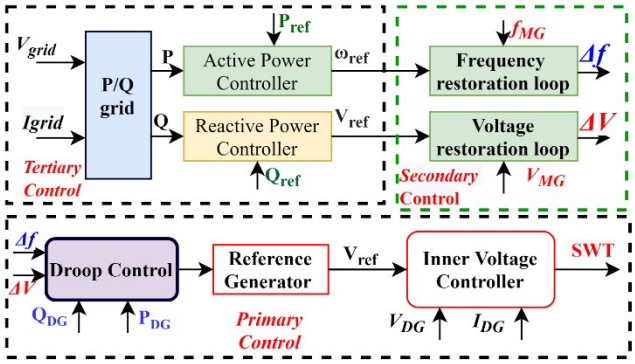

Figure 11. Block diagram of hierarchical control architecture for a DER unit in an MG (Publication III)

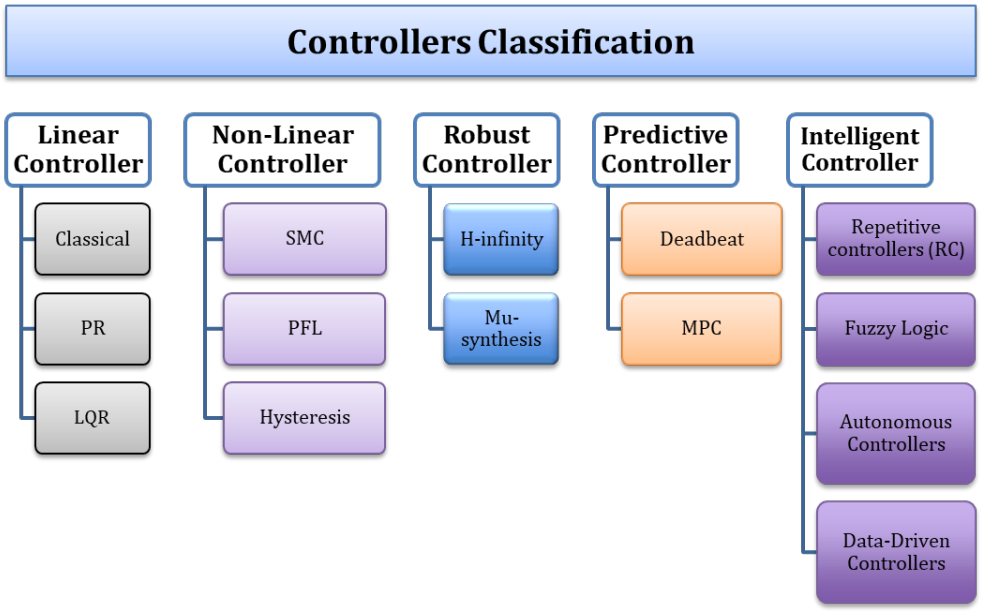

Figure 12. Comprehensive classification of control strategies for DERs found in the literature (Aghdam et al., 2020; Athari et al., 2017; Hossain et al., 2017; Q. Liu et al., 2020)

2.3.1 Linear Control Techniques

Linear control techniques, also called 'classical control methods', include PI, PR and PID controllers, which are often used in cascaded setups. The industry widely uses these controllers to develop products because they are simple, based on well-known mathematics and easy to implement (Chattopadhyay et al., 2014; X. Li et al., 2018). These control techniques rely on mathematical models and feedback-cascaded loops to regulate state variables, such as voltage, current and frequency. These controllers simplify complex systems into single-input single-output (SISO) loops or linearise the design around an operating point within a limited range (Ang et al., 2005). However, conventional linear control methods face significant limitations when applied to multi-input multi-output (MIMO) or nonlinear systems with constraints.

However, traditional linear controllers have several key limitations when used in modern power systems. Tuning linear gains is often labour intensive and requires significant expertise. Although methods exist, such as Ziegler–Nichols, relay autotuning or optimisation-based techniques, their use is limited to nonlinear or MIMO systems. Additionally, the performance of tuned parameters is typically reliable under normal operating conditions. It cannot be guaranteed during abnormal events, such as grid faults, rapid load changes or sudden disturbances. Linear

controllers also tend to have poor dynamic transient responses and cannot effectively control multiple parameters, such as voltage and current. Their narrow bandwidth leads to weak disturbance rejection and reduced robustness in uncertain conditions.

To address these challenges, researchers have proposed adaptive approaches to improve the performance of linear controllers. For instance, in Arnold et al. (2022) and H. Li et al. (2010), an adaptive voltage control method was developed to manage distributed generation (DG) in microgrids, demonstrating improved integration capabilities and excellent instantaneous response compared to conventional methods. In Xu et al. (2014), a robust PI-based control system was introduced for grid-side current, achieving zero steady-state error. The performance of this approach remains satisfactory even when the capacitor current is distorted, with the total harmonic distortion (THD) of the grid current remaining below 3%. Similarly, cascaded inner–outer loop structures have been proposed for grid-connected systems, achieving improved stability and current regulation (Twining & Holmes, 2003).

Although these developments have enhanced performance, their fundamental dependence on linear control structures still limits their applicability to modern power system environments. Their inability to provide reliable robustness, adaptability and multi-objective control emphasises the need to explore advanced nonlinear, adaptive and intelligent control methods that can meet the stringent requirements of next-generation microgrids.

2.3.2 Nonlinear Control

Due to the limitations of linear controllers, researchers are shifting towards advanced control methods, where the error between the reference and actual values is managed based on various theories. Slide mode control (SMC) is derived from the variable structure control theory and operates in two phases: reaching phase and sliding. SMC has robust performance against parametric variations and external disturbances (Lascu, 2020; Rajakumar et al., 2020). However, it is challenging to determine the sliding layer, and chattering phenomena are a significant disadvantage of SMC (L. Wu et al., 2022).

Partial feedback linearisation or state feedback control (SFC) is another type of nonlinear controller. However, its performance is not robust against parametric variations, external load disturbances and noise. The controller's performance is highly dependent on exact system modelling (Callegaro et al., 2018; Chen et al., 2023).

Hysteresis control operates by maintaining the controlled variable within predetermined upper and lower boundary limits. Switching actions occur when these thresholds are crossed, forcing the system back towards the reference trajectory. The primary limitations include unpredictable switching frequency variations that complicate filter design and system optimisation as well as significant current ripple content that affects power quality. Additionally, the control exhibits inherent oscillatory behaviour around the set point, with stability margins that depend critically on the hysteresis bandwidth selection and system dynamics. A comprehensive analysis of various hysteresis-based control methodologies is presented in Z. Li et al. (2016).

Considering the trade-offs of each nonlinear control technique, choosing the right control strategy depends on application needs, system features and performance goals. While SMC offers greater robustness but causes chattering, partial feedback linearisation is mathematically elegant but requires accurate modelling. Moreover, hysteresis control is simple but faces issues with frequency variation. To overcome these limitations and improve control performance, predictive control methods have become a promising option that can manage system constraints and optimise future performance through model-based predictions.

2.3.3 Predictive Controllers

Predictive controllers (PC) represent a class of advanced control strategies that rely on the prediction of future plant behaviour to determine present control actions. PC techniques were introduced in the 1980s for power electronics (Holtz, 1983). They were not further explored until the 2000s due to limited computational resources. Advancements in microprocessor technology have revitalised research in predictive control among power electronics researchers. This has led to the development of various predictive control methods designed for power electronic converter applications (Cortés et al., 2008). Figure 13 presents a detailed classification of PC developed for power converters.

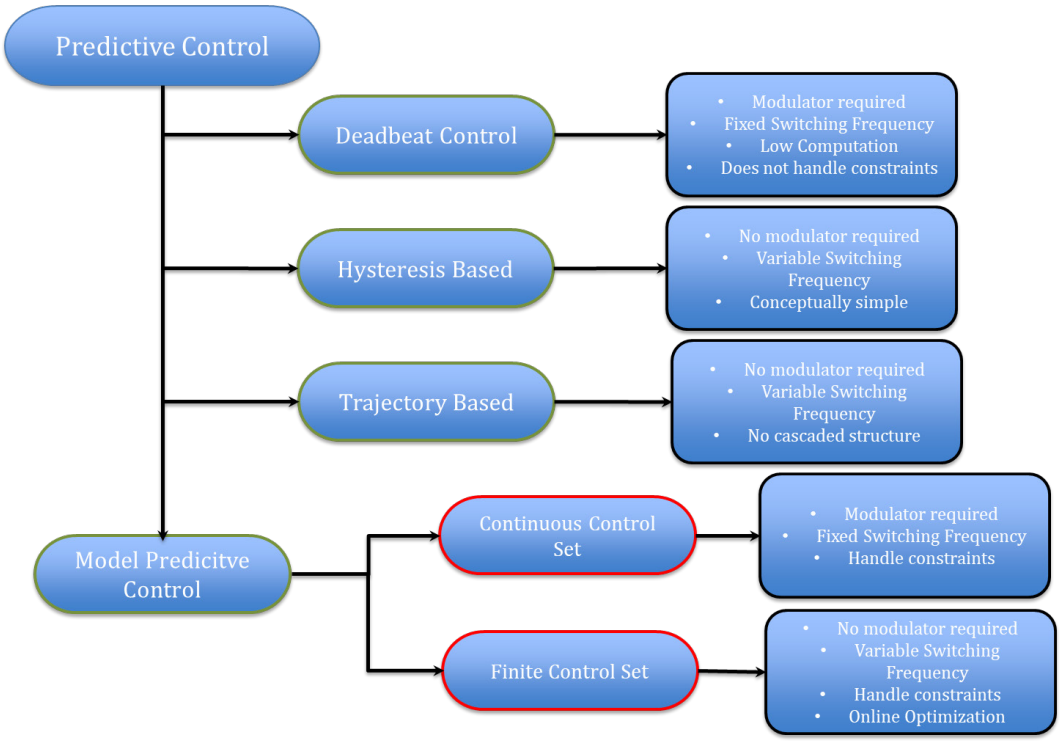

Figure 13. Design considerations and feature comparison of predictive control algorithms (Rodriguez & Cortes, 2012)

Different predictive control approaches use various optimisation criteria to achieve their control objectives. Hysteresis-based predictive control aims to keep the controlled variable within the predefined limits of a hysteresis area (Holtz, 1983), targeting boundary management rather than exact tracking. Trajectory-based control requires variables to follow a predefined reference trajectory (Mutschler, 1998), emphasising accurate path following and tracking performance. Additionally, deadbeat control uses an aggressive optimisation criterion, where the optimal actuation reduces the error to zero by the next sampling instant, focusing on rapid error elimination (Kukrer, 2002).

Among the PCs, model predictive control (MPC) has gained significant attention in the field of power electronics due to its ability to incorporate system models, predict future states and optimise control actions in real time. Unlike conventional linear controllers, MPC eliminates the need for cascaded PI regulators, enabling the direct control of converter behaviour. MPC utilises a more adaptable optimisation criterion, expressed as a cost function. This cost function is minimised to determine the best control action (Morari & Lee, 1999). This adaptability enables multi-objective optimisation and constraint management. MPC can be divided into two main types:

- Continuous control set MPC (CCS–MPC)

- Finite control set MPC (FCS–MPC)

CCS–MPC functions similarly to deadbeat predictive control but processes continuous signals. It requires a modulator to generate switching signals for power electronic devices, and any modulation scheme, such as space vector modulation (SVM) or pulse width modulation (PWM), can be used. The primary advantage of CCS–MPC is its ability to maintain constant switching frequencies, which are advantageous for applications that require predictable switching behaviour (Ahmed et al., 2017; Arias-Esquivel et al., 2022).

FCS–MPC accounts for the discrete nature of power electronics by directly computing switching states. It internally generates switching signals without requiring an additional modulation stage, making it particularly suitable for power electronic devices (PEDs). FSC–MPC has gained significant attention from researchers and is one of the most studied techniques among predictive controls. Unlike conventional control methods, FCS–MPC eliminates the need for traditional cascaded PI controllers and their associated modulation stages (Cortés et al., 2008). The technique offers several distinctive advantages, including the ability to handle multiple control variables simultaneously, a fast dynamic response due to its predictive nature and a simplified design structure that reduces implementation complexity. Additionally, FSC–MPC directly incorporates system nonlinearities and constraints into the control law, consolidates multiple nested control loops into a single unified framework and demonstrates robustness against system parameter variations while effectively handling control delays (Cortés et al., 2010; Yaramasu & Wu, 2013). Table 2 compares PI and FCS–MPC controllers in power electronics applications.

Table 2. Comparison between classical PI and MPC approaches

Description	PI controller	FCS–MPC controller
System Model	Linear load model	Discrete time model
Design of the Controller	PI tuning + modulator design	Define the objective function
Type of Controller	Linear	Optimisation based
Implementation Platform	Both	Only digital
Switching Frequency	Fixed	Variable
Modulation Scheme	PWM/SVM/SPWM	Not needed
Constraint Addition	Not possible	Easily possible
Complex Design	Moderate with SVM	Easy

Description	PI controller	FCS–MPC controller
Steady State Performance	Satisfactory in the DQ frame	Same in all three frames of reference
Computational Burden	Medium	High
Dynamic Behaviour	Average	Outstanding
Multivariable	Coupled	Decoupled

FCS–MPC utilises the mathematical model of the plant to anticipate the future response of the control variables based on a predefined cost function (CF). The CF is typically defined as the square of the Euclidean distance between the measured and reference signals (Cheng et al., 2017). FCS–MPC internally generates switching pulses, eliminating the need for PWM generation units, and directly incorporates system constraints into the cost function to achieve the desired performance. For example, the same CF can be used to achieve primary control objectives such as voltage, current and power, while handling secondary objectives such as switching frequency reduction, thermal stress balancing and DC link voltage regulation. These characteristics make FCS–MPC particularly suitable for regulating power conversion devices, as demonstrated by extensive research documented in recent literature (Babayomi, Madonski, et al., 2025; Camacho & Bordons, 1999; X. Liu et al., 2023; Morari & Lee, 1999; Rocabert et al., 2012) that showcases various MPC implementations for power electronic applications and their theoretical foundations. Despite these advantages, FCS-MPC has not yet been widely adopted in the industry. The main challenges associated with FCS–MPC are real-time implementation and mathematical stability concerns, which are discussed in the following sections.

2.3.3.1 Real-Time Implementation Challenges

FCS–MPC has several practical limitations, including sampling time, computational complexity and prediction horizons. This control approach requires fast sampling rates to accurately predict system dynamics, which raises the computational burden. However, increasing the prediction horizon ($N > 1$) further raises the computational effort, as the algorithm must forecast the future state for all switching states. However, long horizon prediction improves system performance, and if $N = \infty$, it ensures system stability, though it requires a lot of time to compute all cases (Wan et al., 2025). For example, in the case of a two-level voltage source converter (VSC), there are eight possible switching states. For $N = 2$, the classical FCS–MPC must determine switching states 64 times in each sampling instant. Figure 14 showcases the VSI switching state prediction, where $N = 1$ (a) and in (b) when $N = 2$, the two-step-ahead prediction with the assumption that the switching time is small. In

addition, (c) presents reduced-complexity multistep approaches that balance prediction accuracy with computational efficiency (implemented in Publication I). H. S. Khan et al. (2019) propose that the computational burden is reduced by predicting states seven times, as there are six active and two zero vectors. Thus, there is a trade-off among the computational burden, prediction horizon and accuracy (Zafra, Vazquez, Dragičević et al., 2023).

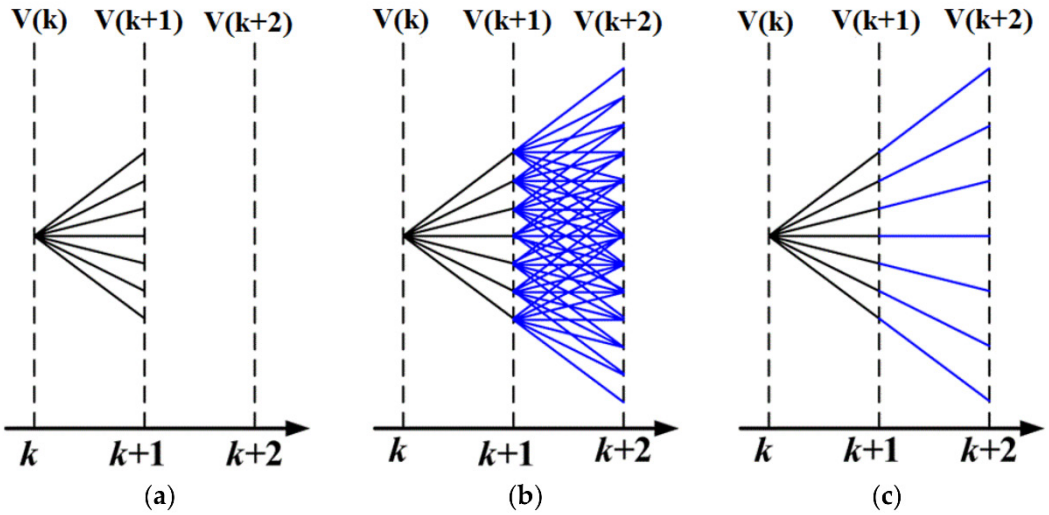

Figure 14. Computational burden reduction scheme for N = 2 (Publication II)

Following the work included in this thesis, subsequent research has advanced the implementation of the long-prediction-horizon FCS–MPC. The article (Zafra, Vazquez, Geyer et al., 2023) presents a comprehensive approach to implementing the long prediction horizon FCS–MPC using a branch-and-bound tree search, addressing key computational challenges. It demonstrates improved control performance but highlights scalability limitations due to exponentially growing complexity. While effective for selected converter topologies, its generalisation to broader systems remains an open question. Zafra et al. (2024) provide a computational analysis of LPH–FCS–MPC by reformulating it as an integer least squares (ILS) problem. It highlights how matrix factorisation methods and exploration modes (FTE vs. BTE) impact computational efficiency. Simulation and experimental results confirm that forward-time exploration significantly reduces computational costs while maintaining control performance.

2.3.3.2 Mathematical Stability of the FCS–MPC

The FCS–MPC is a time-domain nonlinear control method. Therefore, analytic techniques based on linear control theory, such as eigenvector analysis and Bode plots, are not ideal for assessing MPC stability. Additionally, FCS–MPC handles plants

with integer inputs, where the stability of such systems is fundamentally difficult to analyse and rigorously prove. The closed-loop stability of FCS–MPC remains a major theoretical challenge due to the discrete nature of switching inputs. Although a universally accepted mathematical framework for proving MPC stability in such systems does not exist, many researchers have employed Lyapunov stability theory as a foundational approach. Statistical model checking methods have been proposed to validate MPC stability within the power converter domain (Novak et al., 2018), while Lyapunov function-based MPC formulations have been developed for specific converter topologies, including four-leg inverters (Alam et al., 2018) and AC/DC converters in battery energy storage applications (Akter et al., 2015). Despite these advances, deriving Lyapunov-based stability criteria for two-level three-phase DC/AC converters remains unexplored in the current literature, representing an important research gap.

Alternative validation methods have involved extensive parametric sensitivity analysis through simulation studies (Fard et al., 2013; Yaramasu et al., 2012), where a system's performance is assessed under various operating conditions, model uncertainties and parameter variations. These studies, typically benchmarked against traditional PI control schemes and validated through experiments, have demonstrated that control performance exhibits asymmetric sensitivity to inductance parameter estimates, specifically degrading with underestimated inductance values while remaining robust to overestimation. Although these comprehensive simulation studies demonstrate satisfactory steady-state and transient performance, they have inherent limitations in terms of time complexity and computational burden, making exhaustive validation impractical. Table 3 offers a detailed overview of the literature addressing performance evaluation and stability analytic methods developed for the FCS–MPC.

Li et al. (2023) adopted a stability-focused approach to MPC design for DC–DC boost converters, utilising the Jacobian matrix to assess the impact of small changes in system states on stability. By applying Lyapunov-based conditions and analysing local dynamics via the Jacobian matrix, the controller maintains stable operation around setpoints. While the method is mathematically robust, its dependence on linearisation means stability is only ensured near nominal conditions, making it less reliable under large disturbances or model inaccuracies (Y. Li et al., 2023). Novak et al. (2019) provide a tutorial that effectively demonstrates the potential of statistical model checking (SMC) for verifying the FCS–MPC in power electronic converters, offering a novel bridge between formal verification and control engineering. While the use of Uppaal SMC introduces a rigorous and modular modelling framework, its reliance on timed automata and stochastic modelling presents a steep learning curve for practitioners outside formal methods. The paper could benefit from broader

application examples and more practical implementation guidance to enhance its accessibility and real-world relevance. Nonetheless, it lays a strong foundation for future research on robust control verification under uncertainty (Novak et al., 2019).

Table 3. Stability analysis methods applied to FCS–MPC in power converters, with their main strengths and limitations (Publication III)

Application	Method	Pros	Cons	Stability study
DC–DC converter (Aguilera & Quevedo, 2011) **Multicell converter (Aguilera & Quevedo, 2010)**	Lyapunov stability theory	Lyapunov stability theory (verification)	Complex cost function design	✓
Multi-Modular converter (MMC) (Yaramasu et al., 2012) **Four-leg VSC (Fard et al., 2013)**	Multi-simulations Parameter changing	Easy, fast, simple CF design	Closed-loop stability not defined, not validated	X
Active front end rectifier (Akter et al., 2015)	Lyapunov stability criteria	Lyapunov stability theory (verification)	Complex CF design Not a classical MPC	✓
VSC (Novak et al., 2018)	Benchmarking Multiple experiments	Design for industry engineers	Time consuming Benchmarking	✓

2.3.4 Intelligent Controls

In recent years, intelligent controllers have gained significant attention because they can better manage the complex, nonlinear dynamics and uncertainties of power systems compared to traditional controls. Although it is difficult to classify these controllers, this dissertation divides them into four main categories, as shown in the figure. Additionally, in disparate studies (e.g. Babayomi, Li et al., 2025; Gutiérrez-Escalona et al., 2024) authors thoroughly discuss intelligent controls and their types.

A fuzzy logic controller (FLC) primarily operates based on 'if–then' control rules (Lee, 1990). FLCs are intuitive, easy to implement, capable of handling uncertainties and

do not require prior knowledge of a system. In Hannan et al. (2015), a fuzzy-based current control method is proposed for grid-connected inverters. The authors replaced the PI with fuzzy controllers and used a modulator to generate pulses for the inverter. However, a fuzzy controller is implemented indirectly. Studies by Long et al. (2021) have explored the use of FLC to mitigate the chattering phenomenon inherent in SMC. One of the main challenges with fuzzy controllers is determining the correct set of rules, as these are often based on intuition or trial and error, which can limit the controller's performance. Because these rules are discrete and not derived from a formal model, fuzzy controllers may have difficulty with scalability, tuning and maintaining stability, especially in more complex systems.

ANN-based control, also called 'data-driven' or 'model-free control', mimics the human nervous system. It can maintain a consistent switching frequency for the power converter. The data-driven controller does not need information about the system's model, but requires accurate data on a system's operation and behaviour (C. Zhang & Lu, 2021). Most of the work in this domain focuses on improving the performance of power electronics controllers. In Sun et al. (1999), a linear controller is used to extract data, followed by an ANN to regulate voltage and generate pulses through a PWM modulator. However, the performance of this technique is similar to that of a linear controller. In Mohamed et al. (2019), an ANN is trained on data from an FSC–MPC. The ANN's performance is more robust than that of the MPC and requires less computational power. An ANN is also used to tune the weighting factor in the MPC (Dragičević & Novak, 2018). Mohamed et al. (2019) proposed MPC-assisted ANN-based voltage control for a two-level VSC to improve performance and reduce THD. Additionally, an ANN-based MPC for a three-level flying capacitor converter is examined in D. Wang et al. (2021) to demonstrate how an ANN can reduce the computational load of an MPC. Gao et al. (2023) provide a technical overview of how AI is enhancing the performance of controllers in power converter-based systems. It also explored the application of AI in both linear and nonlinear control strategies, addressing real-time parameter tuning, surrogate modelling and imitation learning. Emerging techniques, such as federated and transfer learning, are discussed for their potential in distributed and data-limited scenarios. The article also addresses challenges such as stability analysis, computational demands and the interpretability of AI-based controllers in practical deployment. Furthermore, an ANN-based predictor is developed to update the reference voltage in the DC/DC converter to improve the transient response in Maruta et al. (2016). An ANN-based algorithm to adjust the PID parameter and structure for the DC/DC converter is proposed in J. Liu et al. (2022).

A key limitation of AI-based controllers in power converter controls is their black-box nature, where the relationship between network layers and control actions

cannot be explicitly understood. The performance of such controllers depends heavily on the quality of the training data, as there is a risk that the controller performance deteriorates outside the training range. Establishing mathematical stability in closed-loop systems is challenging, particularly for ANNs, which present significant challenges due to their inherent nonlinearity, high dimensionality and data-driven nature. Berberich et al. (2020) proposed a data-driven MPC scheme that ensures stability using Lyapunov analysis and recursive feasibility, using Hankel matrix representations for linear time-invariant (LTI) systems. Bongard et al. (2022) analysed the robust stability of a data-driven MPC scheme without terminal constraints, proving practical exponential stability with a sufficiently long prediction horizon, even under noisy measurements.

2.4 Comparative Analysis

The comparative analysis in Table 4 evaluates seven control methods (linear, hysteresis, SFC, SMC, FCS–MPC, FLC and ANN) across performance criteria. The assessment considers both theoretical foundations and practical implementation factors, including computational load, design complexity and operational capabilities, such as constraint management and handling nonlinearity. MPC stands out from traditional and robust control techniques, such as PI control, hysteresis, SFC and SMC, by combining constraint management, prediction and optimisation within a single framework. While PI and SFC have strong theoretical bases and are simple to compute, they assume linear system behaviour and face difficulties with nonlinearity and constraint enforcement. Hysteresis control is favoured for its simplicity and quick response; however, it lacks a fixed switching frequency or systematic stability tools. The SMC is reliable against parameter changes and performs well in nonlinear systems. Nonetheless, it can cause chattering and has less intuitive tuning. Conversely, MPC effectively manages multivariable, constrained and nonlinear systems, delivering smoother control and improved performance, especially in safety-critical and high-efficiency applications.

Table 4. Comparative analysis of control methods for DER units

	Linear	Hysteresis	SFC	SMC	FCS–MPC	Fuzzy	ANN
Theoretical Background	Strong	Strong	Strong	Strong	Strong	Medium	Weak
Stability Analysis Tools	Strong	Strong	Strong	Strong	Weak	Average	NO
Computational Complexity	Low	Average	Low	Medium	High	Medium	Low
Intuitive Design	Low	Average	Medium	Medium	High	Low	Low
Handling System Constraints	NO	NO	NO	NO	YES	NO	YES
Handling Non-linearities	No	Yes	NO	YES	YES	YES	YES
Modulation Stage	Req	NO	Req	Req	NO	NO	YES
Parameter Sensitivity	Strong	Tunable	Tunable	Robust	Model-Dependent	Tunable	Data-Dependent

Unlike SFC and SMC, which rely on well-defined models and are sensitive to system parameters, MPC is more flexible and can incorporate model inaccuracies to a certain extent through robust or adaptive variants. The computational complexity of MPCs is indeed higher, though ANN-aided MPC has less computational burden. Importantly, MPC allows intuitive controller design by formulating control goals as an optimisation problem, balancing performance, constraint satisfaction and robustness. Compared to all other listed methods, MPC is the only one that directly incorporates system constraints into the control formulation, making it uniquely capable in practical systems where input limits, thermal constraints or safety margins are essential.

Despite the evident advantages of MPC, several research gaps still exist, as discussed in subsections 2.4.3.1 and 2.4.3.2. The main issue is the computational complexity of MPC, which can restrict real-time implementation in environments with limited resources. Additionally, MPC's model dependency raises concerns about performance when there are parameter uncertainties and changing operating conditions. Moreover, stability analysis tools for MPC are less developed than those for classical linear methods, highlighting the need for more advanced stability frameworks.

2.5 Chapter Summary

This chapter established the theoretical foundation for the dissertation by reviewing the shift of traditional power systems towards decentralised grids, the operational framework of microgrids and the control strategies applied to DERs. The discussion emphasised how the increasing penetration of renewable energy sources, along with the dependence on power electronic interfaces, has reshaped the requirements for stability, power quality and control in modern power systems.

A detailed overview of microgrid classifications and their hierarchical control architecture highlights the distinct roles of the primary, secondary and tertiary layers of ensuring reliable operations. Linear controllers, although widely used in practice, are proven to be insufficient under nonlinear operating conditions, parametric uncertainties and fault scenarios. Nonlinear controllers, including sliding mode and hysteresis techniques, offer robustness but often introduce high switching stress and design complexity. Predictive controllers, especially finite control set model predictive control (FCS–MPC), are recognised as a promising alternative because of their ability to directly manage converter switching states, system constraints and multi-objective formulations. However, challenges such as computational burden, model dependency and limited stability guarantees still need to be addressed.

Finally, the review highlighted the increasing importance of intelligent control strategies, including AI–based methods, in addressing the limitations of traditional approaches. Comparative analysis demonstrated that data-driven and learning-based solutions can improve adaptability, computational efficiency and robustness in future microgrid applications.

Overall, the chapter provides a comprehensive theoretical background, pinpointing key research gaps that drive the development of improved predictive control strategies and AI-driven frameworks discussed in the following chapters.

3 IMPROVED FCS–MPC FOR DISTRIBUTED ENERGY RESOURCES IN AC MICROGRIDS

The growing adoption of DERs has become a key solution for achieving carbon-free energy production. These DER units incorporate various renewable energy sources, typically connected to the MG via power electronic interfaces (PEIs). PEIs handle critical energy conversion tasks, such as AC/DC conversion, and regulate voltage, current and power. Nevertheless, integrating renewable energy sources presents major challenges, including their intermittent nature, harmonic distortions, the nonlinear behaviour of power converters and dynamic loads, which complicate voltage, power and frequency regulation.

Classical linear controllers, such as proportional-integral (PI) or proportional-resonant (PR) controllers, have been widely adopted for regulating DERs. However, the shortcomings of linear controllers necessitate the development of more advanced control strategies that can ensure reliable power sharing, fast dynamic response and enhanced stability, even under uncertain conditions.

FCS–MPC offers a promising solution to address these challenges. Unlike traditional controllers, it directly uses a discrete-time model of a system to predict future states and select optimal switching actions based on a cost function. It also has the capability to handle multiple control objectives simultaneously, improve transient response and facilitate the inclusion of system constraints and uncertainties.

This chapter presents a synthesis of control strategies developed in Publications I–III, focusing on improving voltage regulation, enhancing fault tolerance and establishing hierarchical predictive control frameworks for islanded AC microgrids. Significantly, the articles use the terms ‘MPC’ and ‘predictive control’, even though these terms specifically refer to FCS–MPC. This chapter addresses the following research questions:

RQ1: How can decentralised nonlinear predictive control achieve reliable voltage regulation and power sharing in AC microgrids with diverse load conditions?

RQ2: How can hierarchical predictive control strategies be designed and validated to ensure robust, decentralised voltage and frequency control in renewable-rich power systems under varying load conditions and parametric uncertainties?

3.1 Brief Overview of FCS–MPC

This section will establish the FCS–MPC as the foundation for the advanced control strategies developed in this dissertation. Unlike conventional cascaded controllers, FCS–MPC directly utilises the discrete switching nature of power converters, allowing the simultaneous optimisation of multiple objectives and explicit handling of system constraints. Presenting this basis is crucial for understanding how the proposed improvements later address longstanding challenges in DER control.

FCS–MPC operates on the principle of prediction and optimisation. At each sampling instant, the controller predicts the plant response for all feasible switching states using a discrete-time model and selects the state that minimises a predefined cost function. This method eliminates the need for PWM stages and reduces control delays, leading to faster transient performance. The prediction model used by MPC is derived from the state–space representation of the VSI and its filter. For a three-phase two-level VSI with an LC filter, the discrete-time model can be expressed as follows:

$$\begin{aligned} x(k+1) &= A_d x(k) + B_d\big(u(k)\big) \\ y(k) &= Cx(k) \end{aligned} \qquad \ldots(1)$$

where x(k) is the state variable, such as the system's voltage or current, u(k) is the control input, and y(k) represents the output. Figure 15 presents the working principal overview of the FCS–MPC current control for a grid-tied converter. The switching state of the converter at the current sampling instant is denoted as $S(t_k)$, and its predicted future value is $S(t_{k+1})$. The measured output current at sampling instant k is i_k. The prediction model forecasts the future current response i_{k+2} based on the system parameters R and L and the applied switching state. The cost function minimisation block evaluates the predicted current against the reference and selects the switching state that minimises the error. The optimal control action is then applied to the converter in the next sampling instant.

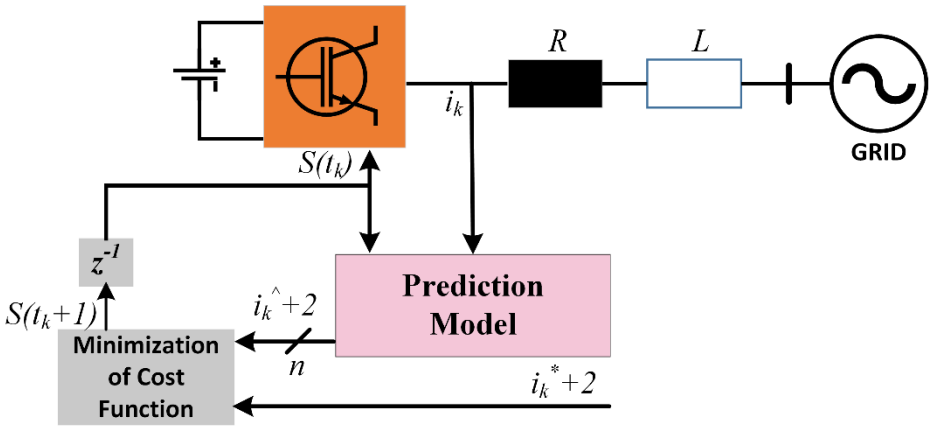

Figure 15. Schematic of a finite control set model predictive control (FCS–MPC) framework, where future states are predicted and the optimal switching signal is selected by minimising a cost function

3.1.1 Cost Function

In FCS–MPC, the design of CF is crucial for implementation, and it is based on the square of the Euclidean distance between the desired system response (reference value) and the predicted response of each possible switching state for a power converter. The general CF equation can be defined as follows:

$$G_{Gen} = \sum_{i=t_k}^{t_k+N-1} \|v_{fe}(i)\|_2^2 + h_{lim}(i) + \lambda_u sw^2(i) \qquad \ldots(2)$$

where v_{fe} denotes the tracking error between the reference and the (predicted) system output and it defines the primary objective of the cost function. For a two-level VSI operating in an islanded microgrid, the main goal is to regulate voltage at the PCC. Secondary objectives, such as current limitations, the explicit regulation of switching activity and power sharing among parallel VSIs, are added as penalty terms to the cost function. These terms inevitably create trade-offs; for instance, tightening current limits or reducing switching activity generally increases the voltage error or THD and vice versa. Therefore, the proper normalisation and weighting of each term are crucial to meet system-level targets.

In Publications I and III, FCS–MPVC minimises a voltage-tracking CF evaluated on the PCC voltage vector in the stationary αβ frame with a prediction horizon of N = 2.

$$G_{Primary} = \left(v_{pc}^*(t_k+2) - v_{pc}^{act}(t_k+2)\right)^2 \qquad \ldots(3)$$

$G_{primary}$ presents the squared Euclidean distance between the droop-generated reference and the model-predicted PCC voltage. The prediction horizon N = 2 follows the restricted two-step scheme, which holds the same space vector for two consecutive samples, thereby retaining dynamic behaviour while reducing switching frequency and computation (eight evaluations instead of 49). In Publication II, dual-objective CF is used for voltage tracking with an explicit current-limiting term. To match the limited two-step hold and actuation delay, the PCC voltage error is penalised at the second switching instant (t_k+2), while the current term is applied at the first switching instant (t_k+1). The secondary term of the dual objective CF activates upon fault detection to keep the surge current within limits, accepting increased voltage error/THD to protect semiconductor devices.

$$G_{DO} = \lambda_v \left(v_{pc}^{*}(t_k + 2) - v_{pc}^{act}(t_k + 2) \right)^2 + \lambda_i \left(i_f^{*}(t_k + 1) - i_f^{act}(t_k + 1) \right)^2 \quad \ldots(4)$$

Figure 16 illustrates the workflow chart of the FCS–MPVC algorithm presented in Publications I–III.

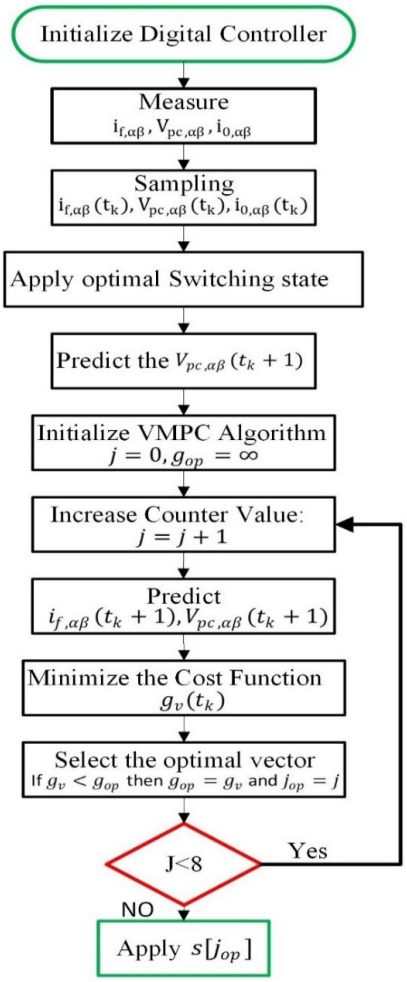

Figure 16. Flow chart of FCS-MPVC algorithm, illustrating the process (Publication I)

3.1.2 Two Steps Ahead Switching Frequency and Computational Burden Reduction Scheme

The converter's switching frequency is the main factor influencing semiconductor losses and thermal stress. Classical one-step FCS–MPC switches at each sampling period, while two-step MPC (N = 2) reduces current ripple but requires evaluating 49 switching sequences, all possible voltage vectors, as depicted in Figure 14. This computational load makes real-time implementation difficult on embedded hardware platforms.

Publications I and II address this problem using a modified two-step-ahead scheme. Instead of evaluating all vector combinations, this method utilises the same space vector for two consecutive sampling periods, assuming sufficiently small sampling times. This reduces the candidate set from 49 to just eight voltage vectors: the

fundamental vectors of a two-level voltage source inverter (VSI), including six active vectors plus two zero vectors (with one zero-vector redundancy removed). The algorithm predicts the system state at time t_{k+2} under this two-sample hold strategy and calculates the primary voltage-tracking cost function at t_{k+2} against the droop-generated reference. This change maintains dynamic performance, such as a lower current ripple and total harmonic distortion (THD), while reducing the average switching frequency and computational complexity to nearly one-step levels.

In practical use, this approach offers several advantages, including reduced hardware resource utilisation, improved voltage quality and simplified real-time implementation. The constraint evaluation and cost function calculations are performed on a small, fixed set, after which the best vector is applied for two consecutive sampling intervals, greatly simplifying control while maintaining high performance.

3.2 FCS–MPC Mathematical Stability Analysis

One of the key contributions of this thesis is the stability evaluation of FCS–MPC, an aspect often overlooked by previous studies. This section introduces a Lyapunov-based framework to formally analyse the closed-loop stability of the proposed predictive controller, thereby enhancing confidence in its use for DER units, where dependable operation under changing load and parameter conditions is essential. The stability analysis, originally detailed in Publication III, focuses on the inner FCS–MPC loop of a two-level voltage source inverter (VSI) with an LC filter in an islanded system. Unlike linear controllers, which can be sufficiently analysed with eigenvalue- or frequency-domain methods, FCS–MPC presents unique challenges because of its discrete time and nonlinear characteristics. These features require specialised mathematical formulations, for which a Lyapunov-based approach is employed to establish rigorous closed-loop stability criteria.

Traditional stability validation for MPC systems typically relies on extensive simulation studies or experimental verification, as discussed in Subsection 2.4.3.2. While these approaches provide valuable insights, they cannot guarantee stability across all operating conditions. The Lyapunov-based approach developed here provides theoretical stability guarantees through mathematical proof, ensuring robust system operation within defined constraints. The discrete Lyapunov function based on voltage tracking error is defined as follows:

$$L(k) = \frac{1}{2}[V_{err}]^T[V_{err}] \quad \ldots(5)$$

Where V_{err} is the error between the actual and reference voltage, and its one-step change can be written as:

$$\Delta L(k) = L(V_{err}[t_k + 1]) - L(V_{err}[t_k]) \quad \ldots(6)$$

The system is declared asymptotically stable if $V_{err}[t_k]$ evolves within a positively invariant set A and the following inequality holds with strictly positive constants L_3 through L_4, with $s \geq 1$:

$$\Delta V(t_k) < -L_3 \|V_{err}[t_k]\|_s + L_4 \quad \ldots(7)$$

The inverter output voltage at the sampling instant t_k+1 can be expressed as:

$$V_i[t_k + 1] = \vec{V_i}[t_k + 1] + \Delta[t_k + 1] \quad \ldots(8)$$

where $V_i[t_k+1]$ represents the continuous voltage vector and $\Delta[t_k+1]$ represents the quantisation error bounded by $|\Delta(t_k+1)| \leq \delta_1$. Substituting the LC filter and discrete system model gives a clear expression for $\Delta V(t)$, with coefficients determined by system parameters and sampling time. The discrete-time LC filter model's parameters are defined as follows:

$$k_1 = \frac{L_f}{T_s}, k_2 = \left(1 - \frac{L_f}{T_s}\right), k_3 = \frac{L_f C_f}{T_s^2}, k_4 = \frac{R_s T_s}{L_f} - \frac{L_f}{T_s} \quad \ldots(9)$$

With quantisation errors δ_1, δ_2 and δ_3 introduced for the voltage, current and load, respectively, the change in the Lyapunov function ΔV becomes:

$$\Delta V(t_k) \leq -\frac{1}{2}[V_{err}]^T[V_{err}] + \frac{1}{2}\left(\frac{1}{k_3}\delta_1 - \frac{k_1}{k_3}\delta_2 - \frac{k_2}{k_3}\delta_3\right)^2 \quad \ldots(10)$$

The stability conditions are met when:

$$L_1 = L_2 = 1, L_3 = \frac{1}{2}, L_4 = \left(\frac{1}{k_3}\delta_1 - \frac{k_1}{k_3}\delta_2 - \frac{k_2}{k_3}\delta_3\right)^2 \quad \ldots(11)$$

Because ΔV has a negative sign, the error energy decays to zero as the time approaches infinity. Therefore, the system is asymptotically stable. In summary, Publication II presents a discrete Lyapunov function-based FCS–MPC stability analysis, demonstrating that the value of the Lyapunov function decreases under the predictive control law, thereby establishing asymptotic stability in the nominal model with bounded quantisation effects.

3.3 Results

This section explains the validation of the proposed FCS–MPC approach's effectiveness (developed in Publications I–III) through extensive simulation studies and FPGA-in-the-loop testing under diverse operating conditions. Demonstrating robust performance across linear, nonlinear and uncertain scenarios provides strong evidence of its suitability for DER integration. The results also highlight how the proposed improvements, such as the two-step-ahead scheme and dual-objective cost function, address the limitations of conventional approaches. The MG simulation model was developed to evaluate the performance of the proposed control strategy. The control implemented for the DER unit is illustrated in Figure 17. In Publication III, the secondary PI voltage and frequency loop and droop control are implemented atop the proposed FCS–MPVC. A dual objective cost function-based FCS–MPVC was implemented to control the fault current under symmetrical faults in Publication I. Publication II includes primary droop control to accurately share power among the DER units and FCS–MPVC with a two-step-ahead prediction method. First, the proposed control is tested on a single DER unit and then on the MG test bench system. A diagram of the MG test bench system developed in Simulink is presented in Figure 18, where two DER units are connected in parallel to a common AC bus. The simulation model parameters are shown in Table 5. Each DER unit is represented by a two-level voltage source inverter along with an LC filter to mitigate the harmonics connected to the load via the common AC bus. The performance of the proposed control strategy was validated under various loading conditions. To evaluate the controller's effectiveness, transient load conditions were simulated with sudden increases in load from 0% to 100% capacity. The performance was assessed under both linear and nonlinear load scenarios.

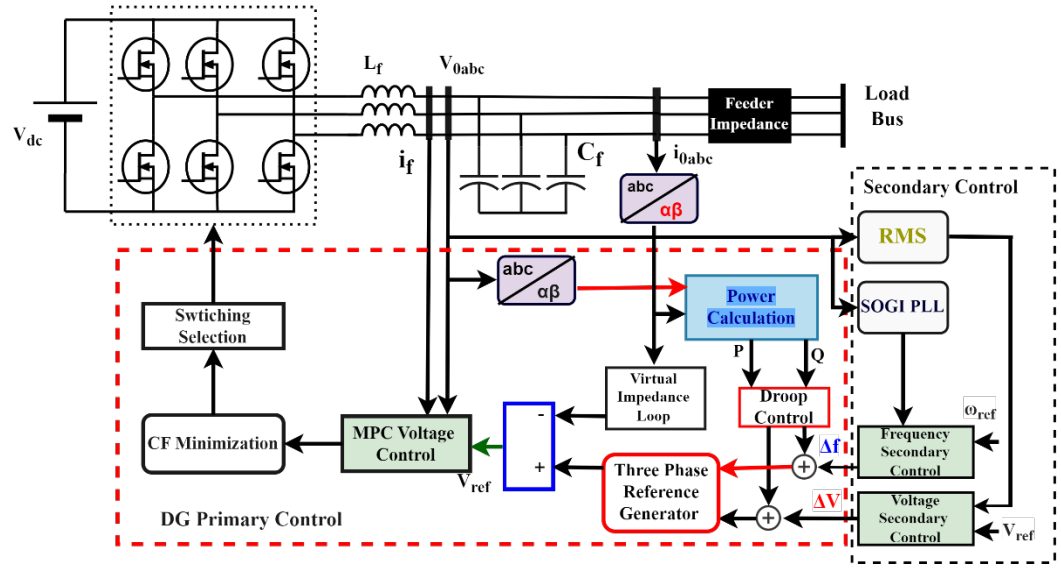

Figure 17. Block diagram of the proposed PI+ FCS–MPVC approach for DER units in an islanded MG (Publication III)

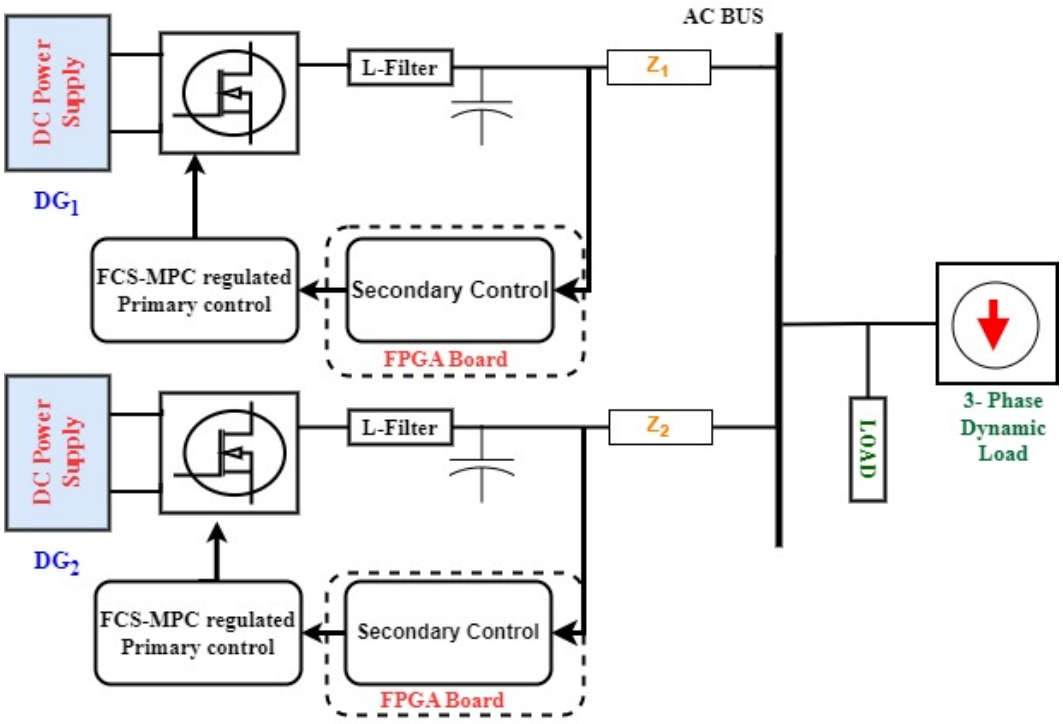

Figure 18. Block diagram representation of the MG test bench system developed to test the proposed technique on FIL (Publication III)

Table 5. Simulation model parameters

Parameter	Value
DC Input Voltage	V_{dc} = 1,000V
Sampling Time	T_s = 20µs
LC Filter Inductance	L_f = 2mH
LC Filter Capacitance	C_f = 250µF
Rated System Frequency	F_{nom} = 60 Hz (Publications I and II) and 50 Hz (Publication III)

3.3.1 Controller Performance Under Linear Load (Publication I)

In the simulation with linear loads, a three-phase RL load with a power rating of 18 kW and 7 kVARs was connected to the microgrid. At t = 0.1 seconds, the load was disconnected, and it was reconnected at t = 0.15 seconds. The proposed FCS–MPC strategy maintained the output voltage at approximately 220V throughout these transitions. The controller exhibited minimal overshoot during the load's disconnection and reconnection, demonstrating effective voltage regulation, as illustrated in Figure 19. The total harmonic distortion (THD) of the output voltage was recorded at 0.89%, which is well within acceptable limits, indicating the controller's capability to manage harmonic content effectively.

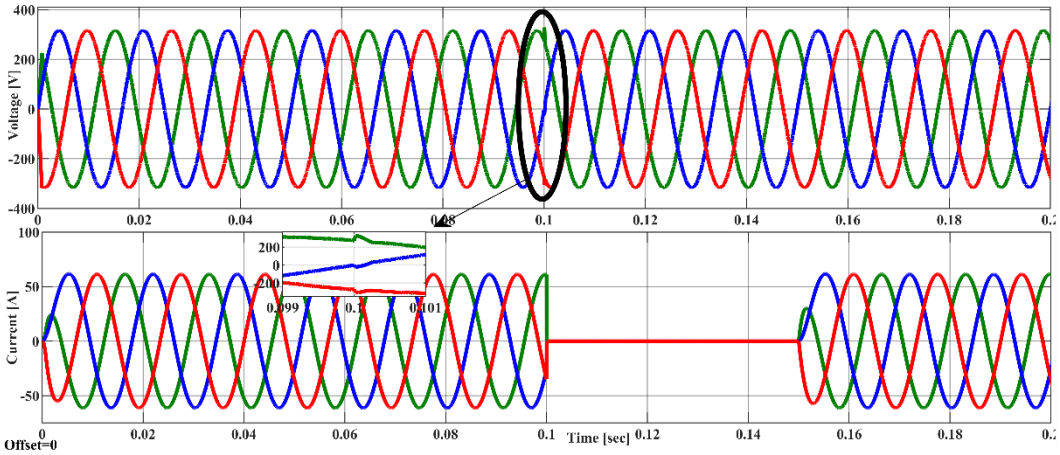

Figure 19. Simulation results of the proposed FCS–MPC under a three-phase RL load (Publication I)

3.3.2 Controller Performance Under Nonlinear Load (Publication I)

In the case of nonlinear loads, the system initially operated with a load of 10 kW. At t = 0.12 seconds, the nonlinear load doubled, increasing the demand to 20 kW. The proposed FCS–MPC strategy effectively managed this sudden change, as presented in Figure 20. Despite the increased complexity of the load, the controller maintained voltage stability during the transient response. The THD for the output voltage under nonlinear load conditions was observed at 1.40%. This result indicates that while the controller effectively manages nonlinearities, there is a slight increase in harmonic content compared to linear loads, though still under IEEE/IEC standards.

The results from linear and nonlinear load scenarios under the step change of load illustrate that the proposed FCS–MPC strategy effectively mitigates the voltage dips associated with sudden load changes while maintaining acceptable levels of THD across all conditions.

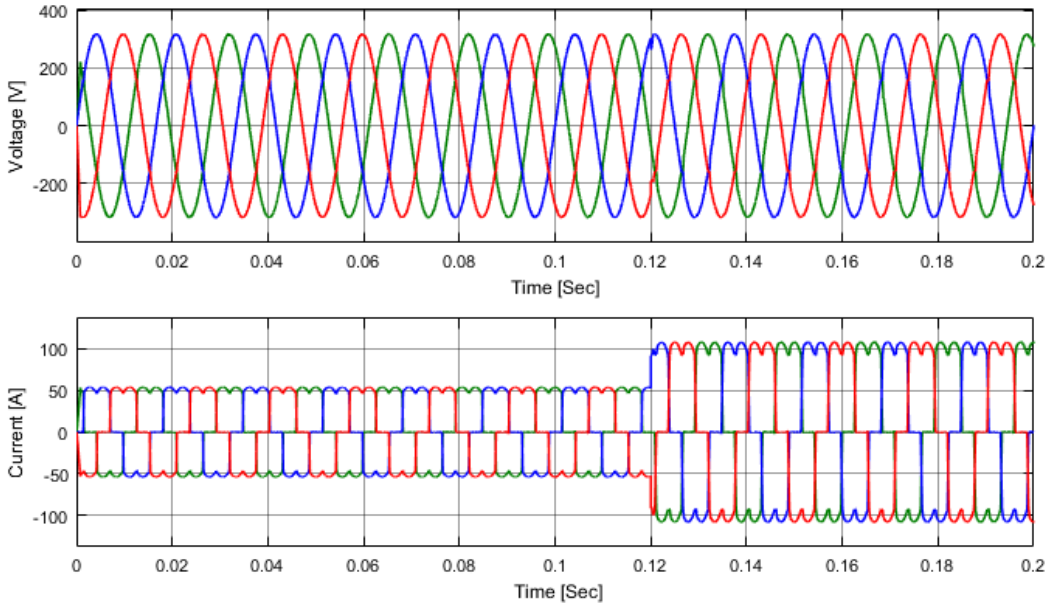

Figure 20. Simulation results of the proposed FCS–MPC under a nonlinear load (Publication I)

3.3.3 Controller Performance Parametric Uncertainty

The performance of the proposed controller was tested under parametric uncertainty to assess its robustness and reliability in real-world applications. Testing the controller's performance under these conditions is crucial because variations in system parameters, such as inductance, can occur due to environmental changes,

ageing components or operational fluctuations. Such uncertainties can significantly impact the stability and efficiency of the control system.

Specifically, the inductance value of the filter in the distributed generation (DG) system was changed from 2 mH to 1 mH at t = 0.4 seconds. As demonstrated in Figure 21, the results showed that the proposed FCS–MPC controller remains stable and effectively regulates the voltage. The THD of the converter's output voltage has increased from 0.95% to 1.88% with a 100% change in inductor value. This significant difference highlights the FCS–MPC's robustness in maintaining voltage quality despite variations in system parameters. These findings demonstrate that the proposed controller effectively adapts to changes in system conditions, ensuring stable operation and compliance with performance standards. The ability to maintain low THD under varying inductance conditions illustrates the suitability of the FCS–MPC strategy for practical applications in islanded AC microgrids.

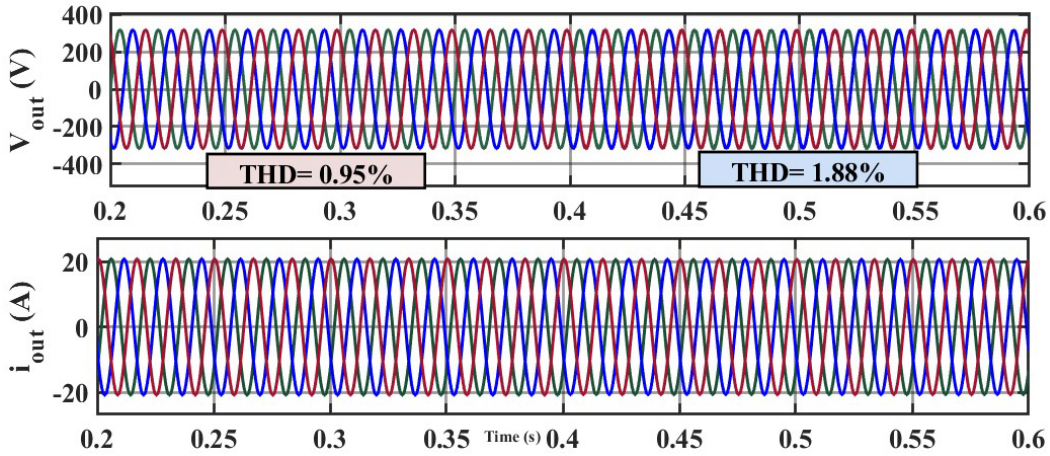

Figure 21. Simulation results of the proposed control under filter parametric variation (Publication III)

3.3.4 Dual Objective CF (Publication I)

In Publication I, a dual-objective cost function was implemented as part of the improved FCS–MPVC strategy. This cost function is designed to regulate the output voltage and minimise the fault current under fault conditions. Figure 22 illustrates that this dual-objective approach significantly enhances the system's performance under fault conditions. While the introduction of the secondary term to manage the current under faults slightly increased the THD of the output voltage to 1.09%, it effectively limited the fault current, keeping it within safe operational limits.

The dual objective cost function enabled a balanced trade-off between maintaining voltage quality and managing current during faults, showcasing the controller's robustness. The results demonstrate the effectiveness of the dual-objective cost function in enhancing the control strategy's ability to handle both voltage regulation and fault conditions, making it a valuable addition to the control framework for islanded AC microgrids.

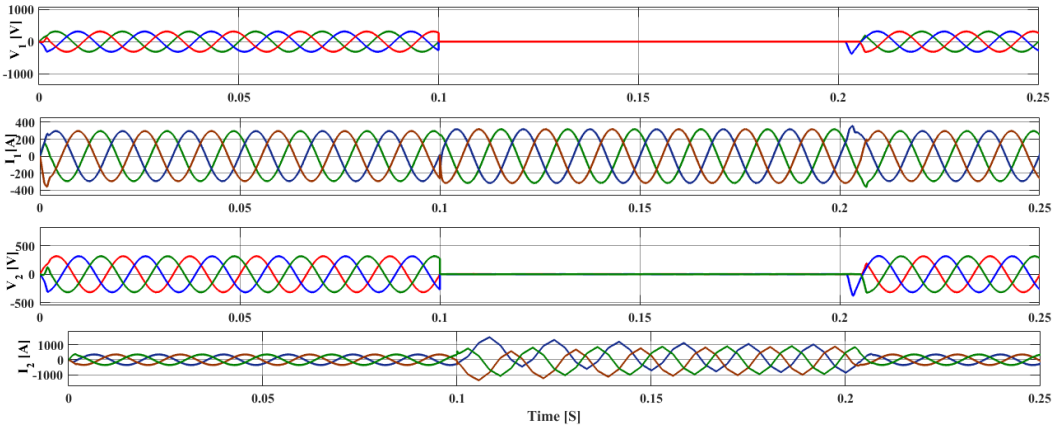

Figure 22. Simulation results of the improved FCS–MPVC with a dual-objective cost function, showing effective voltage regulation and fault current limitations during fault conditions (Publication I)

3.4 Controller Hardware in the Loop (CHIL) Using FPGA-in-the-Loop

The proposed control strategy was validated through extensive testing using controller hardware in the loop (CHIL) methods, specifically employing FPGA-in-the-loop (FIL) techniques. This approach enables the real-time testing of the controller in a simulated environment, ensuring that the control algorithms perform as expected under realistic operating conditions.

The FPGA ZYBO Z7 board was used for this purpose, allowing rapid prototyping and the effective integration of control algorithms. The FIL setup involved generating a VHDL code for the controller, which was then deployed on the FPGA, while the remaining microgrid model was simulated in MATLAB/Simulink. Communication between the FPGA and the simulation environment was facilitated through a JTAG cable, enabling two-way interaction.

Figure 23 illustrates the working principle of the FPGA-in-loop simulation environment, while Figure 24 provides a systematic view of the experimental setup.

This setup enabled thorough testing of the proposed control algorithm, further verifying its robustness and effectiveness under the microgrid's dynamic conditions.

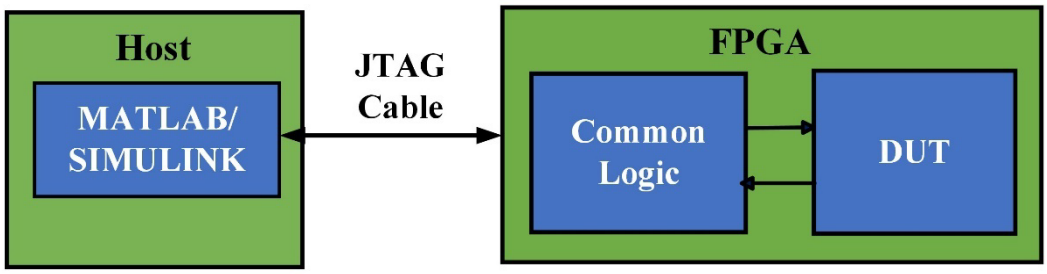

Figure 23. Overview of the FPGA-in-the-Loop (FIL) setup, showing the working principle where MATLAB/Simulink on the host computer communicates with the FPGA device under test (DUT) through a JTAG interface (Publication III)

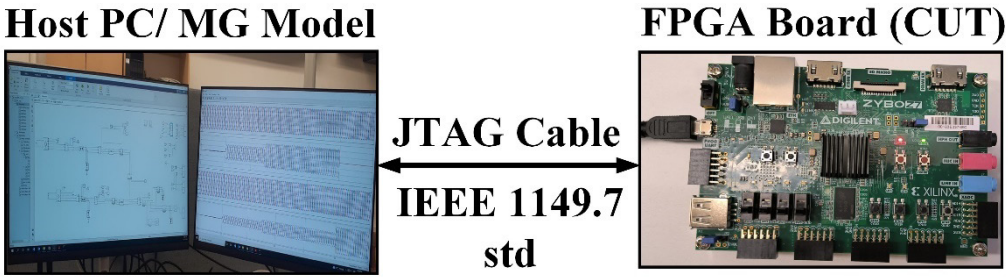

Figure 24. Systematic overview of the experimental FPGA-in-the-Loop (FIL) setup, where the host PC running the microgrid (MG) model communicates with the Zybo Z7 FPGA board (CUT) via a JTAG interface based on the IEEE 1149.7 standard (Publication III)

3.4.1 Dynamic Loads (Publication III)

Dynamic loads (DL) are characterised by varying power consumption based on changes in voltage and frequency. The mathematical model of DL as a function of voltage can be written as:

$$P = P_0 \left[\frac{V}{V_0}\right]^{n_p} (1 + n_{pf}\Delta f Q = Q_0 \left[\frac{V}{V_0}\right]^{n_q} (1 + n_{qf}\Delta f) \quad \ldots(12)$$

The parameters P_0 and Q_0 represent the baseline power consumption values for the load under nominal conditions. P and Q represent the frequency-dependent and voltage-dependent power consumption of the load. The exponents n_p and n_q are the

load characteristic parameters that determine the voltage sensitivity of the load. These exponents equal one for constant current loads and two for constant impedance loads. The frequency weighting factors n_{pf} and n_{qf} influence the load's frequency sensitivity. Under constant impedance conditions, the power–voltage relationship shows quadratic behaviour, while constant current loads exhibit a linear power–voltage relationship. In contrast, constant power loads are unaffected by voltage changes. Table 6 summarises the dynamic load characteristics and their corresponding power ratings, as presented in Publication III. The performance of the proposed control strategy was tested under various dynamic load conditions, including constant current (CI), constant impedance (CZ) and constant power (CP) loads. This evaluation is essential for understanding how effectively the control system can adapt to real-world situations.

Table 6. Load model parameters for different load types (Publication III)

Load Type	Load Constants		P_0 (kWatt)	Q_0 (kVar)
	n_p	n_q		
CP	0	0	8	6
CZ	2	2	2	0
CI	1	1	6	4
Industrial Motor	0.1	0.6	15	7

1. **Constant Impedance (CZ) Load**

When a 2 kW CZ load was connected at t = 0.3 seconds, the voltage and frequency remained stable, indicating the controller's ability to handle power variations without significant disturbances, as shown in Figure 25. The THD of the current was recorded at 0.65%, demonstrating effective harmonic suppression.

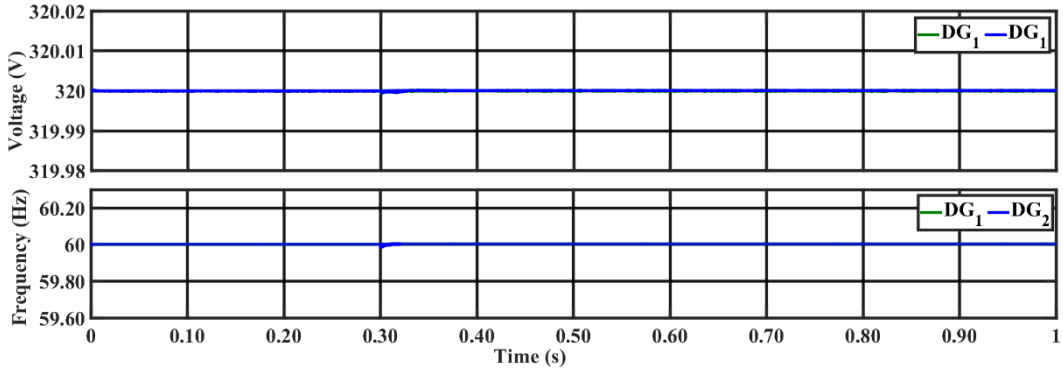

Figure 25. Voltage and frequency response under 2 kW CZ load with droop + FCS–MPVC + PI secondary control, showing stable operations and 0.65% current THD (Publication III)

2. **Constant Current (CI) Load**

For a 6 kW CI load connected at t = 0.3 seconds, the system experienced a drop in voltage and frequency due to the additional load, as shown in Figure 26. However, the proposed control strategy quickly adjusted, maintaining low harmonic levels with a voltage THD below IEEE standards. The current harmonics measured approximately 0.47%.

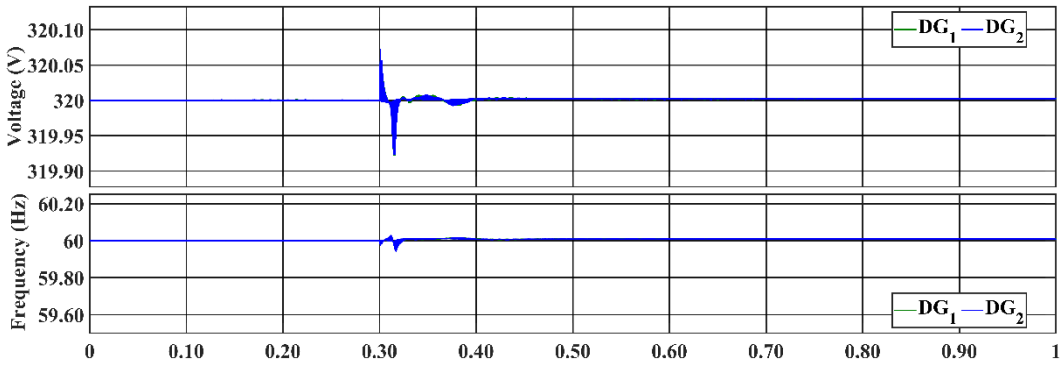

Figure 26. Voltage and frequency response under a 6 kW CI load with a droop and FCS–MPVC at the primary level and PI-based secondary control (Publication III)

3. **Constant Power (CP) Load**

In the case of a CP load of 8 kW, the system displayed some disturbance upon connection. However, the controller rapidly restored the voltage and frequency to their nominal values, as depicted in Figure 27. The current harmonics were observed at approximately 0.33%, demonstrating the controller's ability to maintain power quality even under fluctuating load conditions.

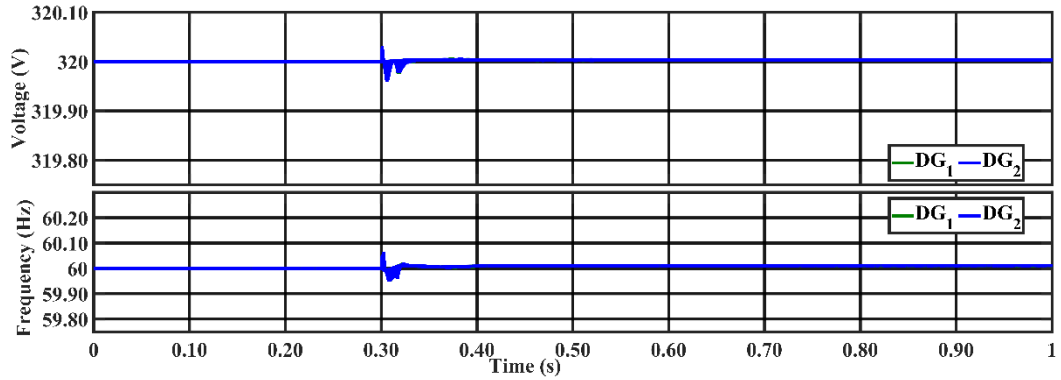

Figure 27. Voltage and frequency response under an 8 kW CP load with a droop and FCS–MPVC at the primary level and a PI-based secondary control (Publication III)

4. **Industrial Motor Load**

An industrial motor load of 16.55 kVA was tested, revealing a dip in voltage and current due to the switching of circuit breakers. Figure 28 shows that the controller effectively mitigated these transients, stabilising the system within 0.1 seconds after the load changes.

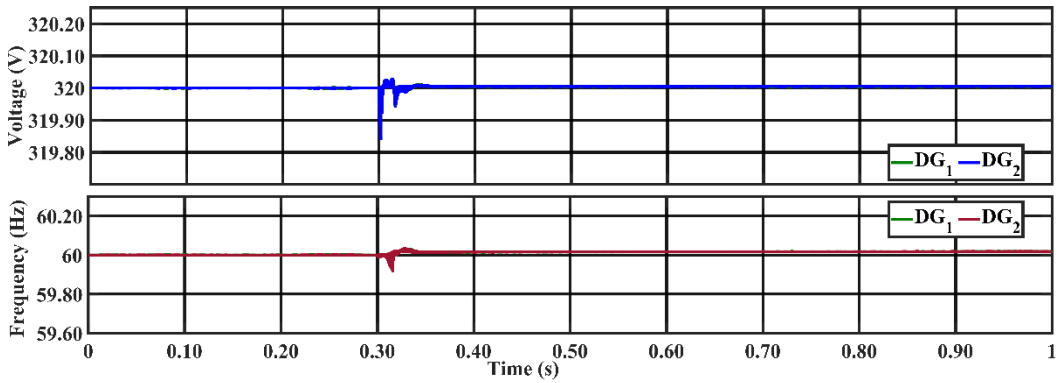

Figure 28. Voltage and frequency response under a 6 kW CI load with a droop and FCS–MPVC at the primary level and a PI-based secondary control (Publication III)

Table 7 presents the THD performance of the controller proposed in Publication III under different complex load types, such as CZ, CI, and CP loads. The results are compared against two established hierarchical control strategies reported in the literature: the PR-based hierarchical control approach and the MPC-based hierarchical control method. These literature values serve as reference benchmarks, illustrating the performance level typically achieved by conventional voltage control schemes under similar load conditions.

As shown in the Table 7, the controller from Publication III achieves a substantially lower THD level across all load categories, outperforming both the PR-based and MPC-based hierarchical controllers. While conventional approaches exhibit THD values around 7.10% and 3.69% respectively, the proposed controller consistently achieves a THD of 0.98%. This significant reduction highlights the improved voltage quality and enhanced disturbance-handling capability of the developed control scheme, particularly under demanding and nonlinear load conditions.

Table 7. THD performance of the controller studied in Publication III under complex load conditions, compared against conventional hierarchical control methods (Publication III)

Types	Conventional PR based hierarchical control (THD) (Jayachandran & Ravi, 2019; Ziouani et al., 2018)	MPC based hierarchical control (THD) (Jayachandran & Ravi, 2019)	Publication III (THD)
CI Load	7.10 %	3.69%	0.98%
CZ Load	7.10 %	3.69%	0.98%
CP Load	7.10 %	3.69%	0.98%

3.5 Discussion

This chapter demonstrated the effectiveness of an improved finite control set model predictive control (FCS–MPC) for DERs in islanded AC microgrids. The novelty of this work lies in three main aspects. First, the integration of a dual-objective cost function enables simultaneous voltage regulation and current limitations during fault conditions. This addresses a known weakness of conventional single-objective predictive controllers, which primarily focus on voltage tracking without considering converter protection under abnormal scenarios. Second, the adoption of a two-step-ahead prediction reduces the computational burden while maintaining robust steady-state and transient performance. Finally, the controller's robustness is validated not only under linear and nonlinear loading conditions, but also in the presence of parametric uncertainties and dynamic load variations, supported by FPGA-in-the-loop testing.

Compared to linear control strategies, such as PI or PR regulators, for MG primary and secondary controls, the proposed predictive scheme demonstrates a faster dynamic response, improved disturbance rejection and superior handling of

nonlinearities. While nonlinear techniques, such as sliding mode or hysteresis control, also offer robustness, they often suffer from high stress on power devices or increased implementation complexity. In contrast, the proposed FCS–MPC approach offers a path to incorporate multiple objectives into the cost function, achieving both high power quality (THD < 1% in most test cases) and fault tolerance.

Classical predictive control methods have been criticised for their high computational demands and lack of formal stability guarantees. This work shows that computational complexity can be reduced through efficient two-step horizon schemes and switching-reduction strategies. Simultaneously, stability is formally examined using Lyapunov criteria for three-phase, two-level inverters. Such stability analyses, which have rarely been attempted in earlier MPC studies, improves the credibility of the method and supports its practical deployment.

Furthermore, the hierarchical implementation discussed here employs FCS–MPC for voltage regulation at the primary layer. Proportional power sharing among DER units is managed through droop control, while PI-based secondary control corrects voltage and frequency deviations. This configuration provides a practical, decentralised solution for microgrids that operate without communication links. The implemented method keeps predictive control within a manageable complexity suitable for FPGA-based real-time platforms.

Overall, this work advances the FCS–MPC through three key improvements. The enhanced controller incorporates dual-objective CF optimisation, lower computational complexity and rigorous stability guarantees. The resulting framework provides scalable and fault-tolerant operations for islanded MG applications. These contributions not only advance theoretical understanding but also lay the groundwork for the practical deployment of predictive controllers in next-generation resilient MGs.

3.6 Chapter Summary

This chapter provided a comprehensive summary of Publications I–III within a unified FCS–MPC framework specifically designed for a two-level VSI in islanded MGs. The proposed approach utilises a cost function evaluated at t_k+2, which is synchronised with measurement, computation and gating delays. It utilises a restricted two-step-ahead prediction technique on the selected space vector to sustain a low switching frequency with nearly one-step computational effort. A dual-objective CF introduces current shaping to mitigate fault currents during symmetrical

faults while ensuring acceptable voltage quality. Discrete Lyapunov analysis was employed to verify the stability of the closed-loop system for the inner predictive controller. Simulation and FPGA-in-the-loop using the Zybo Z7 validate real-time feasibility, power-quality compliance under dynamic load conditions and proper operation within parallel inverter configurations. Overall, the proposed structure meets the requirements for voltage regulation, protection and computation, making it suitable for implementation on practical embedded platforms.

4 AI-BASED CONTROL FOR DC MICROGRIDS

This chapter is based on Publications IV–VI, which collectively advance the use of artificial neural networks (ANNs) for voltage regulation in DC MGs. The main objective of this chapter is to demonstrate how ANN-based control strategies can overcome the limitations of conventional approaches, such as PI and MPC, particularly in challenging scenarios such as constant power loads (CPLs), and to validate these strategies for practical deployment.

The contributions follow a clear development in structure. Publication IV developed an ANN-based control framework for a DC/DC boost converter, trained using datasets generated by MPC, and confirmed its performance through MATLAB/Simulink simulations. Publication V expands the work developed in Publication IV by addressing CPL-induced instability. It demonstrates that ANN controllers outperform traditional methods in terms of transient response and robustness, and verifies the approach in real time using FPGA-in-the-loop (FIL) technology. Publication VI presents a reduced-sensor ANN control strategy that uses Quasi-Stationary Line (QSL) modelling for multibus DC microgrid operation and confirms its feasibility with hardware-in-the-loop (HIL) testing on an OPAL–RT test bench.

Together, these works emphasise a significant contribution to this dissertation: shifting from simulation-based validation to real-time hardware demonstration of AI-driven control. This chapter summarises the main findings of the three publications and addresses the following research questions:

- RQ3: Can ANN-based control provide reliable voltage regulation in DC microgrids?
- RQ4: Can AI-based control, with reduced sensor requirements, outperform conventional approaches (e.g. PI or MPC) for modern power system voltage regulation, particularly under challenging scenarios such as CPLs?

4.1 DC Microgrids and Control Challenges

Understanding the operation of DC microgrids is essential because it frames the motivation for adopting ANN-based solutions in subsequent sections. The rapid integration of renewable energy resources, such as photovoltaic systems, wind power and distributed storage, has accelerated the deployment of direct current (DC) microgrids. DC microgrids outperform their AC counterparts in several ways. Integration of RERs in EPS becomes easier because many RER resources generate

power in DC. Energy efficiency improves by reducing conversion losses. Control systems are also simpler due to the absence of frequency and reactive power. These advantages make DC MGs viable for applications ranging from residential and commercial energy systems to electric vehicles, naval ships and telecommunication infrastructures.

Despite these advantages, DC MGs face significant control challenges, including voltage regulation at the DC bus, stability under dynamic loading, coordination among distributed energy resources (DERs) and the mitigation of constant power load (CPL) effects, all of which are critical for smooth operation. Traditional linear controllers, such as PI and PID, have been widely adopted by industry due to their simplicity. However, they exhibit poor performance under parametric uncertainty, limited disturbance rejection capability and difficulty handling the nonlinear behaviours typical of power converters. Nonlinear control strategies, such as SMC and MPC, have been proposed as alternatives. Nonetheless, these approaches either face issues such as chattering and variable switching frequencies or require extensive computational resources. These challenges present opportunities for enhanced control performance and robustness, which form the foundation for the AI-based contributions developed later in this chapter.

4.1.1 Role of AI in Power Electronics

Power converters in DC MGs face a unique set of challenges that traditional control methods struggle to address effectively. These systems are inherently nonlinear, particularly under demanding conditions, such as constant power loads (CPLs), where their behaviour deviates significantly from linear approximations. Converters operate with a finite number of switching states that must be selected and executed with microsecond-level precision to maintain stable voltage regulation. Adding to this complexity, these systems must respect strict physical constraints, including voltage, current and thermal limits, which define safe operating boundaries.

Modern control platforms have advanced to address these challenges, employing discrete-time implementations with sampling intervals in the microsecond range and compatibility with high-speed digital hardware, such as FPGAs and real-time simulators. Nonetheless, these sophisticated platforms still rely on precise converter models and face the fundamental challenge of modelling complex nonlinear behaviours.

ANNs have become a key solution for bridging the gap between converters' complexity and control systems' requirements. Unlike traditional approaches, ANN-based controllers learn systems' behaviours directly from data, removing the need

for explicit mathematical models. This data-driven approach captures the nonlinear dynamics of converters, taking into account both switching constraints and physical limitations.

Once trained, ANNs offer several advantages for power converter control, including a fast transient response with a reduced computational burden compared to MPC, while maintaining superior performance under parameter variations and unknown disturbances. The model-free nature of ANNs makes them particularly robust against uncertainties compared to traditional control strategies. Additionally, ANN-based approaches offer opportunities to reduce the number of physical sensors required, thereby lowering system costs and improving overall reliability.

Recent research has demonstrated the practical effectiveness of ANN applications across multiple aspects of power electronics, including prediction and fault detection. Figure 29 demonstrates that ANNs serve as a crucial integrating element, translating the complex, nonlinear behaviour of power converters into optimal, real-time control signals suitable for modern digital platforms. This unique positioning makes ANN-based controllers not just a theoretical advancement but a practical and forward-looking approach that addresses the fundamental challenges of power electronics converter control in DC MGs.

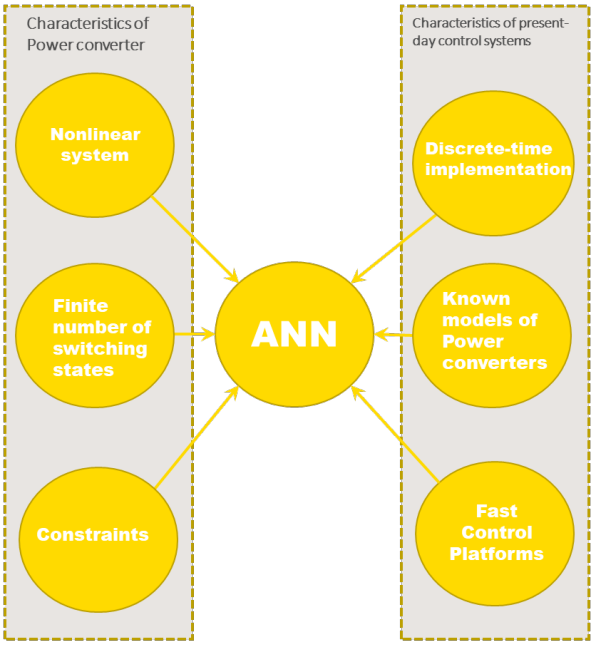

Figure 29. Characteristics of power converters and drives that motivate ANN-based control

4.1.2 Negative Impedance Characteristics of CPL

A key reason for focusing on ANN-based controllers in this chapter is their potential for counteracting one of the most destabilising features of DC microgrids: the negative incremental impedance of constant power loads (CPLs). Addressing this phenomenon represents a central contribution of the work presented in Publication V. Unlike conventional resistive loads, where the current decreases with a falling voltage, CPLs maintain a fixed power demand regardless of supply voltage fluctuations. Such behaviour is typical in tightly regulated power electronic loads, including DC motor drives, telecom power supplies and server infrastructures. The current–voltage relationship of a CPL can be expressed as:

$$i_{cpl} = \frac{P}{V_{cpl}}; \forall V_{cpl} > \varepsilon \qquad \ldots(13)$$

This inverse dependency gives rise to negative incremental impedance. When the bus voltage drops slightly, the CPL increases its current demand to maintain constant power, which further depresses the voltage and drives the system away from equilibrium. Conversely, a small increase in voltage reduces the current demand, amplifying the upward deviation. Figure 30 illustrates the negative impedance properties of the CPLs. This forms a destabilising positive feedback loop that can lead to oscillations or even voltage collapse.

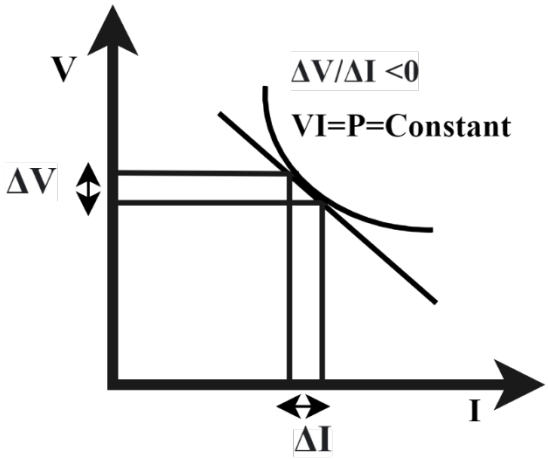

Figure 30. CPL I–V characteristic illustrating negative incremental resistance (Publication V)

As highlighted in recent studies (Singh et al., 2017; Abdurraqeeb et al., 2024; Moradi-Khaligh et al., 2025), equilibrium points with CPLs are inherently unstable, unlike

resistive loads that exhibit positive incremental resistance, as shown in Figure 31. This unique feature makes CPLs a key factor in destabilising DC microgrids, highlighting the need for advanced, robust control strategies that can counteract their negative effects and ensure stable voltage regulation.

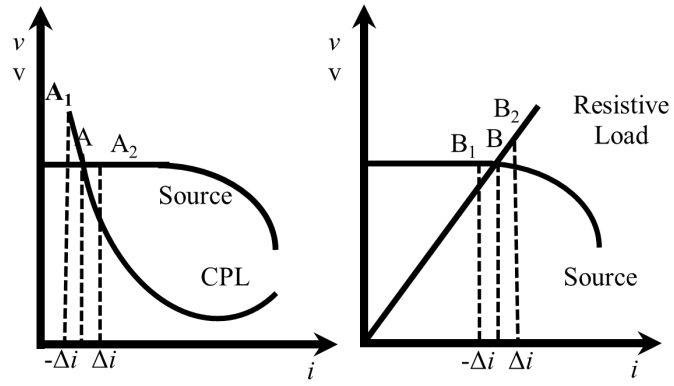

Figure 31. Small-signal I–V characteristics highlighting CPLs' negative incremental impedance versus a resistor and a voltage source (Publication V)

4.2 ANN-Based Voltage Control Principles

Building on the challenges and opportunities outlined in Section 4.1, this section contributes by introducing ANN-based voltage control strategies that address the limitations of classical PI and computationally demanding MPC approaches. The following subsections progressively demonstrate how ANNs can be trained using MPC-generated datasets designed with suitable architectures and extended to reduced-sensor operation in multi-bus DC microgrids.

4.2.1 MPC as an Expert for Data Generation

MPC has long been recognised as a powerful digital control approach for power converters because of its ability to predict future system states, explicitly incorporate system constraints and optimise switching states at every sampling instant. However, its implementation in practical microgrids faces two critical challenges: (i) the reliance on accurate converter models, which may lose validity under parameter variations, and (ii) its high computational burden, especially in fast-switching power electronics applications.

To address these limitations, a hybrid control strategy is implemented, utilising MPC as an expert controller to generate datasets for training ANNs. According to this approach, the MPC initially controls the DC/DC converter across operational scenarios, with the relevant system variables, including the reference voltage, capacitor voltage and inductor current, serving as input features. The resulting switching signals were used as target outputs for data extraction. After training, the ANN successfully imitates the MPC's control logic while using significantly less computational resources and eliminating the need for explicit mathematical modelling. The proposed method achieves control performance comparable to MPC while capitalising on the computational efficiency and adaptive capabilities of neural network-based methods.

4.2.2 ANN Structures for DC/DC Converter Control

The ANNs implemented in Publications IV–VI are designed as feed-forward neural networks (FF–ANNs) capable of learning nonlinear mappings between system states and optimal switching states. The overall structure of the applied ANN (see Figure 32) comprises the following:

- **Input features**: selected from converter states, such as reference voltage (*Vref*), measured capacitor voltage (*Vc*) and inductor current (*iL*)
- **Hidden layers**: trained with Bayesian regularisation or similar optimisation techniques to minimise overfitting while capturing nonlinear dynamics
- **Output layer**: producing the optimal switching state (*Sopt*) of the DC/DC converter

In Publication IV, an ANN-based voltage control for a step-up DC/DC boost converter is developed, utilising MPC-generated datasets to train the ANN to regulate bus voltage under variable loading conditions. Simulation results showed better voltage tracking and disturbance rejection than the conventional PI control.

In Publication V, the ANN design is extended to handle CPLs, which are notorious for their destabilising negative impedance effect. The ANN demonstrates robustness against CPL-induced instability and achieves a superior transient response compared to both MPC and PI controllers. The proposed approach was tested using FPGA-in-the-loop simulations.

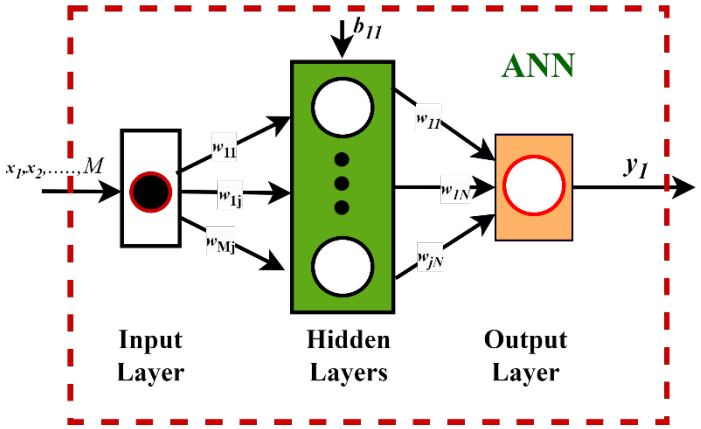

Figure 32. Overview of a multi-layer ANN with multiple inputs and a single output (Publication VI)

The studies presented in Publications IV–VI demonstrate that ANNs can serve as model-free surrogates for MPC, enabling generalisation across different operating points and facilitating the practical application of real-time control systems.

4.2.3 Reduced-Sensor Voltage Control (Publication VI)

Conventional converter control strategies often require multiple sensors (current and voltage) for feedback. However, sensors increase system costs, introduce delays and serve as potential points of failure. Table 8 summarises the existing studies that propose reduced sensor control approaches and compares them with the control approach implemented in Publication VI.

The proposed approach reduces the number of required sensors by designing the ANN so it is primarily based on voltage error signals as input while ensuring accurate voltage regulation. Quasi-Stationary Line (QSL) modelling is employed to approximate line dynamics and account for uncertainties in distributed generation (DG) units. By incorporating QSL-based dynamics into the dataset generation phase, the ANN achieves robust performance in multi-bus DC microgrid configurations under varying load and plug-and-play conditions, that is the connection or disconnection of DER units and loads without disrupting the overall system's stability.

Table 8. Overview of sensorless control strategies for DC MGs (Publication VI)

References	(Kim & Ahn, 2020)	(Tavan et al., 2023)	(EL-Ebiary et al., 2024)	(Obeidi et al., 2022)	(Akpolat, Dursun et al., 2021; Akpolat, Habibi et al., 2021)	Publication VI
Controller	Proportional Derivative (PD)	Fifth Dimensional Estimator	Lyapunov-Based State Observer	Pre-defined Objective Function	Deep Learning	ANN
Load Variation	✓	✓	✓	✓	✓	✓
Plug and Play	-	-	✓	-	-	✓
Parametric Variation	-	✓	-	-	-	✓
Stability Analysis	-	✓	✓	✓	-	✓
Application	DC/DC Boost Converter	AC/DC Converter	DC MG	Buck-Boost Converter	PV Converter	DC/DC Boost Converter
Sensor Reduction	Current	Current	Current, Voltage	Current	Current	Current

4.3 Data Extraction, Training and Deployment

4.3.1 Dataset Generation via MPC

ANN controllers require high-quality datasets that capture the nonlinear behaviour of converters under diverse operating conditions. In the publications included in this dissertation, FCS–MPVC was used as the 'expert' controller to generate the datasets. It regulates the DC/DC converter voltage across varying scenarios, and its switching pulses, state responses and control signals are logged for offline ANN training. Table 9 presents the input features and output targets used in the publications.

Table 9. Dataset features generated by MPC for the training and validation of ANN-based voltage controllers

Publication	Input Features	Control Variable	Disturbance Conditions
IV	Reference voltage, Output voltage, Inductor current	Switching signal	-Step changes in load -Fluctuations in input voltage
V	Reference voltage, Output voltage, Inductor current	Switching signal	-Fluctuations in input voltage -CPL loads
VI	Reference voltage, Output voltage	Switching signal	-Step changes in load -Fluctuations in input voltage -Step changes in reference voltage

In Article IV, a dataset of 30,001 samples was generated, capturing converter dynamics under multiple voltage references and load variations. In Article V, more than 180,000 samples were collected, including challenging CPL cases, to ensure that the ANN could maintain stable operations at highly nonlinear operating points. In Article VI, datasets were generated for multibus DC microgrids using FCS–MPC and quasi-stationary line (QSL) approximations, ensuring that the reduced-sensor ANN control remained valid under network uncertainties.

In all cases, the MPC-generated dataset serves as a knowledge base, enabling the ANN to replicate expert-level control decisions without requiring explicit system models or extensive sensor feedback.

4.3.2 Offline Training Approaches

The datasets generated by MPC are systematically divided into training, validation and testing subsets using random partitioning to ensure the robust development of the ANN controller. The reviewed literature predominantly employs feed-forward artificial neural networks (FF–ANNs) trained using the Bayesian Regularisation (trainbr) algorithm. This approach effectively minimises overfitting while improving generalisation capabilities and eliminating the computational overhead associated with extensive cross-validation procedures.

The comprehensive training workflow encompasses three critical phases that ensure optimal network performance. Initially, feature selection is performed to identify

optimal input variables, such as reference voltage (Vref), capacitor voltage (Vc) and inductor current (iL), carefully balancing prediction accuracy against sensor requirements and system complexity. Subsequently, offline training is conducted using Bayesian regularisation to systematically optimise network weights and biases, enabling the ANN to learn the complex mapping between system states and optimal switching decisions. Finally, rigorous performance evaluation validates the trained network using established statistical metrics, including confusion matrices to measure the correct classification of switching states, mean squared error (MSE) to assess prediction accuracy during both training and testing phases, and overall accuracy percentages to quantify correct predictions relative to expert MPC outputs. Publication IV achieved approximately 97% classification accuracy, with MSE values approaching zero, indicating exceptional learning performance and minimal prediction errors. Similarly, Publication V reported 97.2% accuracy when evaluated on 180,006 data samples, achieving an MSE value of 0.02143, as presented in Figure 33. Performance validation was confirmed through a comprehensive confusion matrix analysis, as represented in Figure 34. Furthermore, Publication VI consistently demonstrated high ANN accuracy across challenging scenarios, including plug-and-play and dynamic load variations, providing strong evidence for the practical feasibility of reduced-sensor control strategies in real-world power electronics applications.

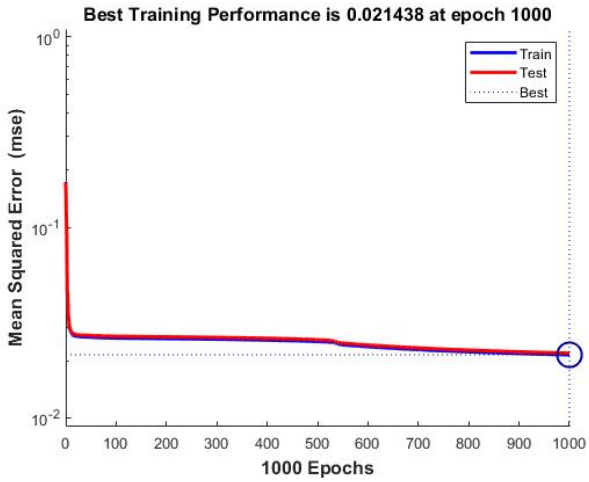

Figure 33. A mean square error value of 0.02143 in the proposed network was achieved during training up to 1,000 epochs (Publication V)

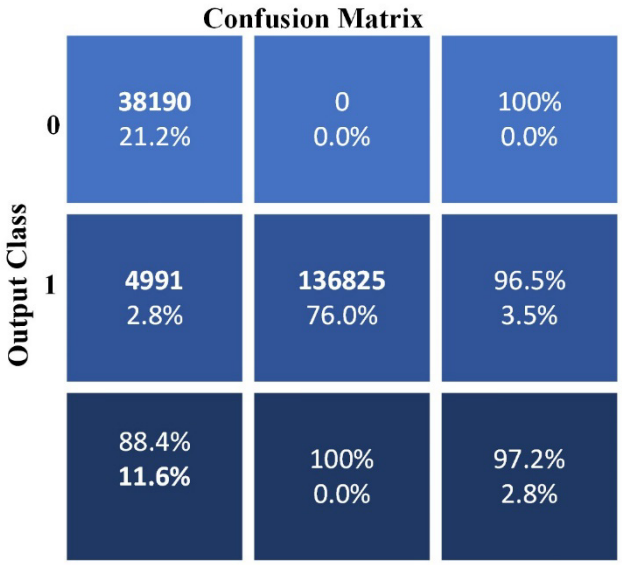

Figure 34. The confusion matrix illustrates the classification accuracy of the trained controller (Publication V)

4.3.3 Online Deployment in MATLAB/Simulink and HIL Environments

The transition from offline-trained ANN models to real-time implementation is a critical step in validating their practical feasibility. This study followed a progressive deployment strategy, beginning with MATLAB/Simulink-based testing, extending to hardware-in-the-loop (HIL) platforms and finally implementing the controller on FPGA hardware, testing it using Simulink and the FPGA-in-the-Loop (FIL) approach. Figure 35 graphically illustrates the entire development procedure of the ANN controller.

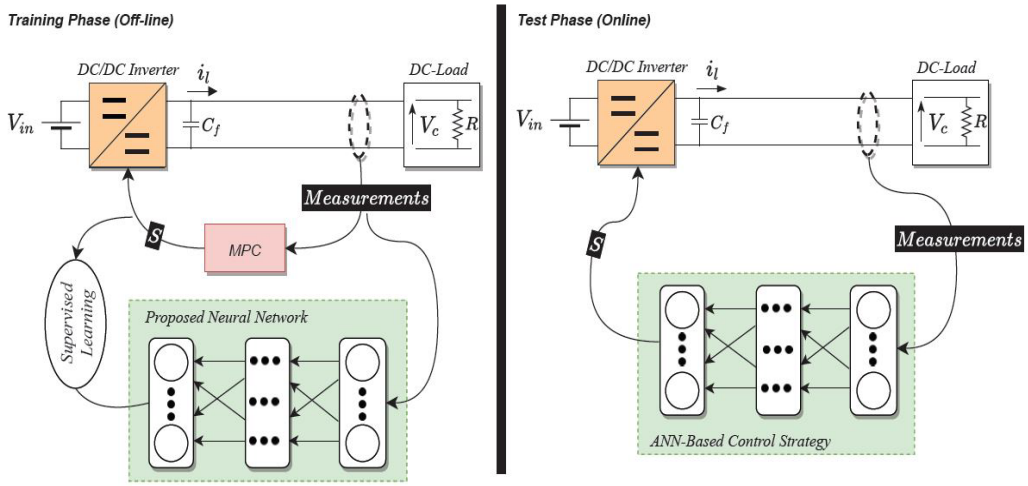

Figure 35. Overview of the development of the proposed controller. During training, FCS–MPC regulates the DC/DC converter to extract the dataset. In testing, the trained ANN replaces MPC as the controller to regulate the converter's voltage (Publication IV)

4.3.3.1 MATLAB/Simulink Deployment

The first validation was conducted in MATLAB/Simulink, where the trained ANN controller was imported into the simulation model and directly linked to the DC/DC converter subsystem. Initially, a switching model of a step-up DC/DC converter with its associated loads was created in Simulink. The ANN controller block was generated from the trained neural network in MATLAB's Neural Network Toolbox and imported into the Simulink environment. During operation, the ANN replaced the MPC block, producing switching signals (Sopt) based on inputs (Vref, Vc, iL). Various test cases, including step load variations, input voltage disturbances and constant power load scenarios, were conducted to compare the ANN with the PI and MPC controllers. This stage verified that the ANN operated correctly in a closed-loop environment, showing improved voltage tracking and transient responses compared to conventional controllers.

4.3.3.2 FPGA-in-the-Loop Testing with Zybo Z7-7020

Building on this foundation, the second stage focused on real-time feasibility using field-programmable gate array (FPGA) hardware. Publication V validated the ANN controller on FPGA hardware to assess its embedded real-time performance. In this case, the trained ANN was converted into VHDL. code and implemented on a Zybo Z7-7020 development board. The FPGA executed the controller logic, while the

converter and load were simulated in MATLAB/Simulink, with communication handled through a JTAG interface in an FPGA-in-the-Loop (FIL) arrangement. The FPGA operated at a clock speed of 125 MHz, utilising approximately 13,300 logic slices, 106,400 flip-flops and 630 KB of embedded RAM for ANN weight storage and computations. Despite modest resource use, the FPGA delivered real-time control decisions with negligible delays. FIL implementation is accomplished with the following steps:

- The controller under testing is specified using a Simulink subsystem. Then, the inputs and outputs of the subsystem are defined as fixed data types (this operation can be performed using the Simulink Fixed-Point Tool).
- After defining data types, select the controller under test (CUT) subsystem, open the HDL workflow, and run all tasks.
- After running all tasks successfully, MATLAB will generate the VHDL code of CUT and write it up on the FPGA board.

4.3.3.3 Hardware-in-the-Loop (HIL) with OPAL–RT

The final stage of extended validation transitioned from a single converter to a system-level microgrid using an OPAL–RT 4510 platform, as described in Publication VI. At this stage, the ANN controller was integrated into a hardware-in-the-loop (HIL) setup, allowing interaction with a real-time digital twin of a multi-bus DC microgrid. The ANN controller operates on the host computer, interfacing with OPAL–RT through the RT–LAB environment. Low-latency analogue/digital interfaces ensured that communication between OPAL–RT and the controller met the timing demands of real power converters. Unlike earlier stages, the controller was designed with fewer sensor requirements, primarily relying on bus voltage feedback rather than full current and voltage measurements. To improve robustness, quasi-stationary line (QSL) modelling was incorporated into the training process, allowing the ANN to learn the effects of line dynamics and parameter variations. Several challenging scenarios were tested, including the plug-and-play of distributed generators, parametric uncertainties in line impedances, load changes and topology reconfigurations. In each case, the ANN controller maintained stable DC bus voltage, outperforming both the PI and MPC controllers in terms of resilience and adaptability. These HIL experiments demonstrated that reduced-sensor, ANN-based control is cost effective and reliable, making it a promising option for practical microgrid environments.

4.4 ANN-Based Control for Stability Enhancement

Data-driven controls, such as MPC-aided ANN, have gained significant attention in control applications due to their ability to approximate complex nonlinear functions and provide a comprehensive understanding of system dynamics. However, ensuring mathematical stability in these systems presents unique challenges compared to traditional control methods. ANNs introduce complications due to their inherent nonlinearity, high-dimensionality and data-driven nature, making formal stability proofs significantly more complex. Bongard et al. (2022) attempted to address these challenges by proposing data-driven MPC schemes that ensure stability through Lyapunov analysis for linear time-invariant systems (Bongard et al., 2022), while Berberich et al. (2020) analysed robust stability without terminal constraints by proving practical exponential stability with sufficiently long prediction horizons. However, achieving similar stability guarantees for ANNs is challenging due to their non-convex optimisation landscapes, the absence of explicit state-space models, nonlinear activation functions, high-dimensional weight matrices and the stochastic nature of parameter updates through gradient descent, all of which make stability analysis more complex. Considering these mathematical complexities, this study adopts a practical approach by analysing the controller's stability using Lyapunov's direct method and confirming the robustness of the ANN controller through numeric simulations to assess the system's convergence. This approach recognises that proving the mathematical stability of data-driven control techniques remains a major challenge in the field. The analysis begins with the definition of a quadratic Lyapunov candidate function based on voltage error:

$$V(x) = \frac{1}{2} V_{error}^2 \quad \ldots(14)$$

Where the voltage error is defined as:

$$V_{error} = V_{ref} - V_{actual} \quad \ldots(15)$$

This function satisfies the positive definiteness condition: $V(x) > 0$ for all $x \neq 0$ and $V(0)$, ensuring that it represents the 'energy' associated with voltage deviations. The time derivative of the Lyapunov function is then given by

$$\dot{V}(x) = V_{error} . \dot{V}_{error} \quad \ldots(16)$$

For stability, the requirement is that $\dot{V}(x) \leq 0$, meaning that the error energy does not increase over time but decreases to zero as time approaches infinity. Numerical simulations in Publication VI show that under ANN control, the Lyapunov function monotonically decreases and converges to zero, indicating that bus voltage errors

converge towards zero as time increases to infinity. Therefore, the controller is asymptotically stable.

4.5 Results

This section consolidates the empirical evidence across three publications, following the progression from simulation to FIL under CPL and finally to reduced-sensor HIL in a multibus DC microgrid. Initially, the common simulation model parameters used in Publications IV to VI are presented in Table 10.

Table 10. Simulation model parameters (Publication VI)

Parameter	Value
DC Input	70–80V
Inductor	0.4µH
ESR Resistance	10mΩ
Capacitor	600µF
DC Output Voltage	98–102V
Line Parameters Z_{12}	R = 0.51Ω, L = 10µH
Line Parameters Z_{13}	R = 2Ω, L = 70µH
Line Parameters Z_{24}	R = 0.51Ω, L = 12.1µH
Line Parameters Z_{43}	R =4Ω, L = 60µH
PI Parameters	K_p = 0.00547, K_i = 7

4.5.1 Step Change of Load (Publication IV)

ANN voltage control for the DC/DC step-up converter was developed in Simulink, where three inputs (reference voltage, measured voltage and inductor current) were chosen using the hit-and-trial method, and the switching state was set as the output. It is essential to note that the ANN is trained on a single reference value under different loading conditions and tested on the same reference value. Figure 36 presents a comparison of the proposed controller response with the conventional PI controller. It can be observed from the figure that during a step change in load, the PI controller shows a dip in voltage and an overshoot in current. Moreover, the ANN-based control approach offers better wave quality and less distortion than the ANN.

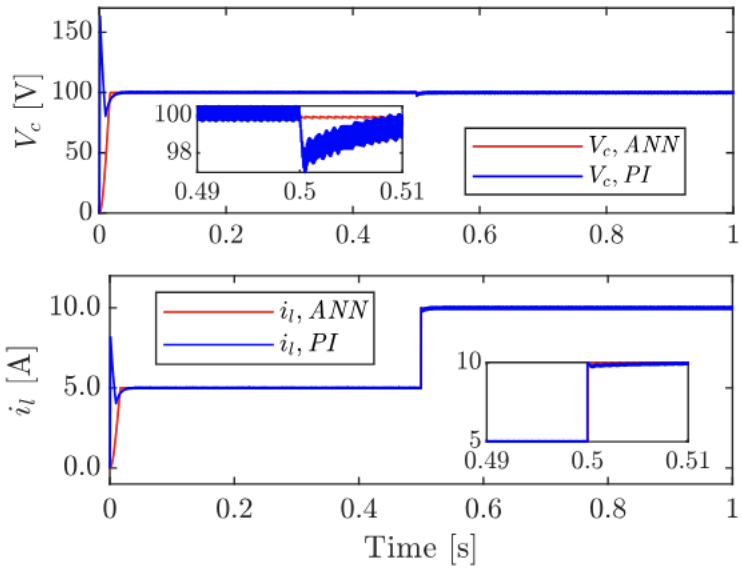

Figure 36. Dynamic performance analysis of output voltage and current in a DC boost converter employing PI and ANN-based control schemes under step load variations (Publication IV)

4.5.2 FPGA-in-the-Loop Under CPL and Input-Voltage Disturbances (Publication V)

To assess the performance and robustness of the proposed controller developed in Publication V under CPL, FPGA-in-the-loop-based validation is conducted. The proposed ANN controller is run on the FPGA board ZYBO Z7, while the DC/DC converter model and load are simulated on the host PC using MATLAB/Simulink. The communication between the FPGA and the host PC takes place through a JTAG cable using the IEEE 1149.7 standard. Closed-loop waveforms demonstrate that the ANN achieves a lower overshoot than MPC during reference changes with CPL, as shown in Figure 37. Robustness against input-voltage perturbations (±5%/50 Hz ripple; steps from 80V to 95V and 75V) is confirmed in Figure 38, where the ANN shows better voltage and current quality than the PI controller. Hence, the proposed controller easily mitigates the effects of AC ripple content on the input voltage.

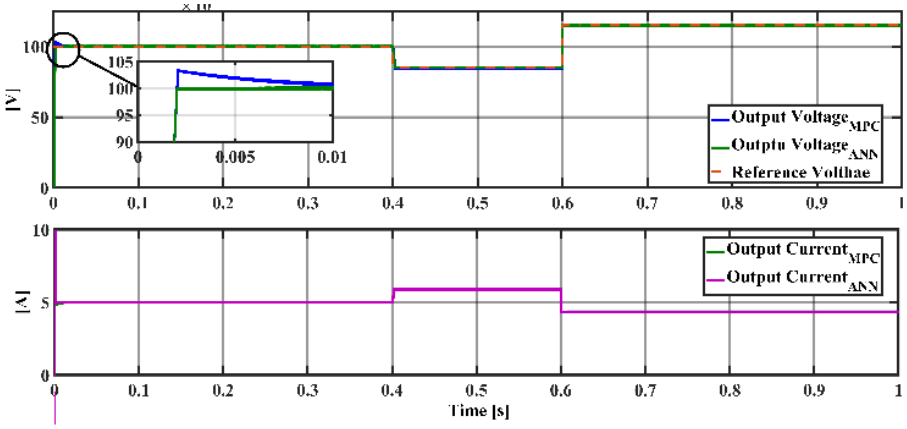

Figure 37. ANN vs. MPC reference tracking under CPL (Publication V).

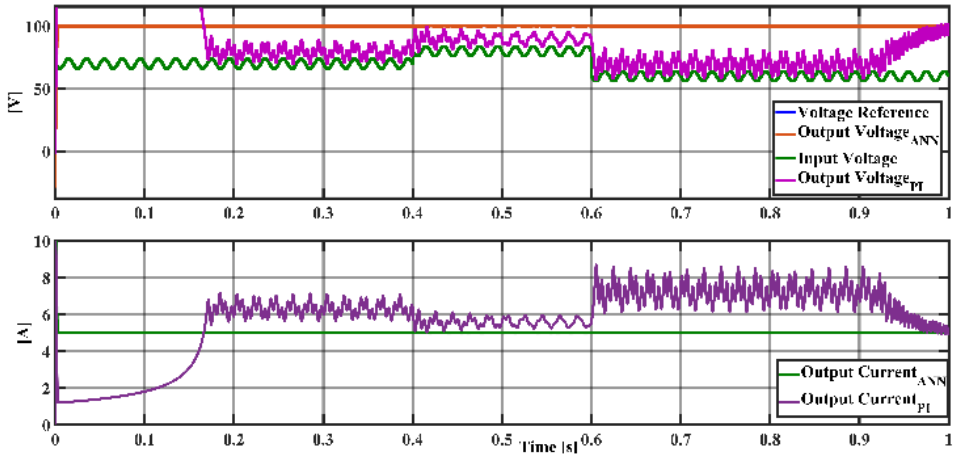

Figure 38. Disturbance rejection under input-voltage ripple/steps vs. PI (Publication V)

4.5.3 Reduced-Sensor HIL in a Multibus DC MG (Publication VI)

This subsection reports a system-level, real-time validation of an OPAL–RT 4510 platform using an ANN controller with voltage-only feedback, as studied in Publication VI. The training data incorporate quasi-stationary line (QSL) effects to account for DC MG uncertainties and disturbances. Figure 39 demonstrates the block diagram of the reduced-sensor ANN approach for a single DER unit. The ANN receives only the bus voltage reference and the measured PCC voltage; it outputs the switching command for the step-up converter. Eliminating inductor/load-current sensing reduces wiring and costs while retaining regulation capability; the missing state's context is compensated through QSL-based training.

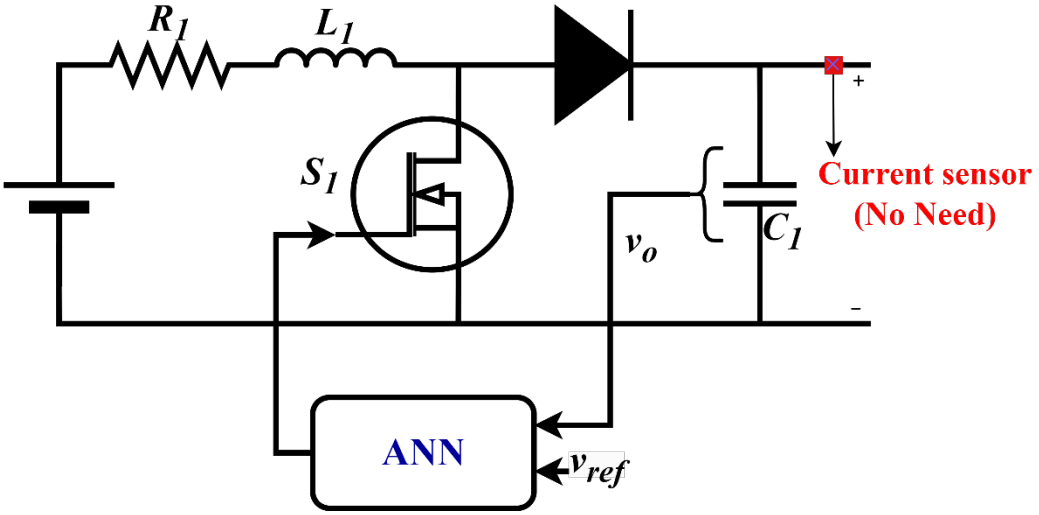

Figure 39. Reduced-sensor ANN for a single DER unit (Publication VI)

Figure 40 displays the DC MG testbench used for hardware-in-the-loop validation, featuring four DER units arranged in a ring topology with the line impedances Z12, Z13, Z24 and Z43. Each DER connects to the common bus through a boost converter with a reference voltage of 100 V. This multi-DER ring setup creates a comprehensive networked testing framework that allows the thorough evaluation of the controller's performance across three key operational scenarios: accurate voltage tracking under varying load conditions, seamless plug-and-play (PnP) integration of new distributed energy resources and dynamic system reconfiguration during topology changes. The HIL platform operates in hardware-synchronised mode, with carefully configured analogue inputs and outputs for optimal performance. The output voltages and currents of each DER are measured through a simulator analogue output board and then fed back via wired connections to an analogue input board, as shown in Figure 41. This loop-back configuration accurately captures critical real-world factors, including system delays, electrical noise and signal interference. The high-fidelity testing environment enables the rigorous evaluation of controller performance under real-time operating conditions. Additionally, the performance of the proposed controller is compared with traditional PI and MPC techniques.

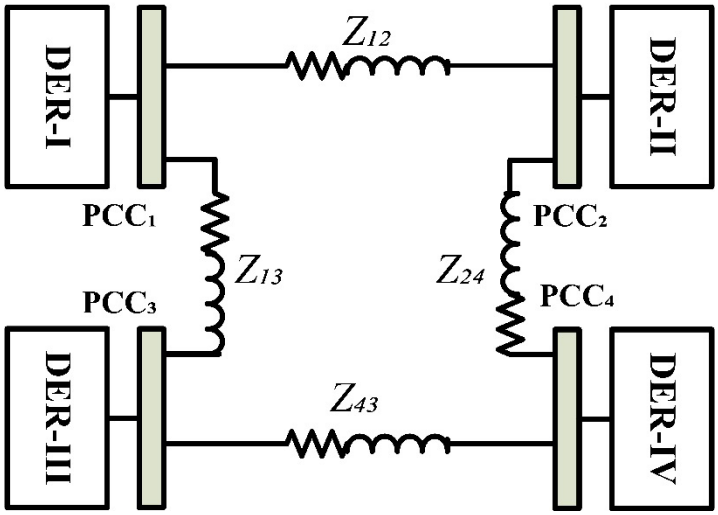

Figure 40. Layout of the DC MG test bench, which has four DER units connected in a ring configuration (Publication VI)

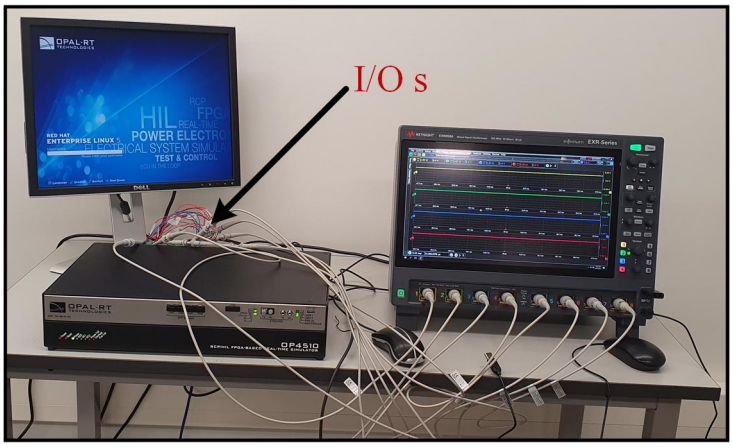

Figure 41. OPAL–RT 4510 hardware-in-the-loop configuration with analogue input/output signal routing for real-time validation (Publication VI)

Plug-and-play functionality is a key operational requirement for distributed energy resource control architectures due to the intermittency of RERs. The transient response of the proposed control algorithm under PnP scenarios is analysed by systematically disconnecting DER-IV from the ring at t = 1.0 seconds, then reconnecting it at t = 1.5 seconds, while keeping a continuous load connection at PCC_4.

The experimental validation, as shown in Figure 42, demonstrates the superior controller dynamics during PnP operation. When DER–IV is isolated from the system and its instantaneous power injection stops, DER–II and DER–III take the load. DER–II and DER–III show proportional current regulation based on their respective capacity ratings, ensuring seamless load transfer without voltage deviation. The bus

voltages remained stable with zero steady-state errors, as revealed in Figure 42. These findings support the effectiveness of the proposed PnP implementation within the islanded DC MG operational framework, demonstrating compliance with IEEE standards for the interconnection of distributed generation.

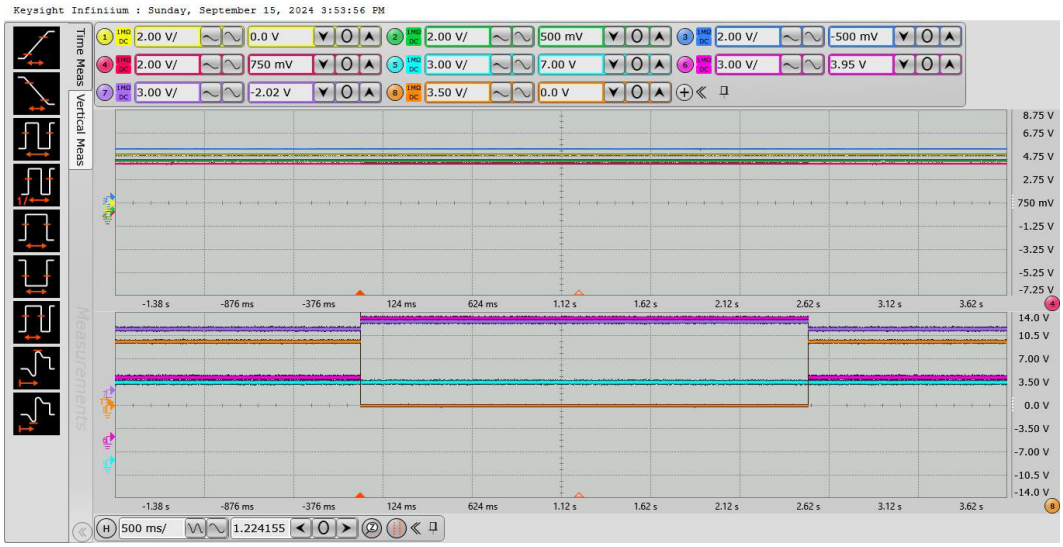

Figure 42. DER–IV plug-and-play event: Voltages remain regulated; neighbouring DER currents redistribute and recover upon reconnection (Publication VI)

Table 11 compares the performance of the different controllers based on the overshoot and settling times. The closed-loop step response in the case of a single DER unit shows that the proposed ANN has achieved a settling time of 99 µs with a minimal overshoot of 0.325%, compared to 124 µs / 0.445% for MPC and 19.9 ms / 180% for PI. These results highlight the ANN controller's enhanced transient response capabilities, delivering approximately 25% faster settling than MPC and a more-than 200-fold improvement relative to the PI controller, while maintaining excellent stability margins with minimal voltage overshoot.

Table 11. Performance comparison of control techniques implemented in Publication VI.

Implemented Technique	Settling Time	Overshoot in %
PI	19.9	180
FCS–MPC	124 µsec	0.445
Proposed ANN	99 µsec	0.325

4.6 Discussion

The results presented in this chapter collectively highlight the contribution of AI techniques, particularly ANNs, to enhancing voltage control in DC microgrids. The key contribution discussed in this chapter is the use of FCS–MPC as a parent technique to develop an ANN-based controller, which shows robust control performance with reduced sensing requirements and lower computational overhead than traditional PI and MPC. Furthermore, the mathematical stability of the ANN was studied. This methodological transition addresses several shortcomings of existing control approaches.

Traditional linear controllers similar to PI and PID are commonly used in industry due to their simplicity; however, they are limited in their ability to cope with nonlinear system dynamics, parametric variations and the destabilising effects of constant power loads (CPLs). Nonlinear controllers, including sliding mode and MPC, offer improved robustness but suffer from challenges such as chattering, variable switching frequencies and significant computational burdens. The studies summarised here demonstrate that ANN-based control can preserve the dynamic performance of MPC while alleviating its dependency on precise system models and high real-time computational requirements.

The ongoing development across the three publications highlights the novelty of the contribution. In Publication IV, the ANN was trained using MPC-generated datasets and shown in the simulation to outperform PI control under dynamic loading conditions, achieving accurate voltage regulation and the high classification accuracy of switching states. Publication V advanced this framework by validating the ANN controller on an FPGA platform feeding CPLs, thereby confirming its capability to mitigate the destabilising effects of negative impedance and to provide a superior transient response compared with both MPC and PI controllers. Finally, Publication VI extended the concept to reduced-sensor operation in a multibus DC microgrid, employing quasi-stationary line (QSL) modelling to account for system uncertainties. Hardware-in-the-loop (HIL) experiments demonstrated that the reduced-sensor ANN maintained stable operation under plug-and-play and topology reconfiguration while improving reliability by reducing the number of potential sensor failure points.

In DC microgrid applications, this study demonstrates that ANN-based voltage controllers achieve superior transient response and maintain bus voltage stability even under challenging conditions, such as CPL effects. These results were validated through hardware implementations using FPGA platforms and hardware-in-the-loop (HIL) testing, confirming their readiness for real-world deployment.

4.7 Chapter Summary

This chapter examined the role of AI in addressing the control challenges of DC MGs, with a particular focus on ANN-based voltage control. Beginning with the limitations of traditional linear and nonlinear controllers, this chapter discussed a series of studies in which MPC acts as an expert in generating training datasets, which then allow ANN models to replace computationally intensive FCS–MPC controllers. The results showed that ANN-based voltage control achieved superior dynamic performance compared with PI and MPC controllers, both in simulation and experimental validation. Furthermore, the reduced-sensor approach was shown to enhance system reliability while maintaining stability in multibus microgrid configurations.

In summary, this research contributes to the advancement of intelligent control in DC MGs by introducing a data-driven methodology that is computationally efficient, experimentally validated and adaptable to sensor-limited environments. These findings enrich the body of knowledge on AI-driven power electronic control and provide a foundation for future research on scalable, resilient and cost-effective MG operations.

5 CONCLUSION

This chapter first addresses the research questions formulated in Chapter 1, followed by a synthesis of the main contributions of the dissertation. It concludes by outlining potential directions for future research.

5.1 Research Outcomes

The refined answers (A) to the research questions (RQ) formulated in Chapter 1 are presented as the primary outcomes of this dissertation.

RQ1: How can decentralised nonlinear predictive control achieve reliable voltage regulation and power sharing in AC MGs with diverse load conditions?

A1: This dissertation demonstrates that FCS–MPC is capable of ensuring robust voltage regulation and accurate power sharing in islanded AC MGs. By incorporating a dual-objective cost function, the proposed controller not only maintained voltage quality but also effectively regulated the output current under symmetrical fault conditions. The integration of droop characteristics enabled autonomous power sharing among DERs without requiring communication links, thus enhancing the system's scalability. FCS–MPC demonstrated superior transient response, disturbance rejection and fault tolerance compared to conventional PI controllers (Publications I–II).

RQ2: How can hierarchical predictive control strategies be designed and validated to ensure robust, decentralised voltage and frequency control in renewable-rich power systems under varying load conditions and parametric uncertainties?

A2: The dissertation introduced a hierarchical control architecture combining FCS–MPC-based primary voltage regulation with droop control for power sharing and PI-based secondary loops for voltage and frequency restoration. A two-step prediction horizon reduced the computational burden and switching frequency while maintaining the controller's performance. Mathematical stability is formally supported through Lyapunov-based analysis, and robustness against parametric uncertainties is confirmed in both simulations and FPGA-in-the-loop hardware validation. Compared to linear hierarchical controllers, the proposed scheme provided enhanced resilience under constant power and dynamic loads, with THD values maintained within IEEE/IEC standards (Publication III).

RQ3: Can ANN-based control provide reliable voltage regulation in DC MGs?

A3: The dissertation verified that ANN-based controllers trained using MPC-generated datasets can achieve reliable voltage regulation in DC MGs. The ANN-based control reduced the dependency on detailed converter models and offered superior adaptability under non-linear and constant power load conditions. Experimental results in HIL environments confirmed that ANN-based voltage controllers match or surpass MPC performance, particularly in terms of reduced steady-state error and faster convergence while maintaining low harmonic distortion. This outcome confirms the feasibility of AI-based approaches for controlling next-generation DC MGs (Publication IV).

RQ4: Can AI-based control with reduced sensor requirements outperform conventional approaches (e.g. linear PI or MPC) for modern power system voltage regulation, particularly under challenging scenarios such as constant power loads?

A4: The dissertation shows that reduced-sensor ANN-based control can outperform both linear PI and predictive MPC approaches when regulating voltage in DC MGs under CPL conditions. By relying only on voltage measurements, the reduced-sensor ANN controller lowered hardware complexity and cost while still providing stable operation. The ANN-based reduced-sensor controller demonstrated computational efficiency, robustness to measurement noise and ease of deployment on digital real-time simulators compared to its parent FCS–MPC technique. These findings indicate that sensor-efficient AI-based controllers offer a viable pathway for scaling predictive and intelligent control to practical, cost-sensitive MG applications (Publications V–VI).

5.2 Main Contributions

In Chapter 1 (Section 1.2), the overall objectives are introduced, and the specific contributions are outlined in Section 1.4. Here, the consolidated contributions of this dissertation are summarised as follows:

1. **Development of fault-tolerant predictive control for AC MGs**: An improved FCS–MPVC was proposed, featuring a dual-objective cost function that simultaneously ensures voltage regulation and fault current limitations. This approach enhanced system reliability under symmetrical fault conditions and provided an alternative to classical PI controllers (Publications I–II).

2. **Introduction of a predictive hierarchical control framework:** A two-layer predictive architecture is designed that combines FCS–MPC for primary voltage regulation, droop control for power sharing and PI-based secondary loops for voltage and frequency restoration. The method reduced computational complexity using a two-step prediction horizon and formally established stability through Lyapunov-based analyses (Publication III).

3. **Validation through FPGA- and hardware-in-the-loop testing:** The proposed controllers are validated in real time using FPGA-in-the-loop (FIL) and controller-hardware-in-the-loop (CHIL) environments. These experiments verified practical feasibility, robustness to parametric uncertainties and compliance with IEEE/IEC standards (Publications III, V and VI).

4. **Advancement of AI-driven control in DC microgrids:** A novel ANN-based voltage control framework is developed with datasets generated from FCS–MPC control models. The ANN controllers exhibited fast convergence, low steady-state error and adaptability under both nonlinear and constant power loads, demonstrating their potential to replace or complement FCS–MPC in practical applications (Publications IV–V).

5. **Proposal of reduced-sensor ANN control for cost-efficient deployment:** To lower implementation costs, a voltage-only ANN controller was designed and validated in a multi-bus DC MG testbed. This reduced-sensor strategy maintained stability and power quality while reducing measurements' complexity, making AI-based controllers more practical for scalable microgrid deployments (Publication VI).

6. **Establishment of mathematical stability proofs:** This dissertation studies rigorous Lyapunov-based stability proofs for predictive controllers applied to AC microgrids and a theoretical stability basis for ANN-based DC/DC converter controls. These results strengthen confidence in the safe deployment of advanced predictive and AI-based controllers (Publications III and VI).

7. **Promotion of open science and reproducibility:** To support transparency and further research, the dissertation releases open-source repositories containing datasets, simulation models and FPGA board definition files. This contribution promotes reproducibility and enables collaborative advancement in the field of intelligent MG control (Publication III).

This dissertation provided an extensive comparison of predictive, linear and AI-based control methods across AC and DC MGs. It demonstrated how predictive and ANN-based controllers overcome the limitations of PI/PR schemes, sliding-mode control and other nonlinear techniques, thus contributing new insights to the body of knowledge on decentralised and intelligent MG control.

5.3 Limitations and Potential Areas for Future Research

The research in this dissertation identifies several potential areas for future investigation and development. While the proposed predictive and AI-based control strategies have been successfully validated, emerging challenges and technological opportunities highlight important directions for ongoing research.

The controllers developed in this dissertation were primarily demonstrated within single-LV MG environments, and their scalability to interconnected or nested microgrids was not addressed. Extending these strategies to multi-MG coordination, which involves several AC and DC systems operating under both technical and economic objectives, is an important direction for further exploration.

Another limitation involves communication aspects. While decentralised and reduced-sensor approaches naturally lower the dependence on communication networks, the impacts of delays, packet loss or cyberphysical vulnerabilities were not explicitly examined. Incorporating these factors into predictive and ANN-based controllers would improve their practical reliability in real-world applications.

Additionally, the validation of these methods was limited to OPAL–RT and FPGA-in-the-loop experiments. Although these offer valuable real-time insights, the additional testing of physical MG prototypes or pilot field demonstrations is necessary to fully confirm long-term reliability, hardware stress effects and resilience against operational disturbances.

Finally, the AI component of this dissertation focuses on feedforward ANN architectures trained on MPC-generated datasets. Future research should explore more adaptive approaches, such as reinforcement learning, recurrent networks or hybrid AI–MPC systems, while addressing challenges regarding explainability and operator trust

References

Abdurraqeeb, A. M., Al-Shamma'a, A. A., Alkuhayli, A., Alharbi, M., Farh, H. M. H., Alsaif, F., Omotoso, H. O., Addoweesh, K. E., & Qamar, A. (2024). Stabilization of constant power loads and dynamic current sharing in DC microgrid using robust control technique. *Electric Power Systems Research*, *230*, 110258. https://doi.org/10.1016/j.epsr.2024.110258

Aghdam, M. M., Li, L., & Zhu, J. (2020). Comprehensive study of finite control set model predictive control algorithms for power converter control in microgrids. *IET Smart Grid*, *3*(1), 1–10. https://doi.org/10.1049/iet-stg.2018.0237

Agreement, P. (2015). Paris agreement. *Report of the Conference of the Parties to the United Nations Framework Convention on Climate Change (21st Session, 2015: Paris). Retrived December*, *4*(2017), 2. https://heinonline.org/hol-cgi-bin/get_pdf.cgi?handle=hein.journals/intlm55&section=46

Aguilera, R. P., & Quevedo, D. E. (2010). On stability of finite control set MPC strategy for multicell converters. *2010 IEEE International Conference on Industrial Technology*, 1277–1282. https://doi.org/10.1109/ICIT.2010.5472626

Aguilera, R. P., & Quevedo, D. E. (2011). On stability and performance of finite control set MPC for power converters. *2011 Workshop on Predictive Control of Electrical Drives and Power Electronics*, 55–62. https://doi.org/10.1109/PRECEDE.2011.6078688

Ahmed, A. A., Koh, B. K., & Lee, Y. I. (2017). A comparison of finite control set and continuous control set model predictive control schemes for speed control of induction motors. *IEEE Transactions on Industrial Informatics*, *14*(4), 1334–1346.

Ahmethodzic, L., & Music, M. (2021). Comprehensive review of trends in microgrid control. *Renewable Energy Focus*, *38*, 84–96.

Akpolat, A. N., Dursun, E., & Kuzucuoglu, A. E. (2021). Deep Learning-Aided Sensorless Control Approach for PV Converters in DC Nanogrids. *IEEE Access*, *9*, 106641–106654. https://doi.org/10.1109/ACCESS.2021.3100857

Akpolat, A. N., Habibi, M. R., Dursun, E., Kuzucuoglu, A. E., Yang, Y., Dragicevic, T., & Blaabjerg, F. (2021). Sensorless Control of DC Microgrid Based on Artificial Intelligence. *IEEE Transactions on Energy Conversion*, *36*(3), 2319–2329. https://doi.org/10.1109/TEC.2020.3044270

Akter, M. P., Mekhilef, S., Tan, N. M. L., & Akagi, H. (2015). Modified model predictive control of a bidirectional AC–DC converter based on Lyapunov function for energy storage systems. *IEEE Transactions on Industrial Electronics*, *63*(2), 704–715.

Alam, K. S., Akter, M. P., Shakib, S. S. I., Xiao, D., Zhang, D., & Rahman, M. F. (2018). Lyapunov-function based predictive approach for load voltage control of four-leg inverter with an output LC filter. *2018 IEEE Energy Conversion Congress and Exposition (ECCE)*, 6880–6885. https://doi.org/10.1109/ECCE.2018.8557385

Almasabi, S., Shaf, A., Ali, T., Zafar, M., Irfan, M., & Alsuwian, T. (2024). Securing Smart Grid Data With Blockchain and Wireless Sensor Networks: A Collaborative Approach. *IEEE Access*, *12*, 19181–19198. https://doi.org/10.1109/ACCESS.2024.3361752

Ang, K. H., Chong, G., & Li, Y. (2005). PID control system analysis, design, and technology. *IEEE Transactions on Control Systems Technology*, *13*(4), 559–576.

Arias-Esquivel, Y., Cárdenas, R., Urrutia, M., Diaz, M., Tarisciotti, L., & Clare, J. C. (2022). Continuous control set model predictive control of a modular multilevel converter for drive applications. *IEEE Transactions on Industrial Electronics*, *70*(9), 8723–8733.

Arnold, D., Saha, S., Ngo, S.-T., Roberts, C., Scaglione, A., Johnson, N. G., Peisert, S., & Pinney, D. (2022). Adaptive control of distributed energy resources for distribution grid voltage stability. *IEEE Transactions on Power Systems*, *38*(1), 129–141.

Athari, H., Niroomand, M., & Ataei, M. (2017). Review and Classification of Control Systems in Grid-tied Inverters. *Renewable and Sustainable Energy Reviews*, *72*, 1167–1176. https://doi.org/10.1016/j.rser.2016.10.030

Babayomi, O., Li, Y., Zhang, Z., & Park, K.-B. (2025). Advanced control of grid-connected microgrids: Challenges, advances and trends. *IEEE Transactions on Power Electronics*. https://doi.org/10.1109/TPEL.2025.3526246

Babayomi, O., Madonski, R., Zhang, Z., Rodriguez, J., Davidson, I., & Kim, D.-S. (2025). Robust Model Predictive Control of Converter-Based Microgrids. *IEEE Transactions on Power Electronics*. https://doi.org/10.1109/TPEL.2025.3586709

Berberich, J., Köhler, J., Müller, M. A., & Allgöwer, F. (2020). Data-driven model predictive control with stability and robustness guarantees. *IEEE Transactions on Automatic Control*, *66*(4), 1702–1717.

Beus, M., Banis, F., Pandžić, H., & Poulsen, N. K. (2020). Three-level hierarchical microgrid control—Model development and laboratory implementation. *Electric Power Systems Research*, *189*, 106758.

Bird, L., Milligan, M., & Lew, D. (2013). *Integrating variable renewable energy: Challenges and solutions*. National Renewable Energy Lab.(NREL), Golden, CO (United States). https://www.osti.gov/biblio/1097911

Bongard, J., Berberich, J., Köhler, J., & Allgöwer, F. (2022). Robust stability analysis of a simple data-driven model predictive control approach. *IEEE Transactions on Automatic Control*, *68*(5), 2625–2637.

Buso, S., Caldognetto, T., & Brandao, D. I. (2016). Dead-Beat Current Controller for Voltage-Source Converters With Improved Large-Signal Response. *IEEE Transactions on Industry Applications*, *52*(2), 1588–1596. https://doi.org/10.1109/TIA.2015.2488644

Callegaro, L., Ciobotaru, M., Pagano, D. J., & Fletcher, J. E. (2018). Feedback linearization control in photovoltaic module integrated converters. *IEEE Transactions on Power Electronics*, *34*(7), 6876–6889.

Camacho, E. F., & Bordons, C. (1999). *Model Predictive Control* (1st ed.). Springer Nature.

Chattopadhyay, R., De, A., & Bhattacharya, S. (2014). Comparison of PR controller and damped PR controller for grid current control of LCL filter based grid-tied inverter under frequency variation and grid distortion. *2014 IEEE Energy Conversion Congress and Exposition (ECCE)*, 3634–3641. https://doi.org/10.1109/ECCE.2014.6953895

Chen, M., Zhou, D., Tayyebi, A., Prieto-Araujo, E., Dörfler, F., & Blaabjerg, F. (2023). On power control of grid-forming converters: Modeling, controllability, and full-state feedback design. *IEEE Transactions on Sustainable Energy*, *15*(1), 68–80.

Cheng, L., Acuna, P., Aguilera, R. P., Jiang, J., Wei, S., Fletcher, J. E., & Lu, D. D. (2017). Model predictive control for DC–DC boost converters with reduced-prediction horizon and constant switching frequency. *IEEE Transactions on Power Electronics*, *33*(10), 9064–9075.

CO2 Emissions in 2022 – Analysis. (2023). https://www.iea.org/reports/co2-emissions-in-2022

Cortés, P., Kazmierkowski, M. P., Kennel, R. M., Quevedo, D. E., & Rodríguez, J. (2008). Predictive control in power electronics and drives. *IEEE Transactions on Industrial Electronics*, *55*(12), 4312–4324.

Cortés, P., Wilson, A., Kouro, S., Rodriguez, J., & Abu-Rub, H. (2010). Model predictive control of multilevel cascaded H-bridge inverters. *IEEE Transactions on Industrial Electronics*, *57*(8), 2691–2699.

Dragičević, T., & Novak, M. (2018). Weighting factor design in model predictive control of power electronic converters: An artificial neural network approach. *IEEE Transactions on Industrial Electronics*, *66*(11), 8870–8880.

Ekechukwu, D. E., & Simpa, P. (2024). The importance of cybersecurity in protecting renewable energy investment: A strategic analysis of threats and solutions. *Engineering Science & Technology Journal*, *5*(6), 1845–1883.

EL-Ebiary, A. H., Marei, M. I., Attia, M. A., & Mokhtar, M. (2024). A sensorless cyberattacks mitigation technique based on braided lyapunov state observer. *Electric Power Systems Research*, *235*, 110881. https://doi.org/10.1016/j.epsr.2024.110881

Eltigani, D., & Masri, S. (2015). Challenges of integrating renewable energy sources to smart grids: A review. *Renewable and Sustainable Energy Reviews*, *52*, 770–780.

Fard, R. N., Nademi, H., & Norum, L. (2013). Analysis of a modular multilevel inverter under the predicted current control based on finite-control-set strategy. *2013 3rd International Conference on Electric Power and Energy Conversion Systems*, 1–6. https://doi.org/10.1109/EPECS.2013.6713046

FERC Order No. 2222: Fact Sheet | Federal Energy Regulatory Commission. (n.d.). Retrieved July 27, 2025, from https://www.ferc.gov/media/ferc-order-no-2222-fact-sheet

Ferdous, Z., & Barman, S. C. (2025). *A Systematic Review of Sustainable Renewable Energy Applications, Procedures, Challenges, and Limitations*. In Review. https://doi.org/10.21203/rs.3.rs-5740831/v1

Gao, Y., Wang, S., Dragicevic, T., Wheeler, P., & Zanchetta, P. (2023). Artificial Intelligence Techniques for Enhancing the Performance of Controllers in Power Converter-Based Systems—An Overview. *IEEE Open Journal of Industry Applications*, *4*, 366–375. https://doi.org/10.1109/OJIA.2023.3338534

Garg, S., & Tyagi, S. (2024). A comprehensive review on opportunities and challenges of grid integration of renewable energy resources. *2024 Second International Conference on Smart Technologies for Power and Renewable Energy (SPECon)*, 1–6. https://doi.org/10.1109/SPECon61254.2024.10537518

Guerrero, J. M., Chandorkar, M., Lee, T.-L., & Loh, P. C. (2012). Advanced control architectures for intelligent microgrids—Part I: Decentralized and hierarchical control. *IEEE Transactions on Industrial Electronics*, *60*(4), 1254–1262.

Guerrero, J. M., Vasquez, J. C., Matas, J., De Vicuña, L. G., & Castilla, M. (2010). Hierarchical control of droop-controlled AC and DC microgrids—A general approach toward standardization. *IEEE Transactions on Industrial Electronics*, *58*(1), 158–172.

Gunduz, M. Z., & Das, R. (2020). Cyber-security on smart grid: Threats and potential solutions. *Computer Networks*, *169*, 107094. https://doi.org/10.1016/j.comnet.2019.107094

Gutiérrez-Escalona, J., Roncero-Clemente, C., Husev, O., Matiushkin, O., & Blaabjerg, F. (2024). Artificial Intelligence in the Hierarchical Control of ac, dc and Hybrid ac/dc Microgrids–A Review. *IEEE Access*. https://doi.org/10.1109/ACCESS.2024.3486382

Hannan, M. A., Ghani, Z. A., Mohamed, A., & Uddin, M. N. (2015). Real-time testing of a fuzzy-logic-controller-based grid-connected photovoltaic inverter system. *IEEE Transactions on Industry Applications*, *51*(6), 4775–4784.

Hirsch, A., Parag, Y., & Guerrero, J. (2018). Microgrids: A review of technologies, key drivers, and outstanding issues. *Renewable and Sustainable Energy Reviews*, *90*, 402–411.

Holtz, J. (1983). A predictive controller for the stator current vector of ac machines fed from a switched voltage source. *IPEC-Tokyo, 1983*, 1665–1675.

Hossain, M. A., Pota, H. R., Issa, W., & Hossain, M. J. (2017). Overview of AC Microgrid Controls with Inverter-Interfaced Generations. *Energies*, *10*(9), 1300. https://doi.org/10.3390/en10091300

IEC TS 62898-1:2017. (n.d.). Retrieved July 27, 2025, from https://webstore.iec.ch/en/publication/28363

IEEE Guide for Design, Operation, and Integration of Distributed Resource Island Systems with Electric Power Systems. (2011). https://doi.org/10.1109/IEEESTD.2011.5960751

IEEE Standard for Interconnection and Interoperability of Distributed Energy Resources with Associated Electric Power Systems Interfaces. (2018). https://doi.org/10.1109/IEEESTD.2018.8332112

Katiraei, F., Iravani, M. R., & Lehn, P. W. (2005). Micro-grid autonomous operation during and subsequent to islanding process. *IEEE Transactions on Power Delivery*, *20*(1), 248–257.

Khan, H. S., Aamir, M., Ali, M., Waqar, A., Ali, S. U., & Imtiaz, J. (2019). Finite control set model predictive control for parallel connected online ups system under unbalanced and nonlinear loads. *Energies*, *12*(4), 581.

Khan, H. S., Khan, M. K., & Kauhaniemi, K. (2025). Distributed Energy Resource Behavior During Faults: Navigating Voltage Ride-Through Compliance Within the Realm of EN 50549. *IET Generation, Transmission & Distribution*, *19*(1), e70131. https://doi.org/10.1049/gtd2.70131

Khan, M. Y. A., Liu, H., Yang, Z., Wang, J., & Zhang, Y. (2025). Hierarchical control of microgrid: A comprehensive study. *Electrical Engineering*. https://doi.org/10.1007/s00202-025-03230-4

Kim, S.-K., & Ahn, C. K. (2020). Proportional-derivative voltage control with active damping for DC/DC boost converters via current sensorless approach. *IEEE Transactions on Circuits and Systems II: Express Briefs*, *68*(2), 737–741.

Kukrer, O. (2002). Discrete-time current control of voltage-fed three-phase PWM inverters. *IEEE Transactions on Power Electronics*, *11*(2), 260–269.

Kundur, P. (2007). Power system stability. In *Leonard L. Grigsby (1st ed.) Power System Stability and Control* (pp. 1–7). CRC Press.

Lascu, C. (2020). Sliding-mode direct-voltage control of voltage-source converters with LC filters for pulsed power loads. *IEEE Transactions on Industrial Electronics*, *68*(12), 11642–11650.

Lee, C.-C. (1990). Fuzzy logic in control systems: Fuzzy logic controller. I. *IEEE Transactions on Systems, Man, and Cybernetics*, *20*(2), 404–418.

Li, H., Li, F., Xu, Y., Rizy, D. T., & Kueck, J. D. (2010). Adaptive voltage control with distributed energy resources: Algorithm, theoretical analysis, simulation, and field test verification. *IEEE Transactions on Power Systems*, *25*(3), 1638–1647.

Li, Q., Zhou, Y., Wei, F., Li, S., Wang, Z., Li, J., Zhou, G., Liu, J., Yan, P., & Yu, D. (2024). Multi-time scale scheduling for virtual power plants: Integrating the flexibility of power generation and multi-user loads while considering the capacity degradation of energy storage systems. *Applied Energy*, *362*, 122980. https://doi.org/10.1016/j.apenergy.2024.122980

Li, X., Lin, P., Tang, Y., & Wang, K. (2018). Stability design of single-loop voltage control with enhanced dynamic for voltage-source converters with a low LC-resonant-frequency. *IEEE Transactions on Power Electronics*, *33*(11), 9937–9951.

Li, Y., Sahoo, S., Dragičević, T., Zhang, Y., & Blaabjerg, F. (2023). Stability-oriented design of model predictive control for DC/DC boost converter. *IEEE Transactions on Industrial Electronics*, *71*(1), 922–932.

Li, Z., Zang, C., Zeng, P., Yu, H., Li, S., & Bian, J. (2016). Control of a grid-forming inverter based on sliding-mode and mixed ${H_2}/{H_\backslashinfty} $ control. *IEEE Transactions on Industrial Electronics*, *64*(5), 3862–3872.

Liu, J., Wei, T., Chen, N., Liu, W., Wu, J., & Xiao, P. (2022). A neural network PID controller with dynamic structure adjustment for DC-DC switching converters. *2022 7th International Conference on Integrated Circuits and Microsystems (ICICM)*, 356–360. https://doi.org/10.1109/ICICM56102.2022.10011394

Liu, Q., Caldognetto, T., & Buso, S. (2020). Review and Comparison of Grid-Tied Inverter Controllers in Microgrids. *IEEE Transactions on Power Electronics*, *35*(7), 7624–7639. https://doi.org/10.1109/TPEL.2019.2957975

Liu, X., Qiu, L., Fang, Y., Wang, K., Li, Y., & Rodriguez, J. (2023). Finite control-set learning predictive control for power converters. *IEEE Transactions on Industrial Electronics*, *71*(7), 8190–8196.

Long, B., Lu, P. J., Chong, K. T., Rodriguez, J., & Guerrero, J. M. (2021). Robust fuzzy-fractional-order nonsingular terminal sliding-mode control of LCL-type grid-connected converters. *IEEE Transactions on Industrial Electronics*, *69*(6), 5854–5866.

Lopes, J. P., Moreira, C. L., & Madureira, A. G. (2006). Defining control strategies for microgrids islanded operation. *IEEE Transactions on Power Systems*, *21*(2), 916–924.

Marnay, C., Chatzivasileiadis, S., Abbey, C., Iravani, R., Joos, G., Lombardi, P., Mancarella, P., & von Appen, J. (2015). Microgrid Evolution Roadmap. *2015 International Symposium on Smart Electric Distribution Systems and Technologies (EDST)*, 139–144. https://doi.org/10.1109/SEDST.2015.7315197

Maruta, H., Taniguchi, H., & Kurokawa, F. (2016). A study on effects of different control period of neural network based reference modified pid control for DC-DC converters. *2016 15th IEEE International Conference on Machine Learning and Applications (ICMLA)*, 460–465. https://doi.org/10.1109/ICMLA.2016.0081

Mattavelli, P. (2005). An improved deadbeat control for UPS using disturbance observers. *IEEE Transactions on Industrial Electronics*, *52*(1), 206–212.

Meegahapola, L., Mancarella, P., Flynn, D., & Moreno, R. (2021). Power system stability in the transition to a low carbon grid: A techno-economic perspective on challenges and opportunities. *WIREs Energy and Environment*, *10*(5), e399. https://doi.org/10.1002/wene.399

Mehrizi-Sani, A., & Iravani, R. (2010). Potential-function based control of a microgrid in islanded and grid-connected modes. *IEEE Transactions on Power Systems*, *25*(4), 1883–1891.

Miveh, M. R., Rahmat, M. F., Ghadimi, A. A., & Mustafa, M. W. (2016). Control techniques for three-phase four-leg voltage source inverters in autonomous microgrids: A review. *Renewable and Sustainable Energy Reviews*, *54*, 1592–1610. https://doi.org/10.1016/j.rser.2015.10.079

Mohamed, I. S., Rovetta, S., Do, T. D., Dragicević, T., & Diab, A. A. Z. (2019). A neural-network-based model predictive control of three-phase inverter with an output LC filter. *IEEE Access*, *7*, 124737–124749.

Moradi-Khaligh, E., Karimi, S., & Sadabadi, M. S. (2025). Robust LMI-based voltage control strategy for DC microgrids under disturbances and constant power load uncertainties. *Electric Power Systems Research*, *241*, 111333. https://doi.org/10.1016/j.epsr.2024.111333

Morari, M., & Lee, J. H. (1999). Model predictive control: Past, present and future. *Computers & Chemical Engineering*, *23*(4–5), 667–682.

Moroz, A., & Lyeonov, S. (2024). Stimulating Financial-Fiscal Instruments of Supporting Development of Renewable Energy Sources: Bibliometric Analysis. *Financial Markets, Institutions and Risks*, *8*(4), 179–203.

Mousavi, Y., Bevan, G., Kucukdemiral, I. B., & Fekih, A. (2022). Sliding mode control of wind energy conversion systems: Trends and applications. *Renewable and Sustainable Energy Reviews*, *167*, 112734. https://doi.org/10.1016/j.rser.2022.112734

Mutschler, P. (1998). A new speed-control method for induction motors. *Proc. Conf. Rec. PCIM*, 131–136.

Nguyen, N., Pandit, D., Quigley, R., & Mitra, J. (2021). Frequency Response in the Presence of Renewable Generation: Challenges and Opportunities. *IEEE Open Access Journal of Power and Energy*, *8*, 543–556. https://doi.org/10.1109/OAJPE.2021.3118393

Novak, M., Nyman, U. M., Dragicevic, T., & Blaabjerg, F. (2018). Analytical design and performance validation of finite set MPC regulated power converters. *IEEE Transactions on Industrial Electronics*, *66*(3), 2004–2014.

Novak, M., Nyman, U. M., Dragicevic, T., & Blaabjerg, F. (2019). Statistical model checking for finite-set model predictive control converters: A tutorial on modeling and performance verification. *IEEE Industrial Electronics Magazine*, *13*(3), 6–15.

Obeidi, N., Kermadi, M., Belmadani, B., Allag, A., Achour, L., & Mekhilef, S. (2022). A Current Sensorless Control of Buck-Boost Converter for Maximum Power Point Tracking in Photovoltaic Applications. *Energies*, *15*(20), 7811. https://doi.org/10.3390/en15207811

Olivares, D. E., Mehrizi-Sani, A., Etemadi, A. H., Cañizares, C. A., Iravani, R., Kazerani, M., Hajimiragha, A. H., Gomis-Bellmunt, O., Saeedifard, M., & Palma-Behnke, R. (2014). Trends in microgrid control. *IEEE Transactions on Smart Grid*, *5*(4), 1905–1919.

Palizban, O., & Kauhaniemi, K. (2015). Hierarchical control structure in microgrids with distributed generation: Island and grid-connected mode. *Renewable and Sustainable Energy Reviews*, *44*, 797–813.

Power Grid Efficiency—Sources of Grid Losses. (2022, August 12). *Cogeneration.Pro*. https://cogeneration.pro/energy-losses-and-inefficiencies-in-the-traditional-power-grid/

Rajakumar, V., Anbukumar, K., & Selwynraj A, I. (2020). Sliding mode controller-based voltage source inverter for power quality improvement in microgrid. *IET Renewable Power Generation*, *14*(11), 1860–1872. https://doi.org/10.1049/iet-rpg.2019.1305

Rashid, S. M. (2024). Employing advanced control, energy storage, and renewable technologies to enhance power system stability. *Energy Reports*, *11*, 3202–3223. https://doi.org/10.1016/j.egyr.2024.03.009

Rathnayake, D. B., Akrami, M., Phurailatpam, C., Me, S. P., Hadavi, S., Jayasinghe, G., Zabihi, S., & Bahrani, B. (2021). Grid forming inverter modeling, control, and applications. *Ieee Access*, *9*, 114781–114807.

Rocabert, J., Luna, A., Blaabjerg, F., & Rodriguez, P. (2012). Control of power converters in AC microgrids. *IEEE Transactions on Power Electronics*, *27*(11), 4734–4749.

Rodriguez, J., & Cortes, P. (2012). *Predictive control of power converters and electrical drives*. John Wiley & Sons.

Roser, M. (2020). Why did renewables become so cheap so fast? *Our World in Data*. https://ourworldindata.org/cheap-renewables-growth

Sani, S. B., Celvakumaran, P., Ramachandaramurthy, V. K., Walker, S., Alrazi, B., Ying, Y. J., Dahlan, N. Y., & Rahman, M. H. A. (2020). Energy storage system policies: Way forward and opportunities for emerging economies. *Journal of Energy Storage*, *32*, 101902. https://doi.org/10.1016/j.est.2020.101902

Shrivastava, S., & Subudhi, B. (2020). Comprehensive review on hierarchical control of cyber-physical microgrid system. *IET Generation, Transmission & Distribution*, *14*(26), 6397–6416. https://doi.org/10.1049/iet-gtd.2020.0971

Singh, S., Gautam, A. R., & Fulwani, D. (2017). Constant power loads and their effects in DC distributed power systems: A review. *Renewable and Sustainable Energy Reviews*, *72*, 407–421. https://doi.org/10.1016/j.rser.2017.01.027

Sun, X., Xu, D., Leung, F. H., Wang, Y., & Lee, Y.-S. (1999). Design and implementation of a neural-network-controlled UPS inverter. *IECON'99. Conference Proceedings. 25th Annual Conference of the IEEE Industrial Electronics Society (Cat. No. 99CH37029)*, *2*, 779–784. https://doi.org/10.1109/IECON.1999.816499

Tang, Z., Yang, Y., & Blaabjerg, F. (2022). Power electronics: The enabling technology for renewable energy integration. *CSEE Journal of Power and Energy Systems*, *8*(1), 39–52. https://doi.org/10.17775/CSEEJPES.2021.02850

Tavan, M., Sabahi, K., Shahparasti, M., Hajizadeh, A., Soltani, M., & Savaghebi, M. (2023). Sensorless Control of a Single-Phase AC–DC Boost Converter Without Measuring Input Voltage and Current. *IEEE Access*, *11*, 59059–59070.

Ton, D. T., & Smith, M. A. (2012). The U.S. Department of Energy's Microgrid Initiative. *The Electricity Journal*, *25*(8), 84–94. https://doi.org/10.1016/j.tej.2012.09.013

Twining, E., & Holmes, D. G. (2003). Grid current regulation of a three-phase voltage source inverter with an LCL input filter. *IEEE Transactions on Power Electronics*, *18*(3), 888–895.

Wan, Y., Zhang, Y., & Xu, Q. (2025). Computationally Efficient Long-Horizon Predictive Control for Power Converter: A Reinforcement Learning Approach. *IEEE Transactions on Industrial Electronics*, 1–12. https://doi.org/10.1109/TIE.2025.3555033

Wang, D., Shen, Z. J., Yin, X., Tang, S., Liu, X., Zhang, C., Wang, J., Rodriguez, J., & Norambuena, M. (2021). Model predictive control using artificial neural network for power converters. *IEEE Transactions on Industrial Electronics*, *69*(4), 3689–3699.

Wang, Y., Qiu, D., Teng, F., & Strbac, G. (2025). Two-Stage TSO-DSO Services Provision Framework for Electric Vehicle Coordination. *IEEE Transactions on Power Systems*, *40*(4), 3117–3130. https://doi.org/10.1109/TPWRS.2024.3510653

Wu, D., Seo, G.-S., Xu, L., Su, C., Kocewiak, L., Sun, Y., & Qin, Z. (2024). Grid Integration of Offshore Wind Power: Standards, Control, Power Quality and Transmission. *IEEE Open Journal of Power Electronics*, *5*, 583–604. https://doi.org/10.1109/OJPEL.2024.3390417

Wu, L., Liu, J., Vazquez, S., & Mazumder, S. K. (2022). Sliding Mode Control in Power Converters and Drives: A Review. *IEEE/CAA Journal of Automatica Sinica*, *9*(3), 392–406. https://doi.org/10.1109/JAS.2021.1004380

Xu, J., Xie, S., & Tang, T. (2014). Improved control strategy with grid-voltage feedforward for LCL-filter-based inverter connected to weak grid. *IET Power Electronics*, *7*(10), 2660–2671. https://doi.org/10.1049/iet-pel.2013.0666

Yaramasu, V., Rivera, M., Wu, B., & Rodriguez, J. (2012). Model predictive current control of two-level four-leg inverters—Part I: Concept, algorithm, and simulation analysis. *IEEE Transactions on Power Electronics*, *28*(7), 3459–3468.

Yaramasu, V., & Wu, B. (2013). Predictive control of a three-level boost converter and an NPC inverter for high-power PMSG-based medium voltage wind energy conversion systems. *IEEE Transactions on Power Electronics*, *29*(10), 5308–5322.

Zafra, E., Vazquez, S., Dragičević, T., Alcaide, A. M., Leon, J. I., & Franquelo, L. G. (2023). Prediction window selection in FCS-MPC for two-level VSI applications. *IEEE Transactions on Power Electronics*, *39*(3), 3135–3143.

Zafra, E., Vazquez, S., Geyer, T., Aguilera, R. P., & Franquelo, L. G. (2023). Long prediction horizon FCS-MPC for power converters and drives. *IEEE Open Journal of the Industrial Electronics Society*, *4*, 159–175.

Zafra, E., Vazquez, S., Geyer, T., Aguilera, R. P., Freire, E., & Franquelo, L. G. (2024). Computational analysis of the long horizon FCS-MPC problem for power converters. *IEEE Transactions on Power Electronics*, *39*(10), 12762–12773.

Zhang, C., & Lu, Y. (2021). Study on artificial intelligence: The state of the art and future prospects. *Journal of Industrial Information Integration*, *23*, 100224.

Zhang, Z. (2024). Combined Cycle Power Plants and Renewable Energy Integration—Hybrid Systems for Sustainable Energy Solutions. *Highlights in Science, Engineering and Technology*, *120*, 586–591. https://doi.org/10.54097/r5awxf20

Ziouani, I., Boukhetala, D., Darcherif, A.-M., Amghar, B., & El Abbassi, I. (2018). Hierarchical control for flexible microgrid based on three-phase voltage source inverters operated in parallel. *International Journal of Electrical Power & Energy Systems*, *95*, 188–201. https://doi.org/10.1016/j.ijepes.2017.08.027

Design and Implementation of Model Predictive Control for Parallel Distributed Energy Resource in Islanded AC Microgrids.

Hussain Sarwar Khan
School of Technology and Innovations
University of Vaasa
Vaasa, Finland
Hussain.khan@uwasa.fi

Jagdesh Kumar
School of Technology and Innovations
University of Vaasa
Vaasa, Finland
jagdesh.kumar@uwasa.fi

Kimmo Kauhaniemi
School of Technology and Innovations
University of Vaasa
Vaasa, Finland
kimmo.kauhaniemi @uwasa.fi

***Abstract*— This study proposes the voltage control strategy for distributed energy resource (DER) in islanded AC microgrids (MG). Typically, AC MG can maintain a constant voltage at the point of common coupling (PCC) as well as perform power-sharing among the DERs. However, linear controllers have several restrictions such as slow transient response, poor disturbance rejection capability etc. Therefore, this study presents an FCS-MPC for a DER with effective voltage regulation capability. The investigated work demonstrates excellent steady-state performance, a low computational burden, better response under transients and have low switching frequency as compared to linear control. First, the benefits of FCS-MPVC for single DER has been studied, then the same topology along with droop control is employed for multiple DERs in AC MG to serve the load. Droop control shows improved power-sharing among the DERs. The performance of the proposed control technique is demonstrated through MATLAB/Simulink simulations for single DG and AC MG under linear, non-linear loading conditions.**

Keywords*— *Distributed Energy Resource (DER) Model Predictive Control (MPC); Primary Control of MG.

I. Introduction

Microgrids (MG) is one of the fundamental technologies which make the electrical grids more intelligent, flexible, and distributed and the incursion of distributed energy resources (DERs) is possible in electrical grids. MG is a localized cluster of adaptive loads, distributed energy storage, and distributed generation (DG) and has effective control. MG with installed DGs able to work in islanded and grid-connected (GC) mode or both. In GC mode, MG can be utilized to provide auxiliary services to power systems such as voltage support, peak load shaving, and load shifting [1, 2]. In the case of a power outage from the utility grid or low power quality, MG can seamlessly disconnect from the utility grid and pursue to provide high-quality power to load in standalone mode. The standalone mode can be further classified into two categories in the context of time. Temporary standalone mode occurs due to preplanned maintenance or due to spontaneous failure in transmission lines between MG and utility grid.

The permanent islanded mode is capable to supply power to remote communities, where energy from the electrical grid is not favourable [3]. In this study, permanent islanded MG is considered. Direct current (DC) MG has a more appealing feature in terms of efficiency, control, and simplicity than AC MG, but the wide majority of load requires ac supply [4]. Consequently, it is mandatory to establish ac MG architecture. AC and DC parts of MG is interfaced through voltage source converters (VSC) [5]. For critical load applications, paralleled connected VSCs operation present redundancy, high reliability, and flexibility. In many cases, it is effectively viable to distribute a high power load between several VSC despite using power devices with a high rating. Commonly, VSCs are connected parallelly to form AC MG.

For the parallel operation of multiple DGs in islanded mode, it is highly expedient to design a decentralized controller, i.e., no external communication network between VSC based DGs. Therefore, a droop control approach is commonly employed and serves as an outer loop. It produces a voltage reference that is delivered to the corresponding VSCs inner loop. The inner loop consists of a voltage compensation loop. The purpose of the voltage regulation loop is to compensate for the output voltage of VSC according to reference. For the voltage control loop of VSC in MG, a linear control along with pulse with modulation (PWM) is widely found in literature and vastly used by the power electronics industry. However, these control techniques have many practical restrictions, and they are incapable of reducing the steady-state error to zero and also had not the capacity to overcome the nonlinearity of the system [6]. Hysteresis control is a type of non-linear controller, it takes the error to zero within a few-cycle and has variable switching frequency, which produces severe stress on VSI switches. This stress decreases the life of the inverter [7, 8].

Finite control Set Model predictive control (FCS-MPC) is a digital control method, and its basic principle is different from linear control. It uses the discrete model of VSC along with its filter to determine the future behavior for all possible input combinations. One of the inputs, which have the least value of predefined cost function (CF) is selected to be applied for the next sampling instant instead of drafting a separate loop for each controlled variable and cascading them together as in linear control system. CF is a square of the Euclidean distance between controlled and reference signals. MPC with load current observer is presented in [9]. The control technique proposed in [9] is quite simple, but the total harmonic distortion (THD) of the output voltage is high. In [10], predictive control is presented, and the author has not investigated the performance

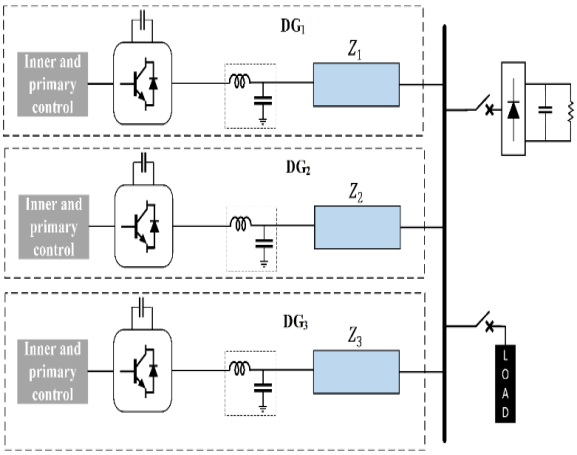

Figure 1. Islanded MG contains Three DG's with VSI and different type of loads.

of the control technique for the non-linear load. The robustness, exemplary transient behavior and easy inclusion of non-linearities make the FCS-MPC the best alternative for the control of power converters [11].

This paper presents a robust voltage control approach for VSC to control the output voltage of single and also for multiple DGs in an islanded MG. The key contributions in this paper are summarized as follows: The proposed two-step prediction FCS-MPVC for single DG in the islanded mode of MG. Discuss the results of single DG with the proposed control technique under different loading conditions and shows that the proposed controller has improved both steady-state response and transient response. The droop control is employed for accurate power-sharing between the DGs in AC MG. Moreover, the proposed control strategy capability is examined for multiple DG units. The real-time simulation is accomplished in the MATLAB/Simulink environment.

The rest of the paper is presented as follows: The proposed control strategy is explained and it provides the comprehensive mathematical model of two-level VSC with linked LC filter and the discretization aspects of FCS-MPC implementation are discussed in section II. Further, the FCS-MPC working and operation are explained in this section. In section III presents droop control and its boundaries. In Section IV, the detailed simulation results are presented. Finally, the last section comprises the conclusion.

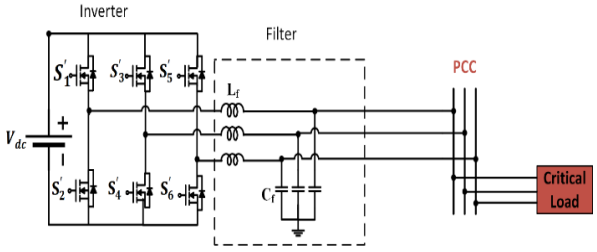

Figure 2. Circuit diagram of VSC having filter serving load at PCC.

II. MODELLING OF THE DER SYSTEM

Fig.1 shows that three VSIs are connected with a common ac bus through a transmission line with impedance and serving local loads. This section explained the proposed system configuration in which VSCs work and describe the discrete-time converter and its filter model which is used by MPC to find the optimal action by minimizing the CF and optimal control action is anticipated for next sampling time. A precise mathematical model of VSC and filter is required to attain adequate control performance. Mainly in AC MG, two-level VSC topology is used and, as shown in Fig. 2 and also presents a constant dc source that is connected with VSC. The output LC filter is used to eliminate the high-frequency components, which are undesirable.

VSC modelling is done in the stationary orthogonal frame of reference. The following initial conditions are considered: the VSC is in a balanced state. Three phases x-y-z are transformed into αβ frame by using Clarke transformation X:

$$\bar{v}=v_\alpha+jv_\beta=\bar{T}[v_x,v_y,v_z] \quad (1)$$

$$\bar{i}=i_\alpha+ji_\beta=\bar{T}[i_x,i_y,i_z]' \quad (2)$$

$$\bar{T}=\frac{1}{3}\left[1 \quad e^{j\frac{2}{3}\pi} \quad e^{j\frac{4}{3}\pi}\right] \quad (3)$$

A. Converter Model

It consists of three legs (S_x,S_y,S_z) and each leg has two switches, so there are two possible switching states for each leg, which are described below:

$$S_x=\begin{cases}1, \text{ if } S_1' \text{ is ON and } S_4' \text{ is OFF}\\ 0, \text{if } S_1' \text{ is OFF and } S_4' \text{ is ON}\end{cases} \quad (4)$$

$$S_y=\begin{cases}1, \text{ if } S_2' \text{ is ON and } S_5' \text{ is OFF}\\ 0, \text{if } S_2' \text{ is OFF and } S_4' \text{ is ON}\end{cases} \quad (5)$$

$$S_z=\begin{cases}1, \text{ if } S_3' \text{ is ON and } S_6' \text{ is OFF}\\ 0, \text{if } S_3' \text{ is OFF and } S_6' \text{ is ON}\end{cases} \quad (6)$$

However, two-level VSC has eight possible switching arrangements. the voltage between N point and leg can be computed by taking the product of dc-link voltage with the present state of the corresponding leg:

$$\begin{aligned}v_{xN}&=S_x.v_{dc}\\ v_{yN}&=S_y.v_{dc}\\ v_{zN}&=S_z.v_{dc}\end{aligned} \quad (7)$$

To find the voltage between phase to neutral (from x, y, z to n point) by subtracting the common voltage from (6). A common voltage is determined by applying the concept of Kirchhoff's voltage law:

$$v_{nN}=\frac{v_{xN}+v_{yN}+v_{zN}}{3} \quad (8)$$

Phase voltage is:

$$v_{xn}=v_{xN}-v_{nN} \quad (9)$$

$$v_{yn}=v_{yN}-v_{nN}$$

$$v_{zn}=v_{zN}-v_{nN}$$

Clark transformation is applied to find eight possible switching states. Which are shown in Table 1.

Table 1. Switching arrangement of VSI.

Space-Vector		On-state switches	Vector placing
Zero Vector	$\overrightarrow{V_{0,7}}$	S_1', S_3', S_5' S_4', S_6, S_2'	$\overline{v_{0,7}}=0$
Active Vector	$\overrightarrow{V_1}$	S_1', S_6', S_2	$\overline{v_1}=\frac{2}{3}v_{dc}$
	$\overrightarrow{V_2}$	S_1', S_3', S_2	$\overline{v_2}=\frac{1}{3}v_{dc}+j\frac{\sqrt{3}}{3}v_{dc}$
	$\overrightarrow{V_3}$	S_4', S_3', S_2	$\overline{v_3}=-\frac{1}{3}v_{dc}+j\frac{\sqrt{3}}{3}v_{dc}$
	$\overrightarrow{V_4}$	S_4', S_3', S_5'	$\overline{v_4}=-\frac{2}{3}v_{dc}$
	$\overrightarrow{V_5}$	S_1', S_5', S_4'	$\overline{v_5}=-\frac{1}{3}v_{dc}-j\frac{\sqrt{3}}{3}v_{dc}$

B. LC Filter

To eliminate the switching harmonics, an LC filter is coupled at the VSI's output terminal, as shown in Fig. 2. The filter is consisting of an inductor with an inductance L_f , damping resistance R_f having current i_f, and a capacitor with capacitance C_f and the voltage across the capacitor is v_{pc}. i_f and v_{pc} are the state variables in this system. The filter response is explained by (10) and (11). Eq (10) describes the inductive nature, and the capacitance nature of the filter is defined by (11). Both equations are stated as:

$$L_f\frac{di_f}{dt}=v_t-v_{PC}-i_fR_f \quad (10)$$

$$C_f\frac{dV_{pc}}{dt}=i_f-i_0 \quad (11)$$

$$\frac{d}{d}\begin{bmatrix} i_f \\ v_{PC}\end{bmatrix}=\mathbf{A}\begin{bmatrix} i_f \\ v_{PC}\end{bmatrix}+\mathbf{B}\begin{bmatrix} v_t \\ i_0\end{bmatrix} \quad (12)$$

$$\mathbf{A}=\begin{bmatrix} \frac{-R_f}{L_f} & \frac{-1}{C_f} \\ \frac{1}{C_f} & 0\end{bmatrix} \quad (13)$$

$$\mathbf{B}=\begin{bmatrix} \frac{1}{L_f} & \mathbf{0} \\ \mathbf{0} & -\frac{1}{c_f}\end{bmatrix} \quad (14)$$

C. Discrete-Time Modelling of Filter.

To implement the proposed control on the digital platform, the continuous-time state-space model is converted to discrete-time state-space model. Discretization techniques are usually used, but this study uses the zero-order hold (ZOH) technique. This technique provides the direct conversion of the CTSS model to the DTSS model for every sampling in stair-case inputs. In this paper, a couple of assumption is made such as the value of dc-link voltage (V_{dc}) is a constant. Eq (12) is converted into the discrete time mathematical model and is written as:

$$\begin{bmatrix} i_f(t_k+1) \\ v_{PC}(t_k+1)\end{bmatrix}=\mathbf{A_d}\begin{bmatrix} i_f(t_k) \\ v_{PC}(t_k)\end{bmatrix}+\mathbf{B_d}\begin{bmatrix} v_t(t_k) \\ i_0(t_k)\end{bmatrix} \quad (15)$$

$$\mathbf{A_d}=e^{AT_s} \quad (16)$$

$$\mathbf{B_d}=\int_0^{T_s} e^{A\tau}\ B\ d_\tau \quad (17)$$

T_s is sampling instant. It is assumed that T_s is very small so the exponential matrix is approximated as:

$$e^{AT_s}\approx 1+AT_s \quad (18)$$

By using (15), the capacitor voltage at instant (t_k+1) can be determined by the following equation:

$$v_{pc}(t_k+1)=v_{pc}(t_k)+\frac{T_s}{C_f}(i_f(t_k)-i_0(t_k)) \quad (19)$$

To regulate the capacitor voltage. The cost function is defined as:

$$g_v=(v^*_{pc,\alpha}(t_k)-v_{pc,\alpha}(t_k+2))^2+(v^*_{pc,\beta}(t_k)-v_{pc,\beta}(t_k+2))^2 \quad (20)$$

$v_{pc,\alpha}$ and $v_{pc,\beta}$ are real and imaginary parts of predicted capacitor voltage. Among all the voltage vectors, a vector that has a minimum value of g_v can be applied to the next sampling instant.

III. Droop Control

Originally each DG is designed to generate power according to its reference at the base frequency, i.e., 60 Hz in this study, In the case of Islanded MG, the main aim of the local controller of DG is to compensate the voltage and frequency within MG. But there is a need for the secondary controller to control the voltage and frequency of MG. Droop control is extensively adopted in MG to control the voltage and frequency and for proper sharing of active and reactive power between the DGs [12]. In this work, droop control is used for accurate sharing of the active and reactive power of each DG proportional to its ratings. Droop control can be expressed as follows:

$$V_{ref}=V_{nom}-k_qQ_{cal} \quad (21)$$

$$f_{ref}=f_{nom}-k_pP_{cal} \quad (22)$$

Where, V_{ref} and f_{ref} are reference voltage amplitude and frequency used to synthesis the $V_{ref,\alpha\beta}$. V_{nom} and f_{ref} are nominal voltage amplitude and frequency. Following equations are used to calculate the P_{cal} and Q_{cal} as:

$$P_{cal}=v_{pc,\alpha}i_{0,\alpha}+v_{pc,\beta}i_{0,\beta} \quad (23)$$

$$Q_{cal}=v_{pc,\beta}i_{0,\alpha}-v_{pc,\alpha}i_{0,\beta} \quad (24)$$

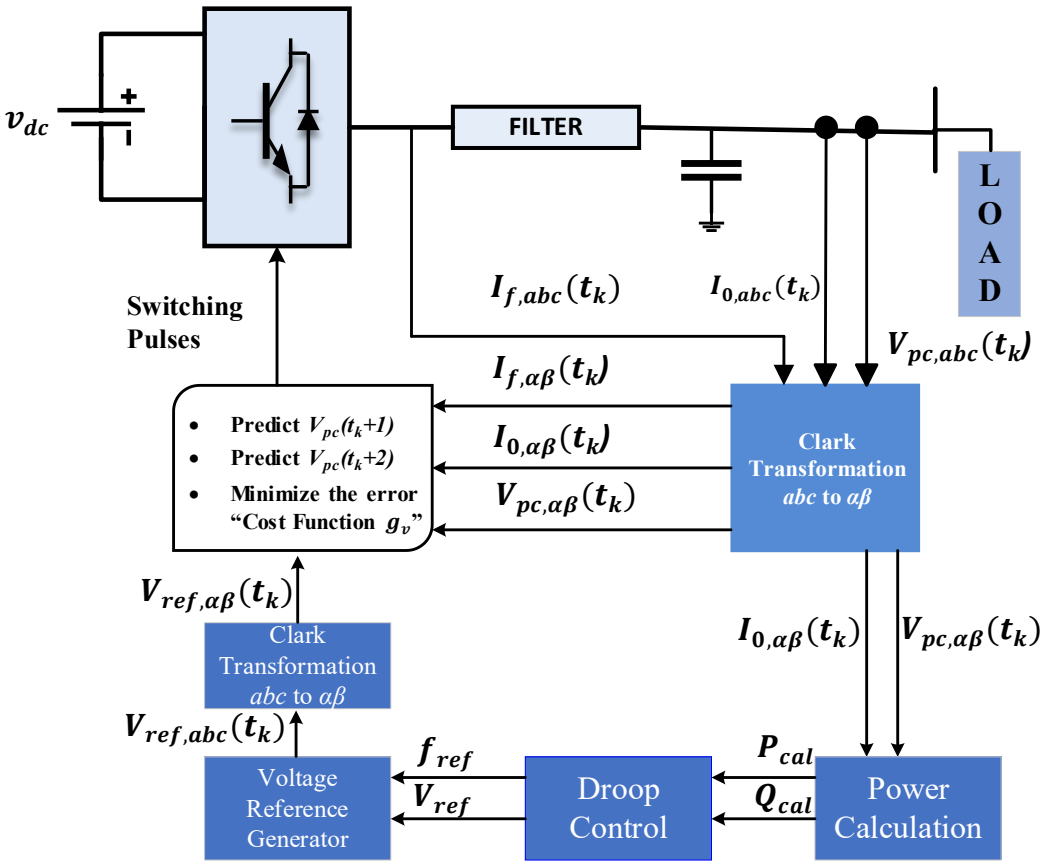

Figure 3. Block diagram of investigating control scheme along with droop control in islanded mode of MG.

Power can be determined by using (23) and (24) then it is processed through a lowpass filter to attenuate the oscillations. However, the lowpass filter has produced delays during transients. k_p and k_q are droop power coefficients. Voltage regulation and coefficients show an inverse relationship. So, there is a trade-off between them to find the best possible solution Droop curves is also based on voltage delta and coefficients of droop. Coefficients of droop is stated as:

$$k_q = \frac{\Delta V}{Q_{max}} \quad (25)$$

$$k_p = \frac{\Delta f}{P_{max}} \quad (26)$$

ΔV and Δf are extremely allocated divergence of voltage and frequency. Q_{max} and P_{max} are the maximum reactive and active power rating of the DER. The control technique expressed in (20) and (21) is normally known as conventional droop control, and it is fully decentralized. But it has several practical restrictions.

IV. SIMULATION RESULTS

For validation of control technique, extensive real-time simulations are carried out in MATLAB/Simulink for both single inverter and tested MG. Different simulations scenarios are performed to evaluate the capabilities under various load conditions. Different types of loads, such as linear and non-linear loads, are considered in this study. The linear load consists of a three-phase RL load with the active and reactive power demand of P= 18 kW and Q= 7 kvar.

In order to verify the claimed novelties such as the response of the proposed control approach and its robustness, scenario-based simulation is done in MATLAB/Simulink. First of all, the performance of DER with the proposed controller is verified under the steady-state condition, and voltage reference is a sinusoidal wave. Afterwards, Different tests, such as linear and non-linear loading condition, disturbance in the system due to change of load, are performed to verify the stability and robustness of the controller. In the end, two DERs are working in parallel along with the proposed controller in the inner loop and droop control is implemented as part of primary control of MG. Droop control is used to share accurate power between the DGs. Fig. 3 demonstrates the whole implementation of proposed control technique for single DG in AC MG.

Table 2. Simulation Parameters.

DC link Voltage	v_{dc}=1000V
Sampling Time	T_s=20μs

LC-filter	C_f=250μF,L_f=2mH
Damping Resistance	R_f=0.94Ω
Linear load	P=18kW,Q=7kVar
Non-linear load (diode rectifier)	P=10kW,Q=4kVar
Nominal Voltage	V_{nom}=318V
Rated Frequency	f_{nom}=60Hz
Droop coefficients	k_q=0.001,k_p=0.001

A. Steady-State Analysis

Fig 4 illustrates the result of a DER under normal conditions when linear RL load is connected. DER supplied the 18-kW active and 7 kVar reactive power to meet the load demand. The frequency of the MG is 60 Hz and the RMS voltage are set to 220V. Load current and voltage are sine waves with little harmonics. The THD of the voltage in this study is 0.90 %, which is within the acceptable limit of IEEE criteria. It is also compared with standard literature, in which MPVC is implemented for two level inverter and 2.93 % is Voltage THD found under linear load in [13]. . In order to test the performance of the controller under non-linear load. The results of non-linear load connected with the system is illustrated in Fig. 5. Due to non-linear load, the current of DG becomes distorted but the voltage remains sine wave with the THD of 1.23%. So, the investigating scheme easily handles the non-linearity of the system.

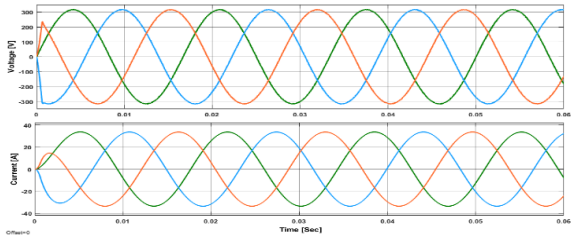

Fig.4. Load current and output voltage of single DG under linear load.

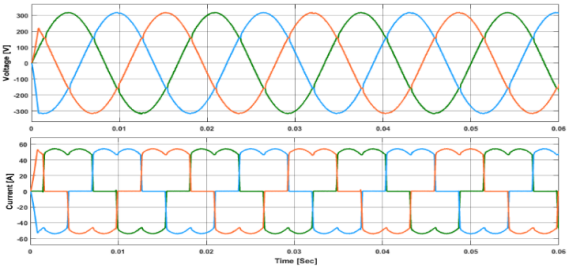

Fig.5. Load current and output voltage of single DG under nonlinear load.

B. Load Tresients Study

In this section, the load transient performance is evaluated to determine the system transient response and overshoot under varying load conditions from 100% load to 0% load and vice versa. Fig. 6 demonstrates the controller response under sudden change of load from no load to full load and vice-versa. It is seen from the results at time t=0.03s total load is disconnected from the bus and now the system is under no-load condition. Again, at the time, t= 0.04s all load is again connected to the system, but during the whole time, the output voltage of the system remains unaffected.

The same test is performed for the non-linear load. Fig. 7 shows that at time t=0.03s load is disconnected from the system, and it becomes under no-load condition. But it is noticed that output voltage shows a spike and remains sinusoidal., The performance of the proposed controller under various loading conditions are tested and verified through the simulations results.

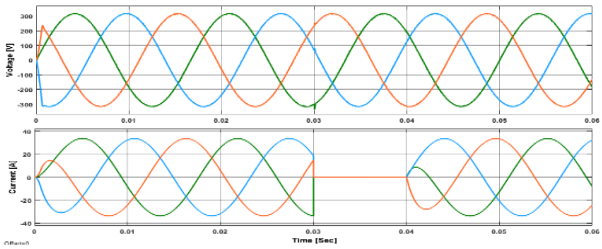

Fig. 6. Output voltage and load current under linear load variations.

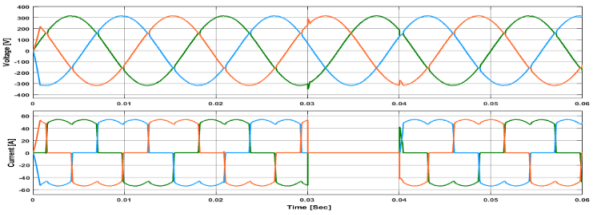

Fig. 7. Output voltage and load current under non-linear load transients.

C. Multiple DGs: Results and Discussion

After validation of proposed control for single DER, this technique is finally developed for two inverters connected in parallel to serve an available load, and simulation is done in MATLAB/Simulink environment. The results are discussed below. At the same time, classical droop-control is also implemented at the upper level of primary control to share the proper power among the DERs. To increase the system stability and for cost reduction, different rating DG are connected together in MG. The features of power-sharing and load transients are investigating. Power-sharing among the inverters are presented in Fig. 8. It expressed that active and reactive power sharing among the DGs. At time t= 0.03s, power demand becomes double. In order to meet load demand, both DGs immediately increase their power production. Fig. 8 (a), (b), (e), and (f) illustrate the resulted current and voltage of DG_1 and DG_2. It is to be shown that at t=0.03s due to an increase in demand, the current of both inverters increases, and voltage remains throughout the time. The droop equally shares active and reactive power because both DGs are of equal rating. All simulation results verify that MPC is more robust and far superior to any other classical linear controller. Table 3 explains the comparison in terms of THD and controller complexity among non-linear and linear control techniques. The presented control technique has a better transient response, low voltage THD, and has the capability to handle the nonlinearity.

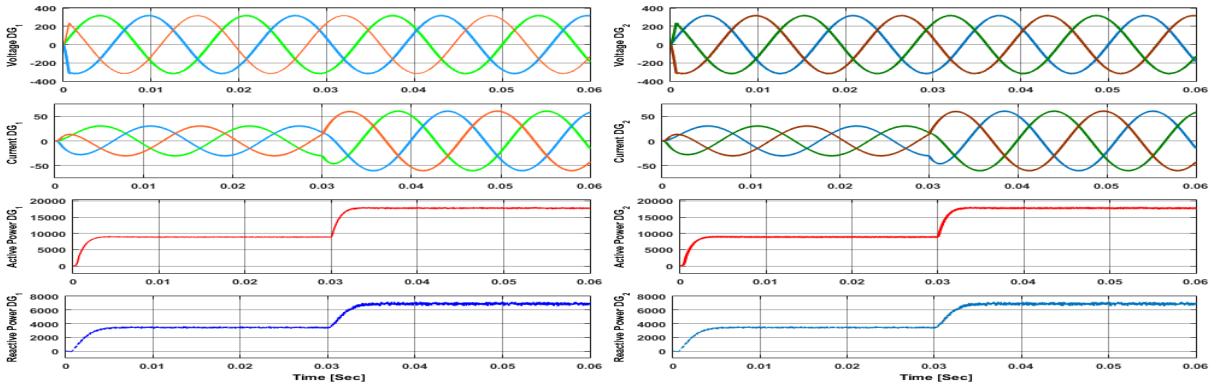

Fig. 8. voltage, load current, active and reactive power of both DG_1 and DG_2 under load transients.

Table 3. Comparison of different control methods.

References	Techniques Implemented	Voltage Quality with Linear-Load (THD)	Voltage Quality with NonLinear-Load (THD)	Implementation Complexity
[14]	Proportional Integral	16	42	Low
[15]	Dead-beat	2.1	4.8	Medium
[16]	Proportional Resonant	1.4	4.6	Low
[17]	Slide Mode Control	--	2.66	High
[18]	Classical MPC	5.1	6.7	High
[9]	Observer based MPC	2.82	3.8	Medium
[13]	Implicit based MPC	2.93	Not studied	Medium
Proposed	**Improved FCS-MPC**	**0.90**	**1.23**	**Medium**

V. Conclusion

The improved FCS-MPC based voltage control has been studied for single and multiple DERs in AC MG. The performance of the proposed predictive controller has been verified by executing the various simulations in the MATLAB/Simulink. Simulation results demonstrate that the proposed controller attains excellent voltage regulation under linear loads and non-linear loads. The proposed controller doesn't need any external or internal parameters for adjustment. It only requires the system model to predicts the controlled variables. Additionally, no modulator is required. Thus the gate signals are directly provided by the controller. The proposed controller offers flexibility and eliminates the cascaded configuration to control output voltage directly. Droop control is implemented for accurate power-sharing among the DGs. The results verify the response and effectiveness of droop-control to share the proper power among the DERs in both steady-state and transient conditions under linear and non-linear loading conditions.

Acknowledgment

This work is carried out by the financial support provided by the Walter Ahlström Foundation Finland with grant # 2021/40. Some parts of this work are done in the SolarX research project with the financial support provided by Business Finland with Grant No. 6844/31/2018. The financial support provided through these funding organizations is highly acknowledged.

References

1. Saad, W., et al., *Game-theoretic methods for the smart grid: An overview of microgrid systems,demand-side management, and smart grid communications.* IEEE Signal Processing Magazine, 2012. **29**(5): p. 86-105.
2. Madureira, AG and J.P. Lopes, *Coordinated voltage support in distribution networks with distributed generation and microgrids.* IET renewable Power generation, 2009. **3**(4): p. 439-454.
3. Tavakoli, A., et al. *A decentralized control strategy for multiple distributed generation in islanded mode*. in *PES General Meeting| Conference & Exposition, 2014 IEEE*. 2014. IEEE.
4. Dragičević, T., et al., *DC microgrids—Part I: A review of control strategies and stabilization techniques.* IEEE Transactions on power electronics, 2016. **31**(7): p. 4876-4891.
5. Liu, X., P. Wang, and PC. Loh, *A hybrid AC/DC microgrid and its coordination control.* IEEE Transactions on smart grid, 2011. **2**(2): p. 278-286.
6. Golestan, S., J.M. Guerrero, and J.C. Vasquez, *A PLL-Based Controller for Three-Phase Grid-Connected Power Converters.* IEEE Transactions on Power Electronics, 2018. **33**(2): p. 911-916.
7. Blaabjerg, F., et al., *Overview of control and grid synchronization for distributed power generation systems.* IEEE Transactions on industrial electronics, 2006. **53**(5): p. 1398-1409.
8. Ali, M., et al., *Lyapunov Stability and Performance Analysis of the Fractional Order Sliding Mode Control for a Parallel Connected UPS System under Unbalanced and Non-linear Load Conditions.* Energies, 2018. **11**(12): p. 3475.
9. Cortés, P., et al., *Model predictive control of an inverter with output $ LC $ filter for UPS applications.* IEEE Transactions on Industrial Electronics, 2009. **56**(6): p. 1875-1883.
10. Ahmed, K.H., et al., *A modified stationary reference frame-based predictive current control with zero steady-state error for LCL coupled inverter-based distributed generation systems.* IEEE Transactions on Industrial Electronics, 2011. **58**(4): p. 1359-1370.

11. Khan, H.S., et al., *Finite Control Set Model Predictive Control for Parallel Connected Online UPS System under Unbalanced and Non-linear Loads.* Energies, 2019. **12**(4): p. 581.
12. Sao, C.K. and PW. Lehn, *Autonomous load sharing of voltage source converters.* IEEE Transactions on Power Delivery, 2005. **20**(2): p. 1009-1016.
13. Nauman, M. and A. Hasan, *Efficient implicit model-predictive control of a three-phase inverter with an output LC filter.* IEEE Transactions on Power Electronics, 2016. **31**(9): p. 6075-6078.
14. Sun, X., Y.-S. Lee, and D. Xu, *Modeling, analysis, and implementation of parallel multi-inverter systems with instantaneous average-current-sharing scheme.* IEEE Transactions on Power Electronics, 2003. **18**(3): p. 844-856.
15. Mattavelli, P., *An improved deadbeat control for UPS using disturbance observers.* IEEE Transactions on Industrial Electronics, 2005. **52**(1): p. 206-212.
16. Hasanzadeh, A., et al., *A proportional-resonant controller-based wireless control strategy with a reduced number of sensors for parallel-operated UPSs.* IEEE Transactions on Power Delivery, 2010. **25**(1): p. 468-478.
17. Komurcugil, H., *Rotating-sliding-line-based sliding-mode control for single-phase UPS inverters.* IEEE Transactions on Industrial Electronics, 2011. **59**(10): p. 3719-3726.
18. Yaramasu, V., et al., *Model predictive approach for a simple and effective load voltage control of four-leg inverter with an output $ LC $ filter.* IEEE Transactions on Industrial Electronics, 2014. **61**(10): p. 5259-5270.

Engineering Science and Technology, an International Journal 24 (2021) 694–705

HOSTED BY

ELSEVIER

Contents lists available at ScienceDirect

Engineering Science and Technology, an International Journal

journal homepage: www.elsevier.com/locate/jestch

Full Length Article

Improved finite control set model predictive control for distributed energy resource in islanded microgrid with fault-tolerance capability

Hussain Sarwar Khan [a,*], Muhammad Aamir [b], Kimmo Kauhaniemi [c], Mohsin Mumtaz [d], Muhammad Waqar Hassan [d], Muhammad Ali [d]

[a] School of Technology and Innovation, University of Vaasa, Finland
[b] Pak-Austria Fachhochschule, Institute of Applied Sciences and Technology, Haripur, Pakistan
[c] School of Technology and Innovation, University of Vaasa, Finland
[d] Department of Electrical Engineering, Bahria University, Islamabad, Pakistan

ARTICLE INFO

Article history:
Received 12 July 2020
Revised 1 November 2020
Accepted 13 December 2020
Available online 20 February 2021

Keywords:
Distributed energy resource
Fault-tolerance capability
MPC
Microgrid

ABSTRACT

In this paper, improved finite control set model predictive voltage control (FCS-MPVC) is proposed for the distributed energy resource (DER) in AC islanded microgrid (MG). Typically, AC MGs have two or more power electronic-based DERs, which have the ability to maintain a constant voltage at the point of common coupling (PCC) as well as perform power sharing among the DERs. Though linear controllers can achieve above-mentioned tasks, they have several restrictions such as slow transient response, poor disturbance rejection capability etc. The proposed control approach uses mathematical model of power converter to anticipate the voltage response for possible switching states in every sampling period. The proposed dual-objective cost function is designed to regulate the output voltage as well as load current under fault condition. Two-step horizon prediction technique reduces the switching frequency and computational burden of the designed algorithm. Performance of the proposed control technique is demonstrated through MATLAB/Simulink simulations for single distributed generator (DG) and AC MG under linear and non-linear loading conditions. The investigated work presents an excellent steady state performance, low computational overhead, better transient performance and robustness against parametric variations in contrast to classical controllers. Total harmonic distortion (THD) for linear and non-linear load is 0.89% and 1.4% respectively as illustrated in simulation results. Additionally, the three-phase symmetrical fault current has been successfully limited to the acceptable range.

1. Introduction

Microgrid (MG) is one of the fundamental technologies, which makes the electrical power systems more intelligent, flexible and distributed. The incursion of distributed energy resources (DERs) is possible in conventional power system. Basically, MG is a localized cluster of adaptive loads, energy storage systems, and distributed generations (DG) with their effective control operating in the coordinated pattern. It can operate in islanded and grid-connected (GC) mode or both. In GC mode, MG provides auxiliary services to power systems such as voltage support, peak load shaving and load shifting [1–3]. In the case of isolation from the utility grid due to fault, regular maintenance or low power quality, MG provides high-quality power to the load in standalone mode [4]. The standalone mode can be further classified into two categories in the context of time. Temporary standalone mode occurs due to pre-planned maintenance or due to spontaneous failure in transmission lines between MG and utility grid while the permanent islanded mode is created to feed the remote communities, where power from the electrical grid is unfavorable and uneconomical [5]. In this study, permanent islanded MG is considered.

Direct current (DC) MG has more appealing features in terms of efficiency and control simplicity than AC MG however, majority of loads requires AC supply [6,7]. Consequently, it is mandatory to establish AC MG architecture which can provide regulated power with effective control. AC and DC parts of MG are interfaced through voltage source converters (VSC) [8,9]. For critical load applications, parallel operated VSCs provide high redundancy, high reliability, and more flexibility. In many cases, it is viable to distribute high power load between several VSCs instead of using a

* Corresponding author.
E-mail addresses: hussain.khan@uwasa.fi, hussainsarwar1994@yaho.com (H.S. Khan), muhammad.aamir@fecid.paf-iast.edu.pk (M. Aamir), Kimmo.Kauhaniemi@uwasa.fi (K. Kauhaniemi), mohsin143.comsats@gmail.com (M. Mumtaz), mwaqarhassan53@gmail.com (M.W. Hassan), m.turi21@gmail.com (M. Ali).

https://doi.org/10.1016/j.jestch.2020.12.015
2215-0986/

single power device with high rating. Commonly, VSCs connected in parallel and feeding a common load form an AC MG.

For the parallel operation of multiple DGs in islanded mode, many control schemes have been proposed in the literature like, average load-sharing technique [10], master–slave control [11,12], centralized based-control [13,14], etc. Though above-mentioned control techniques involved a communication structure among the DGs for smooth operation, using these techniques increase the system's complexity and reduces the reliability. Consequently, it is necessary to use a technique like droop control to govern the power-sharing between the DGs. In [15], the authors present the analysis of the droop control. It is advantageous to design a decentralized controller i.e. no external communication network between VSC-based DGs. The objectives of droop control in AC MG are power sharing among the DGs in AC MG and regulating the frequency and voltage at the AC bus.Droop control serves as an outer loop of VSC while the voltage control technique is used in the inner control loop of VSC in MG.

Various linear controls with pulse width modulation (PWM) are widely found in literature like PI, PR, PID [16,17], but, the linear control techniques have many practical restrictions such as their inability to track the sinusoidal reference with zero steady-state error, tuning of gains, poor disturbance rejection capability and incapability to handle the non-linearities of the power system [18]. Therefore, non-linear control techniques such as $H\infty$ [13], deadbeat [19,20],μ-synthesis [12], and slide mode control (SMC) [21,22] are vastly used by the power electronics industry. In[19], deadbeat (DB) control has been proposed, which moves all the system poles at zero axis line. consequently, the error drops to zero in no time thus, providing fastest dynamic response towards achieving stability. Still, its key shortcomings are parametric variations, external disturbances, and measurement noise. Observer-based DB control is proposed in [20] to increase the system stability but there is a trade off between system stability and performance of control parameters.

Another approach is $H\infty$ which effectively handles the system uncertainties,it working principle based on the hysteresis. Using the feedback loop, control action ensure position the state variable with in the hysteresis but it's variable switching frequency causes a severe stress on switches and reduces the inverter's life, thus making the filter design a bit complicated [23].μ-synthesis guarantees only local stability [24].

In comparison to linear controllers, Non-linear controllers such as slide mode control (SMC) is based on variable structure control theory. Its basic principle is divided into 2 stages. In start, the system states trajectory is forcefully taken into user-defined sliding layer, this phase is known as reaching phase then state trajectories remains in the layer and known as sliding phase. It has better performance, is robust against parametric variations, and possesses magnificent transient response under different loading conditions. Still, chattering phenomena, high switching losses and its complex mathematical modeling are the main barriers in its implementation[25,26]. Artificial intelligence-based approaches i.e. using neural networks [27], fuzzy logic and interactive learning control [28] have the ability to enhance the controller's steady-state performance. However, the approaches illustrate slower transient response and needs much time in training of models. So, an amalgam of the different control approaches balancing out their disadvantages is also found in literature [29].

FCS-MPC is a digital control method and its basic principle is different from linear control. It uses the discrete time model of VSI along with its filter to anticipate the behavior for all possible input combinations. One of the inputs having the least value of the predefined cost function (CF) is selected and applied to the coming sampling instant despite drafting a separate loop for each controlled variable and cascading them together. CF is basically, a square of the Euclidean distance between controlled and reference signal. Current observer-based MPC is proposed in [30]. The authors claim that the cost of system decreases but its performance is poor in term of THD under normal load conditions. Current sensor-less MPVC is proposed for inverter instead of measuring the inductor current. It is assumed that the system cost and computational burden have been reduced, but the proposed control scheme has not shown an effective performance under transients and the authors have not investigated the performance of the system under fault conditions [31]. In [32], predictive control is proposed using improved stationary reference frame, but the performance of control technique for the non-linear load is not investigated. In [33], an implicit VMPC is proposed for power converter with LC filter in autonomous mode, but this approach shows vulnerability to parametric variations and external uncertainties. Likewise, it requires high computational time as compared to other MPC-based approaches. In [34], VMPC for parallel connected UPS is proposed to increase the stability of the system and to reduce the system cost. Due to its robustness, outstanding transient behavior and easy addition of restraints makes FCS-MPC becomes the best alternative for the control of power converters and it can be implemented to a vast range of power electronic applications [35].

The power system faults are further divided into two categories i.e. Symmetrical and unsymmetrical faults. All three phase to ground short circuit is known as symmetrical fault while single phase to ground or two phase to ground short circuits are lies in unsymmetrical faults type. However symmetrical faults are more sever than unsymmetrical faults. This study focuses on the symmetrical faults. Ideally under fault and overload conditions, VSI Output current remains in limit to restrain the damage of the VSI's switches because the converter has low thermal inertia.Normally, the output current increases up to three times of the load current.In order to reduce the damage usually latched limit and instantaneous saturation limit techniques is used. In latched limit, a predefined current reference is introduced in place of actual reference and voltage loop is disconnected due to change of reference. Converter voltage becomes distorted and increases in healthy phases. while in instantaneous saturation strategy, a limiter is added to limit the current. however, this method is easy to implement but output becomes distorted for sinusoidal signal. In [36] a virtual resistance is introduced to reduced the reference current but this technique also reduces the system output voltage.In [37] current limit control based on Instantaneous saturation is proposed for parallel UPS, working in master–slave configuration. The reference for slave converter is generated by master converter by reducing the reference amplitude. consequently the quality of current wave becomes distorted.It also required the communication setup.To limit the fault current, harmonics components of power is used to generate the current reference for grid-tied inverter and proposed in [38].In [39] hardware components is used to limit the current under faults conditions. Hardware based along with instantaneous limit technique is proposed in [40]. although implementation of external devices increases the system cost and reduce the reliability and reduction of the fault limiter size is an important factor to be considered.

Table 1 shows the summary of above discussed control techniques based on parameter, which is used to analysis the performance of control techniques. The linear control scheme is mature and well recognized in literature and extensively uses by PE industry. Instead of that, modern control techniques include new ideas, complex mathematical modeling, the frame of reference transformation, and the often-required microprocessor. Among control schemes, hysteresis control has the easiest approach. System data is not required for the hysteresis and ANN control. But ANN control demands the preceding information and perception of designers

Table 1
Overview of advanced control techniques.

	Linear control	Dead-beat	Slide mode control	ANN	Model predictive control
	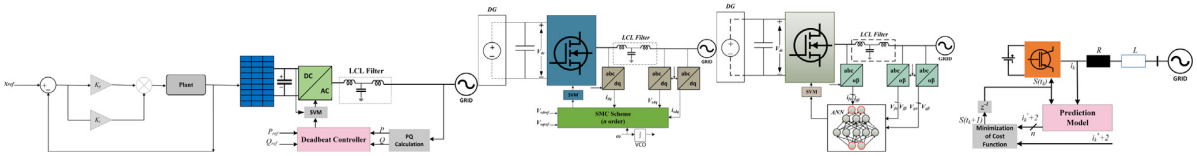				
Theoretical background	Strong	Moderate	Strong	Weak	Strong
Stability analysis tools	Strong	Strong	Strong	No	Initial Results
Computational complexity	Low	Average	Medium	Low	High
Intuitive design	Low	Average	Medium	Low	High
Handling system constraints	No	No	No	Yes	Yes
Handling non-linearities	No	Yes	Yes	Yes	Yes
Parameter sensitivity	Strong	Average	Robust	Data Dependent	Tunable
Fault tolerance capability	No	No	Yes	Not-studied	Yes

and its performance is directly related to training data. The constraints are handle by the ANN and MPC.ANN is newly introduced in the power electronics domain and have weak theoretical literature. The response of hysteresis and MPC has exceptional performance under different loading conditions. SMC required complex mathematical modeling and has high computational burden. Despite high computational burden. MPC is better in all aspects discussed in 1.

This paper presents an improved voltage control strategy for VSC in order to regulate the output voltage of single and parallel DG units operating in an islanded mode of MG. The key contributions in this paper includes;

1. A dual objective cost function-based two-step prediction horizon FCS-MPVC for single DG in the islanded mode.
2. The systems mathematical model is used to predict the imminent action of the system for possible switching sequences in a sampling period.
3. The cost function is designed to determine the optimum action and then it is applied to the coming sampling period.
4. A two-step prediction horizon-based CF is formulated to decrease the converter switching frequency and also to increase the system efficiency.
5. In order to control fault current under fault condition, a dual-objective cost function is designed, the primary objective of the CF is to compensate the voltage error and its secondary function is to control the current under fault conditions.

Proposed control technique is validated for single DG under linear, non-linear, and unbalance loading condition. More importantly, the controller exhibits efficient performance under fault condition. Similarly, multiple DGs parallel operation has been simulated for the proposed control and droop technique is analyzed for accurate power sharing.

The remaining paper is arranged as follows. The proposed control strategy is explained while providing the comprehensive mathematical model of two-level VSC with linked LC filter and discussing the discretization aspects of FCS-MPC implementation in Section 2. Further, the FCS-MPC operating principle is explained in this section. Cost function design is explained in Section 3 while Section 4 presents the switching reduction mechanism. The Section 5 explains the droop control for proper power sharing between the DGs and its restrictions are also presented. In Section 6, the detailed simulation results are explained. Finally, the last section comprises of the conclusion.

2. Mathematical modelling of DER system

A detailed block diagram of MG having renewable energy resources connected with AC bus through PE interface, each converter have it's own primary and secondary control and also connected with MG central controller for the smooth operation of MG is illustrated in 1. The MPC uses the discrete time converter model and its filter parameters to find the optimal action by minimizing the CF. Based on minimized CF, optimal control action is anticipated for the next sampling time. Precise mathematical model of the VSC and filter is required to attain good control performance. Particularly in AC MG, two-level VSC topology is used as shown in 2. The output LC filter is used to eliminate the high frequency current components which are undesirable. VSC modelling is done in the stationary orthogonal frame of reference. The two assumptions are considered i.e. the VSC is in balanced condition and all three phases are balanced.Three phases x-y-z are transformed into $\alpha\beta$ frame by using the Clarke transformation: see Fig. 3.

(2)

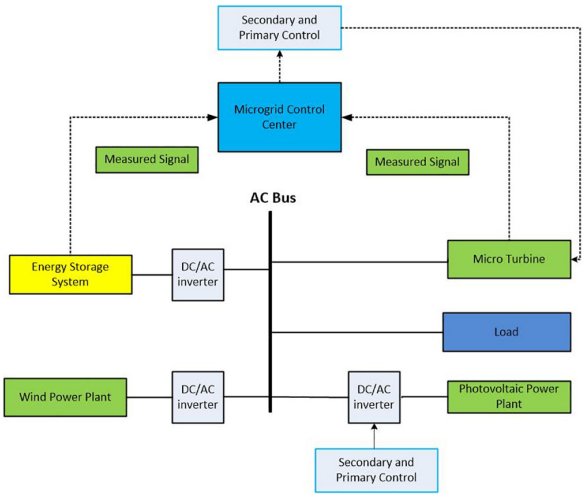

Fig. 1. Islanded MG contains three DG's with VSI and different type of loads.

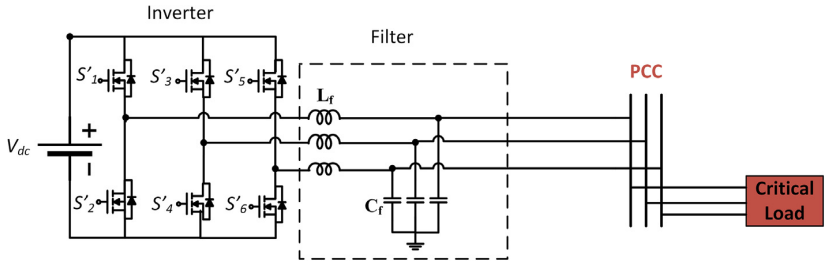

Fig. 2. Circuit representation of 3-phase VSC with output LC filter connected with load at PCC.

$$T = \frac{1}{3}\left[e^{j\frac{2}{3}\pi}e^{j\frac{2}{3}\Pi}\right] \tag{3}$$

2.1. Converter model

The converter consists of three legs $(S_x, S_y, S_z)$and each leg has two switches so there are two possible switching states for each leg, which are described below:

$$S_x = \begin{cases} 1, & S'_1 \text{ is ON and } S'_4 \text{ is OFF} \\ 0, & S'_1 \text{ is OFF and } S'_4 \text{ is ON} \end{cases} \tag{4}$$

$$S_y = \begin{cases} 1, & S'_2 \text{ is ON and } S'_5 \text{ is OFF} \\ 0, & S'_2 \text{ is OFF and } S'_5 \text{ is ON} \end{cases} \tag{5}$$

$$S_z = \begin{cases} 1, & S'_4 \text{ is ON and } S'_6 \text{ is OFF} \\ 0, & S'_4 \text{ is OFF and } S'_6 \text{ is ON} \end{cases} \tag{6}$$

However, two-level VSC has eight possible switching arrangements. The voltage between N-th point and leg can be computed

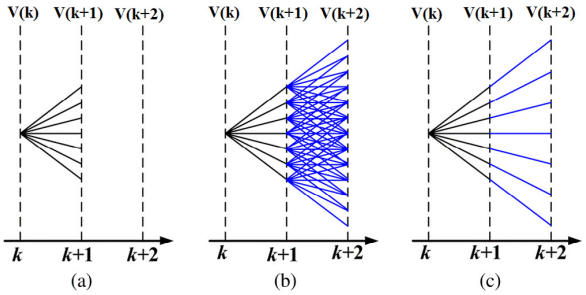

Fig. 3. Demonstration of prediction approach. (a) N = 1, (b) N = 2, In every sampling time, different voltage vectors are using. (c) N = 2, but same vector is taking into account for two consecutive sampling time.

by taking the product of the DC link voltage with the present state of the corresponding leg:

$$\begin{aligned} V_{xN} &= S_x.V_{dc} \\ V_{yN} &= S_y.V_{dc} \\ V_{zN} &= S_z.V_{dc} \end{aligned} \tag{7}$$

The voltage between phase to neutral (from x, y, z to n-th point) is determined by subtracting the common voltage from 7. Common voltage is determined by executing Kirchhoff's voltage law:

$$V_{nN} = \frac{V_{xN} + V_{yN} + V_{zN}}{3} \tag{8}$$

Phase voltage is:

$$\begin{aligned} V_{xn} &= V_{xN} - V_{nN} \\ V_{yn} &= V_{yN} - V_{nN} \\ V_{zn} &= V_{zN} - V_{nN} \end{aligned} \tag{9}$$

Clark transformation is applied to find eight possible switching states. These are expressed in Table 2.

2.2. Filter modelling

To suppress the switching harmonics, a LC filter is coupled at VSC's output terminal as illustrated in 2. LC filter has an inductor L_f, and capacitor C_f and damping resistance R_f with current I_f and voltage V_{pc} across the load. I_f and $_{V_{pc}}$ are the state variables in this system. The Eq. 10 and 11 explain the filter dynamics. Inductive behaviour of the filter is described in 10, while 11 demonstrates the capacitive response of the filter. The equations are stated as:

$$L_f \frac{d_{i_f}}{d_t} = v_t - v_{pc-i_f R_f} \tag{10}$$

$$C_f \frac{d_{V_{pc}}}{d_t} = i_f - i_0 \tag{11}$$

$$\frac{d}{d}\begin{bmatrix} i_f \\ V_{pc} \end{bmatrix} = \mathbf{A}\frac{d}{d}\begin{bmatrix} i_f \\ V_{pc} \end{bmatrix} + \mathbf{B}\frac{d}{d}\begin{bmatrix} v_t \\ i_0 \end{bmatrix} \tag{12}$$

$$\mathbf{A} = \begin{bmatrix} \frac{-R_f}{L_f} & \frac{-1}{C_f} \\ \frac{1}{C_f} & 0 \end{bmatrix} \tag{13}$$

Table 2
Feasible switching sequence for power converter.

Space-Vector		On-state switches	Vector placing
Zero vector	$\vec{V_{0,7}}$	S'_1, S'_3, S'_5	$\bar{v_{0,7}} = 0$
Active Vector	$\vec{V_1}$	S'_1, S'_6, S'_2	$\bar{v_1} = \frac{2}{3} v_{dc}$
	$\vec{V_2}$	S'_1, S'_3, S'_2	$\bar{v_2} = \frac{1}{3} v_{dc} + j\frac{\sqrt{3}}{3} v_{dc}$
	$\vec{V_3}$	S'_4, S'_3, S'_2	$\bar{v_3} = -\frac{1}{3} v_{dc} + j\frac{\sqrt{3}}{3} v_{dc}$
	$\vec{V_4}$	$S'_{44}, S'_{33}, S'_{55}$	$\bar{v_4} = -\frac{2}{3} v_{dc}$
	$\vec{V_5}$	S'_4, S'_3, S'_5	$\bar{v_5} = -\frac{1}{3} v_{dc} - j\frac{\sqrt{3}}{3} v_{dc}$
	$\vec{V_6}$	S'_1, S'_4, S'_5	$\vec{v_6} = \frac{1}{3} v_{dc} - j\frac{\sqrt{3}}{3} v_{dc}$

$$\mathbf{B} = \begin{bmatrix} \frac{1}{lf} 0 \\ 0 \frac{-1}{Cf} \end{bmatrix} \tag{14}$$

2.3. Discrete time modelling of the LC filter

For the practical implementation of the proposed control approach on digital control platforms, continuous time state space (CTSS) model of the filter is essentially converted into discrete time state space (DTSS) model. In order to convert the model to DTSS, different discretization techniques are used, but in this study, Zero order-hold technique is implemented. Actually, Zero order-hold technique is implemented. Actually, it provides the exact transformation of CTSS to DTSS model for each sampling period in stair type inputs. In this paper, the value of the dc-link voltage V_{dc} is taken constant and the mathematical model of the DTSS is described as:

$$\begin{bmatrix} i_f(t_{k+1}) \\ V_{pc}(t_{k+1}) \end{bmatrix} = A_d \begin{bmatrix} i_f(t_{k+1}) \\ V_{pc}(t_{k+1}) \end{bmatrix} + B_d \begin{bmatrix} v_t(t_k) \\ i_0(t_k) \end{bmatrix} \tag{15}$$

$$A_d = e^{AT_s} \tag{16}$$

$$\mathbf{B}_d = \int_0^{\vec{T_s}} e^{A\tau} B d_\tau \tag{17}$$

T_s is the sampling instant. It is assumed that T_s is very small so the exponential matrix is approximated as:

$$e^{AT_s} = 1 + AT_s \tag{18}$$

By using 15, the capacitor voltage at instant (t_{k+1}) is determined by the following equation:

$$v_{pc}(t_{k+1}) = v_{pc}(t_k) + \frac{T_s}{C_f}\left(i_f(t_k) - i_0(t_k)\right) \tag{19}$$

19 is used to find the voltage at the next sampling instant.

3. Cost function

The working of investigating MPVC algorithm is briefly explained below:

- $v_{pc}, i_f$and $i_0$are measured through sensors in the beginning of every sampling period.
- The measured values of voltages and currents are used to anticipate system variable via (19), for all probable switching arrangements.
- Pre-defined CF (21) or (22) is evaluated using predicted state values (19) then switching pattern (Table 1) at which CF has minimal value. It is applied to converter in coming sampling instant.

In order to implement FCS-MPC, CF formulation is fundamental. Basically, CF gives the error between the reference and the forecast value. MPC can handle the multiple objective based-issues.By defining these in cost function as expressed in 20:

$$g_{Gen} = \sum_{i=t_k}^{t_k+N-1} \left\| v_{fe}(i) \right\|_2^2 + h_{lim}(i) + \lambda_u sw^2(i) \tag{20}$$

$v_{fe}(i)$ is the anticipated tracking error,$h_{lim}(i)$ is the current limitation, $sw^2(i)$defines the reduction of switching frequency and is regulated by weighting factor λ. CF employed in the study is expressed in 21. It is a specialized type of 20 with $N = 2$, Its primary role is to lessen the Euclidean distance at every sampling instant. CF used in this study is described below:

$$g_v = \left(v^*_{(pc)}\alpha(t_{k+2}) - v_{(pc)\alpha}(t_{k+2})\right)^2 + \left(v^*_{(pc)}\beta(t_{k+2}) - v_{(pc)_\beta}(t_{k+2})\right)^2 \tag{21}$$

$v^*_{(pc)}\alpha$and $v^*_{(pc)}\beta$ are real & imaginary parts of the voltage reference at t_{k+2} instant, usually provided by the droop approach in AC MG.$v_{(pc)_\alpha}$ and $v_{(pc)_\beta}$ are anticipated output voltages at the t_{k+2} instant. Above defined CF provides us a voltage error.

3.1. Dual-objective cost function for symmetrical fault

Basically, dual objective cost function is designed to regulate the AC bus voltage and also to minimize the fault current under fault conditions. The dual objective cost function is defined as:

$$G_{DO} = \left(v^*_{(pc)_{\alpha\beta}}(t_{k+2}) - v_{(pc)_{\alpha\beta}}(t_{k+2})\right)^2 + \left(i^*_{(f)_{\alpha\beta}}(t_{k+1}) - i_{(f)_{\alpha\beta}}(t_{k+1})\right)^2 \tag{22}$$

Load current term is introduced in the new CF to regulate the load current under fault conditions. By introducing the new term of the current in CF as mentioned in 22, There is a trade-off between voltage quality in terms of THD and the current waveform, but the THD of voltage slightly increases whereas the current waveform remains sinusoidal and surge in a current is limited under fault conditions. Consequently, the advantages of addition of a new term outweighs its disadvantages. Among all the voltage vectors, the vector which has minimum value of g_v is applied to the next sampling instant.

4. Switching frequency reduction scheme

The switching frequency of the converter plays a vital role in power generation. If the switching frequency is high, more losses will occur. Consequently, efficiency of the system decreases and vice versa. In this study, a two-step prediction horizon approach is realized to attain low switching frequency for better efficiency. If one-step prediction horizon is taken into account, only eight possible voltage vectors are estimated for each sampling instant. For the implementation of the prediction horizon where N = 2, two voltage vectors are evaluated. One voltage vector is determined for the 1st sampling period and other vector is applied for the 2nd sampling period. So, 49 combinations of voltage vectors are possible and may be determined as demonstrated in Fig. 3b. This scheme increases the computational burden, which causes problems in implementation stages.

To lessen the switching frequency, a simple two-step prediction is implemented in this paper. For both sampling periods, the same voltage vector is determined [41]. Subsequently, only 7 voltage vectors are evaluated instead of 49 vectors for both sampling instants, as illustrated in Fig. 3c. The implemented scheme gives same performance with very low switching frequency. Voltage for instant t_{k+2} is anticipated by using 19. This approach lowers the switching frequency and also reduces the voltage ripples and increases the wave quality.

5. Droop control

Originally each DG is designed to generate a power according to its reference at base frequency i.e. 60 Hz in this study. In the case of islanded MG, the main aim of the local controller of DG is to com-

pensate the voltage and frequency within MG. But there is a need of secondary controller to control the voltage and frequency of MG. Droop control is extensively adopted in MG to control the voltage and frequency, as well as proper sharing of active and reactive power between the DGs [24]. In this work, droop control is used for accurate sharing of the active and reactive power of each DG proportional to its ratings. Droop control can be expressed as follows:

$$V_{ref} = V_{nom} - k_q Q_{cal} \tag{23}$$

$$f_{ref} = f_{nom} - k_p P_{cal} \tag{24}$$

where as $f_{ref}$and V_{ref} are reference frequency and voltage respectively used to determine the $V_{ref,\alpha\beta}$. $V_{nom}$and f_{nom} are nominal voltage and frequency respectively. Following equations are used to calculate the active power P_{cal} and reactive power Q_{cal}.

$$P_{cal} = v_{pc,\alpha} i_{0,\alpha} + v_{pc,\beta} i_{0,\beta} \tag{25}$$

$$Q_{cal} = v_{pc,\beta} i_{0,\alpha} - v_{pc,\alpha} i_{0,\beta} \tag{26}$$

Low-pass filter is used to mitigate the harmonics in the calculated power. However, it shows slow-response under step change of load. k_q and k_p are droop power coefficients. Basically, voltage control and coefficients of droop are inversely proportional. Hence, adjustment between both the parameters is essential to find an optimal solution. The slope of the droop curves are also calculated using droop coefficients and expressed as:

$$k_q = \frac{\delta V}{Q_{max}} \tag{27}$$

$$k_p = \frac{\delta f}{P_{max}} \tag{28}$$

ΔV and Δf represent the allowable variations in voltage and frequency respectively. Q_{max} and P_{max} are the nominal active and reactive power provided by the system.Control technique expressed in (23) and (24) is commonly known as droop control as expressed in Fig. 4. Table 3 presents the comparison among the resistive-impedance and inductive-impedance based droop approach. see Fig. 5–7

Table 3
Evaluation among different impedance-based droop control.

Parameter	Resistive type$\varnothing = 90^{\circ}$ Z = r	Inductive type $\varnothing = 90^{\circ}$ Z = jx
Active power	$P = \frac{EV\cos\varnothing - V^2}{r} \cong \frac{v}{r}(E - v)$	$P = \frac{EV}{X}\sin\varnothing \cong \frac{EV}{X}\varnothing$
Reactive power	$Q = -\frac{ev}{R}\sin\varnothing \cong \frac{ev}{r}\varnothing$	$Q = \frac{ev\cos\varnothing - v^2}{x} \cong \frac{v}{x}(e - v)$
Frequency Equation	$\omega - k_P Q = \omega^*$	$\omega + k_P P = \omega^*$
Amplitude equation	$E = E^* - k_Q P$	$E = E^* - k_Q Q$
Droop coefficient	$k_P = \frac{\Delta\omega}{Q_N}$	$k_P = \frac{\Delta\omega}{P_N}$
Droop coefficient	$k_Q = \frac{\Delta E}{P_N}$	$k_Q = \frac{\Delta E}{2Q_N}$

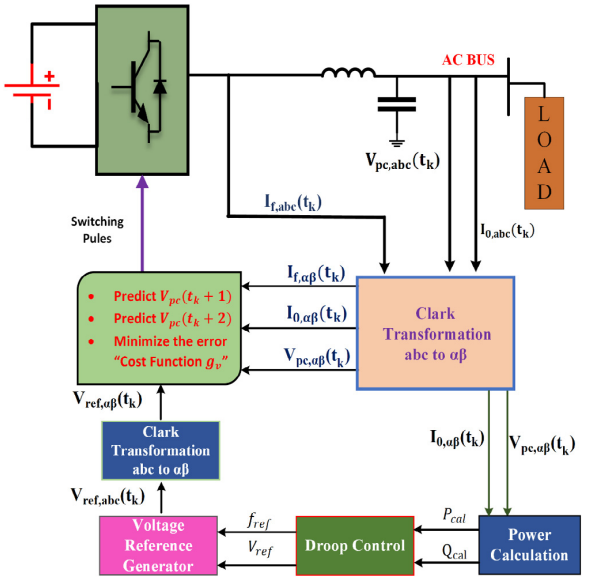

Fig. 5. Block diagram of investigating control scheme along with droop control in islanded mode of MG.

6. Simulation: results & discussion

For the validation of the proposed control technique, extensive real-time simulations are carried out in MATLAB/Simulink for both single DG and parallel DG in islanded MG. Different simulation scenarios are simulated under different loading & fault conditions to present the robustness and effectiveness of the control strategy under study. Both linear and non-linear as well as unbalanced loads are considered in this study. Linear load consists of three phase RL load with the active and reactive power of P = 18 kW and Q = 7 kVar respectively. Fig. 5 presents the complete block diagram of VSC along with its control structure. First, steady-state simulation for an VSI has been done to authenticate the performance of the proposed controller under sinusoidal voltage reference. Then, transient conditions, a step change of load, and system performance under non-linear load is inspected to illustrate the system robustness and stability. Finally, two DERs with proposed controller are connected in parallel to serve the common load at AC bus in islanded MG. Accurate power sharing between the DGs are achieved by applying the droop approach. Different parameters used in this study is given in Table 4.

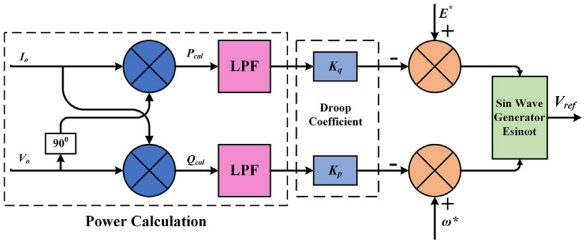

Fig. 4. Droop control.

6.1. Steady state analysis

Fig. 6 presents the results of a DG under linear RL balanced load, when RL load is connected. During operation, 18 kW active and 7 kVar reactive power is generated by the DG to meet the load demand. Both voltage and current are sine waves with negligible distortions. The execution of the proposed control scheme is equated with the standard literature [33]. In [33], output voltage THD is 2.93%. However, the proposed strategy reduces the output voltage THD to 0.89% and also with in the limit of IEEE criterion. Fig. 7 illustrates the simulation results of the voltage and current waveform for single

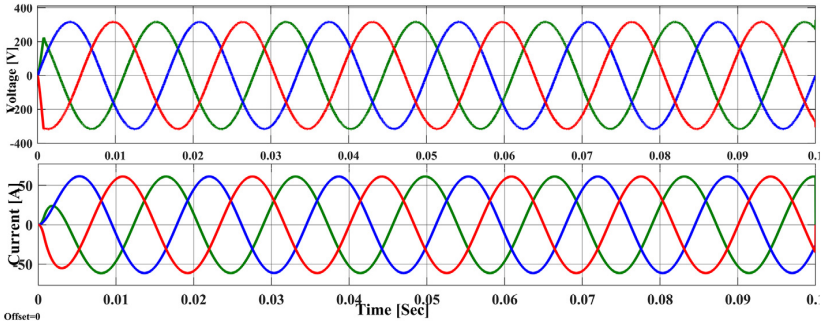

Fig. 6. Load current and output voltage of single DG under linear load.

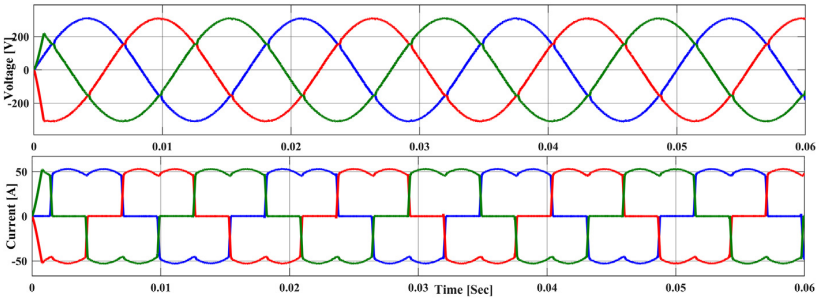

Fig. 7. Load current and output voltage of single DG under non-linear load.

Table 4
Simulation parameters.

Parameters	Values
DC link voltage	$v_{dc} = 1000$ V
Sampling time	$T_s = 20$ μ S
LC-filter	$C_f = 250$ μ$F, L_f = 2$ mH
Damping resistance	$R_f = 0.94$ W
Linear loads	$P = 18$ kW, $Q = 7$ kVar
Non-linear load (diode rectifier)	$P = 10$ kW, $Q = 4$ kVar
Nominal voltage	$V_{nom} = 311$ V
Rated frequency	$F_{ref} = 60$ Hz
Droop coefficients	$k_q = 0.008$ $k_p = 0.001$
PI parameter	$K_P = 42$ $K_I = 0.15$

DG under non-linear load condition with proposed controller. It should be seen in results that the voltage wave is a sine wave even now with THD of 1.40% regardless of the distorted output current.

6.2. Load transients studies

The load transient analysis of the system with proposed controller is performed to determine the system transient response and overshoot under varying load conditions. Fig. 8 illustrates the transient response of the system under step change in load from 0% to 100% and 100% to 0%. At time 0.1s system load becomes zero or under no load condition and a smaller spike of voltage is shown in the magnified window.which occurs due to switching of the load. However, this spike cannot create produce the stress on the switches of VSI. Then at time is 0.15s, load is again con-

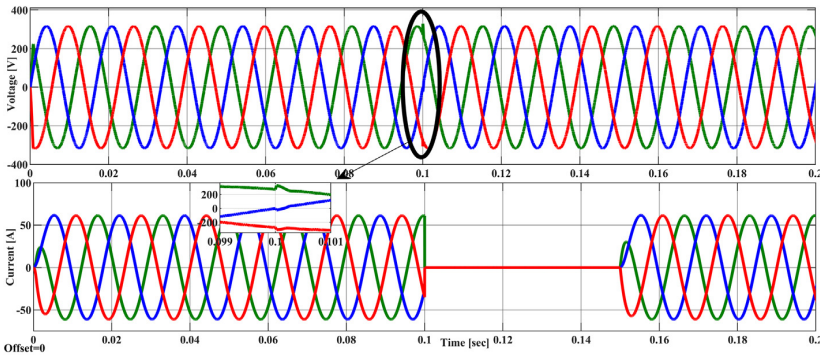

Fig. 8. Output voltage and line current results for load variations.

nected with the system. During the whole period, the output voltage of the system remains stable and the output current varies with the load. Fig. 9 demonstrates the simulation results with PI controller as a voltage regulator. At time 0.5s, extra load is added to in the system to observe the behavior of PI. Due the increase in load, a voltage dip is observe along with the distortion in current wave. The controller takes time regain its position and to start work smoothly. The THD of voltage, in the case of PI is above 4%. To validate the performance of the proposed controller, step change in load test under non-linear loading condition is per-

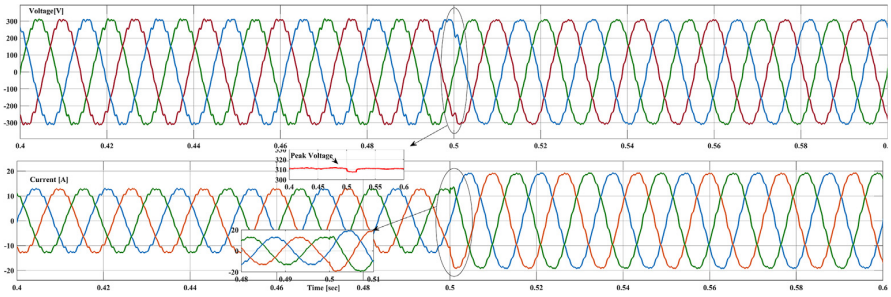

Fig. 9. Output voltage and line current results for load variations, when PI controller is employed.

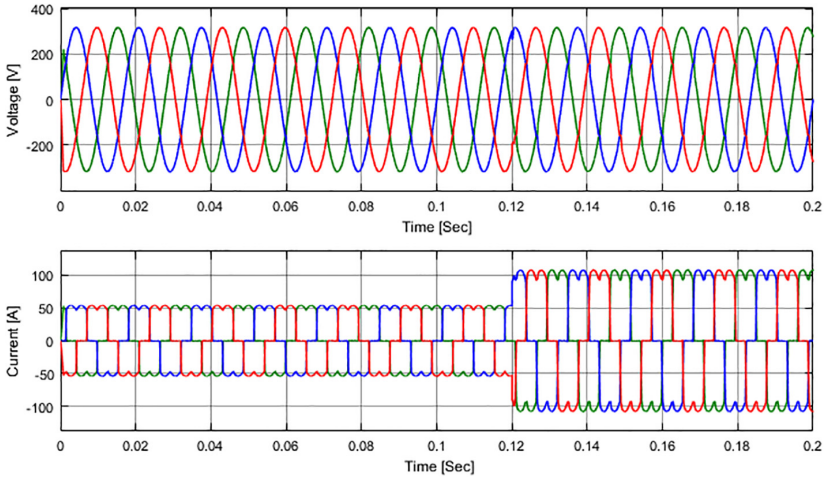

Fig. 10. Voltage and current results in step change of load.

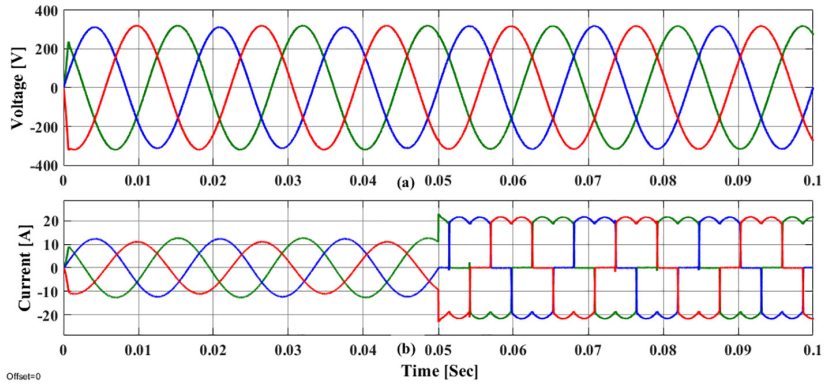

Fig. 11. Simulation results of voltage and current under unbalanced and non-linear loads using MPC controller.

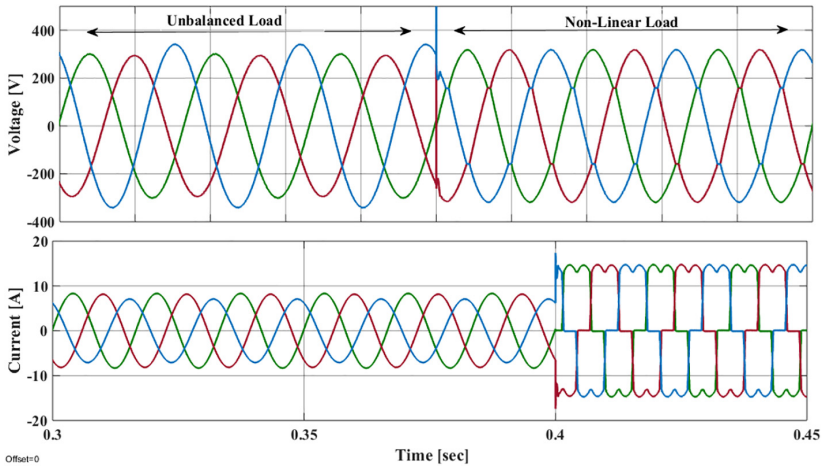

Fig. 12. Voltage and current results under non-linear and unbalanced loads using PI controller.

Table 5
THD comparison among the implemented control techniques.

	Linear load	Non-linear load
PI controller	3.53%	12.16%
Single-objective CF MPC	0.89%	1.40%
Dual-objective CF MPC	1.09%	–

formed. Fig. 10 shows that at time t = 0.12s, the non-linear load connected to the system becomes double. It can be noted that the output voltage waveform remains sinusoidal but shows a ditch during switching period as depicted in Fig. 10.

At t = 5 ms, the non-linear load is connected with system and at same time, the connected unbalanced load is disconnected to show the transition between different loading conditions. It is seen in Figs. 11(b) and 12(b) that the current becomes distorted because non-linear load is switched on. Fig. 12(a) demonstrates that the linear controller is unable to suppress the harmonics so, the quality of the output voltage becomes bad. But, the proposed control approach handles the non-linearity and the harmonics in output voltage is less, as presents in Fig. 12(a).

Table 5 present the comparison of the control strategy, discussed in this study in the form of total harmonic distortion (THD). THD is calculated using SIMULINK build-in FFT tool. Highest THD under both loading conditions is observed in the case of linear control. while single objective CF based MPC has lowest value of THD. In the case of dual objective CF, There is trade off between control parameter such as voltage and current. Slightly Increase the voltage THD but limit the current under fault conditions.

6.3. Multiple DGs: results and discussion

After validation of the proposed control for single DER. Now finally, this technique is tested for two DGs connected in parallel to serve a single load. Simulation is done in MATLAB/Simulink environment. Droop control strategy is employed for the better regulation of power between the DGs. The features of power-sharing and load transients are being investigated. Power sharing among the DERs is presented in Fig. 13. At 30 ms, the total system load doubles. Consequently, power generated by DGs also grows by the same rate to meet the system demand. Fig. 13(a), (b), (e) and (f) illustrate the load current and output voltage of DG_1 and DG_2. It is shown that at t = 0.03s, due to the increase in demand, the current of both inverters increases, while the voltage remains stable. Active and reactive power is equally shared by the droop control because both DGs have equal KVA rating as demonstrated in 13.

6.3.1. Dual objective CF under faults conditions

This section present the simulation results of PI controller, single objective CF based MPC and then for dual objective CF based MPC under symmetrical faults. In literature, many research studies have been found to address the faults but in mainly studies, sec-

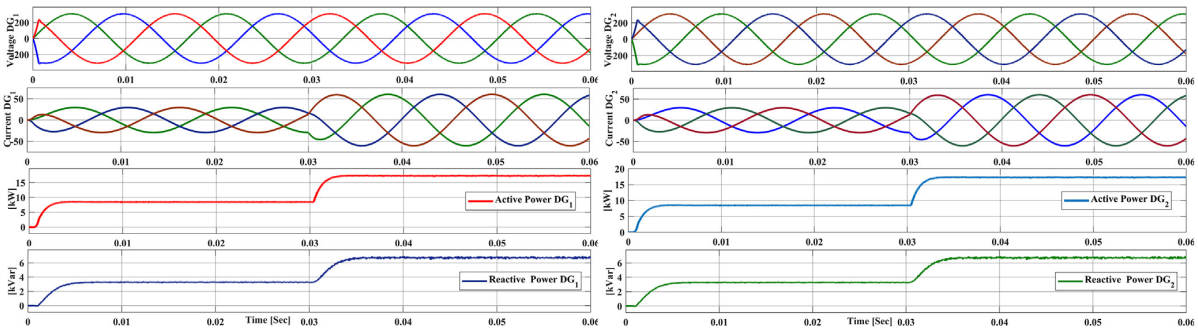

Fig. 13. Voltage, load current, active and reactive power of both DG_1 and DG_2 under load transients.

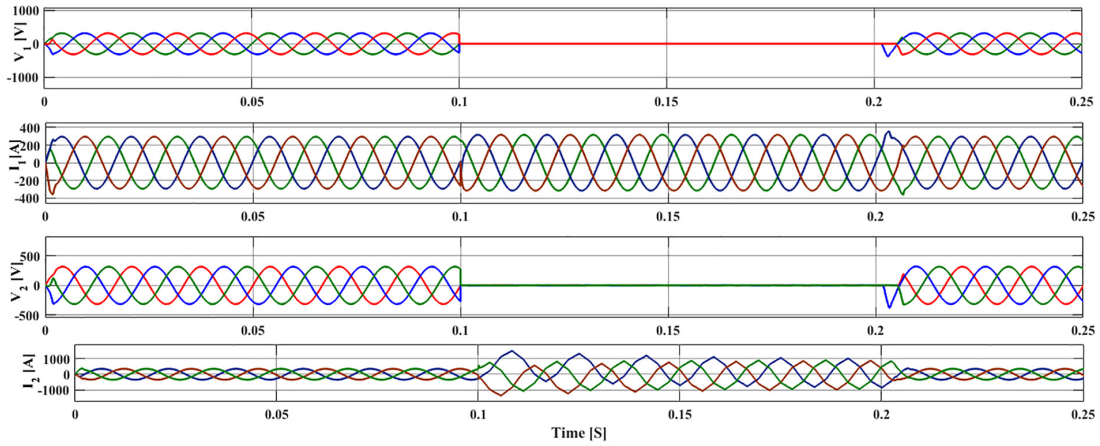

Fig. 14. Voltage and load current waveform of both DG_1 and DG_2 during 3-phase fault period.

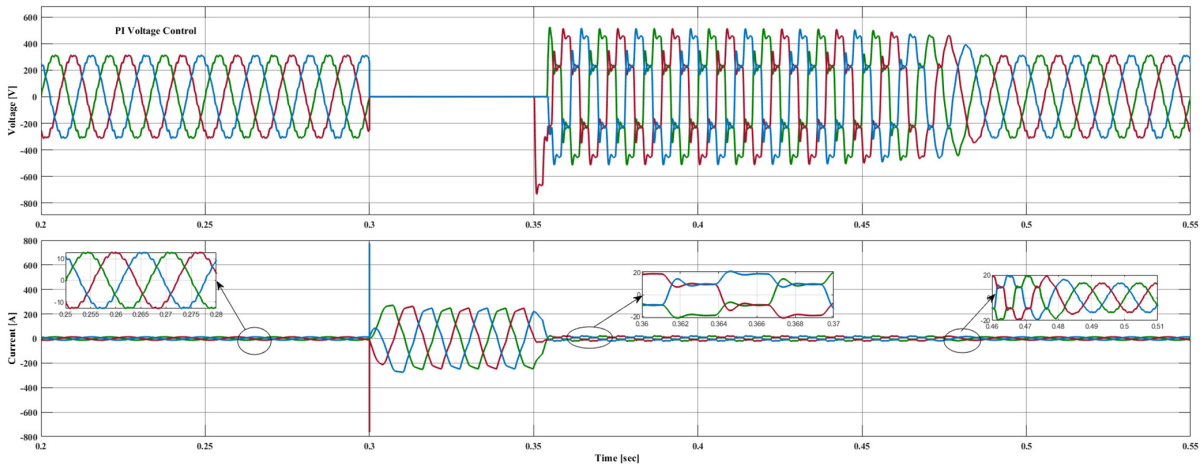

Fig. 15. Voltage and load current waveform of PI controller during 3-phase fault period.

ondary controller or hardware based devices is used to limit the fault current. However, authors don't find any literature to address this issue using converter basic control.In the dual objective CF,the primary objective of CF is to regulate the bus voltage and secondary function of CF is to compensate the output current under three-phase line to ground fault. However, the use of secondary term deteriorate the performance of controller in term of THD But advantages are far superior than the cons. In this scenario, a novel dual-objective CF is employed on DG_1. But the DG_2 having the single objective CF as described in (18).

14 illustrates the performance of newly designed dual-objective cost function in comparison with single objective CF. Output volt-

Table 6
Comparison of different control techniques.

References	Techniques Investigated	Voltage quality under Linear load (THD)	Voltage quality under Non-linear load (THD)	Controller implementation Complexity	Application
[16]	Proportional-Integral	9	30	Low	MG (Islanded), UPS
[17]	Proportional-Resonant	1.4	4.6	Low	MG,UPS
[19]	Dead-beat	2.1	4.8	Medium	MG, UPS
[26]	Slide Mode Control	Not given	2.66	High	General
[42]	Model Predictive Control	5.1	6.7	High	General
[30]	Observer-based MPC	2.82	3.8	Medium	UPS, MG (Islanded)
[33]	MPC (Implicit)	2.93	Not Given	Medium	General
[27]	ANN-MPC	1.09	2.89	High	General
Proposed	Improved FCS-MPC	**0.89**	**1.40**	Medium	MG (Islanded), UPS

age THD is more in the case of DG_1 as compared to DG_2 as shown in the Fig. 14. At t = 0.1s, three-phase line to ground fault occurs in the system, the voltage of the both DGs becomes zero and the load current of system rises and becomes distorted simultaneously, but at same time the current waveform of DG_1 remains sinusoidal and the current of the system increases but remains in safe limit. But the current of DG_2 increases by 3× of the load current.

15 illustrates the results of PI controller under fault condition. It is shown in the Fig.15 that at time 0.3s, a symmetrical phase is introduced in the system.The voltage og the system becomes zero but current shows a large spike. Fault is cleared at 0.35s, But the voltage and current of the system remains distorted and amplitude of the voltage is much higher than the reference. So, the controller is not following the reference and behave like as in transient period. PI controller takes 0.13s to becomes stables and works smoothly. All the simulation results verify that proposed MPC has better performance than any other classical controller.

Table 6 presents the comparison among the existing linear and non-linear control techniques found in literature with proposed control technique. The control approach under investigation demonstrates a better dynamic response and it effectively suppresses the harmonics and has excellent performance in comparison to the other controllers found in literature.

7. Conclusion

In this paper, a new dual objective CF-based FCS-MPC control technique has been studied for a single and multiple DGs in AC MG. The effectiveness of the proposed control technique has been verified by doing extensive simulations in the MATLAB/Simulink. Results based on simulations demonstrate that the proposed strategy attain excellent voltage regulation under linear and non-linear loads. Fault current is also regulated by a new CF under fault condition. The proposed controller does not need any external or internal parameters for adjustment. It only requires the system model in order to anticipate the state variables. Additionally, no modulator is required, thus the gate signals are directly provided by the controller. The proposed controller provides flexibility and eliminates the cascaded configuration to control the output voltage directly. Results are compared with conventional MPC and PI controllers. The proposed model demonstrates a significant decrease in the THD of the system and the switching frequency. Results also indicate that the output current remains sinusoidal under symmetrical faults. For proper power-sharing between the DGs in AC MG, Droop strategy is employed. The results depict perfect power regulation among the DERs in different loading conditions.

Declaration of Competing Interest

The authors declare that they have no known competing financial interests or personal relationships that could have appeared to influence the work reported in this paper.

Acknowledgment

The authors would like to thank the editors and anonymous reviewers for providing insightful suggestions and comments to improve the quality of research paper.

References

[1] W. Saad, Z. Han, H.V. Poor, T. Basar, Game-theoretic methods for the smart grid: an overview of microgrid systems, demand-side management, and smart grid communications, IEEE Signal Process. Mag. 29 (5) (2012) 86–105. URL: https://doi.org/10.1109/MSP.2012.2186410.

[2] A.G. Madureira, J.P. Lopes, Coordinated voltage support in distribution networks with distributed generation and microgrids, IET Renew. Power Gen. 3 (4) (2009) 439–454. URL:https://doi.org/10.1049/iet-rpg.2008.0064.

[3] M. Mumtaz, H.S. Khan, M. Aamir, M. Ali, A. Rehman, Load flow analysis of cigre benchmark model using etap, in: Proceedings of the International Conference on Renewable, Applied and New Energy Technologies, ICRANET, pp. 19–22..

[4] M. Aamir, K.A. Kalwar, S. Mekhilef, Uninterruptible power supply (ups) system, Renew. Sustain. Energy Rev. 58 (2016) 1395–1410. URL:https://doi.org/10.1016/j.rser.2015.12.335..

[5] H. Bakir, A.A. Kulaksiz, Modelling and voltage control of the solar-wind hybrid micro-grid with optimized statcom using ga and bfa, Eng. Sci. Technol. Int. J. 23 (3) (2020) 576–584. URL:https://doi.org/10.1016/j.jestch.2019.07.009.

[6] T. Dragicevic, X. Lu, J.C. Vasquez, J.M. Guerrero, Dc microgrids–part i: a review of control strategies and stabilization techniques, IEEE Trans. Power Electron. 31 (7) (2016) 4876–4891. URL:https://doi.org/10.1109/TPEL.2015.2478859.

[7] C. Chellaswamy, L. Balaji, T. Kaliraja, Renewable energy based automatic recharging mechanism for full electric vehicle, Eng. Sci. Technol. Int. J. 23 (3) (2020) 555–564. URL:https://doi.org/10.1016/j.jestch.2019.07.007.

[8] X. Liu, P. Wang, P.C. Loh, A hybrid ac/dc microgrid and its coordination control, IEEE Trans. Smart Grid 2 (2) (2011) 278–286. URL:https://doi.org/10.1109/TSG.2011.2116162.

[9] U. Datta, A. Kalam, J. Shi, Frequency performance analysis of multi-gain droop controlled dfig in an isolated microgrid using real-time digital simulator, Eng. Sci. Technol. Int. J. 23 (5) (2020) 1028–1041. URL:https://doi.org/10.1016/j.jestch.2019.11.008.

[10] X. Sun, Y.S. Lee, D. Xu, Modeling, analysis, and implementation of parallel multi-inverter systems with instantaneous average-current-sharing scheme, IEEE Trans. Power Electron. 18 (3) (2003) 844–856. URL:https://doi.org/10.1109/TPEL.2003.810867.

[11] Y.J. Cheng, E.K.K. Sng, A novel communication strategy for decentralized control of paralleled multi-inverter systems, IEEE Trans. Power Electron. 21 (1) (2006) 148–156. URL:https://doi.org/10.1109/TPEL.2005.861194.

[12] T. Caldognetto, P. Tenti, Microgrids operation based on master–slave cooperative control, IEEE J. Emerg. Select. Top. Power Electron. 2 (4) (2014) 1081–1088. URL:https://doi.org/10.1109/JESTPE.2014.2345052.

[13] J.M. Guerrero, L. Hang, J. Uceda, Control of distributed uninterruptible power supply systems, IEEE Trans. Industr. Electron. 55 (8) (2008) 2845–2859. URL: https://doi.org/10.1109/TIE.2008.924173.

[14] M.M.A. Abdelaziz, M.F. Shaaban, H.E. Farag, E.F. El-Saadany, A multistage centralized control scheme for islanded microgrids with pevs, IEEE Trans. Sustain. Energy 5 (3) (2014) 927–937. URL:https://doi.org/10.1109/TSTE.2014.2313765.

[15] U.B. Tayab, M.A.B. Roslan, L.J. Hwai, M. Kashif, A review of droop control techniques for microgrid, Renew. Sustain. Energy Rev. 76 (2017) 717–727. URL:https://doi.org/10.1016/j.rser.2017.03.028.

[16] P.C. Loh, M.J. Newman, D.N. Zmood, D.G. Holmes, A comparative analysis of multiloop voltage regulation strategies for single and three-phase ups systems, IEEE Trans. Power Electron. 18 (5) (2003) 1176–1185. URL: https://doi.org/10.1109/TPEL.2003.816199.

[17] A. Hasanzadeh, O.C. Onar, H. Mokhtari, A. Khaligh, A proportional-resonant controller-based wireless control strategy with a reduced number of sensors for parallel-operated upss, IEEE Trans. Power Delivery 25 (1) (2010) 468–478. URL:https://doi.org/10.1109/TPWRD.2009.2034911.

[18] S. Golestan, J.M. Guerrero, J.C. Vasquez, A pll-based controller for three-phase grid-connected power converters, IEEE Trans. Power Electron. 33 (2) (2018) 911–916. URL:https://doi.org/10.1109/TPEL.2017.2719285.

[19] P. Mattavelli, An improved deadbeat control for ups using disturbance observers, IEEE Trans. Industr. Electron. 52 (1) (2005) 206–212. URL: https://doi.org/10.1109/TIE.2004.837912.

[20] M.A.U. Rasool, M.M. Khan, M.T. Faiz, S. Tahir, W. Zhang, An optimized disturbance observer based digital deadbeat control technique for three-phase voltage source inverter (2018). doi: 10.1145/3277453.3286094. URL: https://doi.org/10.1145/3277453.3286094.

[21] M. Ali, M. Aamir, H.S. Khan, A. Waqar, F. Haroon, A.R. Jafri, Lyapunov stability and performance analysis of the fractional order sliding mode control for a parallel connected ups system under unbalanced and nonlinear load conditions, Energies 11 (12) (2018) 3475. URL:https://doi.org/10.3390/en11123475.

[22] O. Kukrer, H. Komurcugil, A. Doganalp, A three-level hysteresis function approach to the sliding-mode control of single-phase ups inverters, IEEE Trans. Industr. Electron. 56 (9) (2009) 3477–3486. URL:https://doi.org/10.1109/TIE.2009.2016512.

[23] M.A.U. Rasool, M.M. Khan, Z. Ahmed, M.A. Saeed, Analysis of an h8 robust control for a three-phase voltage source inverter, Inventions 4 (1) (2019) 18. URL:https://doi.org/10.3390/inventions4010018.

[24] C.K. Sao, P.W. Lehn, Autonomous load sharing of voltage source converters, IEEE Trans. Power Delivery 20 (2) (2005) 1009–1016. URL:https://doi.org/10.1109/TPWRD.2004.838638.

[25] M. Ali, M. Aamir, H.S. Khan, A.A. Khan, F. Haroon, Design and implementation of fractional-order sliding mode control for parallel distributed generations units in islanded microgrid, in: 2019 IEEE 28th International Symposium on Industrial Electronics (ISIE), IEEE, pp. 64–69. URL:https://doi.org/10.1109/ISIE.2019.8781383..

[26] H. Komurcugil, Rotating-sliding-line-based sliding-mode control for single-phase ups inverters, IEEE Trans. Industr. Electron. 59 (10) (2012) 3719–3726. URL:https://doi.org/10.1109/TIE.2011.2159354..

[27] I.S. Mohamed, S. Rovetta, T.D. Do, T. Dragicevic, A.A.Z. Diab, A neural-network-based model predictive control of three-phase inverter with an output *lc*, IEEE Access 7 (2019) 124737–124749. URL:https://doi.org/10.1109/ACCESS.2019.2938220.
[28] W. Lu, K. Zhou, D. Wang, M. Cheng, A general parallel structure repetitive control scheme for multiphase dc–ac pwm converters, IEEE Trans. Power Electron. 28 (8) (2013) 3980–3987. URL:https://doi.org/10.1109/TPEL.2012.2229395.
[29] H.K. Kang, C.H. Yoo, I.Y. Chung, D.J. Won, S.I. Moon, Intelligent coordination method of multiple distributed resources for harmonic current compensation in a microgrid, J. Electr. Eng. Technol. 7 (6) (2012) 834–844. URL:https://doi.org/10.5370/JEET.2012.7.6.834.
[30] P. Cortés, G. Ortiz, J.I. Yuz, J. Rodríguez, S. Vazquez, L.G. Franquelo, Model predictive control of an inverter with output *lc* filter for ups applications, IEEE Trans. Industr. Electron. 56 (6) (2009) 1875–1883. URL:https://doi.org/10.1109/TIE.2009.2015750.
[31] C. Zheng, T. Dragicevic, F. Blaabjerg, Current-sensorless finite-set model predictive control for lc-filtered voltage source inverters, IEEE Trans. Power Electron. URL:https://doi.org/10.1109/TPEL.2019.2914452..
[32] K.H. Ahmed, A.M. Massoud, S.J. Finney, B.W. Williams, A modified stationary reference frame-based predictive current control with zero steady-state error for lcl coupled inverter-based distributed generation systems, IEEE Trans. Industr. Electron. 58 (4) (2011) 1359–1370. URL:https://doi.org/10.1109/TIE.2010.2050414.
[33] M. Nauman, A. Hasan, Efficient implicit model-predictive control of a three-phase inverter with an output lc filter, IEEE Trans. Power Electron. 31 (9) (2016) 6075–6078. URL:https://doi.org/10.1109/TPEL.2016.2535263.
[34] H.S. Khan, M. Aamir, M. Ali, A. Waqar, S.U. Ali, J. Imtiaz, Finite control set model predictive control for parallel connected online ups system under unbalanced and nonlinear loads, Energies 12 (4) (2019) 581, https://doi.org/10.3390/en12040581.
[35] C. Zheng, T. Dragicevic, B. Majmunovic, F. Blaabjerg, Constrained modulated-model predictive control of an lc)filtered voltage source converter, IEEE Trans. Power Electron. URL:https://doi.org/10.1109/TPEL.2019.2917634..
[36] C.A. Plet, T.C. Green, A method of voltage limiting and distortion avoidance for islanded inverter-fed networks under fault, in: Proceedings of the 2011 14th European Conference on Power Electronics and Applications, IEEE, pp. 1–8..
[37] E. Ebrahimi, G. Gharehpetian, J. Milimonfared, A novel scheme to protect distribution networks in presence of inverter-based distributed generation, in: International Conference on Renewable Energies and Power Quality..
[38] I. Sadeghkhani, M.E.H. Golshan, J.M. Guerrero, A. Mehrizi-Sani, A current limiting strategy to improve fault ride-through of inverter interfaced autonomous microgrids, IEEE Trans. Smart Grid 8 (5) (2016) 2138–2148.
[39] X. Pei, Y. Kang, Short-circuit fault protection strategy for high-power three-phase three-wire inverter, IEEE Trans. Industr. Inf. 8 (3) (2012) 545–553.
[40] I. Ngamroo, T. Karaipoom, Improving low-voltage ride-through performance and alleviating power fluctuation of dfig wind turbine in dc microgrid by optimal smes with fault current limiting function, IEEE Trans. Appl. Superconduct. 24 (5) (2014) 1–5.
[41] J. Hu, J. Zhu, D.G. Dorrell, Model predictive control of grid-connected inverters for pv systems with flexible power regulation and switching frequency reduction, IEEE Trans. Ind. Appl. 51 (1) (2015) 587–594. URL:https://doi.org/10.1109/TIA.2014.2328785.
[42] V. Yaramasu, M. Rivera, M. Narimani, B. Wu, J. Rodriguez, Rodriguez, Model predictive approach for a simple and effective load voltage control of four-leg inverter with an output *lc* filter, IEEE Trans. Industr. Electron. 61 (10) (2014) 5259–5270. URL:https://doi.org/10.1109/TIE.2013.2297291.

Hussain Sarwar Khan is born in Muzaffargarh, Pakistan in 1994. He received the B. Sc. degrees in electrical (Power) engineering from the Islamia University of Bahawalpur, Pakistan in 2016 and completed the master studies degree in electrical engineering with specialization in power systems from Bahria University Islamabad, Pakistan in 2018.

From 2017 to 2018, he was a Design Engineer (R&D) at a research project funded by Higher Education Commission, Pakistan at Bahria University Islamabad. He is currently serving as a Project Researcher at School of Technology and Innovations, University of Vaasa, Vaasa, Finland. His research interests include model predictive control, UPSs, control of power converter, renewable energy and microgrid.

Muhammad Aamir received the B.E. (Hons.) degree in electrical engineering from the University of Engineering and Technology (UET), Peshawar, Pakistan, in 2007, the Master's degree in electrical engineering from Hanyang University, Seoul, South Korea, in 2011 and Ph.D. degree in electrical engineering from Power Electronics and Renewable Energy Research Laboratory (PEARL), University of Malaya, Kuala Lumpur, Malaysia in 2016. He is currently working as Assistant Professor at Pak-Austria Fachhochschule Institute of Applied Sciences and Technology Haripur, Pakistan. His research interests include UPSs, power conversion, Microgrid and control of power converters.

Kimmo Kauhaniemi was born in Kankaanpaa, Finland, in 1963. He received the M. Sc. and Dr. Tech. degrees in electrical engineering from the Tampere University of Technology, Finland, in 1987 and1993, respectively. He was with the VTT Technical Research Centre of Finland. He is currently a Professor and the Head of the Smart Electric Systems (SES) Research Group in electrical engineering with the University of Vaasa, Finland. He has long-term experience on transient simulation of various power systems. His research interests include electricity distribution systems, relay protection, smart grids, and microgrids.

Muhammad Waqar Hassan was born in D. G. Khan, Pakistan in 1996. He received the B.Sc. and MS degrees in electrical (Power) engineering from the Islamia University of Bahawalpur, Pakistan in 2017 and 2020 respectively. Muhammad Waqar Hassan became a Member of Pakistan Engineering Council in 2017. His research interests are grid-tied inverter, power regulation, microgrid, and model predictive control.

Engineering Science and Technology, an International Journal 48 (2023) 101557

Contents lists available at ScienceDirect

Engineering Science and Technology, an International Journal

journal homepage: www.elsevier.com/locate/jestch

Design and FPGA-in-loop based validation of predictive hierarchical control for islanded AC microgrid

Hussain Sarwar Khan *, Kimmo Kauhaniemi

School of Technology and Innovations, University of Vaasa, Finland

ARTICLE INFO

Keywords:
Decentralized control approach
Distributed generation
Dynamic loads
FPGA-in-loop
Model predictive control
Islanded AC microgrid

ABSTRACT

This paper proposes a decentralized control approach for the flexible operation of an autonomous AC microgrid (MG). AC MG typically consists of two or more voltage source inverters (VSI), capable of simultaneously regulating the voltage at the point of common coupling (PCC) and meeting the local power demand. The classical linear control techniques attain these functions. However, they have many limitations, such as slow transient response, high sensitivity to the parameter variations, and inability to handle the system nonlinearities. This paper aims to address these issues by presenting an improved finite control set model predictive control (FCS-MPC) approach for inverter-based distributed generation (DG). The proposed scheme tracks the voltage trajectory using cost function (CF) over two-step prediction horizons. The proposed control method is employed for the AC MG having two parallel DGs. Droop control is responsible for the power-sharing between the parallel DGs regardless of impedance mismatch at the distribution level of AC MG. The decentralized secondary control is developed to eliminate the deviation in the voltage and frequency caused due to overlooking the primary control. The proposed control scheme has been validated through extensive simulations and real-time controller hardware in the loop tests using an FPGA ZYBO Z7 board. Moreover, the proposed methodology depicts the enhanced transient response, less computational burden than the classic MPC, and shows robustness to parametric uncertainties in terms of THD than hierarchical linear control. The simulations and experimental results visually represent research outcomes, exhibiting the THD of 0.98 % for different dynamic loads, which is within the limit of IEEE and IEC standards. Furthermore, the proposed controller's mathematical stability is further supported by analysis based on the Lyapunov stability theory.

1. Introduction

Due to climate change and global warming, various countries in the world adopted the Paris Agreement to reduce the emission of greenhouse gases and also limit global warming below the 2 °C [1]. Power generation through fossil fuels such as oil, coal, and natural gas is one of the primary causes of greenhouse gases emission. The world is looking for alternative ways of energy generation, which must be clean, reliable, and carbon-free. Therefore, power generation through renewable energy sources has got the world's attention. However, renewable energy resources (RES) are intermittent and produce energy in both AC and DC. Consequently, the concept of distributed generation (DG) is introduced in literature by the research community to integrate RES in conventional power systems and meet the load demand locally [2].

The DGs are connected to the grid through a power electronic interface (PEI). PEIs are responsible for regulating the voltage, current, and power. The high penetration and integration of RES in the power system originate high risks to the power system's stability and reliability. The microgrid (MG) concept is presented to mitigate the problems as mentioned [3,4]. MG is a small distribution power system with a cluster of loads, generation units, and energy storage systems, and it effectively controls each unit [5]. The MG can operate in two modes, i.e., grid-connected and islanded modes. In grid-connected mode, MG has the ability to import and export the power with the utility grid as per grid codes such as EN 50549-1 or EN 50549-2 [6]. In islanded mode, MG is disconnected from the main grid due to regular maintenance, low-quality power generation, or occurred faults. The autonomous MG is also developed for areas far from the power network, such as rural areas. Islanded MG is used in various applications such as avionic [7], marine [8] and automotive [9]. Sometimes, it is economical to distribute the high power among the several DGs with lower current ratings. This mechanism also helps to maximize the system's efficiency. The islanded MG generates power to meet the demand locally and also regulates the voltage at the point of common coupling. However, an energy management system is required to run and optimize the operation of an islanded MG.

* Corresponding author.
E-mail addresses: hussain.khan@uwasa.fi (H.S. Khan), kimmo.kauhaniemi@uwasa.fi (K. Kauhaniemi).

https://doi.org/10.1016/j.jestch.2023.101557
Received 3 April 2023; Received in revised form 16 June 2023; Accepted 19 October 2023
Available online 3 November 2023

Nomenclature

ANN	Artificial Neural Network
CF	Cost Function
CI	Constant Current
CZ	Constant Impedance
CP	Constant Power
DSO	Distribution System Operator
DG	Distributed Generation
DER	Distributed Energy Resources
MG	Microgrid
MPC	Model Predictive Control
MPVC	Model Predictive Voltage Control
PEI	Power Electronic Interface
PC	Power Converter
PI	Proportional Integral
PR	Proportional Resonant
PCC	Point of Common Coupling
SOGI-PLL	Second Order Generalized Integrator Phase Locked Loop
TSO	Transmission System Operator
THD	Total Harmonic Distortion
VSI	Voltage Source Inverter
VSC	Voltage Source Converter

The MG control approaches are categorized as distributed, decentralized, and centralized in literature [10]. Distributed and centralized control techniques require a communication network. The implementation of centralized techniques reduces reliability and increases system complexity. However, the decentralized approach uses local measurements and does not require any communication infrastructure [11].

The hierarchical control of MG is vastly proposed in the literature and it is considered to be the best possible solution to regulate the MG operation. Fig. 1 explains the hierarchical control graphically for easy understanding. MG hierarchical control consists of three different levels, i.e., primary, secondary, and tertiary levels [12,13].

- **Primary control:** It is further divided into inner control and outer droop control loops. The inner control loop regulates the output current and voltage of DERs. The outer droop control is responsible for accurate power-sharing among the DGs and also mitigates the circulating current.
- **Secondary control:** This control level is responsible for mitigating the MG's voltage and frequency deviation. The response of this level is slower than the primary controller.
- **Tertiary Control:** This control level is at the highest level of the MG hierarchy, and its response is slower than the secondary control loop. It is responsible for scheduling and optimizing power generation references for DGs and the techno-economic operation of MG and remains in contact with DSO and TSO.

As aforementioned that tertiary control focuses on economic dispatch and operation scheduling. It is also characterized as coordination between multiple MG, which are interconnected. In [14] tertiary control is implemented to adjust the DG compensating efforts with respect to unbalanced voltage limits of DGs and load buses. Optimal power flow-based tertiary control using MPC is proposed in [15]. In [16], authors proposed a centralized IOT-based tertiary control solution for multi-microgrids.

Many studies are proposed in the literature incorporating primary and secondary control levels and implementing the amalgam of linear and nonlinear controllers. Hierarchical control for grid supporting inverter in AC MG is investigated in [17]. PR based inner and PI based

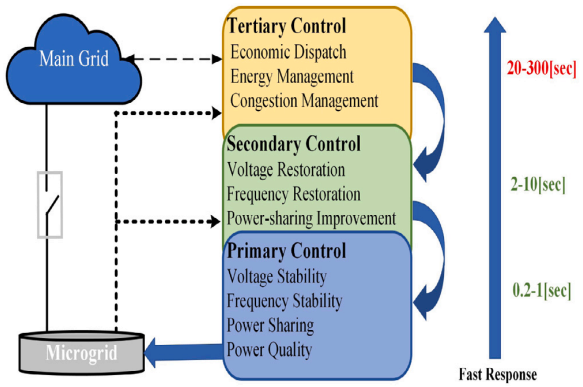

Fig. 1. Control layers typically utilized for hierarchical control of MGs.

secondary loops are proposed in [18] for the islanded AC microgrid. However, multiple resonant controllers are connected in parallel to cope with the fifth and seventh harmonics, which makes the system complex and takes the system towards instability. In [19], the authors proposed the hierarchical control for MG. The PI based linear controller is implemented in the microgrid's (primary and secondary) control levels. However, linear-based controllers cannot track the sinusoidal wave with zero steady state error and poor disturbance rejection capability and cannot handle the power systems' nonlinearity. Flexible secondary control for three VSIs operated in parallel is proposed in [20]. The authors also proposed a new algorithm to optimally tune the various gain of PR controllers. MPC based primary and secondary control is proposed in [21,22]. The predictive voltage hierarchical control for islanded MC with limited communications is studied in [23]. However, implementing predictive control at the secondary level is unsuitable due to the computational burden. Implementing MPC at the secondary level increases the system complexity and decreases the system response due to computational burden. Table 1 summarizes some of the recent studies on the hierarchical control of MG based on different control typologies.

The main task of primary control is to regulate the voltage and also achieve accurate power sharing among the DGs. Different types of linear and nonlinear control techniques have been proposed and investigated in the literature [29]. Linear controllers are limited in their ability to handle the nonlinearities and parameter variations of power systems, as well as other practical issues such as the need for tuning parameters and potential stability problems [20]. Nonlinear controllers perform better than linear controllers but have limitations, such as complex mathematical modeling [30], variable switching frequency [31], and high computational burden [32]. In [33], the author proposed sliding mode control for voltage regulation of a standalone DC/AC converter. Nevertheless, the complex mathematical modeling and chattering (an undesirable phenomenon) reduce the system's performance. MPC based hierarchical control for AC MG is proposed in [34] but the authors did not test the proposed under different dynamic loads and THD (%) is more than the proposed scheme.

The artificial neural network (ANN) aided MPC based voltage regulation technique is proposed in [35,36]. The authors use the MPC as the parent system to train the ANN. The performance of ANN is better than MPC in terms of total harmonic distortion (THD) and computational burden. However, the control technique needs to be more mature. The PID controller and its combinations are matured and vastly implemented by the power electronics industry. However, the nonlinear or advanced control approaches need complex mathematical modeling, and their implementation requires high-speed digital platforms. Table 2 summarized the pros and cons of different advanced control techniques.

Table 1
Comparison of hierarchical control approaches.

References	Control levels			Secondary control scheme	Applications
	Primary	Secondary	Tertiary		
[17]	H/SMC	Agent-based	–	Distributed	Grid-supporting converter
[18]	PR	PI	–	Centralized	VSI
[19,20]	PI	PI	–	Centralized	MG
[21]	MPC	MPC	–	Decentralized	MG
[24]	PI	PI	–	Centralized	MG
[16]	–	–	IOT based	Centralized	MG
[23]	Non-linear control (Lyapunov function)	Event predicted control	–	Centralized	MG
Proposed	MPC	PI	–	Decentralized	MG

Table 2
Comparison of the different linear and nonlinear control techniques.

	Linear control (Generalized)	Slide mode control	Artificial neural network	Model predictive control
Theoretical background	Mature	Mature	Weak	Mature
Computational Complexity	Low	Medium	Low	High
Handling system constraints	Incapable	No	Yes	Yes
Parameter sensitivity	No	Robust	Data dependent	Tunable
Intuitive Design	Average	Medium	Not-studied	Yes
Stability Analysis Tool	Strong	Strong	No	Initial results
Handling non-linearities	No	Yes	Yes	Yes
Frame of Reference	DQ	ALL	ALL	ALL
Implementation	[19,20]	[25]	[26,27]	[28]

This study aims to develop and implement the decentralized hierarchical control technique for attaining enhanced transient stability and accurate power sharing among the DGs under different dynamics loads in islanded AC MG. Fig. 6 elucidates the implemented hybrid MPC-based hierarchical control for DG. The key contributions in this study are as follows:

1. The finite control set model predictive voltage control is introduced at the primary layer to regulate the voltage of the DG and droop control is also implemented to attain accurate power-sharing among the DGs under complex load conditions. MPC uses DER's discrete time domain model to anticipate the future voltage states for each possible switching combination in every sampling time. This technique determines the error using the pre-defined cost function and produces optimal control action for the coming instant based on the error minimization. In order to reduce the switching loss, the switching frequency reduction technique is implemented based on [37].
2. Lyapunov stability studies are carried out to validate the stability of the proposed controller. According to the authors' best knowledge, this analysis has not been previously carried out for 2-level DC/AC three-phase inverters.
3. At the secondary control level, the PI controller based frequency and voltage regulation loop are employed to annihilate the voltage and the frequency deviation overlooked by the primary control in AC MG. The proposed technique uses local measurements to regulate the voltage and frequency of MG.
4. The impact of different dynamics loads, such as commercial, residential, and constant power, on the proposed controller is also studied and evaluated.

Additionally, to validate the system performance in real time, the controller hardware in the loop (CHIL) testing is carried out using the FPGA ZYBO Z7 board. The proposed controller runs on the FPGA board while AC MG is simulated in MATLAB/Simulink. The JTAG cable is used for two way communication. Finally, we also provide an GitHub[1] open repository of the dataset and simulation files and ZYBO Z7 (ZYNQ-7020) board definition files (to integrate the board into the MATLAB FPGA Manager for HIL validation) to the community for further research activities.

The rest of the paper is organized as follows: Section 2 explains the structure of MG. Section 2.1 describes the discrete modeling of DER and MPC and the switching reduction method is written in Section 2.2. The Lyapunov function MPC stability for DC/AC converter is derived in Section 2.3. Section 2.4 discusses the virtual impedance loop while the droop control and its implementation are expressed in Section 2.5. PI-based secondary control and its stability analysis are studied in Section 3. Dynamics loads and their mathematical modeling is explained in Section 4. Section 5 discusses the simulation studies. In contrast, HIL testing of the proposed control scheme is discussed in Section 5.1 while parametric uncertainty tests are presented in Section 5.2. Finally, the conclusion is presented in Section 6.

2. Microgrid

Fig. 2 illustrates the common configuration of a microgrid, which contains multiple DGs, loads, the energy storage system (ESS), transmission lines, and their effective control. MG is connected to the utility grid through a circuit breaker or static transfer switch. DGs are connected to an AC bus through a feeder. MG has the ability to work in grid connected or islanded mode. In this study, only islanded mode operation of MG is studied. Fig. 1 expressed the hierarchical control layers of MG and their roles. Since tertiary control has no role in islanded operation mode, it is not taken into account in this study. Droop control and virtual impedance loop are also discussed in this section.

[1] https://github.com/HS-Khan/-PREDICITVECONTROLUsingFPGAZYNQ7020

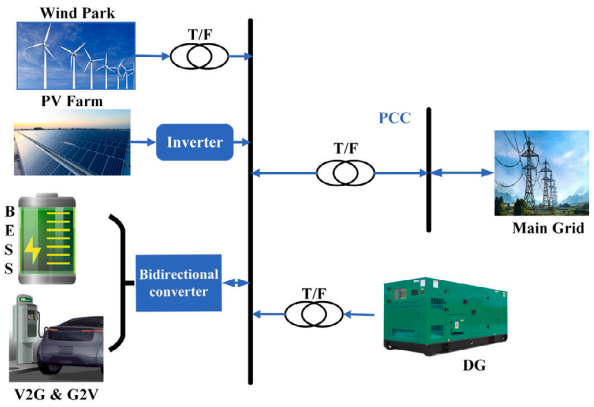

Fig. 2. Possible configuration of an islanded AC MG.

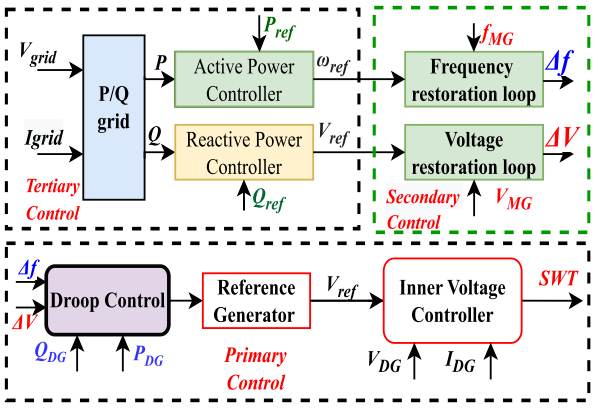

Fig. 3. Classical hierarchical control configuration of islanded AC MG.

2.1. MPC based primary control

This section discusses the discrete time modeling of VSI, the MPC's basic working principle, and its cost function definition. Fig. 3 demonstrates the classical hierarchical control implemented in literature for readers' better understanding. This study uses the Clarke transformation [38,39] to formulate the primary control in the $\alpha\beta$ reference frame. However, the performance of MPC in all frames of reference is evaluated to be the same [40].

The inner control of VSI is based on FCSMPC because it has better performance under transient conditions, the ability to handle the nonlinearity, good disturbance rejection capacity, and improved reference tracking capability [22]. The power converter's discrete-time model and filter are employed to anticipate the future response of DG for probable eight (2^3) switching states. Among these, six states are stated as active states, while two states with zero output are known as zero states as expressed in Eq. (1). The control approach based on MPC theory chooses the switching state, which has the least value of CF among them and is implemented for the next sampling time. Fig. 6 presents the two level three phase voltage source inverter with an LC filter to mitigate the switching harmonics. Each leg of VSC has two switches; they can be in on or off state and represented as 1 and 0, respectively. The output voltage of the VSI depends upon the switching states (000, 100, 110, 010, 011, 001, 101,& 111). At every switching action, VSI has a different output value and is expressed as follows:

$$V_0 = \begin{cases} \frac{2}{3}V_{dc}e^{j(i-1)\frac{\pi}{3}} & (i = 1, 2, \ldots \ldots 6) \\ 0 & (i = 0, 7) \end{cases} \quad (1)$$

The mathematical model of the VSI and its filter can be determined by using Kirchhoff voltage and current law. Eqs. (2) and (3) express the dynamic behavior of the capacitor and inductor, respectively. I_{fabc} is the inductor current through inductor L_f while V_{0abc} is the voltage across capacitor C_f, and i_{0abc} is the output current. V_i is the output of the converter. The equations are as follows:

$$\frac{1}{C_f}\frac{dV_{0abc}(t)}{d(t)} = i_f(t) - i_{0abc}(t). \quad (2)$$

$$V_i = i_f(t)R_f + L_f(t)\frac{di_f(t)}{d(t)} + V_{0abc}(t) \quad (3)$$

The state space model of the system is determined by combining Eqs. (2) and (3) and written as:

$$\frac{d(y)}{d(t)} = Ax + By \quad (4)$$

In Eq. (5), the x matrix represents the system's state variables, and the y matrix explains the output variables of the system.

$$x = \begin{bmatrix} V_{0abc} \\ i_f \end{bmatrix}, y = \begin{bmatrix} V_i \\ i_{0abc} \end{bmatrix} \quad (5)$$

$$A = \begin{bmatrix} 0 & \frac{1}{C_f} \\ -\frac{1}{L_f} & -\frac{R_f}{L_f} \end{bmatrix}, B = \begin{bmatrix} 0 & -\frac{1}{C_f} \\ \frac{1}{L_f} & 0 \end{bmatrix} \quad (6)$$

By solving Eq. (4) using Euler's technique, the discrete time model of the system can be expressed as:

$$\begin{bmatrix} V_{0abc}(t_k+1) \\ i_f(t_k+1) \end{bmatrix} = A_r \begin{bmatrix} V_{0abc}(t) \\ i_f(t) \end{bmatrix} + B_r \begin{bmatrix} V_i(t) \\ i_{0abc}(t) \end{bmatrix} \quad (7)$$

$$A_r = e^{AT_s} \approx 1 + AT_s \quad , \quad B_r = \frac{B}{A}\left(A_r - I\right) \quad (8)$$

where "t" represents the present instant, while $\varepsilon t_k + 1\varepsilon$ is the future sampling instant. Eq. (7) is used to pre-calculate the capacitor voltage for all feasible voltage vectors in the coming instant.

The definition of CF is essential in the design of MPC. CF is used to calculate the lowest error while handling multiple objectives. It is the error between the predefined reference and actual values. The general CF equation is presented in Eq. (9).

$$g_{\text{Gen}} = \sum_{i=t_k}^{t_k+N-1} \left\| v_{fe}(i) \right\|_2^2 + h_{\text{lim}}\,(i) + \lambda_u sw^2(i) \quad (9)$$

where v_{fe} is the anticipated tracking error and primary objective while secondary objectives are $h_l im(i)$ is the current limitation, $sw^2(i)$ defines the reduction of switching frequency and is regulated by weighting factor λ. The CF defined in this study is only based on the primary objective (Voltage) and is expressed as follows:

$$G_{\text{primary}} = \left(V_{0\alpha}^* - V_{0\alpha}^{(t_k+1)}\right)^2 + \left(V_{0\beta}^* - V_{0\beta}^{(t_k+1)}\right)^2 \quad (10)$$

where $V_{0\alpha\beta}^*$ represents the reference voltage for DG in the $\alpha\beta$ reference frame, and $V_{0\alpha\beta}^{(t_k+1)}$ is determined using Eq. (7). The reference voltage is provided by the droop control. The DC-link capacitor voltage is taken as constant throughout the modeling. The working process of the MPVC is illustrated in the flowchart as shown in Fig. 4. After the controller's initialization, measured inputs are taken by the controller to predict the one step ahead voltage and current using Eq. (7). Eq. (10) is used to determine the value of the CF for each possible switching state of the converter. Among all possible switching states, the switching state, which has minimal error value, is applied to the converter for the next switching instant.

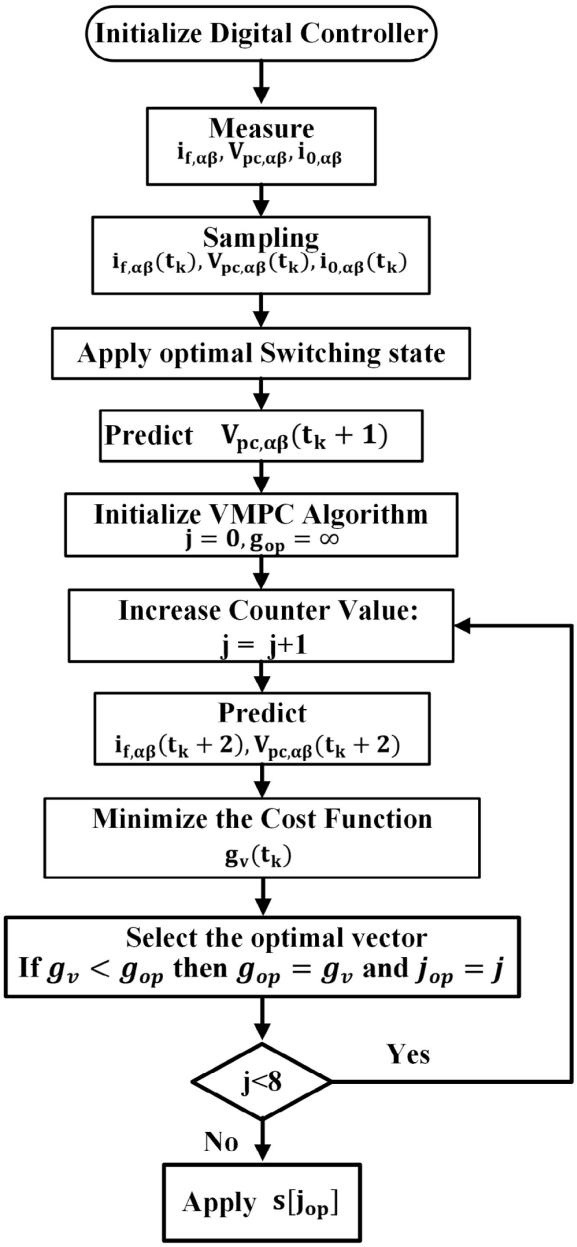

Fig. 4. Flow chart of the proposed predictive controller.

2.2. Two steps ahead switching frequency reduction scheme

The power converters' switching frequency has a major effect on systems' losses. If the switching frequency is high, more loss and more stress on the converter switches will consequently occur, reducing the converter's life and decreasing the system's efficiency. Classical MPC has higher switching losses due to high switching frequency. In order to cope with this issue, a two step ahead reduction approach is implemented in this study. For two level VSI, the converter has

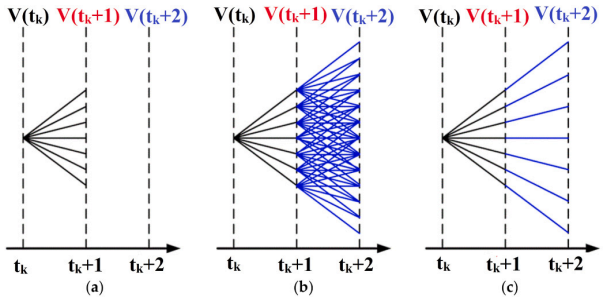

Fig. 5. Demonstration of prediction approach. (a) $N = 1$, (b) $N = 2$, and Different voltage vectors are used every sampling time. (c) $N = 2$, but the same vector is considered for two consecutive sampling times.

eight possible switching states (six active and two zero vector states) in one sampling instant, as shown in Fig. 5a. The switching state fulfills the CF criteria and is applied to the converter for the next sampling instant. In the two steps ahead classical approach, the total possible sequences are 49. So, The algorithm has to run the loop for 49 times, which increases the computation burden and also enhances the MPC performance, as demonstrated Fig. 5b. In this study, the two step prediction is accomplished by taking only eight vectors into account, as illustrated in Fig. 5c. This technique showed similar performance but had a lower switching frequency and computational burden hence using fewer hardware resources and improving the voltage quality in the form of lower THD. The predicted voltage for instant $(t_k + 2)$ is determined by Eq. (7).

2.3. MPC stability analysis

In the case of a linear theory based controller, the power electronic system is considered a linear system. In contrast, the nonlinear controller uses a power electronic system in a discrete time. So, the analysis methods based on eigenvector, bode plot, etc., are not ideal for finding the MPC stability. The Lyapunov stability criteria are widely used for the stability analysis of nonlinear controllers. There is no proper mathematical method to prove MPC stability, but many studies incorporate the Lyapunov stability to establish MPC stability. In [41], a statistical model checking approach is proposed to validate the MPC stability in the PC domain. The Lyapunov function based MPC is proposed for a four leg inverter in [42]. In [43], the authors studied the stability of MPC based on Lyapunov theory for AC/DC converters in battery applications. According to the author's best knowledge, the Lyapunov-based stability for a two level three phase DC/AC converter has not been derived before. In [44,45], multiple simulations are carried out with different system parameters to validate the response of the power converter under model uncertainties and parametric variations. The results of simulations are also verified by experiments and compared with the classical PI benchmark model. It is observed from the results that the control performance deteriorates for underestimated inductance and has no effect on the overestimated inductance. The described cases demonstrate a good steady state and transient response. The downside of this type of study is that the experiments are very time consuming. Table 3 illustrates the overview of literature work done in the domain of performance and stability of FCS-MPC.

The discrete Lyapunov function is expressed as:

$$L(k) = \frac{1}{2}\left[V_{\text{err}}\right]^T \left[V_{err}\right] \tag{11}$$

Table 3
Summary of the state-of-the-art stability and validation of FCS-MPC.

Application	Technique	Pros	Cons	Stability study	Performance validation
DC-DC converter [46] Multicell converter [47]	Lyapunov stability theory	Lyapunov stability theory (verification)	Complex cost function design	Yes	Yes
Multi-Modular converter (MMC) [44] 4-leg VSC [45]	Multi simulations, Parameter changing	Easy, fast, simple CF design	Close loop stability not defined, not validated	No	Yes
Active front end rectifier [48]	Lyapunov stability criteria	Lyapunov stability theory (verification)	Complex CF design, Not a classical MPC	Yes	No
2l-VSC [49]	Lyapunov stability theory	Easy, fast, simple CF design	Close loop stability not defined, not validated	Yes	No
VSC [41]	Benchmarking, Multiple experiments	Design for industrial engineers	Time consuming, Benchmarking	Yes	Yes
Proposed	Lyapunov stability theory	Verified	based on mathematical modeling	Yes	Yes

where V_{err} is the voltage tracking error. The change in the Lyapunov function is as follows:

$$\Delta L(k) = L\left(V_{\text{err}}\,[t+1]\right) - L\left(V_{\text{err}}\,[t]\right) \tag{12}$$

The system is asymptotically stable if the input $V_{err}(t)\epsilon A$ and also satisfies Eq. (13) or Eq. (14). Basically, Eq. (14) is the further elaboration of Eq. (13).

$$\begin{aligned}\|L\left(V_{\text{err}}\,[t+1]\right) - L\left(V_{err}[t]\right)\|_s \le L_1\Big\|\left(V_{err}[t+1]\right) \\ -\left(V_{\text{err}}\,[t]\right)\Big\| \forall V_{err}[t] \in \mathrm{A} \subseteq \mathrm{R}\end{aligned} \tag{13}$$

$$\begin{aligned}\Big\|L\left(V_{\text{err}}\,[t+1]\right) - L\left(V_{\text{err}}\,[t]\right)\Big\| \ge L_2\Big\|\left(V_{\text{err}}\,[t+1]\right) \\ -\left(V_{\text{err}}\,[t]\right)\Big\| \forall V_{\text{err}}\,[t] \in \mathrm{B} \subset \mathrm{A}\end{aligned} \tag{14}$$

$$\Delta V(t) < -L_3\left\|V_{\text{err}}\,[t]\right\|^s + L_4 \tag{15}$$

where $L_1 - L_4$ must be positive values and $s \ge 1$. **A** is a positively invariant set of natural numbers. Now, define the inverter output voltage at t+1 sampling instant and express it as:

$$V_i[t+1] = \vec{V}_i[t+1] + \Delta[t+1] \tag{16}$$

$\vec{V}_i[t+1]$ is the continuous voltage input vector, and $\Delta[t+1]$ represents quantization error and satisfies the condition given in Eq. (16). Where is the quantization error upper limit and is greater than 0:

$$|\Delta(t+1)| \le \delta_1 \tag{17}$$

The change in the Lyapunov function for converter output voltage is:

$$\begin{aligned}\Delta V(t) = \frac{1}{2}\Big(\frac{1}{k_3}V_i(t+1) - \frac{k_1}{k_3}i_{0abc}(t+1) - \frac{k_2}{k_3}V_{0abc}(t+1) \\ -\frac{k_4}{k_3}i_f - V_0^*(t+1)\,)^T \cdot \Big(\frac{1}{k_3}V_i(t+1) - \frac{k_1}{k_3}i_{0abc}(t+1) \\ -\frac{k_2}{k_3}V_{0abc}(t+1) - \frac{k_4}{k_3}i_f - V_0^*(t+1)\,) \\ -\frac{1}{2}\left[V_{err}(t)\right]^T\left[V_{err}(t)\right]\end{aligned} \tag{18}$$

where

$$k_1 = \frac{L_f}{T_s}, k_2 = \left(1 - \frac{L_f}{T_s}\right), K_3 = \frac{L_f C_f}{T_s^2}, \quad k_4 = \frac{R_s T_s - L_f}{T_s} \tag{19}$$

Now rewrite Eq. (18) as per Eq. (16) by converting the load voltage, current, and inverters voltage vector into vector and quantization error. Here, $\delta_1(t+1), \delta_2(t+1), \delta_3(t+1)$ are the quantization errors.

$$\begin{aligned}\Delta V(t) = \frac{1}{2}\Big(\frac{1}{k_3}V_i(t+1) + \frac{1}{k_3}\delta_1(t+1) - \frac{k_1}{k_3}i_{0abc}(t+1) \\ -\frac{k_1}{k_3}\delta_2(t+1) - \frac{k_2}{k_3}V_{0abc}(t+1) - \frac{k_2}{k_3}\delta_3(t+1) - \frac{k_4}{k_3}i_f \\ -V_0^*(t+1)\,)^T \cdot \Big(\frac{1}{k_3}V_i(t+1) + \frac{1}{k_3}\delta_1(t+1) \\ -\frac{k_1}{k_3}i_{0abc}(t+1) - \frac{k_1}{k_3}\delta_2(t+1) - \frac{k_2}{k_3}V_{0abc}(t+1) \\ -\frac{k_2}{k_3}\delta_3(t+1) - \frac{k_4}{k_3}i_f - V_0^*(t+1)\,) - \frac{1}{2}\left[V_{err}(t)\right]^T\left[V_{err}(t)\right]\end{aligned} \tag{20}$$

The VSI voltage vector, load current, and voltage are finite sets and bounded. The change of defined control error in Eq. (15), can be written as:

$$\begin{aligned}\Delta V(t) \le -\frac{1}{2}\left[V_{err}(t)\right]^T\left[V_{err}(t)\right] \\ +\frac{1}{2}\left(\frac{1}{k_3}\delta_1 - \frac{k_1}{k_3}\delta_2 - \frac{k_2}{k_3}\delta_3\right)^2\end{aligned} \tag{21}$$

The stability of the system is satisfied by the given conditions:

$$\begin{aligned}L_1 = L_2 = 1, L_3 = \frac{1}{2}, \\ L_4 = \frac{1}{2}\left(\frac{1}{k_3}\delta_1 - \frac{k_1}{k_3}\delta_2 - \frac{k_2}{k_3}\delta_3\right)^2\end{aligned} \tag{22}$$

As Eq. (21) has a negative sign, the system energy converges to zero with the time towards infinite and defines voltage control error converges as a compact set:

$$\delta = \left[\sqrt{\frac{L_4}{L_3}} \ge \left(V_{\text{err}} \mid V_{\text{err}}\right)\right] \tag{23}$$

2.4. Virtual impedance loop

The virtual impedance loop enhances system stability and damping and provides PQ decoupling. It also lowers the circulating current and power ripple. The virtual DG impedance value is determined from [50]. The voltage drop can be calculated in $\alpha\beta$ reference frame using Eq. (24) as stated:

$$\begin{bmatrix}V_{d\alpha} \\ V_{d\beta}\end{bmatrix} = \begin{bmatrix}R_1 & -\omega L_1 \\ \omega L_1 & R_1\end{bmatrix}\begin{bmatrix}i_{0\alpha} \\ i_{0\beta}\end{bmatrix} \tag{24}$$

Here R_1 and L_1 represent the feeder impedance.

2.5. Droop control

Droop control is responsible for accurate power sharing among the distributed generations and lies at the upper level of primary control of

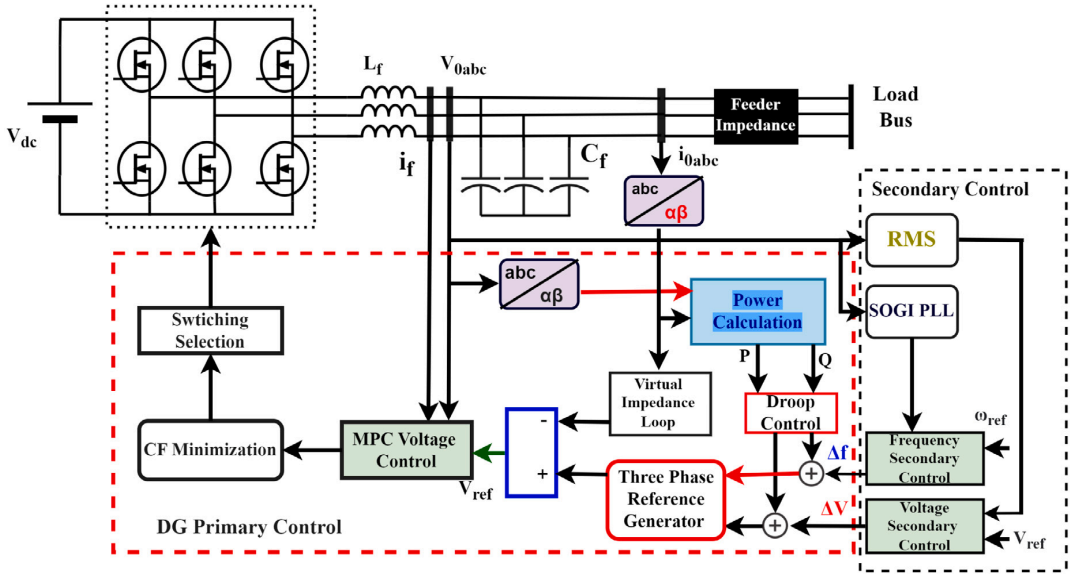

Fig. 6. Block diagram of the proposed decentralized control strategy.

MG, and is widely used due to its communication less structure [18,51]. P-f and Q-v droop strategy is implemented in this study and expressed as follows:

$$f = f_n - K_p(P - P_{ref}) \tag{25}$$

$$V = V_n - K_q(Q - Q_{ref}) \tag{26}$$

P_{ref} and Q_{ref} are zero in the case of islanded MG, and V and f are the voltage amplitude and frequency generated by the droop approach for concern DG. K_p and K_q are droop coefficients and expressed as $K_p = \frac{\Delta f}{P_{max}}$ and $K_q = \frac{\Delta V}{Q_{max}}$. ΔV and Δf are the maximum deviations in voltage and frequency, while P_{max} and Q_{max} are rated active and reactive power of the DG. Droop control keeps the voltage and phase angle stable, eliminating the circulating current. Eqs. (14) to (15) are used to evaluate the P and Q using instantaneous power theory in the $\alpha\beta$ reference frame:

$$P = i_{f\alpha}V_{0\alpha} + i_{f\beta}V_{0\beta} \tag{27}$$

$$Q = i_{f\alpha}V_{0\beta} - i_{f\beta}V_{0\alpha} \tag{28}$$

3. Secondary control

The fundamental responsibility of secondary control is to regulate the voltage and frequency deviation at PCC and forcefully shift the system variables to their nominal reference values with zero steady-state error after each change of generation and load. However, these deviations are generated due to overseeing the primary control. The voltage and frequency deviations are larger in the case of linear theory based controllers while smaller in the case of nonlinear controllers. In order to attenuate these deviations, the PI controller is used as a regulator. The secondary control layer usually consists of a voltage and frequency regulation loop. A second order generalized integrator phase locked loop (SOGI PLL) is used to measure the system's frequency. The secondary voltage and frequency compensation loops are extracted as follows:

$$\Delta V = k_{pv}\left(V_{ref} - V_{Act}\right) + k_{iv}\int\left(V_{ref} - V_{Act}\right)dt \tag{29}$$

$$\Delta f = k_{pf}\left(f_{\text{ref}} - f_{\text{SOGI}}\right) + k_{if}\int\left(f_{\text{ref}} - f_{\text{SOGI}}\right)dt \tag{30}$$

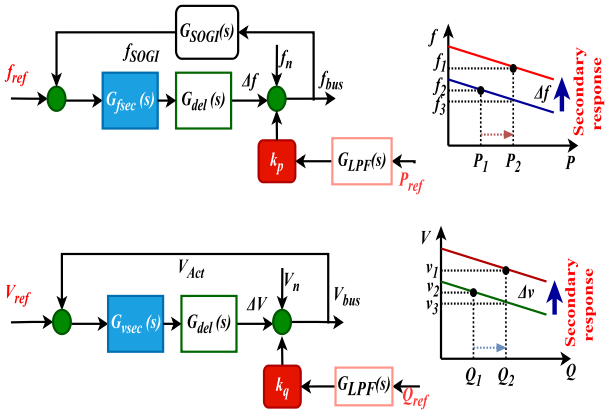

Fig. 7. Block diagram of the secondary control for frequency and voltage restoration.

where k_{pv}, k_{iv}, k_{pf} and k_{if} are the gain parameters of secondary layers regulators. V_{ref} and f_{ref} are the reference voltage and frequency of MG, while f_{SOGI} and V_{Act} are the actual frequency and voltage of AC bus in MG.

Fig. 7 illustrates the complete structure and process and how secondary control works and restores the voltage and frequency deviation. However, the response of the secondary level control is slower than the primary level control. As shown in the p-f graph, with the load increment, primary control acts first accordingly and increases the power generation. However, the system's frequency moves from f_2 to f_3 Hz. Then secondary control adds the δf factor into droop control to shift the characteristic curve to attain the system frequency. The same principle is applied in the voltage droop case. Without secondary control, the amplitude and frequency of MG would be load dependent. To design the regulator and analyze the system's stability, the transfer function is determined for the frequency regulation loop as written in Eq. (32). As shown in Fig. 6, the block model comprises droop control, secondary control gain, second order generalized integrator based phase lock loop, and communication delay. The block model is

mathematically represented as:

$$f_{bus} = \frac{G_{fsec}(s)G_{del}(s)}{1 + G_{fsec}(s)G_{del}(s)G_{\mathrm{SOGI}}(s)} f_{ref} - \frac{k_p G_{LPF}(s)}{1 + G_{fsec}(s)G_{del}(s)G_{SOGI}(s)} P_{ref} \quad (31)$$

Here the transfer function is demonstrated as follows:

$$G_{fsec}(s) = \frac{k_{pf}s + k_{iF}}{s} \quad (32)$$

$$G_{del}(s) = \frac{1}{(s + 1.5\omega_s)} \quad (33)$$

$$G_{LPF}(s) = \frac{\omega_c}{s + \omega_c} \quad (34)$$

The P_{ref} to f_{bus} transfer function can be written as:

$$f_{bus} = \frac{k_p \omega_c s\,(s^2 + sa + b)}{s^4 + s^3 c + s^2 d + se + f} P_{ref} \quad (35)$$

The parameters are given as:

$$\boldsymbol{a} = t + 1.5T_s, \quad \boldsymbol{b} = 1.5T_s tc = 1.5T_s + \omega_c + t \quad (36)$$

$$d = \omega_c\,(1.5T_s + t) + t\,(1.5T_s + k_{pf}) \quad (37)$$

$$e = t\,(\omega_c\,(k_{pf} + 1.5T_s) + k_{iF})\; f = tk_{iF}\omega_c \quad (38)$$

By using this model, the secondary control parameters can be easily adjusted, and the effects of communication delays can also be analyzed. The voltage regulation loop is also modeled and developed using the same procedure.

4. Dynamics loads

The dynamic load is a load in which active and reactive power depends on the voltage and frequency of the systems. However, the voltage variation is in practice larger than the frequency variation [52]. The mathematical model of the load as a function of voltage is as follows:

$$P = P_0 \left[\frac{V}{V_0}\right]^{n_p} (1 + n_{pf}\Delta f) \quad (39)$$

$$Q = Q_0 \left[\frac{V}{V_0}\right]^{n_Q} (1 + n_{qf}\Delta f) \quad (40)$$

P_0 and Q_0 are the nominal power rating of load. P and Q are the net power rating of load w.r.t the frequency and voltage of the system. The n_p and n_q are the load constants that define the load's nature. For constant current load, the value of n_p and n_q equals to one, and the value is two for constant impedance load. n_{qf} and n_{pf} are weighting factors to control the effect of frequency on load. The relationship between power and voltage is quadratic under constant impedance load (CZ), while in constant current load (CI), power is linear with bus voltage. However, constant power (CP) loads are independent of voltage. Table 4 expressed load constants, the power rating of the dynamic loads used in this study.

5. Simulation results

This part of the article discusses the simulation studies of the MG model developed in the MATLAB/Simulink environment to evaluate the performance of the proposed control strategy. Several MATLAB/Simulink simulations are carried out to assess the response of the proposed controller under different types of dynamic loads. In the simulation studies, two DGs with feeder mismatch are tested under different dynamic loads such as constant current, constant impedance, and constant power load to validate the performance of the studied controller, as shown in Fig. 8. The proposed system's control parameters

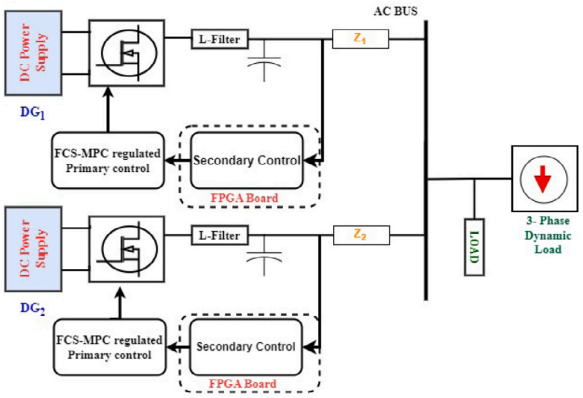

Fig. 8. Simulated communication and physical model of MG.

Table 4
Dynamics load contacts and their power ratings.

Load types	Load constants		Active power rating P_0 (kW)	Reactive power rating Q_0 (kVar)
	n_p	n_q		
Constant Current (CI)	1	1	6	4
Constant Impedance (CZ)	2	2	2	0
Constant Power (CP)	0	0	8	6
Industrial motor load	0.1	0.6	15	7

Table 5
Simulation parameters.

Parameter	Value
DC Input V_{dc}	700 [V]
Inductor value	$L_f = 2\times10^{-3}$ [H]
Nominal Bus Voltage	$V_{bus} = 320$ [V]
Capacitor	$C_f = 250\times10^{-6}$ [F]
System Frequency	50 [Hz]
Droop Coefficients	$K_p = 0.0001$, $K_q = 0.001$
Sampling Time	20×10^{-6} [s]
Secondary Voltage Control Gains	$K_p = 1.01$, $K_i = 0.001$
Secondary Frequency Control Gains	$K_p = 0.165$, $K_i = 0.001$
Switching Frequency	20 [kHz]
Line Impedance	$R_1 = 0.1$ [Ω], $L_1 = 2.4\times10^{-3}$ [H]

are prescribed in Table 5, and the sampling time of the simulation is 20 μs. The results analysis is further divided into two parts; the first part explains the response of the studied controller with secondary and without secondary controller under normal RL load. The second part illustrates the system's performance under different types of dynamic loads.

To validate the performance of the proposed control, two DGs are operated in parallel, having an LC filter, and a feeder impedance is also added to make the system more realistic. The total load of 13 kW and 6 kVar is connected to the common MG AC bus. Fig. 9 shows the voltage and frequency of the DG_1 and DG_2 without secondary control. The initial part of the RL load of 9 kW and 4 kVar is suddenly connected to the system at instant t = 0.2 s So, there is a negligible dip in the voltage and frequency due to connecting the initial load. Again, at instant t = 0.6 s, the load is further increased to 13 kW and 6 kVar. The DGs' voltage and frequency drop and settle at a lower value due to the absence of secondary control.

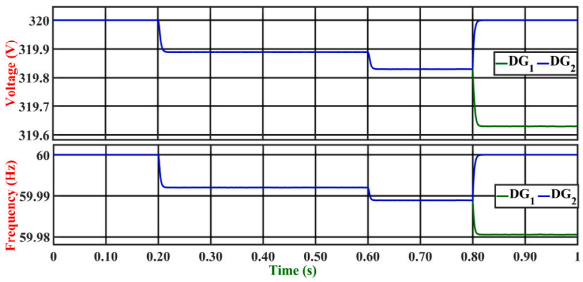

Fig. 9. Frequency and voltage of DGs under RL load, when secondary control is not employed.

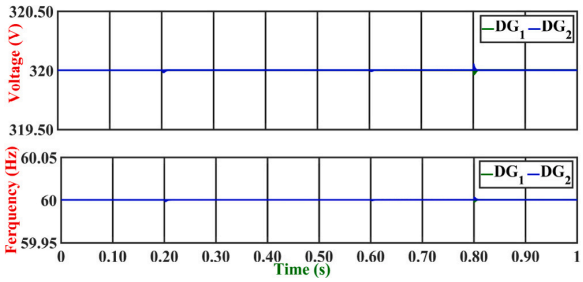

Fig. 10. Frequency and voltage of DGs under RL load, when secondary control is employed.

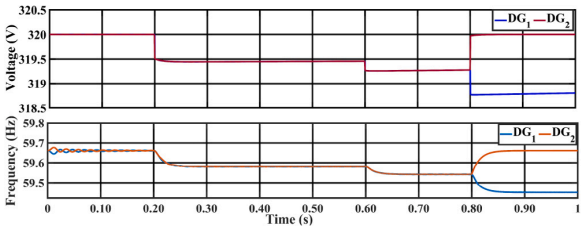

Fig. 11. Frequency and voltage waveform of DGs (PI based primary control) under RL load.

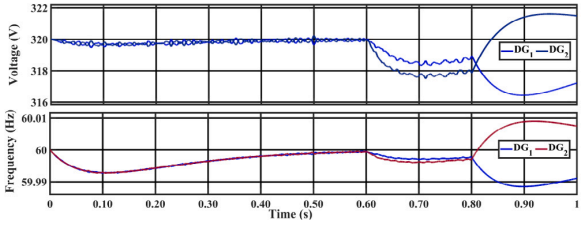

Fig. 12. Frequency and voltage waveform of DGs under RL load, when PI based hierarchical control is implemented.

At t = 0.8 s, the DG_1 is disconnected from the system. Therefore, the frequency of DG_2 drops from its nominal value, and the voltage also falls due to an increased share of the load. DG_2 is under a no load condition, so the voltage and frequency of DG_2 elevate to the predefined reference value.

Fig. 10 illustrates the voltage and frequency of the DGs with secondary control. It can be observed from Fig. 10 that the frequency and voltage demonstrate a slight dip and deviation from the reference values due to the load change. The secondary controller adds the increments to attain the reference value within no time. It is also seen

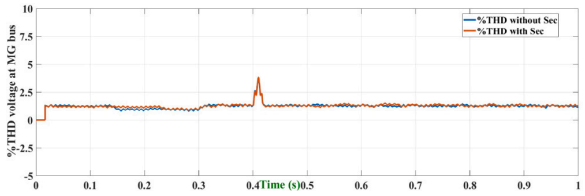

Fig. 13. THD of the MG at PCC.

in Fig. 10 that small transients occur in the system due to the operation of circuit breakers. However, the controller effectively accomplishes its goal of promptly achieving the reference voltage and frequency. Figs. 11 to 12 present DGs' output voltage and frequency when implementing PI-based hierarchical control. As shown in Fig. 11, the voltage and frequency of DGs decrease with the increase in load due to the absence of secondary control loop, and the PI based primary control loop has more deviation in voltage and frequency compared to the proposed controller. Fig. 12 depicts the performance of DGs when PI controller based hierarchical control is implemented. From Fig. 12, it can be observed that the PI based hierarchical control exhibits inferior performance when compared to the proposed control scheme. Fig. 13 illustrates the total harmonic distortion (THD) of the voltage at the AC bus of the MG. The voltage THD remains under 2 percent for the proposed control scheme.

The performance of the proposed PI+MPC based hierarchical control scheme is also analyzed under the different dynamics loads such as CZ, CI, and CP.

Constant Impedance: The output power of CZ load is in a quadratic relationship with voltage. Fig. 14(a) exhibits the voltage and frequency of DG_1 and DG_2 under constant impedance (CZ) load. At t = 0.3 s, the load of 2 kW is suddenly connected to the system. However, the voltage and frequency remain stable despite the switching of the load. The THD percentage of the current is 0.65. So the proposed controller effectively suppressed the voltage and current harmonics.

Constant Current: In this load, the output current remains constant, but the power changes linearly with the voltage. The power rating CI load is 6 kW and 4 kVar, which is connected to the system at t = 0.3 s, as demonstrated in Fig. 14(b). It is observed from the simulation results that the voltage and frequency of the system drop due to the addition of the load. But the proposed control system effectively tracks the reference and shares the DGs' harmonics. The percentage THD of the voltage is less than with the conventional control techniques, as shown in Table 6. At the same time, the current harmonics is about 0.47 percent, far less than the recommended value of IEEE/IEC standards such as IEC 62040, IEEE 1547 [53], and IEEE 519 [54]. The IEEE 519 standard recommends that the total harmonic distortion (THD) for voltage should not exceed 5 percent for systems with a voltage at the point of common coupling (PCC) of 69 kV and below. For individual harmonics, the standard recommends that it should not exceed 3 percent [54].

Constant Power: In this type of load, power remains constant and dependent on the input voltage change. The total load of 8 kW and 6 kVar is applied to the system at 0.3 s, as shown in Fig. 14(c). The system voltage and frequency show some disturbance, attain the reference, and become stable. The current harmonics are observed at PCC due to the feeder mismatch. However, the current harmonics are reduced and properly shared by the DGs. The current harmonic percentage is 0.33 at the PCC. The THD percentage comparison among the different control schemes is presented in Table 6.

Fig. 14(d) illustrates the simulation results of voltage and frequency of islanded MG when the industrial motor load is connected with a power rating of 16.55 kVA. The motor load is connected to the system at 0.3 s and shows the spike in voltage and current waveform due to the switching of the circuit breaker. The nominal voltage

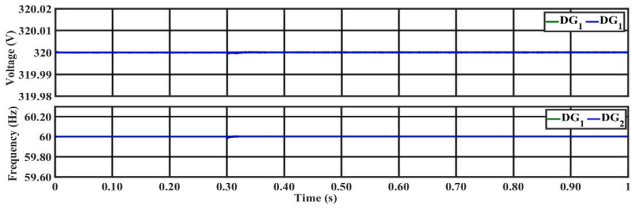

(a) Voltage and frequency of the DG_1 and DG_2 under CZ load.

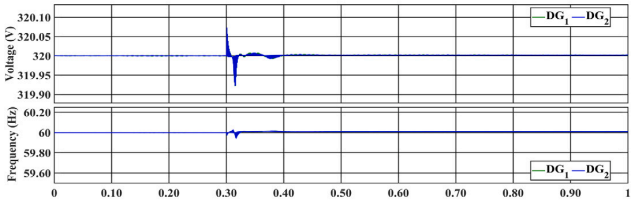

(b) Voltage and frequency of the DG_1 and DG_2 under CI load.

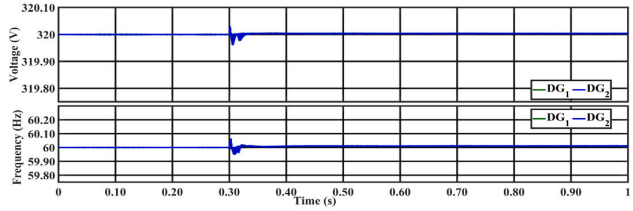

(c) Voltage and frequency of the DG_1 and DG_2 under CP load.

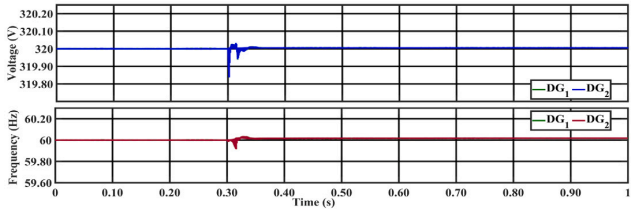

(d) Voltage and frequency of the DG_1 and DG_2 under Small industrial load.

Fig. 14. Impact of different dynamics loads on the voltage and frequency of the AC MG.

and frequency of the DGs deviate from their reference. The proposed secondary controller eliminates voltage and frequency deviation with minor transients in 0.1 s, produced by the droop control due to a change in load. The current harmonics in the case of the industrial motor is 0.22 percent. The active and reactive power generated by the DGs to meet the load demand is illustrated in Fig. 15. The power voltage relation is quadratic in the case of CZ load and also has a large load power variation. At the same time, the CI load has less load power variation compared to CZ and has linear relation between voltage & power. In the case of CP, the voltage is not dependent on power and has a constant power load. Table 6 explains the performance analysis of THD among different control techniques. The proposed hybrid control scheme has achieved less percentage THD in all load types.

Table 6
Voltage quality performance of the proposed controller under complex load conditions.

Load Types	Conventional PR based Hierarchical control (THD) [20,21]	MPC based Hierarchical control (THD) [21]	Proposed (THD)
Constant Current	7.10%	3.69%	0.98%
Constant Impedance	7.10%	3.69%	0.98%
Constant Power	7.10%	3.69%	0.98%

5.1. Controller-HIL studies

FPGA-in-the-loop (FIL) wizard provides the capability to use MATLAB/Simulink for testing controllers in real hardware conditions. The FIL wizard generates the code in VHSIC hardware descriptive language (VHDL) then generated VHDL code of the controller under test (CUT) is burned on the selected FPGA board. The communication between the board and MATLAB/Simulink is carried out through a JTAG cable. In this study, ZYBO Z7 (ZYNQ-7020 development board) is used. The ZYBO Z7 is driven by 125 MHz oscillators and supports the JTAG mode. It has 13300 logic slices, 106,4000 flip flops, and 630 kB embedded RAM. Fig. 16 illustrates the working of the FIL implementation in

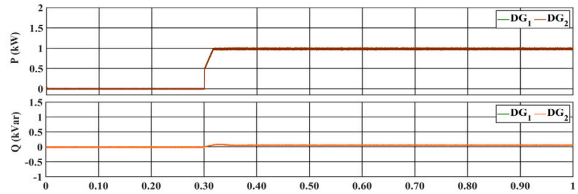

(a) Active and reactive power generated by DG_1 and DG_2 under CZ load.

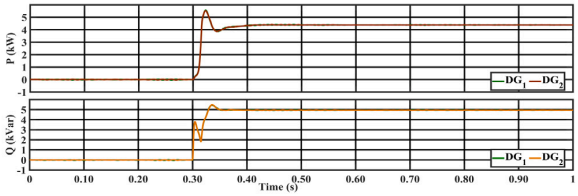

(b) Active and reactive power generated by DG_1 and DG_2 under CI load.

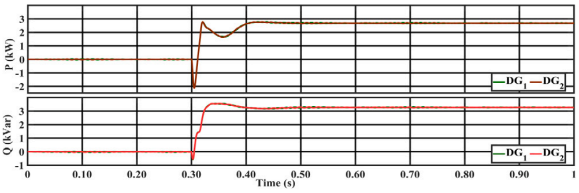

(c) Active and reactive power generated bye DG_1 and DG_2 under CP load.

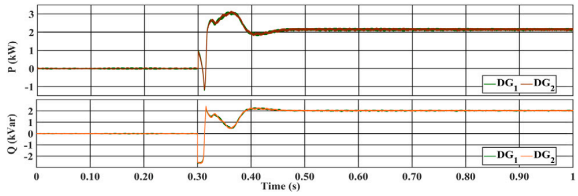

(d) Active and reactive power generated by DG_1 and DG_2 under Small industrial load.

Fig. 15. The response of DGs power generation under different dynamic loads.

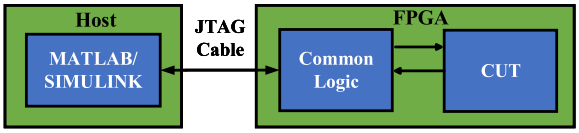

Fig. 16. Working principle of FPGA-in-Loop simulation environment.

SIMULINK. The CUT is burnt on the FPGA board, while the remaining AC MG model is on the MATLAB/Simulink environment. The interactive communication is done through a JTAG cable. FIL Implementation is performed in the following steps:

1. The controller under test is specified using a Simulink subsystem. Then inputs and outputs of the subsystem are defined as fixed data types(This operation can be performed using SIMULINK Fixed Point Tool).
2. After defining data types, select the CUT subsystem, open the HDL workflow, and run all tasks.
3. After running all tasks successfully, Matlab will generate the VHDL code of CUT and write it up on the FPGA board.

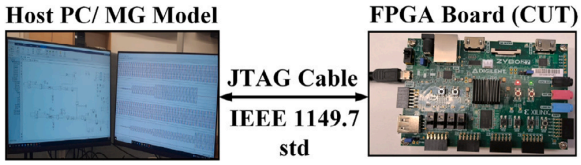

Fig. 17. Systematic view of FPGA controller hardware in the loop simulation environment along with the signal flow.

The performance of the studied controller is verified experimentally. Fig. 17 presents the systematic diagram of the experimental setup utilized for the proposed algorithm. This study implements the secondary controller on an FPGA card, while the AC MG model and MPC-based primary controller are modeled on MATLAB/Simulink environment. The controller hardware in the loop (CHIL) testing is carried out to study the response of the secondary controller in real time. Fig. 8 explains the detailed structure of the studied cases. Fig. 18 expressed the voltage and current of DERs during the step change of load under primary and secondary control. At t = 0.2 s, the RL load is connected to MG at the PCC. Voltage, the output current of the DERs remains stable despite a smaller dip, as shown in Fig. 18. Suddenly further load of 5 kW & 2 KVar is added into the system to see the impact of load on the proposed controller at t = 0.6 s The system remains stable and attains the new power demand in no time. At t = 0.8 s, hot-swap operation is performed. Usually, this type of simulations studies is performed for UPS applications [55]. In this test, one DG suddenly goes out of the system due to a circuit breaker tripping. The remaining DGs take the whole connected load. It can be noticed from the figure that DG_1 instantly increased its power generation to fulfill the load demand. The quality of voltage and current remained stable despite the transition period when DG_2 was isolated from the system. Fig. 19 shows the voltage and frequency of the DGs. It is observed from Fig. 19 that the voltage and frequency of the system remain stable despite disturbances occurring to changes in load. Fig. 20 shows the response of droop control to share the active and reactive power between the DG_1 and DG_2 according to the load demand.

Figs. 21 to 22 present the system's fault study results. At t = 0.3 s, the three phase ground fault occurred at the PCC. DG voltage becomes zero, and the output current increases by 3 times the load current. Fig. 22 illustrates the fault current injection and bus voltage at the point of fault. When the fault is cleared at 0.4 s, the voltage and current of the MG are stabilized within no time.

5.2. Parametric uncertainty tests

This section discusses the performance of the proposed controller under the parameter uncertainty issues. The filter value of the DG is changed at t = 0.4 s from 2 mH to 1 mH. After changing the filter inductance value, The proposed controller performs better than PI, as shown in Figs. 23 to 24. This comparison is carried out based on THD in the converter's output voltage, which is 1.88 percent in the case of the proposed controller, but THD is 4 percent when PI is employed. The results illustrate the suitability and better performance of the studied controller under realistic conditions, and thus the proposed control can be effectively implemented for practical applications.

6. Conclusion

This paper proposed a decentralized hierarchical control comprised of FCS-MPC-based primary control and PI-based secondary approach for islanded AC microgrid to enhance the transient stability, load sharing, and power quality among the parallel connected DGs in AC MG under different dynamic loads (CZ, CI, CP, and industrial load). The mathematical stability of the proposed controller is also justified

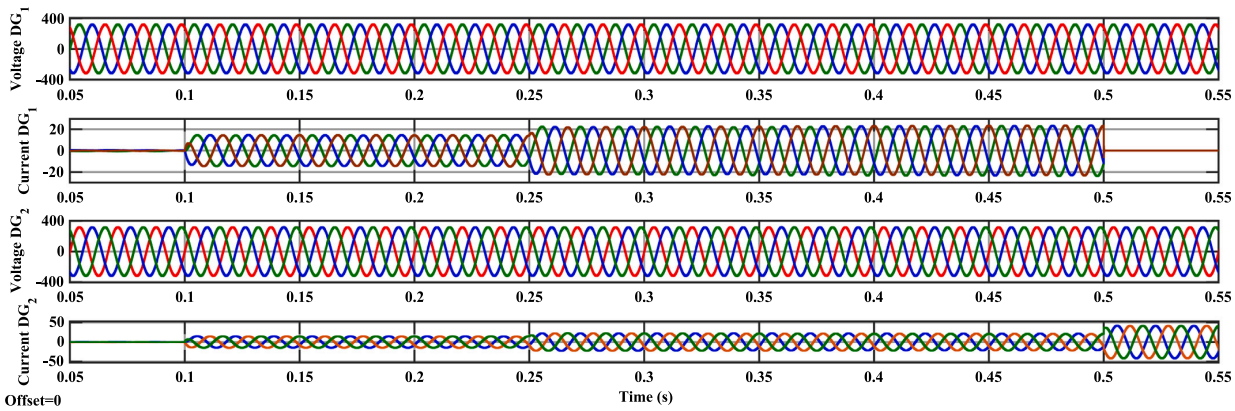

Fig. 18. Three phase voltage of DERs with RL load under step change of load.

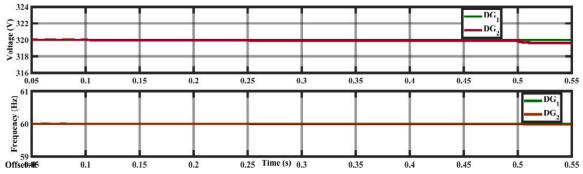

Fig. 19. DERs frequency and output voltage under step change of load.

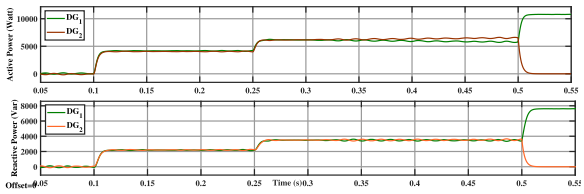

Fig. 20. Active and reactive power generated by the DERs to cope with the load demand.

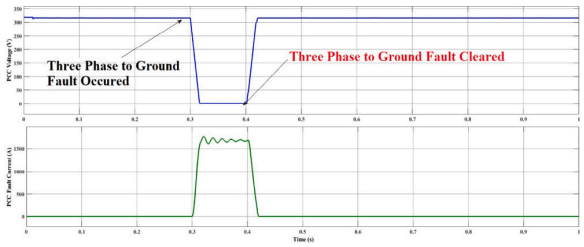

Fig. 21. Voltage and fault current injection during the 3-phase balanced fault at PCC.

using Lyapunov stability criteria. This rigorous mathematical proof confirms that the controller maintains stability within the system. The performance of the proposed control scheme is validated through the realistic MG test bench comprising two DGs operated in parallel along with an LC filter and a feeder impedance. The effectiveness of the proposed control technique was verified by performing simulations in MATLAB/Simulink along with hardware-in-loop testing using the FPGA-in-loop. The simulations and hardware setup results illustrated that the proposed approach tracked the reference with zero steady-state error by effectively regulating the voltage and frequency to its nominal value. The proposed control strategy achieved a THD (%)

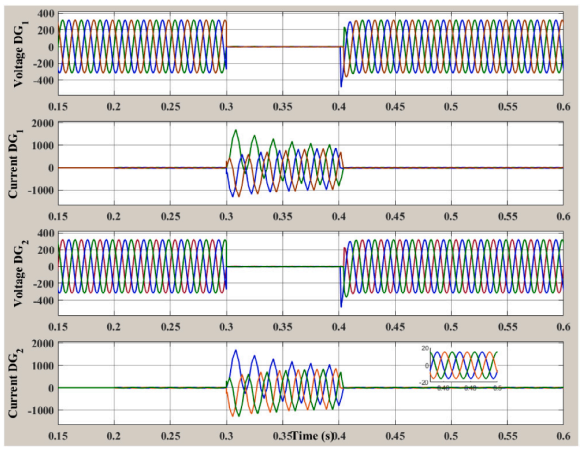

Fig. 22. Three phase voltage and output current of DERs under 3-phase balanced fault.

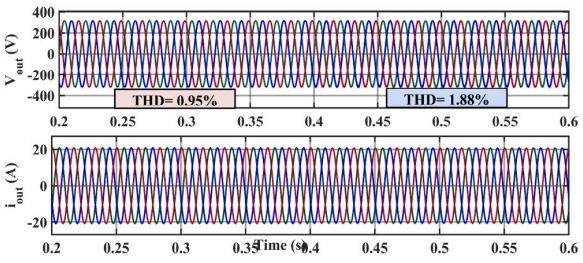

Fig. 23. Performance of the proposed control approach under load inductance changes L = 2 mH to L = 1 mH at t = 0.4 s.

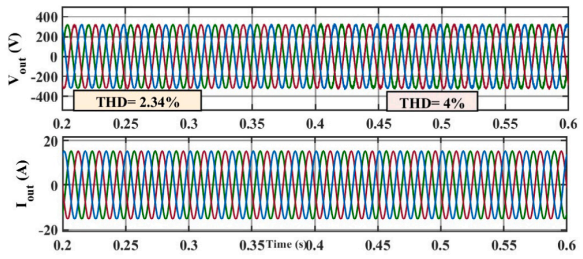

Fig. 24. Performance of the PI control approach under load inductance changes L = 2 mH to L = 1 mH at t = 0.4 s.

of 0.98 percent, much less than required per IEEE standards. Consequently, it enhances the power quality and ensures active and reactive power sharing between the DER under steady-state and transient load conditions.

CRediT authorship contribution statement

Hussain Sarwar Khan: Conceptualization, Methodology, Software & Hardware implementation, Writing – original draft. **Kimmo Kauhaniemi:** Supervision, Proofreading, Modification for the final layout.

Declaration of competing interest

The authors declare that they have no known competing financial interests or personal relationships that could have appeared to influence the work reported in this paper.

Acknowledgments

The authors would like to thank the editors and anonymous reviewers for providing insightful suggestions and comments to improve the quality of the research paper. This work is done in the SolarX and Smart Grid 2.0 research projects with the financial support provided by Business Finland with Grant No. 6844/31/2018 & 1386/31/2022. The financial support provided by the funding organization is highly acknowledged.

References

[1] P. Agreement, Paris agreement, in: Report of the Conference of the Parties to the United Nations Framework Convention on Climate Change (21st Session, 2015: Paris). Retrived December. Vol. 4, HeinOnline, 2015, p. 2017.
[2] M. Ahmed, L. Meegahapola, A. Vahidnia, M. Datta, Stability and control aspects of microgrid architectures–A comprehensive review, IEEE Access 8 (2020) 144730–144766.
[3] A.A. Alkahtani, S.T. Alfalahi, A.A. Athamneh, A.Q. Al-Shetwi, M.B. Mansor, M. Hannan, V.G. Agelidis, Power quality in microgrids including supraharmonics: Issues, standards, and mitigations, IEEE Access 8 (2020) 127104–127122.
[4] Y.-Y. Hong, F.I. Alano, Hierarchical energy management in Islanded networked microgrids, IEEE Access 10 (2022) 8121–8132.
[5] A. Banerji, D. Sen, A.K. Bera, D. Ray, D. Paul, A. Bhakat, S.K. Biswas, Microgrid: A review, in: 2013 IEEE Global Humanitarian Technology Conference: South Asia Satellite, GHTC-SAS, IEEE, 2013, pp. 27–35.
[6] Requirements for Generating Plants to Be Connected in Parallel with Distribution Networks - Part 1: Connection to a LV Distribution Network - Generating Plants Up to and Including Type B, Vol. 2019, Standard, European standard, Brussels, Bel, 2019, EN50549-1:2019.
[7] G. Buticchi, S. Bozhko, M. Liserre, P. Wheeler, K. Al-Haddad, On-board microgrids for the more electric aircraft—Technology review, IEEE Trans. Ind. Electron. 66 (7) (2018) 5588–5599.
[8] C. Wu, D. Zhou, X. Lin, Q. Sui, F. Wei, Z. Li, A novel energy cooperation framework for multi-island microgrids based on marine mobile energy storage systems, Energy 252 (2022) 124060.
[9] M. Srinivasan, A. Kwasinski, Decentralized control of a vehicular microgrid with constant power loads, in: 2014 IEEE International Electric Vehicle Conference, IEVC, IEEE, 2014, pp. 1–8.
[10] Y. Khayat, Q. Shafiee, R. Heydari, M. Naderi, T. Dragičević, J.W. Simpson-Porco, F. Dörfler, M. Fathi, F. Blaabjerg, J.M. Guerrero, et al., On the secondary control architectures of AC microgrids: An overview, IEEE Trans. Power Electron. 35 (6) (2019) 6482–6500.
[11] T. Dragicevic, D. Wu, Q. Shafiee, L. Meng, Distributed and decentralized control architectures for converter-interfaced microgrids, Chin. J. Electr. Eng. 3 (2) (2017) 41–52.
[12] J.M. Guerrero, P.C. Loh, T.-L. Lee, M. Chandorkar, Advanced control architectures for intelligent microgrids—Part II: Power quality, energy storage, and AC/DC microgrids, IEEE Trans. Ind. Electron. 60 (4) (2012) 1263–1270.
[13] J.M. Guerrero, M. Chandorkar, T.-L. Lee, P.C. Loh, Advanced control architectures for intelligent microgrids—Part I: Decentralized and hierarchical control, IEEE Trans. Ind. Electron. 60 (4) (2012) 1254–1262.
[14] L. Meng, F. Tang, M. Savaghebi, J.C. Vasquez, J.M. Guerrero, Tertiary control of voltage unbalance compensation for optimal power quality in Islanded microgrids, IEEE Trans. Energy Convers. 29 (4) (2014) 802–815.
[15] F. Delfino, G. Ferro, M. Robba, M. Rossi, An architecture for the optimal control of tertiary and secondary levels in small-size Islanded microgrids, Int. J. Electr. Power Energy Syst. 103 (2018) 75–88.
[16] Y. Li, T. Zhao, P. Wang, H.B. Gooi, L. Wu, Y. Liu, J. Ye, Optimal operation of multimicrogrids via cooperative energy and reserve scheduling, IEEE Trans. Ind. Inform. 14 (8) (2018) 3459–3468.
[17] Z. Li, C. Zang, P. Zeng, H. Yu, S. Li, Fully distributed hierarchical control of parallel grid-supporting inverters in Islanded AC microgrids, IEEE Trans. Ind. Inform. 14 (2) (2017) 679–690.
[18] J.C. Vasquez, J.M. Guerrero, M. Savaghebi, J. Eloy-Garcia, R. Teodorescu, Modeling, analysis, and design of stationary-reference-frame droop-controlled parallel three-phase voltage source inverters, IEEE Trans. Ind. Electron. 60 (4) (2012) 1271–1280.
[19] X. Hou, Y. Sun, J. Lu, X. Zhang, L.H. Koh, M. Su, J.M. Guerrero, Distributed hierarchical control of AC microgrid operating in grid-connected, Islanded and their transition modes, Ieee Access 6 (2018) 77388–77401.
[20] I. Ziouani, D. Boukhetala, A.-M. Darcherif, B. Amghar, I. El Abbassi, Hierarchical control for flexible microgrid based on three-phase voltage source inverters operated in parallel, Int. J. Electr. Power Energy Syst. 95 (2018) 188–201.
[21] M. Jayachandran, G. Ravi, Decentralized model predictive hierarchical control strategy for Islanded AC microgrids, Electr. Power Syst. Res. 170 (2019) 92–100.
[22] H.S. Khan, M. Aamir, K. Kauhaniemi, M. Mumtaz, M.W. Hassan, M. Ali, Improved finite control set model predictive control for distributed energy resource in Islanded microgrid with fault-tolerance capability, Eng. Sci. Technol. Int. J. 24 (3) (2021) 694–705.
[23] Z. Zhang, C. Dou, D. Yue, B. Zhang, Predictive voltage hierarchical controller design for Islanded microgrids under limited communication, IEEE Trans. Circuits Syst. I. Regul. Pap. 69 (2) (2021) 933–945.
[24] Z. Zhao, P. Yang, Y. Wang, Z. Xu, J.M. Guerrero, Dynamic characteristics analysis and stabilization of PV-based multiple microgrid clusters, IEEE Trans. Smart Grid 10 (1) (2019) 805–818.
[25] M. Ali, M. Aamir, H.S. Khan, A.A. Khan, F. Haroon, Design and implementation of fractional-order sliding mode control for parallel distributed generations units in Islanded microgrid, in: 2019 IEEE 28th International Symposium on Industrial Electronics, ISIE, IEEE, 2019, pp. 64–69.
[26] I.S. Mohamed, S. Rovetta, T.D. Do, T. Dragicević, A.A.Z. Diab, A neural-network-based model predictive control of three-phase inverter with an output *LC* filter, IEEE Access 7 (2019) 124737–124749.
[27] Y.E. Yağan, K. Vardar, Artificial neural networks controllers for three-phase neutral point clamped inverters, Eng. Sci. Technol. Int. J. 41 (2023) 101390.
[28] H.S. Khan, M. Aamir, M. Ali, A. Waqar, S.U. Ali, J. Imtiaz, Finite control set model predictive control for parallel connected online ups system under unbalanced and nonlinear loads, Energies 12 (4) (2019) 581.
[29] D.E. Olivares, A. Mehrizi-Sani, A.H. Etemadi, C.A. Cañizares, R. Iravani, M. Kazerani, A.H. Hajimiragha, O. Gomis-Bellmunt, M. Saeedifard, R. Palma-Behnke, et al., Trends in microgrid control, IEEE Trans. Smart Grid 5 (4) (2014) 1905–1919.
[30] Y. Mousavi, G. Bevan, I.B. Kucukdemiral, A. Fekih, Sliding mode control of wind energy conversion systems: Trends and applications, Renew. Sustain. Energy Rev. 167 (2022) 112734.
[31] S.A.Q. Mohammed, I.M. Alsofyani, K.-B. Lee, Improved adaptive CCS-MPCC for distorted model parameters mitigation of IPMSM drives, IEEE Trans. Ind. Electron. (2023).
[32] K. Rajesh, S. Dash, R. Rajagopal, R. Sridhar, A review on control of ac microgrid, Renew. Sustain. Energy Rev. 71 (2017) 814–819.
[33] M. Ali, M. Aamir, H.S. Khan, A. Waqar, F. Haroon, A.R. Jafri, Lyapunov stability and performance analysis of the fractional order sliding mode control for a parallel connected UPS system under unbalanced and nonlinear load conditions, Energies 11 (12) (2018) 3475.
[34] I. Poonahela, A. Krama, S. Bayhan, U. Fesli, M.B. Shadmand, H. Abu-Rub, M.M. Begovic, Hierarchical model-predictive droop control for voltage and frequency restoration in AC microgrids, IEEE Open J. Ind. Electron. Soc. 4 (2023) 85–97, http://dx.doi.org/10.1109/OJIES.2023.3240070.
[35] J. Kaushal, P. Basak, Power quality control based on voltage sag/swell, unbalancing, frequency, THD and power factor using artificial neural network in PV integrated AC microgrid, Sustain. Energy Grids Netw. 23 (2020) 100365.
[36] H.S. Khan, I.S. Mohamed, K. Kauhaniemi, L. Liu, Artificial neural network-based voltage control of DC/DC converter for dc microgrid applications, in: 2021 6th IEEE Workshop on the Electronic Grid, EGRID, IEEE, 2021, pp. 1–6.
[37] J. Hu, J. Zhu, D.G. Dorrell, Model predictive control of grid-connected inverters for PV systems with flexible power regulation and switching frequency reduction, IEEE Trans. Ind. Appl. 51 (1) (2015) 587–594.
[38] E. Clarke, C. Park, Generalized theory of electrical machines, Trans. Am. Inst. Electr. Eng. Part II: Appl. Ind. 74 (3) (1954) 1292–1301.
[39] W. Duesterhoeft, M.W. Schulz, E. Clarke, Determination of instantaneous currents and voltages by means of alpha, beta, and zero components, Trans. Am. Inst. Electr. Eng. 70 (2) (1951) 1248–1255.
[40] S. Vazquez, J. Leon, L. Franquelo, J. Carrasco, E. Dominguez, P. Cortes, J. Rodriguez, Comparison between FS-MPC control strategy for an UPS inverter application in α-β and abc frames, in: 2010 IEEE International Symposium on Industrial Electronics, IEEE, 2010, pp. 3133–3138.

[41] M. Novak, U.M. Nyman, T. Dragicevic, F. Blaabjerg, Analytical design and performance validation of finite set MPC regulated power converters, IEEE Trans. Ind. Electron. 66 (3) (2019) 2004–2014.
[42] K. Alam, M.P. Akter, S.S.I. Shakib, D. Xiao, D. Zhang, M. Rahman, Lyapunov-function based predictive approach for load voltage control of four-leg inverter with an output LC filter, in: 2018 IEEE Energy Conversion Congress and Exposition, ECCE, IEEE, 2018, pp. 6880–6885.
[43] M.P. Akter, S. Mekhilef, N.M.L. Tan, H. Akagi, Modified model predictive control of a bidirectional AC–DC converter based on Lyapunov function for energy storage systems, IEEE Trans. Ind. Electron. 63 (2) (2015) 704–715.
[44] V. Yaramasu, M. Rivera, B. Wu, J. Rodriguez, Model predictive current control of two-level four-leg inverters—Part I: Concept, algorithm, and simulation analysis, IEEE Trans. Power Electron. 28 (7) (2012) 3459–3468.
[45] R.N. Fard, H. Nademi, L. Norum, Analysis of a modular multilevel inverter under the predicted current control based on finite-control-set strategy, in: 2013 3rd International Conference on Electric Power and Energy Conversion Systems, IEEE, 2013, pp. 1–6.
[46] R.P. Aguilera, D.E. Quevedo, On stability and performance of finite control set MPC for power converters, in: 2011 Workshop on Predictive Control of Electrical Drives and Power Electronics, IEEE, 2011, pp. 55–62.
[47] R.P. Aguilera, On stability of finite control set MPC strategy for multicell converters, in: 2010 IEEE International Conference on Industrial Technology, IEEE, 2010, pp. 1277–1282.
[48] M.P. Akter, S. Mekhilef, N.M.L. Tan, H. Akagi, Modified model predictive control of a bidirectional AC–DC converter based on Lyapunov function for energy storage systems, IEEE Trans. Ind. Electron. 63 (2) (2015) 704–715.
[49] H.A. Young, M.A. Perez, J. Rodriguez, H. Abu-Rub, Assessing finite-control-set model predictive control: A comparison with a linear current controller in two-level voltage source inverters, IEEE Ind. Electron. Mag. 8 (1) (2014) 44–52.
[50] J. He, Y.W. Li, Analysis and design of interfacing inverter output virtual impedance in a low voltage microgrid, in: 2010 IEEE Energy Conversion Congress and Exposition, IEEE, 2010, pp. 2857–2864.
[51] U.B. Tayab, M.A.B. Roslan, L.J. Hwai, M. Kashif, A review of droop control techniques for microgrid, Renew. Sustain. Energy Rev. 76 (2017) 717–727.
[52] W. Price, C. Taylor, G. Rogers, Standard load models for power flow and dynamic performance simulation, IEEE Trans. Power Syst. 10 (CONF-940702-) (1995).
[53] IEEE standard for interconnection and interoperability of distributed energy resources with associated electric power systems interfaces, in: IEEE Std 1547-2018 (Revision of IEEE Std 1547-2003), 2018, pp. 1–138, http://dx.doi.org/10.1109/IEEESTD.2018.8332112.
[54] IEEE recommended practice and requirements for harmonic control in electric power systems, in: IEEE Std 519-2014 (Revision of IEEE Std 519-1992), 2014, pp. 1–29, http://dx.doi.org/10.1109/IEEESTD.2014.6826459.
[55] P. Cortés, G. Ortiz, J.I. Yuz, J. Rodríguez, S. Vazquez, L.G. Franquelo, Model predictive control of an inverter with output *LC* filter for UPS applications, IEEE Trans. Ind. Electron. 56 (6) (2009) 1875–1883.

This paper has been accepted for publication at the 6th IEEE Workshop on the Electronic Grid (eGrid 2021)

Artificial Neural Network-Based Voltage Control of DC/DC Converter for DC Microgrid Applications

Hussain Sarwar Khan*✉, Ihab S. Mohamed†✉, Kimmo Kauhaniemi*, and Lantao Liu†
*School of Technology and Innovations, University of Vaasa, Vaasa, Finland
†Luddy School of Informatics, Computing, and Engineering, Indiana University, Bloomington, IN 47408, USA

***Abstract*—The rapid growth of renewable energy technology enables the concept of microgrid (MG) to be widely accepted in the power systems. Due to the advantages of the DC distribution system such as easy integration of energy storage and less system loss, DC MG attracts significant attention nowadays. The linear controller such as PI or PID is matured and extensively used by the power electronics industry, but their performance is not optimal as system parameters are changed. In this study, an artificial neural network (ANN) based voltage control strategy is proposed for the DC–DC boost converter. In this paper, the model predictive control (MPC) is used as an expert, which provides the data to train the proposed ANN. As ANN is tuned finely, then it is utilized directly to control the step-up DC converter. The main advantage of the ANN is that the neural network system identification decreases the inaccuracy of the system model even with inaccurate parameters and has less computational burden compared to MPC due to its parallel structure. To validate the performance of the proposed ANN, extensive MATLAB/Simulink simulations are carried out. The simulation results show that the ANN-based control strategy has better performance under different loading conditions comparison to the PI controller. The accuracy of the trained ANN model is about 97%, which makes it suitable to be used for DC microgrid applications.**

***Index Terms*—ANN, DC Microgrid, DC/DC boost converter, MPC, Primary control.**

I. Introduction

Renewable energy got attention due to the depletion of fossil fuels and global warming. Due to this, the use of DC/DC converters is rapidly increasing in a vast amount of applications such as wind turbines, photovoltaic systems, electric vehicles, energy storage systems, and in such applications, where different voltage levels loads are connected [1]–[3]. The block diagram of DC MG is expressed in Fig. 1. DC MG mainly includes renewable energy sources (RES) such as solar and wind, energy storage system (*ESS*), and DC load. Every RES and ESS is connected with the bus through a power electronic interface (PEI). It is therefore necessary to have effective control for the PEIs. The research community extensively proposes different types of linear controllers such as proportional–integral (PI) and proportional–integral–derivative (PID) and is vastly used by the PE industry [4]–[6]. However, the linear controller has its practical limitations such as tuning of gains, poor disturbance rejection capability, shifting of the operating point of the converter towards instability due to change of the system parameters, and lacking the capacity to handle the non-linearities of the power system. Many nonlinear control techniques such as model predictive control (*MPC*), sliding mode control (*SMC*), fuzzy-logic control (*FLC*) have been proposed to cope with the issues mentioned above and also try to improve the transient behavior. In [7], FLC for DC converter is presented for PV-based lighting systems. FLC implementation for DC power converter using microcontroller has been studied in [8]. FLC basically works on the if-else statement, and its response depends upon predefined rules using if-else logic. FLC does not need any mathematical system model and also has the ability to handle the non-linearity of the system. Voltage regulation of FLC for DC/DC converter is also good under different conditions. However, many studies prove it as an unreliable controller because it lacks formal analysis. So, the amalgam of varying control techniques is found in the literature to balance the disadvantages of FLC [9].

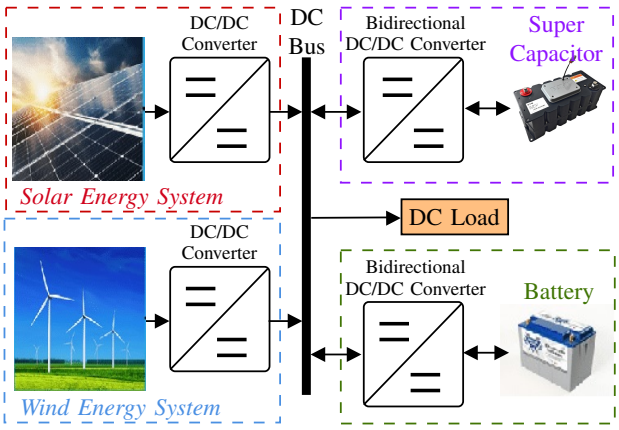

Fig. 1. Possible structure of single bus DC MG, including renewable energy sources such as solar and wind, energy storage systems, and DC load.

Slide mode control and model predictive control are developed and vastly studied in literature and have become promising solutions for power electronic converter applications. Slide mode control is based on variable structure control theory. Its basic principle is divided into two stages. The system state trajectory is forcefully taken into the user-defined sliding layer. This phase is known as the reaching phase, then in the second phase, which is known as the sliding phase, state trajectories remain within the layer, defined by the user on the base of ap-

e-mails in-order: hussain.khan@uwasa.fi, mohamedi@iu.edu, kimmo.kauhaniemi@uwasa.fi, lantao@iu.edu
✉ Corresponding authors: Hussain Sarwar Khan and Ihab S. Mohamed

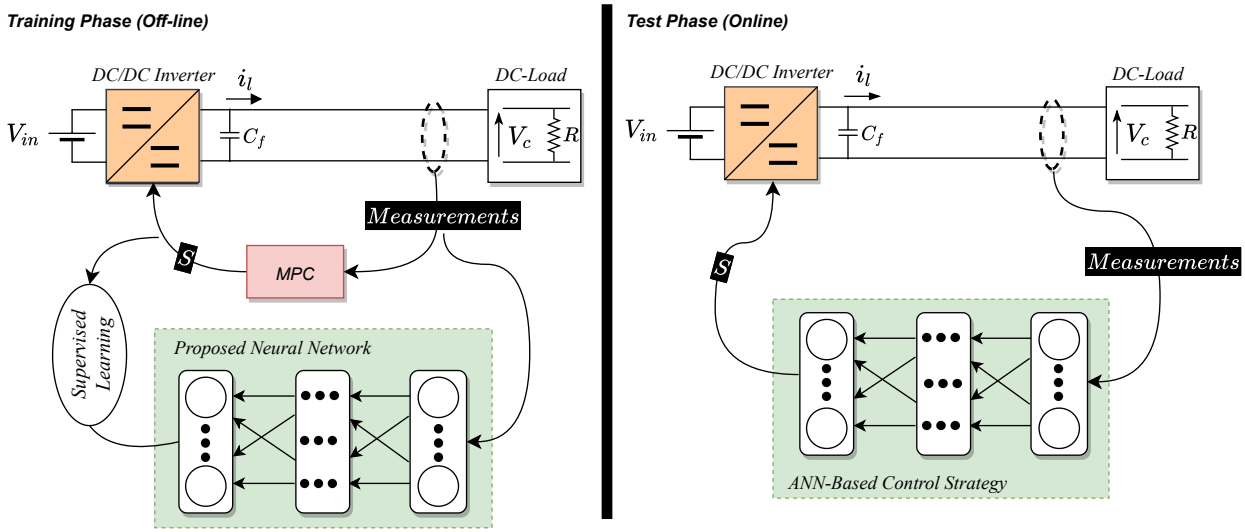

Fig. 2. Overview of the proposed control strategy. During the training phase, the classical MPC is used to control the DC/DC converter and collect the training data. In the test phase, the trained ANN is implemented to control the voltage of the converter instead of MPC [10].

plication. It has better performance, robust against parametric variations, and possesses magnificent transient response under different loading conditions. Still, chattering phenomena, high switching losses, and complex mathematical modeling are the main barriers to its implementation [11], [12].

MPC is a digital control method, and its basic principle is different from linear control. It uses the discrete-time model of the converter along with its filter to anticipate the behavior for all possible input combinations. One of the inputs having the least (i.e., optimal) value of the predefined cost function (CF) is selected and applied to the coming sampling instant despite drafting a separate loop for each controlled variable and cascading them together as in the case of linear controllers [13]. CF is basically a square of the Euclidean distance between controlled and reference signals. However, it has a high computational burden, and its performance depends upon the mathematical model of the system and also has variable switching frequency; however, many new studies proposed a constant switching frequency based MPC for different power electronic applications [12], [14], [15].

Data-driven or model-free control techniques and especially ANN-based methods are growing in the domain of power converters [16]. An ANN-based control scheme has been proposed in [10] to directly control a three-phase inverter with an output LC filter, where a lower THD and a better steady and dynamic performance are achieved. Similarly, authors in [17] proposed an ANN-based control strategy for a three-phase flying capacitor multi-level inverter (FCMLI). In [18], a neural network predictive-based voltage control is proposed for the DC/DC buck converter. The author used PID controller data to train NN. After training, neural network predictive control (NNPC) is used to regulate the voltage. NNPC controller for grid-connected synchronverter is proposed in [19].

Broadly speaking, the ANN-based controllers are better as compared to other controllers due to the following reasons [10], [20]:

- They do not require an explicit mathematical model of the system.
- Their performance is better if they are finely tuned with sufficient data and properly chosen input features [17].
- They can be designed without having expert knowledge.

This paper proposes an artificial neural network-based voltage control for a DC/DC step-up (i.e., Boost) converter for DC microgrid applications. Initially, MPC-based voltage control is implemented for the Boost converter to extract the input features data. After the extraction of required data, a different possible combinations of inputs features are chosen. Finally, the voltage reference, inductor current, and capacitor voltage are selected as input features, while the converter switching state is taken as output feature for the proposed ANN in this study, as illustrated in Fig. 4. Then, these combinations are used to train the ANN. Once the ANN is trained and has good model accuracy, the ANN model is directly used to generate the optimal switching state for the DC converter. Figure 2 illustrates the overview of the proposed control strategy: the training phase combines using MPC to anticipate the converter output voltage converter and collection of state variables data under full-state observation. The collected data is used to train the ANN. In the test phase, the trained neural network is employed online to control the converter's output voltage instead of MPC. The simulation results of the proposed control strategy are also compared with the traditional PI Controller.

The rest of the paper is organized as follows. The mathematical modeling of the DC/DC boost converter and the basic principle of MPC are explained in Section II. While the proposed ANN and its training procedure are elaborated in Section III. Section IV shows the simulation results for both ANN and PI controllers. Then, future work is discussed in

Section V. Finally, Section VI presents the conclusion.

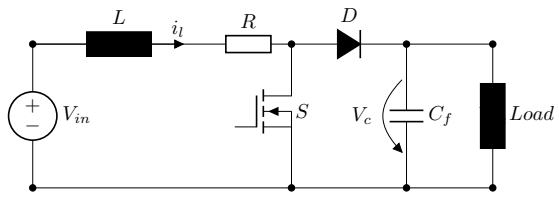

Fig. 3. Circuit diagram of the DC/DC converter.

II. Mathematical Modelling of MPC

Figure 3 illustrates the circuit diagram of the simple step-up boost converter, where S is a controllable switch, R is the damping resistance, the current through the inductor L is i_l, and the voltage across the capacitor C_f is V_c. V_{in} represents the input voltage of the DC source. The second order low pass filter is used to attenuate the ripples and distortion. In order to implement the MPC, it is necessary to develop the discrete time model of the DC converter. The output voltage of the step-up DC converter, namely, V_c, is controlled by varying the duty cycle of pulse width modulation (PWM) signal. But in the case of MPC, the pulse for the switch is directly generated by the MPC. One of the major drawbacks of MPC is its variable switching frequency. Equation (1) explains the inductive nature, while (2) presents the capacitive behavior of the system:

$$\frac{di_l(t)}{d(t)} = -\frac{R}{L}i_l(t) - \frac{V_c(t)}{L} + \frac{V_c(t)}{L}u(t) + \frac{V_{\text{in}}}{L}, \quad (1)$$

$$\frac{dV_c(t)}{d(t)} = \frac{1}{C_f}i_L(t) - \frac{1}{C_f}i_L(t)u(t) - \frac{1}{RC_f}V_c(t). \quad (2)$$

The switch states, S, are defined by function $u(t)$, as shown in (3). If $S = 1$, then switch S is in ON state and if switch $S = 0$, then switch S is in OFF state.

$$u(t) = \begin{cases} 1, & \text{if } S = 1 \\ 0, & \text{if } S = 0 \end{cases} \quad (3)$$

The discrete-time model of the DC converter is expressed in (4) and (5). These equations are used to anticipate the future response of voltage and current.

$$i_l(k+1) = \left(\frac{TR}{L} - 1\right) i_l(k) + (u(k) - 1)\frac{T}{L}V_c(k) \quad (4)$$

$$V_c(k+1) = \frac{T}{C_f}i_l(k) + \left(1 - \frac{T}{C_f R}\right) V_c(k) - \frac{T}{C_f}i_l(k)u(k) \quad (5)$$

Where $k+1$ represents the future or next (coming) instant and T is the sampling time.

The formulation of cost function (*CF*) is an essential part of the development of MPC, and it is the positive value of error between the reference and actual value of the state parameter. The CF, J, chosen in this study is illustrated in (6), where V_c^* is the reference output voltage.

$$J(k) = \left(V_c^*(k+1)^2 - V_c(k+1)\right)^2 \quad (6)$$

The execution of the MPC algorithm can be summarized as follows:

- At the start of the switching instant, the voltage and current of the converter are measured using sensors.
- Equations (4) and (5) are used to predict the current and voltage at instant $k+1$ for all possible switching states, and then the CF is evaluated using (6) for all possible states. In this study, N is taken as one. So, there is only two possible switching states.
- The switching state that minimizes the CF is applied to the converter at the next time instant $k+1$.

III. Proposed ANN-Based Control Strategy

Basically, ANN is a network that has one or more hidden layers and each layer has one or multiple neurons which makes the ANN response similar to the real neural network. In this study, the feed-forward ANN is used, which is called FF-ANN. In FF-ANN, the data moves in forward direction only. The output of single neuron is mathematical expressed as:

$$y = \text{Act}\left(b + \sum_{i=1}^{M} x_i w_i\right), \quad (7)$$

where $Act(.)$, w_i, b, and M are the activation function, weights of each input x_i, bias or correction factor, and number of input elements (or neurons) where the input features $x = \{x_1, x_2, \ldots, x_M\}$, respectively. The most commonly used types of activation functions are given in Table I. By joining the multiple neurons into a single layer, an FF-ANN layer can be developed. The general equation used to compute the output of the multi-input single-output FF-ANN can be expressed as:

$$\begin{aligned} y_1 &= Act\left(\sum_{j=1}^{J} {}^2w_{j1}h_j + {}^2b_1\right), \text{and} \\ h_j &= Act\left(\sum_{m=1}^{M} {}^1w_{mj}x_m + {}^1b_j\right), \quad \forall j = \{1, \ldots, J\}, \end{aligned} \quad (8)$$

where y_1 is the output of the ANN, $({}^1w_{mj}, {}^2w_{j1})$ represent the weights of the hidden and output layers, J represents the number of hidden layers, M represents the number of input neurons, and $({}^1b_j, {}^2b_1)$ refer to the biases of the hidden and output layers, respectively.

Table I
Activation function types.

$Act(.) \equiv f(x)$	Definition
Sigmoid	$f(x) = \frac{1}{1+e^{-x}}$
Hyperbolic Tangent (tanh)	$f(x) = \frac{e^x - e^{-x}}{e^x + e^{-x}}$
Rectified Linear	$f(x) = \begin{cases} 0 & x \leq 0 \\ x & x > 0 \end{cases}$
Binary Step	$f(x) = \begin{cases} 0 & x < 0 \\ 1 & x > 0 \end{cases}$

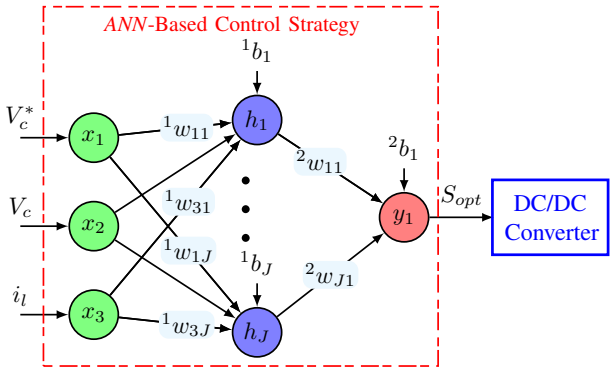

Fig. 4. Block diagram of the proposed ANN-based control scheme for the DC/DC converter. It is trained to map directly from the measured variables, namely, V_c^*, V_c, and i_l, to the *optimum* switching state S_{opt}.

Fig. 5. Confusion matrix of the trained ANN based on the overall training data, where the correct and incorrect observations are highlighted in green and red, respectively.

Figure 4 demonstrates the proposed ANN-based control strategy used in this study. The accuracy of MPC depends on the mathematical modeling of the system. However, the proposed control scheme does not need the model of the system, but it requires the training dataset. It maps directly from the raw input features to the desired outputs. Therefore, the performance of the ANN does not depend upon the system model or its parameter. In this work, the reference voltage V_c^*, capacitor voltage V_c and inductor current i_l are chosen as the input features of the trained ANN-based control strategy, while the optimal switching state S_{opt} is considered as its target or output. Initially, the MPC algorithm is simulated to extract the training data, which consists of the input features and the corresponding output, i.e., input-output pairs. Then, the extracted data is used to train the ANN. In our case, the total number of training data samples is 30001. The control-loop of the proposed ANN-based control strategy, at instant k is summarized as follows:

1) Initially, measure i_l and V_c at instant k.
2) Those measured variables, along with the reference value V_c^*, are utilized by our proposed controller to directly predict the optimal switching state S_{opt}.
3) Then, the optimal switching state is directly applied to the converter without using any modulator.

A grid search tuning method is used for the selection of configuration with 15 neurons. Bayesian regularized technique (BRT) is used to train the ANN and adjust the biases and weights. BRT is more robust than standard propagation methods and can reduce or eliminate the need for lengthy cross-validation [21]. In this research work, 60% of the random input data is used to train the ANN, while 20% is used for testing and 20% validation. Figure 5 presents the overall confusion matrix, which is used to analyze the accuracy of the trained ANN. The correct classification of the data class is presented in the diagonal entries of the matrix, while other entries show the incorrect classification of the data. The trained ANN that has been used, in this study, has an accuracy of 97%. The trained ANN model is exported to Simulink to test

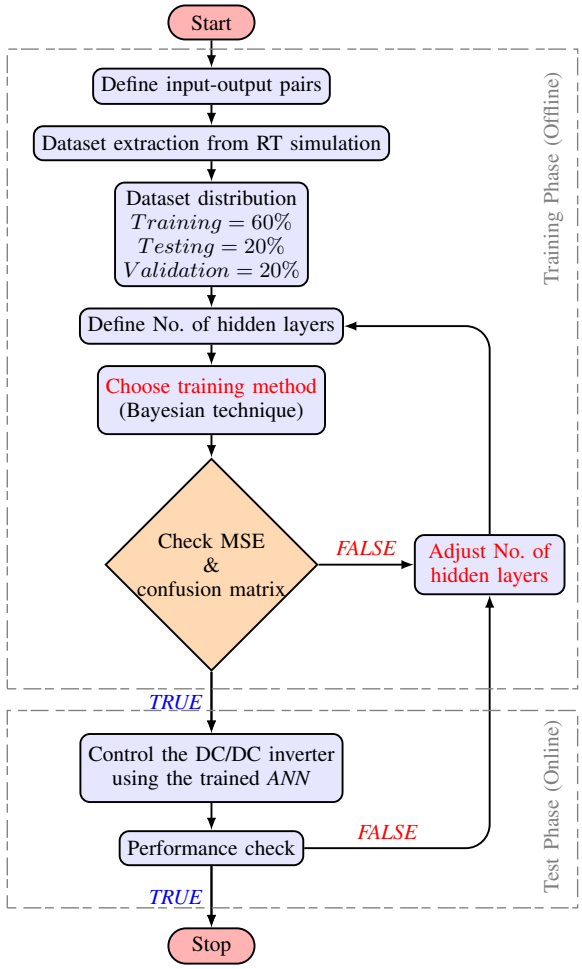

Fig. 6. Main steps of deploying the ANN-based control strategy for the DC/DC converter.

its performance under the original scenario. To sum up, the complete procedure of the learning-based control strategy is illustrated in Fig. 6, highlighting the main steps of the training and test phases.

IV. Simulation Results

The trained ANN model is exported into the Simulink model of the DC/DC converter to validate and verify the performance of the proposed control strategy. Extensive MATLAB/Simulink simulation is carried out. The performance of the boost converter with the proposed control scheme is investigated under normal load and step change of load. The simulation parameters of the converter are given in Table II.

Table II
Simulation Parameters.

Parameter	Value
DC Input V_{in}	70 [V]
Inductor value L	10×10^{-3} [H]
Resistance Value R	80×10^{-3} [Ω]
Capacitor C_f	100 [mF]
Load P	0−1500 [W]
PI Parameter K_p, K_i	0.054, 8.86
Switching Frequency	20 [kHz]

Figure 7 illustrates the performance of our proposed control strategy, considering normal load conditions. The simulation starts at $t = 0\,\mathrm{s}$, where a resistive load of $20\,\Omega$ is connected with the system. The reference voltage is set to $95\,\mathrm{V}$. Initially, the system takes around $20\,\mathrm{ms}$ to reach the reference value. After a transient period, the output voltage and current wave forms remain stable and do not show distortion. Figure 8

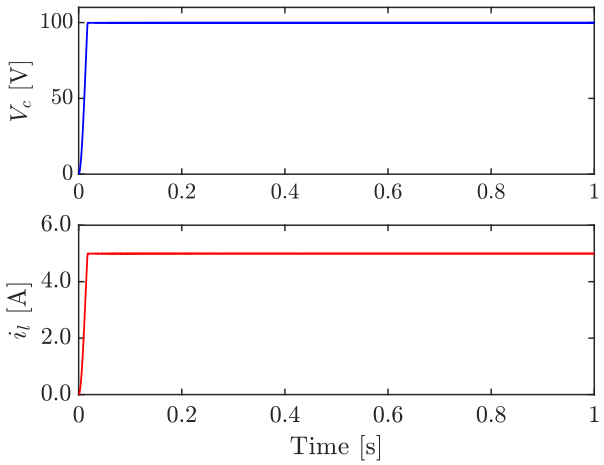

Fig. 7. Simulation results of the output voltage and current of the DC boost converter under normal load conditions.

shows the performance of the proposed controller from full load to no-load condition and vice versa. At $t = 0.4\,\mathrm{s}$, the load is disconnected from the system; i.e., the converter is under no-load condition. It is observed that the voltage remains stable, and the current becomes zero. While at $t = 0.5\,\mathrm{s}$, the load is again connected to the system. The voltage remains stable, while the current is increased to $4.9\,\mathrm{A}$. However, there is no transient observed in the simulation. After the interval of $0.6\,\mathrm{s}$, further loads are added into the system to investigate the response of the proposed controller. It is observed from Fig. 8 that with increasing the load, the voltage remains stable while keeping track of the reference value with un-noticeable distortion, demonstrating the superior performance of the proposed ANN-based control scheme under different loading and transient conditions. Figure 9 presents the simulation

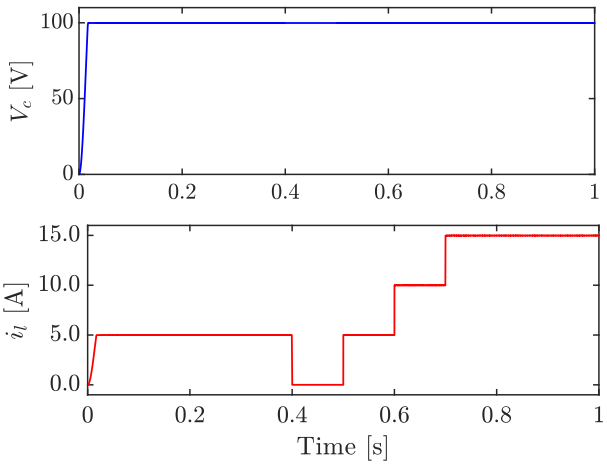

Fig. 8. Simulation results of the output voltage and current of the DC boost converter under full load to no-load test.

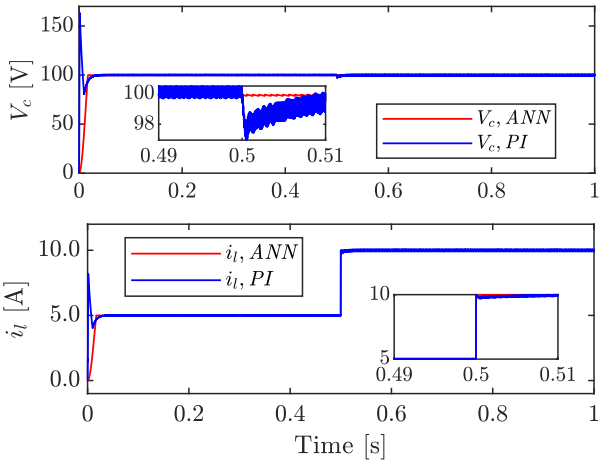

Fig. 9. Simulation results of the output voltage and current of the DC boost converter using PI and ANN-based controllers under step change of load.

results of our proposed controller under step change of load. At $t = 0.5\,\mathrm{s}$, the DC load becomes double. We can observe that the voltage remains stable without any distortion, whereas the current increases with the increase of load. However, the current waveform becomes stable with almost no transient time. Figure 9 also presents a comparison with the PI controller. Under the transient period, the PI controller shows an overshoot

in the voltage and current which may harm the switch of the DC/DC converter; accordingly, a high rating semi-conductor switch is required which increases the converter cost. The ANN-based control scheme has better wave quality and less distortion compared to the PI controller. Moreover, the output current of the PI-based controlled converter is distorted, while the current wave in the case of ANN is constant, stable, and has less loss compared to the PI controller.

V. Discussion and Future Work

In this study, our proposed control strategy is trained on a single reference value (i.e., $V_c^* = 95\,\mathrm{V}$) and also tested on the same reference value under different loading conditions. In the future work, the proposed ANN model will be trained and its performance will be examined on different reference values. Moreover, it will be trained on various parameters such as filter values, switching frequency, etc, proposing a more generic control strategy. We have also observed that the performance of our proposed controller is similar to the MPC used to extract the training data. For this reason, the comparison is carried out with the PI controller. However, the ANN-based controller has an advantage over MPC as it has less computation burden and constant switching frequency.

VI. Conclusion

Within this work, we proposed a feed-forward artificial neural network-based voltage control strategy for the DC/DC step-up converter. Model predictive control is implemented to extract the training data, where the data is used, later on, to train the ANN offline. After training the ANN properly, MPC is removed and the trained ANN successfully regulates the voltage of the DC/DC converter as per reference voltage. The bayesian regularized technique is used to train the ANN and adjust the biases and weights of the ANN. Different types of tests were also performed during simulation, such as step change of load, the shift of load from full load to no load, and vice versa, in order to demonstrate the performance of the proposed controller. It has been observed through simulation results that the overall performance of the proposed control scheme is better than the classical linear controllers. The implementation of the proposed technique would be useful in DC microgrid applications, where the DC boost converters require high accuracy for tuning controller parameters.

VII. Acknowledgment

This work is carried out by the financial support provided by the Walter Ahlström Foundation Finland with grant No. $2021/40$. Some parts of this work are done in the SolarX research project with the financial support provided by Business Finland with Grant No. $6844/31/2018$. The financial support provided through these funding organizations is highly acknowledged.

References

[1] H. S. Khan, M. Aamir, K. Kauhaniemi, M. Mumtaz, M. W. Hassan, and M. Ali, "Improved finite control set model predictive control for distributed energy resource in islanded microgrid with fault-tolerance capability," *Engineering Science and Technology, an International Journal*, vol. 24, no. 3, pp. 694–705, 2021.

[2] H. S. Khan, M. Aamir, M. Ali, A. Waqar, S. U. Ali, and J. Imtiaz, "Finite control set model predictive control for parallel connected online UPS system under unbalanced and nonlinear loads," *Energies*, vol. 12, no. 4, p. 581, 2019.

[3] B. Sahu and G. A. Rincón-Mora, "A low voltage, dynamic, noninverting, synchronous buck-boost converter for portable applications," *IEEE Transactions on power electronics*, vol. 19, no. 2, pp. 443–452, 2004.

[4] K. Hwu and Y. Yau, "Performance enhancement of boost converter based on PID controller plus linear-to-nonlinear translator," *IEEE transactions on power electronics*, vol. 25, no. 5, pp. 1351–1361, 2009.

[5] C.-F. Hsu, I.-F. Chung, C.-M. Lin, and C.-Y. Hsu, "Self-regulating fuzzy control for forward DC–DC converters using an 8-bit microcontroller," *IET Power Electronics*, vol. 2, no. 1, pp. 1–13, 2009.

[6] I. S. Mohamed, S. A. Zaid, M. Abu-Elyazeed, and H. M. Elsayed, "Classical methods and model predictive control of three-phase inverter with output *LC* filter for UPS applications," in *2013 International Conference on Control, Decision and Information Technologies (CoDIT)*. IEEE, 2013, pp. 483–488.

[7] T.-F. Wu, C.-H. Chang, and Y.-H. Chen, "A fuzzy-logic-controlled single-stage converter for PV-powered lighting system applications," *IEEE Transactions on Industrial Electronics*, vol. 47, no. 2, pp. 287–296, 2000.

[8] T. Gupta, R. Boudreaux, R. M. Nelms, and J. Y. Hung, "Implementation of a fuzzy controller for DC-DC converters using an inexpensive 8-b microcontroller," *IEEE transactions on Industrial Electronics*, vol. 44, no. 5, pp. 661–669, 1997.

[9] S. J. Jawhar, N. Marimuthu, and N. A. Singh, "An neuro-fuzzy controller for a non linear power electronic boost converter," in *2006 International Conference on Information and Automation*. IEEE, 2006, pp. 394–397.

[10] I. S. Mohamed, S. Rovetta, T. D. Do, T. Dragicević, and A. A. Z. Diab, "A neural-network-based model predictive control of three-phase inverter with an output *LC* filter," *IEEE Access*, vol. 7, pp. 124 737–124 749, 2019.

[11] S. Oucheriah and L. Guo, "PWM-based adaptive sliding-mode control for boost DC–DC converters," *IEEE Transactions on industrial electronics*, vol. 60, no. 8, pp. 3291–3294, 2012.

[12] H. S. Khan, K. S. Fuad, M. Karimi, and K. Kauhaniemi, "Fault current level analysis of future microgrids with high penetration level of power electronic-based generation," in *2021 IEEE 9th International Conference on Smart Energy Grid Engineering (SEGE)*. IEEE, 2021, pp. 48–53.

[13] I. S. Mohamed, S. A. Zaid, M. Abu-Elyazeed, and H. M. Elsayed, "Improved model predictive control for three-phase inverter with output *LC* filter," *International Journal of Modelling, Identification and Control*, vol. 23, no. 4, pp. 371–379, 2015.

[14] P. Karamanakos, T. Geyer, and S. Manias, "Direct voltage control of DC–DC boost converters using enumeration-based model predictive control," *IEEE transactions on power electronics*, vol. 29, no. 2, pp. 968–978, 2013.

[15] L. Cheng, P. Acuna, R. P. Aguilera, J. Jiang, S. Wei, J. E. Fletcher, and D. D. Lu, "Model predictive control for DC–DC boost converters with reduced-prediction horizon and constant switching frequency," *IEEE Transactions on Power Electronics*, vol. 33, no. 10, pp. 9064–9075, 2017.

[16] B.-R. Lin, "Power converter control based on neural and fuzzy methods," *Electric power systems research*, vol. 35, no. 3, pp. 193–206, 1995.

[17] P. B. Malidarreh, A. Bakeer, I. S. Mohamed, and L. Liu, "An artificial neural network-based model predictive control for three-phase flying capacitor multi-level inverter," *arXiv preprint arXiv:2110.08101*, 2021.

[18] S. Saadatmand, P. Shamsi, and M. Ferdowsi, "The voltage regulation of a buck converter using a neural network predictive controller," in *2020 IEEE Texas Power and Energy Conference (TPEC)*. IEEE, 2020, pp. 1–6.

[19] S. Saadatmand, M. S. S. Nia, P. Shamsi, M. Ferdowsi, and D. C. Wunsch, "Neural network predictive controller for grid-connected virtual synchronous generator," in *2019 North American Power Symposium (NAPS)*. IEEE, 2019, pp. 1–6.

[20] S. Zhao, F. Blaabjerg, and H. Wang, "An overview of artificial intelligence applications for power electronics," *IEEE Transactions on Power Electronics*, 2020.

[21] F. D. Foresee and M. T. Hagan, "Gauss-newton approximation to bayesian learning," in *Proceedings of international conference on neural networks (ICNN'97)*, vol. 3. IEEE, 1997, pp. 1930–1935.

FPGA Validated Advanced Learning-Based Voltage Control of DC/DC Converter Feeding CPL in DC Microgrid Applications

Hussain Sarwar Khan
School of Technology and Innovations
University of Vaasa
Vaasa, Finland
hussain.khan@uwasa.fi

Kimmo Kauhaniemi
School of Technology and Innovations
University of Vaasa
Vaasa, Finland
kimmo.kauhaniemi@uwasa.fi

2023 IEEE 32nd International Symposium on Industrial Electronics (ISIE) | 979-8-3503-9971-4/23/$31.00 ©2023 IEEE | DOI: 10.1109/ISIE51358.2023.10228168

***Abstract*—The high penetration of renewable energy distribution generations enables the concept of microgrids and is widely accepted for future power systems. In this context, the DC microgrid is preferred due to easy integration, less system losses and offer high reliability and efficiency compared to its counterparts. However, the constant power loads (CPL) are a risk to the stability of the power electronics devices due to their negative impedance characteristics and also effects the voltage quality. To overcome these conditions, this paper proposes advanced artificial intelligence-based control of DC/DC converter to regulate the DC voltage in DC microgrid (MG) applications. At the start, model predictive control is implemented as an expert to control the studied converter to extract the dataset. The extracted dataset is used to train the proposed artificial neural network (ANN). The proposed controller is tested under various operating conditions while feeding the constant power loads. The proposed controller presents a superior transient response compared to conventional model predictive control (MPC). The experimental validation of the proposed scheme is carried out by implementing the controller on the FPGA ZYBO Z7-7020 board. The results are also compared with the conventional PI control. The proposed control technique has less computational burden and mitigates destabilizing effects caused by the CPLs.**

Keywords—Artificial Intelligence, Constant Power Load, DC/DC converter, DC Microgrid.

I. INTRODUCTION

The expansion of renewable energy-based distributed generations (DG) systems such as wind, solar, and biomasses becomes more prevalent. Especially the implementation of DGs far away from the main grid. So, to incorporate the DGs in power system systems, DC or AC microgrid is one of the suitable options [1]. The MG is a small-scale independent distribution system with its generation and control. It can also resolve energy issues, improve reliability locally and be operated in islanded or grid-connected mode. The microgrid can be operate as an AC, DC or hybrid system. However, AC MG has disadvantages when compared to DC microgrids, such as skin effect, more complicated control due to the presence of frequency, etc. AC MG also has lower efficiency, high implementation cost and low reliability. In contrast, DC MG are easier to implement due to the absence of reactive power flow, harmonics and voltage unbalances. Additionally, implementation of the DC system lowers the power network weight by 10 tons/MW [2]. The DC MG also acquires attention in different applications such as electric vehicles, naval ships, submarines and telecommunications infrastructure. A basic structural diagram of DC MG is shown in Fig. 1. Many challenges appear in above mentioned applications of DC, but suitable control approach is one of the critical aspects to be considered when aiming for high stability of the system in challenging operation conditions.

With continuous development in control theory, many new control techniques have been proposed to control the power converters [3]. Linear theory-based controllers such as PID and PR and their combinations are mature and widely used by the power electronics industry. But, gains tuning, parametric uncertainty and inability to handle the power system nonlinearity due to the power converters and constant power loads in DC systems are practical limitations of these controllers [4]. Model-free fuzzy logic-based control for DC/DC converter is discussed in [5]. Slide mode control (SMC) and model predictive control (MPC) have been proposed to overcome the abovementioned issues[6], [7]. SMC is a recently developed popular control method for DC/DC converters and is robust against parametric variations, converges towards the sliding surface and can handle external disturbance. First-order SMC is proposed for DC/DC converters in [8], while second-order SMC for DC MG applications is discussed in [9], implementing the nested voltage and current loop to improve the robustness of the parallel converters. But, the second-order SMC enhanced the performance in terms of transient response but required an extra current sensor, which ultimately increases the cost. In [10], [11], authors proposed the SMC for DC/DC converter in DC MG applications. Overall, the chattering phenomena, high overshoot, variable switching frequency and complex mathematical modelling are potential barriers and make it unsuitable for power converters [12].

Model predictive control is optimal digital control, which solves the optimization problem over a prediction horizon for each sampling time. MPC uses the mathematical model of the converter along with its filter to anticipate future states. The state with the least cost function (CF) value is selected, and its switching state is applied to the next sampling duration. CF is the error value between the reference value and the predicted value of the state variables (voltage, current, frequency or power). It also handles the system's nonlinearities and constraints [13]. Decentralized MPC for DC MG with constant power loads (CPL) is presented in [14]. The proposed technique regulates the bus voltage and ensures power-sharing among the multi-parallel converters. However, the disadvantages of MPC are its high computational burden and inaccurate mathematical modelling that takes the system towards instability [15]. Model-free or data-driven control

techniques have become successful in getting the attention of the research community in the PE domain in recent years [16][17]. So, ANN-based controllers have been proposed for short-term prediction [18], voltage sag classification [19] and problem identification [20]. ANN is the subset of artificial intelligence and matching learning. A total harmonic distortion prediction tool is developed using ANN in [21]. In [22], ANN-aided MPC for DC/DC converter is studied to regulate the DC bus voltage. However, the control is not robust against the voltage change.

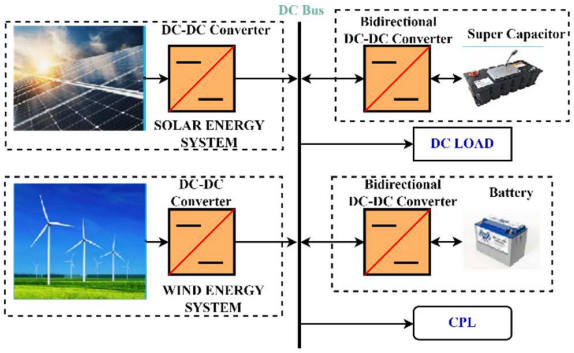

Fig. 1. Typical configuration of DC microgrid.

This paper proposes an artificial neural network-based voltage control strategy for DC-DC converter under constant power loads. In this study, the CPL is the only load connected with the system, which is assumed as the worst-case scenario from a stability point of view. The design of the proposed controller is divided into two stages. Initially, MPC is implemented to regulate the converter voltage and used as an expert for extracting the dataset. In the second stage, the obtained dataset is used to train the proposed ANN. Once the developed ANN has been fine-tuned, the MPC-based controller is replaced with it to test its performance in a closed loop system using MATLAB/SIMULINK. In this study, reference voltage, output voltage, and output current are chosen as input features, and the switching state of the converter is selected as the target. The dataset contains samples from different voltage reference values under different loading conditions, such as step changes in load, changes in input voltages, etc. Moreover, the proposed control is verified by FPGA-in-the-loop (FIL) implementation. The results are also compared with the conventional PI and MPC control.

The rest of the paper is organized as follows: Section II explains constant power loads and its response. The MPC mathematical modelling for DC-DC converter is briefly discussed in section III. The proposed ANN-based control strategy is explained in section IV and the experimental setup and cases are presented in Section V. The last section of the article presents the conclusion.

II. Constant Power Loads

Constant power load is the product of voltage and the current of the load [23], [24]. Let's review the basics of the constant power load. It is observed from Fig. 2 that if the voltage across the CPL changes, the load current will also change. This change in the current creates a destabilization effect on the system. The destabilization effect is annihilated by equalling the source voltage to the CPL voltage, and this point is known as the equilibrium point. The system's operation will become in a steady state at the equilibrium point. The equilibrium point stability of the system is determined from the I-V curves of the load and source. Fig. 3a illustrates the I-V characteristics between CPL and a voltage source. Consider that A is the equilibrium point in the cases of CPL. Further consider that due to a disturbance, the system moves to point A_1, where the load current reduces, and the source voltage is less than the load voltage. Therefore, the current will reduce further, and the operating point will shift further away from point A. The circuit behaves like positive feedback, and current and voltage go to zero and infinity, respectively. In other conditions, if the current increases, then the CPL voltage is less than the source voltage, leading to a further increase in current and moving the equilibrium point further away from point A. Hence, the point A is unstable in the case of CPL.

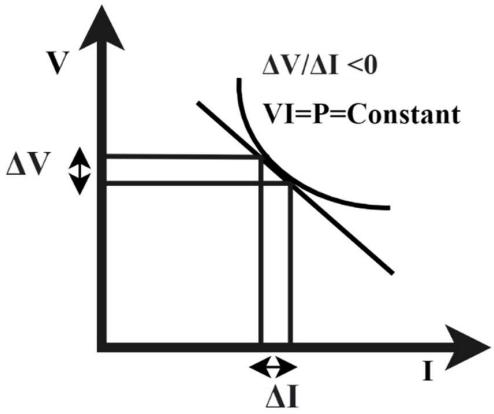

Fig. 2. Negative impedance properties of CPLs.

Fig. 3b represents the V-I curve for the resistive load and voltage source. Let's assume that B is the steady state equilibrium point and the current increase occurs due to the disturbance and the operating point moving to B_1. So, the load voltage is more than the source voltage. The load voltage becomes negative, and the current will decrease. As a result, the operating point will shift back to point B. In the second condition, the current reduces. As a result, the load voltage is less than the source voltage. The load voltage becomes positive, and in response to this behavior, the current will increase and shift the operating point back to equilibrium point B. In fact, the resistive load has positive incremental resistance, while CPL has negative incremental resistance properties which is obvious basing on CPLs mathematical representation:

$$i_{cpl}(t) = \frac{P}{V_{cpl}(t)};\ \forall v_{cpl}(t) > \varepsilon \qquad (1)$$

where P, i_{cpl}, *and* v_{cpl} are the rated power, current, and voltage of the load respectively. v_{cpl} is equal to the converter's output voltage, and ε is a small positive value. To sum up the above discussion, the equilibrium point will be stable when the positive change in current causes the load voltage to be greater

than the source, and a negative change in current originates the load voltage to become less than the source voltage.

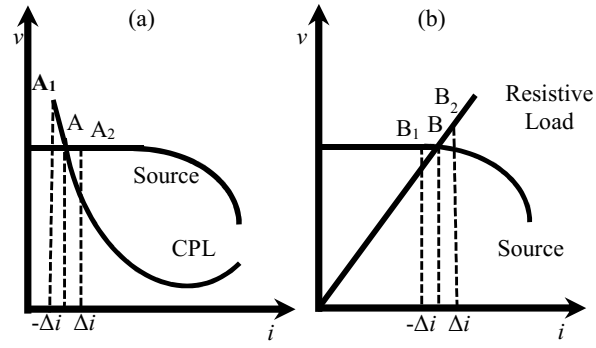

Fig. 3. Voltage- current characteristics of a CPL, resistive load and voltage source.

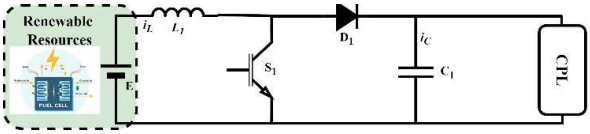

Fig. 4. Circuit diagram of DC/DC converter feeding CPL.

III. Mathematical Modelling of MPC

In order to implement the MPC, it is necessary to develop the discrete-time model of the DC converter. Fig. 4 illustrates the circuit diagram of the DC/DC step-up converter feeding CPL. The output voltage of the step-up DC converter is controlled by varying the duty cycle of the pulse width modulation (PWM) signal. But in the case of MPC, the pulse for the switch is directly generated by the MPC algorithm. In Fig 4. S_1 is a controllable switch, R_1 is the damping resistance, and current through inductor L is i_L, and the voltage across the capacitor C_1 is V_{c1}. V_{in} represents the input voltage of the DC source. Equation (2) explains the inductive nature while (3) presents the capacitive behavior of the dc converter:

$$\frac{di_{L1}(t)}{d(t)} = -\frac{R_1}{L_1} i_{L1}(t) - \frac{V_{c1}(t)}{L_1} + \frac{V_{c1}(t)}{L_1} u(t) + \frac{V_{in}}{L_1} \quad (2)$$

$$\frac{dV_{c1}(t)}{d(t)} = \frac{1}{C_1}\, i_{L_1}(t) - \frac{1}{C_1}\, i_{L_1}(t)u(t) - \frac{1}{R_1 C_1} V_{c1}(t) \quad (3)$$

Switch states (S_1) are defined by function u(t), as shown in (4). If $S_1 = 1$, switch S_1 is in the ON state; if switch $S_1 = 0$, switch S_1 is in the OFF state.

$$u(t) = \begin{cases} 1 & S_1 = 1 \\ 0 & S_1 = 0 \end{cases} \quad (4)$$

The discrete-time model of the DC converter is expressed in (5-6). These equations are used to anticipate the future response of voltage and current.

$$i_l(k+1) = \left(\frac{TR_1}{L_1} - 1\right) i_L(k) + (u(k) - 1)\frac{T}{L_1} V_{c1}(k) + \frac{T}{L_1} V_{in} \quad (5)$$

$$V_{c1}(k+1) = \frac{T}{C_1} i_{L1}(k) + \left(1 - \frac{T}{C_1 R}\right) V_{c1}(k) - \frac{T}{C_1} i_{L1}(k) * u(k) \quad (6)$$

Where (k+1) represents the future or next (coming) instant. T is the sampling time.

The formulation of the cost function (CF) is an essential part of the development of MPC. CF is the positive error value between the reference and actual state parameter value. In this case the positive value is ensured by squaring the error. The CF chosen in this study is illustrated in (7).

$$J_{DV}(k) = (V_C^*(k+1) - V_c(k+1))^2 \quad (7)$$

The execution of the MPC algorithm is as follows:

- At the start of the switching instant, the voltage and current of the converter are measured using sensors.
- Equation (5-6) is used to predict the current and voltage at the coming instant for all possible switching states, and then CF is evaluated using (7) for all possible states. In this study, N is taken as one. So, there are only two possible switching states.
- The state at which CF has a minimum value is chosen. This state is given to the converter switch for the coming instant.

IV. Proposed ANN Control Strategy

The artificial neural network is a subset of machine learning. It creates the mathematical relation based on gains between the inputs and outputs. ANN consists of a set of nodes known as neurons. These neurons create the layers, which are parallelly connected. The output of the single neuron is mathematically expressed as:

$$n_{out} = Act(b + \sum_{o=1}^{m} x_o . w_o) \quad (8)$$

The general equation used to compute the output of multilayers FF-ANN is as follows:

$$n_{ij} = Act_j^i(b_j^i + \sum_{o=1}^{m_{i-1}} n_{(i-1)o} . w_{o\,j}^i) \quad (9)$$

Where i is the number of hidden layers, j represents the number of neurons, and n_{ij} is the neuron's output at the j^{th} layer. It is necessary to have data to implement ANN. So, it requires to have a closed-loop simulation of the plant. In this study, a model predictive voltage control is implemented to extract the data of input features and output (targets). The reference voltage, actual voltage and output current are chosen as ANN's input features, switching pulses are selected as an output or target. The development of ANN is divided into three steps: offline training, testing and validation. The extracted data from simulations is used to train the ANN. After the training, fine-tuned ANN is tested in real-time simulation. The overall principle of the proposed ANN based controller is shown in Fig. 5.

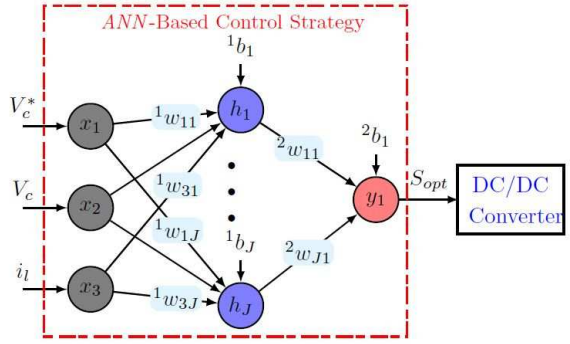

Fig. 5. The principle of the proposed ANN controller.

In this study, A feed-forward neural network is trained on the extracted data. The data set chosen for the offline training of ANN contains random samples of selected variables on different reference voltage values, such as 90V, 95V, 100V and 105V. Furthermore, the data set is randomly divided into three sets: Training set, validation and testing set with the ratio of 60%, 20% and 20%, respectively. The hidden number of neurons in the network is 15, and Bayesian regularized technique "trainbr function" is used as a training function. There are many methods to evaluate the performance of trained ANN but we applied two methods in this study. The first one is the confusion matrix, which evaluates the performance on the basis of output. In our case, the output of the ANN is 0 or 1 (pulse for the switch S_1). So, 78.8% of samples in the dataset belong to output class 1 while 21.2 % of samples are part of the output class 0. The total number of samples in the dataset is 180006. The proposed controller correctly predicts the output class of the random sample by overall accuracy of 97.2%, as shown in Fig. 6. Fig. 7 demonstrates the mean square error (MSE) during the network training. The performance of the trained network is good when the value of MSE is close to zero or zero. In our case, the value of MSE is 0.02143, which is attained during the offline training of the network.

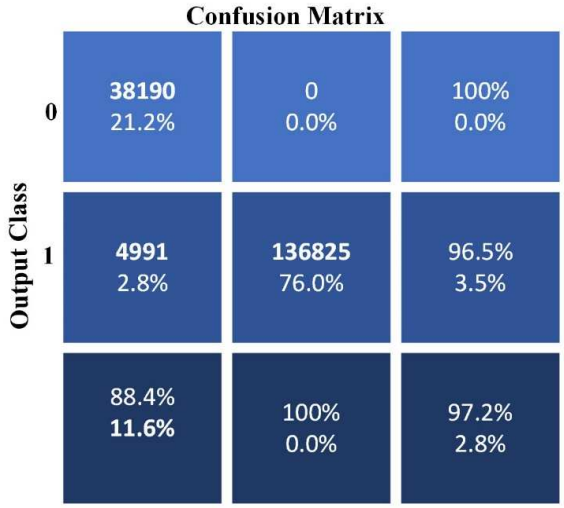

Fig. 6. The confusion matrix presents the accuracy of the trained ANN.

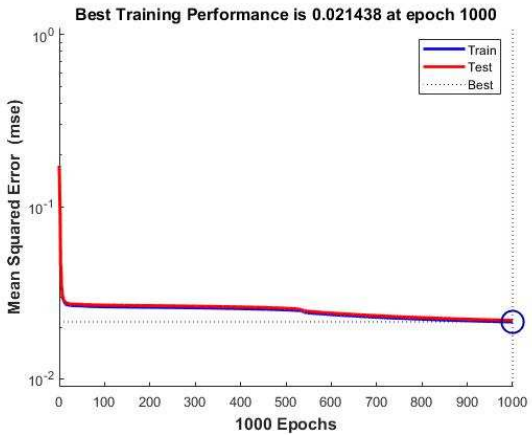

Fig. 7. Mean square error value of the proposed network during the training up to the 1000 epoch size.

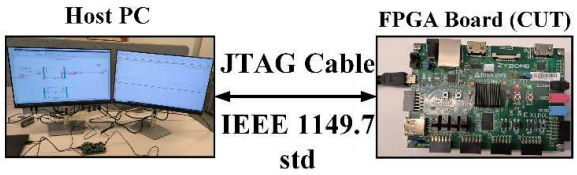

Fig. 8. Experimental setup to validate the proposed control technique.

TABLE I. SIMULATION SYSTEM PARAMETERS.

Parameters	Values
Inductor L	1mH
Capacitor C	1000 µF
Vref	85-115 V
Rated CPL Power	500-1000 W
DC input Vin	65-90V
PI Parameter	Kp=0.054; Ki= 8.86
FPGA Board	Zybo z7=7020

V. EXPERIMENTAL RESULTS

To validate the proposed approach's performance, effectiveness and transient response, the controller FPGA-in-loop-based validation is carried out. The test set is shown in Fig. 8. The system parameters are presented in Table 1. The ANN-based controller runs on the FPGA board, and DC/DC converter and load are simulated in the MATLAB/Simulink environment. The FPGA-in-the-loop (FIL) wizard provides the capability to use MATLAB/SIMULINK for testing controllers in real hardware conditions. The FIL wizard generates the code in VHSIC hardware descriptive language (VHDL). Then the generated VHDL code of the controller under test (CUT) is burned on the selected FPGA board. The communication between the board and MATLAB /SIMULINK is carried out through a JTAG cable. In this study, ZYBO Z7 (ZYNQ-7020 development board) is used. The ZYBO Z7 is driven by 125 MHz oscillators and supports the JTAG mode. It has 13300 Logic slices, 106,4000 flip flops and 630 KB embedded RAM.

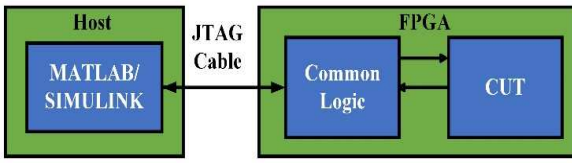

Fig. 9. The working principle of FPGA-in-loop simulation environment.

Fig. 9 illustrates the working of the FIL implementation in MATLAB/SIMULINK. The CUT is burned on the FPGA board while the remaining DC/DC converter model runs on the MATLAB/SIMULINK environment. The interactive communication is done through a JTAG cable. FIL Implementation is performed in the following steps:

1. The controller under test is specified using a Simulink subsystem. Then inputs and outputs of the subsystem are defined as fixed data types (This operation can be performed using SIMULINK Fixed Point Tool).
2. After defining data types, select the CUT subsystem, open the HDL workflow, and run all tasks.
3. After running all tasks successfully, MATLAB will generate the VHDL code of CUT and write it up on the FPGA board.

Furthermore, The PI and MPC results are simulated in MATLAB/SIMULINK environment. In this study, the PI controller was tuned only manually to have adequate performance, but possibly somewhat better tuning could have been possible with some optimal tuning methods. At the same time, the Proposed controller is implemented on the FPGA. The results are split into three cases, and only CPL is connected with the system, which is one of the worst cases from the stability point of view.

A. Reference voltage tracking

In this scenario, the transient response of the DC converter is examined with the change of reference voltage. In the beginning, the reference voltage is set to 100V. As depicted in Fig. 10, the output voltage tracks the reference voltage and output current becomes stable at 0.002 s. There is no disturbance observed in output voltage and output current. In the second scenario, at t=0 s, the CPL load of 500 W is connected with the system and voltage and load current becomes stable in no time. It is observed from the zoomed-in graph of Fig. 11 that the transient response of the proposed controller is slightly better and has less overshoot than conventional MPC. At t=0.4 s, the voltage reference is decreased to 85 V to observe the effect of change in voltage reference and also verify the controller response. However, both controllers track the reference voltage and remain stable without disturbance. Due to the decrease in the voltage, the current escalates to keep the power constant. Again, at t=0.6 sec, the reference voltage suddenly increases to 115 V. Both controllers track the new reference without any distortion, as demonstrated in Fig. 11.

B. Robustness to unknown changes in load

To validate the controller response to the unknown load variations. The constant power load of 500 W is initially connected at the point of common coupling (PCC). At t=0.4 s, the load connected at PCC is increased to 1000 W, and at =0.6s, the connected load is decreased to 500 W, as shown in Fig. 12. It can be seen from Fig. 12 that the performance of the proposed controller is better than the conventional PI controller. There is no variation observed in the proposed controller's case, while the PI controller cannot handle the increase in load and has more voltage deviation with steady-state error. Thus, the proposed controller is robust against load variations.

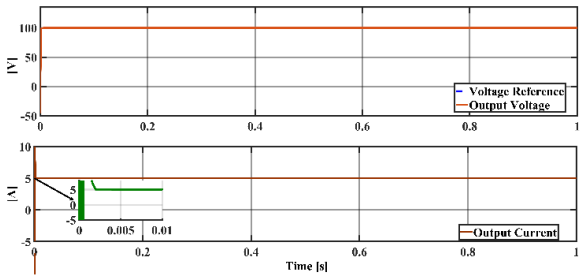

Fig. 10. Start-up response of the proposed controller.

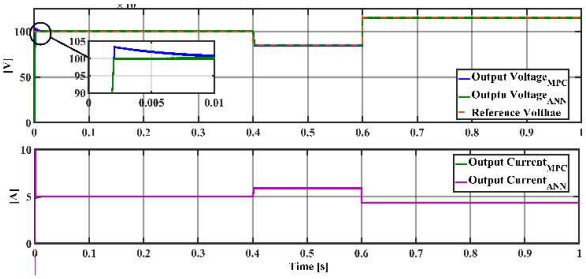

Fig. 11. Voltage reference tracking response of proposed controller compared to conventional MPC.

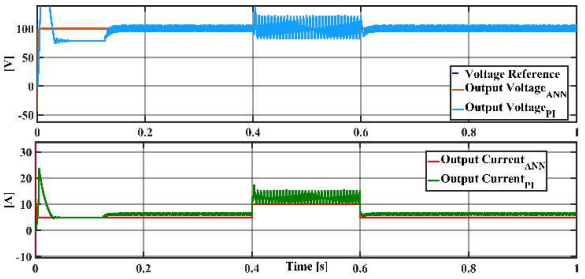

Fig. 12. Performance comparison between proposed ANN and PI controller under a change in load.

C. Robustness against the change of input voltage

In this case, the performance of the proposed controller is evaluated against the variation and noise input voltage. The case represents the PV solar sources and also the diode-based rectifier output. The input voltage of the DC converter is 80 V as shown in the Fig. 13. The ± 5% of the voltage fluctuation at the frequency of 50 Hz is added into the nominal input voltage as exhibited in Fig. 13. At t=0.4 s, the input voltage is increased to the 95 V, and at t=0.6 s, the input voltage is decreased to the 75 V to examine the effect of input voltage change and voltage noise on the performance of the proposed controller. The results show that the proposed controller rejects the disturbances and fluctuations and presents better transient performance. Accordingly, the proposed controller is robust against input voltage variations and fluctuations.

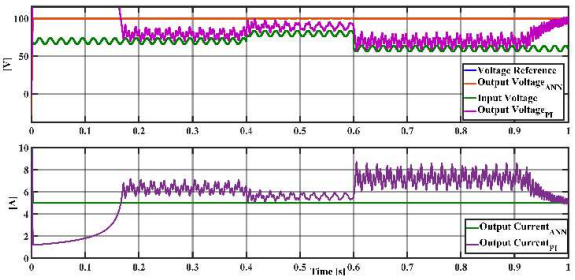

Fig. 13. Proof of proposed controller robustness against the input voltage fluctuations and variations and comparsion with the PI controller.

VI. Conclusion

This paper introduces an ANN-based voltage control approach for DC/DC boost converter under constant power loads (one of the worst cases). Initially, MPC is implemented to extract the dataset, which is used to train the ANN. The Bayesian regularized technique is used to train the ANN and adjust the biases and weights of the ANN. The proposed ANN control's overall performance is better in terms of transient response compared to MPC and conventional PI control strategies and robust against uncertainties, input variations and system nonlinearities. To validate the performance of the proposed control technique, FPGA-in-loop testing is also conducted using ZYBO Z7-7020 FPGA board. The implementation of the proposed technique would be useful in DC microgrid and critical applications, where it requires high robust performance under variations.

Acknowledgment

This work is carried out in project titled: Smart Grid 2.0 with the financial support provided by Business Finland under Grant No. 1386/31/2022. The financial support provided by the funding organization is highly acknowledged.

References

[1] D. Olivares, A. M.-S.-… on smart grid, and undefined 2014, "Trends in microgrid control," ieeexplore.ieee.org, Accessed: Jun. 15, 2022. [Online]. Available:https://ieeexplore.ieee.org/abstract/document/6818494/.

[2] R. W. De Doncker, "Power electronic technologies for flexible DC distribution grids," 2014 Int. Power Electron. Conf. IPEC-Hiroshima - ECCE Asia 2014, pp. 736–743, 2014, doi: 10.1109/IPEC.2014.6869670.

[3] F. A.-I.-I. Access and undefined 2021, "DC microgrid planning, operation, and control: a comprehensive review," ieeexplore.ieee.org, Accessed: Aug. 19, 2022. [Online]. Available: https://ieeexplore.ieee.org/abstract/document/9366476/.

[4] Z. Shuai, J. Fang, F. Ning, Z. S.-R. and S. Energy, and undefined 2018, "Hierarchical structure and bus voltage control of DC microgrid," Elsevier, Accessed: Aug. 19, 2022. [Online]. Available: https://www.sciencedirect.com/science/article/pii/S1364032117314788.

[5] H. Farsizadeh, M. Gheisarnejad, M. Mosayebi, M. Rafiei, and M. H. Khooban, "An Intelligent and Fast Controller for DC/DC Converter Feeding CPL in a DC Microgrid," IEEE Trans. Circuits Syst. II Express Briefs, vol. 67, no. 6, pp. 1104–1108, Jun. 2020, doi: 10.1109/TCSII.2019.2928814.

[6] H. S. Khan, M. Aamir, M. Ali, A. Waqar, S. Umaid Ali, and J. Imtiaz, "Finite control set model predictive control for parallel connected online UPS system under unbalanced and nonlinear loads," Energies, vol. 12, no. 4, 2019, doi: 10.3390/en12040581.

[7] H. S. Khan, M. Aamir, K. Kauhaniemi, M. Mumtaz, M. W. Hassan, and M. Ali, "Improved finite control set model predictive control for distributed energy resource in islanded microgrid with fault-tolerance capability," Eng. Sci. Technol. an Int. J., 2021.

[8] S. Tan, Y. Lai, K. C.-I. transactions on industrial, and undefined 2008, "General design issues of sliding-mode controllers in DC–DC converters," ieeexplore.ieee.org, 2008, doi: 10.1109/TIE.2007.909058.

[9] Z. Cheng et al., "A novel cascaded control to improve stability and inertia of parallel buck-boost converters in DC microgrid," Elsevier, Accessed: Aug. 19, 2022. [Online]. Available: https://www.sciencedirect.com/science/article/pii/S0142061519336075.

[10] S. Singh, D. Fulwani, and V. Kumar, "Robust sliding-mode control of dc/dc boost converter feeding a constant power load," IET Power Electron., vol. 8, no. 7, pp. 1230–1237, Jul. 2015, doi: 10.1049/IET-PEL.2014.0534.

[11] B. A. Martínez-Treviño, R. Jammes, A. El Aroudi, and L. Martínez-Salamero, "Sliding-mode control of a boost converter supplying a constant power load," IFAC-PapersOnLine, vol. 50, no. 1, pp. 7807–7812, Jul. 2017, doi: 10.1016/j.ifacol.2017.08.1055.

[12] Z. Wang, S. Li, Q. L.-I. T. on C. and Systems, and undefined 2019, "Continuous nonsingular terminal sliding mode control of DC–DC boost converters subject to time-varying disturbances," ieeexplore.ieee.org, Accessed: Aug. 19, 2022. [Online]. Available: https://ieeexplore.ieee.org/abstract/document/8915725/.

[13] L. Cheng et al., "Model predictive control for DC–DC boost converters with reduced-prediction horizon and constant switching frequency," ieeexplore.ieee.org, 2017, doi: 10.1109/TPEL.2017.2785255.

[14] Z. ; Karami, Q. ; Shafiee, Y. ; Khayat, M. ; Yaribeygi, T. ; Dragicevic, and H. Bevrani, "Decentralized model predictive control of DC microgrids with constant power load," ieeexplore.ieee.org, vol. 9, no. 1, p. 451, 2021, doi: 10.1109/JESTPE.2019.2957231.

[15] Q. Wei, B. Wu, D. Xu, and N. R. Zargari, "Model Predictive Control of Capacitor Voltage Balancing for Cascaded Modular DC-DC Converters," IEEE Trans. Power Electron., vol. 32, no. 1, pp. 752–761, Jan. 2017, doi: 10.1109/TPEL.2016.2530869.

[16] S. Zhao, F. Blaabjerg, H. W.-I. T. on Power, and undefined 2020, "An overview of artificial intelligence applications for power electronics," ieeexplore.ieee.org, Accessed: Aug. 19, 2022. [Online]. Available: https://ieeexplore.ieee.org/abstract/document/9200511/.

[17] I. S. Mohamed, S. Rovetta, T. D. Do, T. Dragicevic, and A. A. Z. Diab, "A neural-network-based model predictive control of three-phase inverter with an output LC Filter," IEEE Access, vol. 7, pp. 124737–124749, 2019, doi: 10.1109/ACCESS.2019.2938220.

[18] A. Rosato, M. Panella, R. Araneo, and A. Andreotti, "A Neural Network Based Prediction System of Distributed Generation for the Management of Microgrids," IEEE Trans. Ind. Appl., vol. 55, no. 6, pp. 7092–7102, 2019, doi: 10.1109/TIA.2019.2916758.

[19] J. Duan, Z. Yi, D. Shi, C. Lin, … X. L.-I. T. on, and undefined 2019, "Reinforcement-learning-based optimal control of hybrid energy storage systems in hybrid AC–DC microgrids," ieeexplore.ieee.org, Accessed: Aug. 19, 2022. [Online]. Available: https://ieeexplore.ieee.org/abstract/document/8630643/.

[20] M. Khan, A. Haque, … V. K.-I. J. of, and undefined 2020, "Advanced control strategy with voltage sag classification for single-phase grid-connected photovoltaic system," ieeexplore.ieee.org, Accessed: Aug. 19, 2022. [Online]. Available: https://ieeexplore.ieee.org/abstract/document/9277513/.

[21] B. Adineh, M. Habibi, … A. A.-I. T. on, and undefined 2021, "Sensorless voltage estimation for total harmonic distortion calculation using artificial neural networks in microgrids," ieeexplore.ieee.org, vol. 2, no. 7, pp. 2583–2587, 2021, doi: 10.1109/TCSII.2021.3059410.

[22] H. S. Khan, I. S. Mohamed, K. Kauhaniemi, and L. Liu, "Artificial Neural Network-Based Voltage Control of DC/DC Converter for DC Microgrid Applications," 2021 6th IEEE Work. Electron. Grid, eGRID 2021, 2021, doi: 10.1109/EGRID52793.2021.9662132.

[23] S. Singh, A. R. Gautam, and D. Fulwani, "Constant power loads and their effects in DC distributed power systems: A review," Renewable and Sustainable Energy Reviews, vol. 72. 2017, doi: 10.1016/j.rser.2017.01.027.

[24] E. Hossain, R. Perez, A. Nasiri, and S. Padmanaban, "A Comprehensive Review on Constant Power Loads Compensation Techniques," IEEE Access, vol. 6, 2018, doi: 10.1109/ACCESS.2018.2849065.

IET Renewable Power Generation

IET Journals
The Institution of Engineering and Technology

Artificial Intelligence-based Reduced Sensor Voltage Control Strategy for DC Microgrid Applications

ISSN 0000-0000
doi: 0000000000
www.ietdl.org

H. S. Khan[1]* *K. Kauhaniemi*[1]

[1] *School of Technology and Innovations, University of Vaasa, Vaasa, Finland*
* *E-mail: hussain.khan@uwasa.fi*

Abstract: The expeditious advancement in renewable energy technologies enables the concept of microgrids to boost the incorporation of renewable energy into power systems. In this context, distributed generation (DG)-based DC microgrids (MGs) are favoured because of their higher efficiency, greater reliability, and simpler development and control compared to their AC counterparts. This paper presents an artificial neural network (ANN) voltage control for a DC-DC step-up converter to reduce the number of sensors in the DC microgrids. The proposed approach offered cost-effective and better voltage regulation in multi-bus DC MG. The proposed methodology employs Quasi-Stationary Line (QSL) modeling to account for DC MG uncertainties and disturbances, while simultaneously developing and implementing a model predictive voltage control (MPVC) strategy to generate the comprehensive dataset. The converter's voltage error and switching signals, extracted from the generated dataset, serve as input features for offline training of an artificial neural network (ANN). Once trained, the ANN is deployed online to regulate distributed generators (DGs) within a multi-bus DC MG. Real-time hardware-in-the-loop simulations using OPAL-RT 4510 demonstrate that the proposed controller effectively regulates voltage with reduced sensors, ensuring improved reliability and efficiency.

1 Introduction

With the development and advancement of renewable energy technology, modern power systems have become more complex and have undergone extensive changes over the past two decades. Microgrids (MGs) offer a promising solution for the effective integration of renewable energy resources. As crucial smart grid components, these systems will provide carbon-free and sustainable energy to consumers while operating in grid-tied and islanded modes. However, electrical systems are predominantly based on alternating current (AC). Advancements in power electronics technology have made direct current (DC) systems more efficient at all levels, namely generation, distribution, and transmission, and capable of operating in a wide range of voltages.[1]. The advantages of DC MG over AC MG can be summarized as:

- Most renewable energy resources, such as fuel cells, photovoltaic (PV) systems, and battery energy storage systems (BESS), generate DC power. Although wind turbines produce AC power, they can be effectively integrated into DC MGs because of the availability of advanced power converters.
- Most Energy Storage Systems (ESS) are inherently DC-based. This characteristic facilitates easier integration of ESS into DC MGs, resulting in reduced costs, higher efficiency, simpler control, and improved reliability.
- The overall control of DC MGs is simpler due to the absence of factors such as frequency regulation, reactive power management, voltage imbalance, and harmonics.

Due to the advantages above, the DC MG is a well-accepted solution for the utility grid and the transportation sector, such as electric ships and aircraft. Figure 1 illustrates the typical DC MG configuration that contains multiple sources such as photovoltaic panels (PV), wind turbine (WT), and energy storage systems (ESS), which are connected to a common DC bus through a power electronic interface (PEI). The distribution network topology of DC microgrids (MGs) can vary, from radial to ring-type distribution systems.

The primary responsibilities of the control system in a DC microgrid (DC MG) are to address the following issues [2]:

- Regulation of DC-bus voltage.
- Accurate power sharing among the distributed generators (DGs)
- Management of power quality issues.
- Coordination among the distributed energy resources and energy storage systems (ESS).
- Unit commitment and economic dispatch of the DC MG.
- Minimization of transmission losses.
- Utilization of DERs to their full potential.

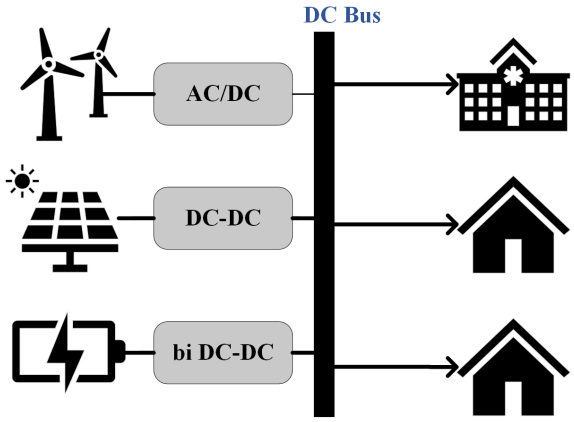

Fig. 1: The typical configuration of an autonomous DC microgrid has DG units, ESS, loads, and their control.

To address the aforementioned issues, the hierarchical control strategy has garnered significant attention due to its multi-layered architecture. This strategy comprises three layers: primary, secondary, and tertiary control, as illustrated in Figure 2. The primary layer includes an inner control loop to regulate the voltage and current of the converter, while droop control is employed to share power

among the distributed energy resources (DER). The secondary control layer is responsible for voltage compensation and improving power-sharing accuracy. At the highest level, the tertiary control layer handles economic dispatch, system optimization, and energy management within the DC microgrid. However, this paper focuses exclusively on primary control; the secondary and tertiary controls are not studied here.

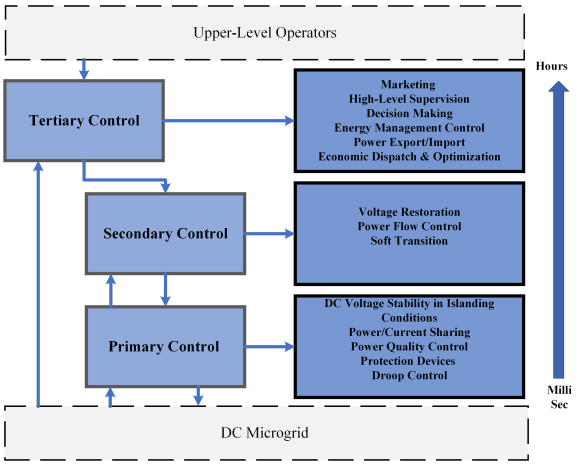

Fig. 2: Control architecture description for autonomous DC microgrid.

Numerous strategies for coordinating multiple distributed generators (DGs) in the autonomous mode of microgrids (MGs) have been proposed in existing research [3]. These strategies include master-slave control [4], load-sharing techniques [5, 6], centralized control [7], and others. These methods typically rely on a communication network among the DGs to ensure efficient and stable operation; however, this requirement adds complexity and can potentially reduce the system's reliability. Consequently, implementing a method like droop control is essential for accurate power sharing among DGs. In [8], the authors introduce decentralized droop control as a beneficial strategy, eliminating the need for an external communication link between power electronic interface-based DGs. The primary objectives of droop control in DC MGs are to share power between DGs and maintain voltage stability at the DC bus. In this context, the droop control functions as the external loop of the power converter, while the voltage control strategies are applied within the inner loop of the DG in the MG.

In the realm of power electronics (PE) control, the research community has extensively explored various linear controllers, notably PI and PID, which are widely implemented as evidenced by numerous studies and are widely used by the PE industry [9, 10]. Despite their prevalent use, these linear theory-based controllers exhibit enormous practical limitations, such as PID parameter tuning, limited ability to reject disturbances, operating point shifts towards instability due to parameter variations, and an inability to address the nonlinear characteristics of power systems adequately.

To address the shortcomings of linear controllers and improve the transient behaviour, various nonlinear control strategies like sliding mode control (SMC), fuzzy-logic control (FLC), and model predictive control (MPC) have been developed. For instance, a fuzzy-logic control approach for DC converters in photovoltaic lighting systems is studied in [11]. The microcontroller implemented the fuzzy logic for the DC power converter, which was explored in [12]. FLC primarily operates on if-else logic, and its response depends on pre-established rules without requiring a mathematical model of the system, adeptly managing nonlinearities. The performance of fuzzy controllers for the DC-DC converter is also effective across a range of operating conditions. However, the reliability of fuzzy controllers is often questioned due to the lack of formal analysis. Therefore, numerous control approaches are amalgamated in the literature to address the limitations of fuzzy logic control [13].

Sliding mode control and model predictive control have been extensively proposed in the literature and have shown promising results in power electronic converter applications. Based on the principles of variable structure control theory, sliding mode control involves two main phases: the reaching phase, where system state trajectories are directed to a predefined sliding surface, and the sliding phase, where they remain within this surface based on predefined criteria. Despite its resilient performance, robustness to parametric variations, and excellent transient response under various loads, its implementation faces significant challenges. It includes issues such as chattering phenomena, high switching losses, and the complexity of its mathematical modelling as the sliding order increases [14] [15]. In [3], the authors presented the intelligent sliding mode control for parallel converters in DC microgrid for constant power load applications.

Model predictive control (MPC) is a digital control strategy that fundamentally differs from traditional linear control methods. Unlike linear controllers, which typically require separate loops for each controlled variable and their subsequent cascading, MPC leverages a discrete-time model of the converter and its filter to predict outcomes for all potential input combinations. The input that minimizes a predefined cost function is selected for the next sampling period. It is typically defined as the square of the Euclidean distance between the measured and reference signals [16]. MPC-based control schemes have been proposed for a wide range of applications, including AC systems [17, 18], DC systems [19, 20] , and hybrid microgrids (MGs) [21, 22]. In AC/DC and AC MGs, MPC strategies have been developed for bidirectional DC/DC converters [18] and AC/DC converters [21, 23]. In the context of DC microgrids, MPC has been employed to enhance stability, optimize power sharing, manage energy systems, improve transient response, and address pulsed power loads in naval DC MGs. Additionally, MPC is used to control DC/DC converters, maximize photovoltaic (PV) power output through maximum power point tracking, and reduce power losses in DC MGs. However, MPC's effectiveness heavily depends on the system's mathematical model's accuracy and has significant computational burden. Moreover, it has a variable switching frequency, which can be a limitation in some applications. To address this, recent research has introduced MPC methodologies that maintain a constant switching frequency, tailored for various power electronic applications [16].

Data-driven or model-free control methods, particularly those utilizing artificial neural networks (ANN), are becoming increasingly common in the field of power converter control. [24]. ANN-based control techniques are proposed for voltage sag classification, fault detection, short-term prediction, etc. ANN-based converter control has been proposed in [25, 26]. In [27], neural network predictive-based voltage control has been introduced for the DC-DC buck converter. PID controller data serve as training data to train ANN. Once trained, neural network predictive control (NNPC) regulates the voltage. An NNPC controller designed for a grid-connected synchronverter is presented in [28]. Furthermore, an improved control strategy has been proposed that combines a proportional-integral controller with an ANN to improve performance metrics such as overshoot, rise time, and settling time [29]. A fuzzy logic-aided ANN power oscillation damping controller is proposed for hybrid AC/DC MG [30]. Sliding Mode robust droop control scheme enhanced by an ANN algorithm for islanded photovoltaic-integrated microgrids is studied in [31]. In [32], the author studied the ANN-based control for nonlinear DC microgrids. Real-time FPGA-based validation of ANN for DC-DC converter is illustrated in [33].The superiority of the ANN controller over other controllers is due to the various key advantages [34]:

- It eliminates the need for a mathematical model of the system.
- Its performance can be enhanced through controller tuning.
- Its design does not necessitate specialized expertise.

Table 1 Overview of sensorless control approaches for DC MG.

References	[29, 35]	[36]	[37]	[38]	[39]	Proposed
Controller	Deep Learning	Lyapunov Based State Observer	Pre-defined Objective Function	Fifth Dimensional Estimator	Proportional Derivative (PD)	ANN
Load Variation	✓	✓	✓	✓	✓	✓
PnP	-	✓	-	-	-	✓
Parametric Variations	-	-	-	✓	-	✓
Stability Analysis	-	✓	✓	✓	-	✓
Application	PV converter	DC MG	Buck-Boost Converter	AC-DC Converter	DC/DC Boost Converter	DC/DC Boost Converter
Sensor Reduction	Current	Current, voltage	Current	Current	Current	Current

This study introduces an innovative reduced-sensor ANN-based voltage control technique for distributed generations in a DC microgrid, specifically focusing on a DC-DC step-up (Boost) converter. Our methodology employs an artificial neural network (ANN) that requires fewer sensors compared to model predictive control, which typically requires at least two sensors. Table 1 summarizes the overall features of various existing reduced sensor control techniques. A quasi-stationary line (QSL) approximation is used to model the uncertainties, disturbances, and line dynamics of the DC MG, as studied in [40]. Initially, model predictive control (MPC) is implemented for the DC-DC converter as a parent control method and also as a tool to extract a dataset comprising input features such as voltage, current, power, and switching pulses under different loading and operating conditions. After extracting the dataset, various combinations of input features are evaluated to identify the most effective for control purposes. The error between the output and reference voltage is ultimately selected as the primary input feature. At the same time, the converter's switching action is chosen as the output feature for the artificial neural network (ANN) in this study. The selected input-output pair simplifies the system to a single input and single output (SISO) configuration, reducing the computational complexity [41] and enabling efficient training of the ANN. The SISO ANN is trained offline using the Bayesian regularization technique, with performance validated through metrics such as mean squared error (MSE) and confusion matrices. Upon achieving high accuracy and reliability during the training, validation, and testing phases, the ANN is integrated into the Simulink environment for control of the Boost converter. Figure 8 illustrates the overview of the proposed control strategy: the training phase combines using MPC to anticipate the converter output voltage and collection of state variables data under full-state observation. The data collected are used to train the ANN. In the test phase, the trained neural network is employed online to control the converter's output voltage instead of the MPC. The simulation results validate the superiority of the proposed ANN-based control strategy, demonstrating enhanced voltage regulation performance and accuracy compared to conventional PI controllers and the model predictive control (MPC) method used in this study. Furthermore, real-time HIL simulations were conducted using the OPAL-RT 4510 platform to assess the controller's effectiveness under various test scenarios, including plug-and-play events, microgrid topology reconfiguration, and responses to unknown load variations. The proposed controller exhibits robust performance in both simulation and hardware-in-the-loop (HIL) environments. Reducing the number of sensors improves system reliability by minimizing potential failure points and improves speed by eliminating communication delays associated with sensors. This leads to a more responsive and efficient system. Additionally, current sensors are generally more susceptible to failure in DC systems than voltage sensors because of their higher exposure to thermal and electrical stresses. Therefore, favoring voltage sensors over current sensors increases the system's resilience and ensures more reliable operation in case of sensor failure. The following are the key features of the proposed approach:

1. Whole system dynamics are incorporated by using QSI approximation.
2. The ANN is implemented by designing the control objectives based on MPC.
3. ANN architecture is developed by merging the feedback from the DC/DC converter with the ANN, creating a unified system.
4. The training of ANN is carried out offline to prevent any stability issues.

The rest of the paper is organized as follows: Mathematical modeling of the DC MG is developed in 2, and the basic principle of model predictive control is explained in section 3. Section 4 delves into the artificial neural network and the training process of the ANN model. Simulation and HIL results are discussed in section 5. Finally, the paper summarizes the key findings and insights in section 6.

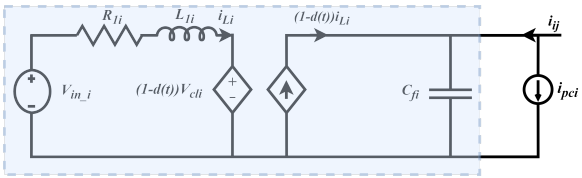

Fig. 3: Equivalent circuit diagram of step-up converter.

2 Mathematical model of islanded DC microgrid

Figure 1 illustrates the configuration of the DC microgrid. Usually, a DC microgrid can consist of PV arrays, wind turbines, fuel cells connected with the bus through a unidirectional DC/DC converter, an energy storage system with a bidirectional DC/DC converter, and fixed and variable DC loads. It may also have an AC load connected via a DC/AC converter. There is the possibility of connecting the DC MG with the AC utility grid through a bidirectional interlink AC/DC converter. The DC MG controls are divided into three types based on communication: decentralized control, centralized control, and distributed control.

The equivalent circuit diagram of the DC-DC boost converter is shown in Figure 3, where V_{in_i} represents the input voltage, which models renewable energy such as PV systems, batteries, etc. Due to the uncertainty in the system load ratings, the system is modelled as a current disturbance i_l. The output of DER_j is denoted as V_{out_j}, while DER_i is represented as V_{out_i}. Other parameters follow a similar notation pattern. Additionally, d(t) represents the duty cycle at the switching instant t in the DC-DC converter. The dynamic response of DER_i and $Line_{ij}$ is determined using Krichoff's current and voltage laws, and their equation are expressed as follows:

$$\frac{dV_{cli}}{dt} = \frac{1}{C_{fi}} i_{L_{1i}} - \frac{1}{C_{fi}} i_{L_{1i}} d(t) - \frac{1}{C_i} i_{pci} + \frac{1}{C_i} i_{ij} \quad (1)$$

$$\frac{di_{Li}}{dt} = -\frac{R_{1i}}{L_{1i}} i_{Li} - \frac{V_{cli}}{L_{1i}} + \frac{V_{cli}(t)}{L_{1i}} d(t) + \frac{V_{in_i}}{L_{1i}} \quad (2)$$

$$Line_{ij} = \frac{dI_{ij}}{dt} = \frac{V_{in_j}}{L_{ij}} - \frac{V_{in_i}}{L_{ij}} - \frac{R_{ij} I_{ij}}{L_{ij}} \quad (3)$$

The DER unit parameters C_{fi} , R_{1i} and L_{1i} are the LC parameters of the circuit. Moreover, the line parameters are specified as $L_{ij} = L_{ji}$ and $R_{ij} = R_{ji}$, ensuring symmetry between the connecting lines and currents flowing between the nodes are equal in magnitude but opposite in directions, maintaining the consistency with the Kirchoff's current law.

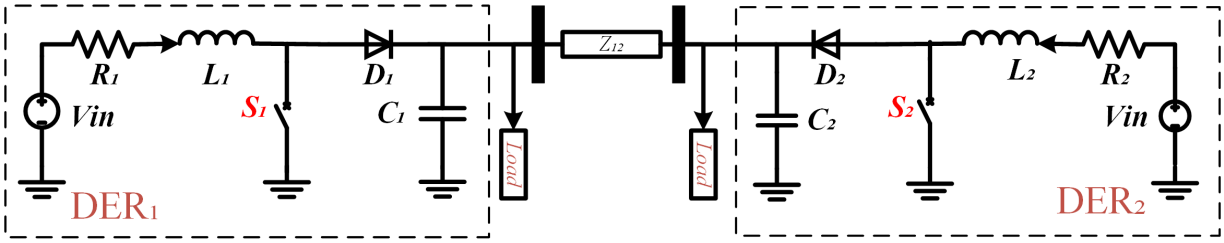

Fig. 4: Schematic diagram of an autonomous DC microgrid with two DERs.

2.1 Quasi-stationary-line (QSL) model approximation

The Quasi-Stationary Line (QSL) model is an approximation used to simplify the analysis of the system by assuming that changes in the system occur over a period long enough for the system to be considered quasi-static yet short enough to prevent it from reaching full equilibrium. In the short transmission line, the line's inductance is relatively small and has a small time constant, allowing the line dynamics to be neglected. Consequently, the rate of change of the inductors' current over time $\frac{dI_{ij}}{dt}$ is negligible and also expressed as QSL approximations [42]. So, This QSL model approximation is only valid for short transmission lines. A comprehensive model based on the quasi-stationary line (QSL) approximation should be developed for medium and long transmission lines to accurately capture electrical behavior and dynamic characteristics over extended distances. Figure 4 illustrates the two coupled distributed energy resource (DER) units, consisting of a DC-DC converter, input source V_{in}, and the local load connected through a line, denoted as "ij," with resistance R_{ij} and inductance L_{ij}, respectively. The proposed control scheme applies to DC microgrids (MG) with radial, parallel, and meshed topologies in this configuration. In this study, a DC-DC boost converter with uncertainties is considered. Based on this assumption, Equation (4) is derived from Equation (3).

$$I_{ij} = \frac{V_{in_j} - V_{in_i}}{R_{ij}} \tag{4}$$

Substituting the Equation (4) to Equation (1) gives the QSL approximation of DER_i, expressed in the Equation (5).

$$\mathrm{DER}_i := \begin{cases} \frac{\mathrm{dV_{c1_i}}}{\mathrm{dt}} = \frac{(1-d_i)}{C_{f_i}} I_{L_i} + \frac{V_{\mathrm{c1}_j}}{R_{\mathrm{ij}} C_{f_i}} - \frac{V_{\mathrm{c1}_i}}{R_{\mathrm{ij}} C_{f_i}} - \frac{1}{C_{f_i}} i_{L_i} \\ \frac{\mathrm{di_{L_i}}}{\mathrm{dt}} = \frac{1}{L_{1_i}} V_{\mathrm{ini}} - \frac{(1-d_i)}{L_{1_i}} V_{\mathrm{c1_i}} - \frac{R_{1_i}}{L_{1_i}} i_{L_i} \end{cases} \tag{5}$$

$$DER_{[i]} = \begin{cases} \dot{\tilde{x}}_{[i]}(t) = A_{[ii}(t)\tilde{x}_{[i]}(t) + B_i(t)\tilde{u}_{[i]}(t) \\ +D_i(t)\tilde{w}_{[i}(t) + \tilde{\zeta}_{[i]}(t) \\ \tilde{y}_i(t) = C_i(t)\tilde{x}_{[i]}(t) \end{cases} \tag{6}$$

The generalized state space representation of QSL is given in Equation (6). This formulation represents a small-signal state vector, which includes the perturbed system variables. The input $\tilde{u}(t) = \tilde{d}_i(t)$, corresponds to the duty cycle of DER_i. The term $\tilde{w}_{[i]}(t) = \left[\tilde{L}_{L_i}, \tilde{v}_{\mathrm{in}_i}\right]^\top$ are small-signal exogenous disturbances, accounting for variations in current and input voltage. Additionally, $\tilde{\zeta}_{[i]}(t) = A_{ij}(t)\tilde{x}_j$ captures the coupling between DER_i and DER_j, indicating the interaction between different distributed energy resources. $\tilde{y}_{[i]}(t)$ is the output vector, which is the function of the system state variables. Equation (5) is rewritten as a state space model and described below.

$$A_{ii}(t) = \begin{bmatrix} \frac{-1}{R_{ij}C_{f_i}} & \frac{(1-\bar{D}_i)}{C_{f_i}} \\ \frac{-(1-\bar{D}_i)}{L_{1_i}} & \frac{-R_{1_i}}{L_{1_i}} \end{bmatrix}, B_i(t) = \begin{bmatrix} \frac{-i_{L_i}}{C_{f_i}} \\ \frac{\bar{V}_{\mathrm{c1_i}}}{L_{1_i}} \end{bmatrix}$$

$$D_i(t) = \begin{bmatrix} \frac{-1}{C_{f_i}} & 0 \\ 0 & \frac{1}{L_{1_i}} \end{bmatrix}, A_{ij}(t) = \mathrm{diag}\left(\frac{1}{R_{ij}C_{f_i}}, 0\right), C_i = I_{2\times 2}$$

The linearised model's applicability in Equation (6) hinges on the premise that fluctuations around the equilibrium point are minor enough to ensure the inherent non-linear system. Equation (5) ensures the asymptotic stability of the system. However, if fluctuations and disturbances extend too high, the linearized representation of the system might lose its accuracy. Building on Equation (6), the small-signal state-space model for the interconnected distributed energy resources depicted in Figure 4, is articulated as follows:

$$\begin{bmatrix} \hat{\dot{x}}_{[i]} \\ \hat{\dot{x}}_{[j]} \end{bmatrix} = \begin{bmatrix} A_{ii}(t) & A_{ij}(t) \\ A_{ji}(t) & A_{jj}(t) \end{bmatrix} \begin{bmatrix} \tilde{x}_{[i]} \\ \hat{x}_{[j]} \end{bmatrix} + \begin{bmatrix} B_i(t) & 0 \\ 0 & B_j(t) \end{bmatrix} \begin{bmatrix} \tilde{u}_{[i]} \\ \tilde{u}_{[j]} \end{bmatrix} + \begin{bmatrix} D_i(t) & 0 \\ 0 & D_j(t) \end{bmatrix} \begin{bmatrix} \tilde{w}_{[i]} \\ \tilde{w}_{[j]} \end{bmatrix}$$
$$\begin{bmatrix} \hat{y}_{[i]} \\ \hat{y}_{[j]} \end{bmatrix} = \begin{bmatrix} C_i & 0 \\ 0 & C_j \end{bmatrix} \begin{bmatrix} \hat{x}_{[i]} \\ \hat{x}_{[j]} \end{bmatrix} \tag{7}$$

The model expressed in Equation (7) describes the interaction between various DER units through coupling terms and also considers the system disturbances. The output matrix $C_i = I_{2x2}$ ensures that the system outputs are directly proportional to the state variables.

Now expand the model for interconnected DER units, Let represent the set of all interconnected DER units and ,$\mathcal{N}_i \subset \mathcal{D}$ is a neighbouring subset of DER_i, which is coupled via electrical links ij. The coupling between different DER units is expressed by the term $DER_{ij}\ \tilde{\xi}_{[i]}(t) = \sum_{j\in N_i} A_{ij}(t)\tilde{x}_{[j]}(t)$. Therefore, the matrix A_{ii} is reevaluated as:

$$A_{\mathrm{ii}}(t) = \begin{bmatrix} \sum_{j\in N_i} \frac{-1}{R_{ij}C_{f_i}} & \frac{(1-\bar{D}_i)}{C_{f_i}} \\ \frac{-(1-\bar{D}_i)}{L_{1_i}} & \frac{-R_{1_i}}{L_{1_i}} \end{bmatrix}$$

The small-signal linear time-variant model of the whole system, including the disturbances, coupling, and dynamics in the compact form, is represented as:

$$\begin{cases} \dot{\tilde{\mathbf{x}}}(t) = \mathbf{A}(t)\tilde{\mathbf{x}}(t) + \mathbf{B}(t)\tilde{\mathbf{u}}(t) + \mathbf{D}(t)\tilde{\mathbf{w}}(t) \\ \tilde{\mathbf{y}}(t) = \mathbf{C}(t)\tilde{\mathbf{x}}(t) \end{cases}$$

Where $\tilde{\mathbf{x}}, \tilde{\mathbf{u}}, \tilde{\mathbf{w}}, \tilde{\mathbf{y}}$ are defined as:

$$\tilde{\mathbf{x}} = \begin{bmatrix} \tilde{x}_{[1]} \\ \tilde{x}_{[2]} \\ \vdots \\ \tilde{x}_{[N]} \end{bmatrix}, \quad \tilde{\mathbf{u}} = \begin{bmatrix} \tilde{u}_{[1]} \\ \tilde{u}_{[2]} \\ \vdots \\ \tilde{u}_{[N]} \end{bmatrix},$$

$$\tilde{\mathbf{w}} = \begin{bmatrix} \tilde{w}_{[1]} \\ \tilde{w}_{[2]} \\ \vdots \\ \tilde{w}_{[N]} \end{bmatrix}, \quad \tilde{\mathbf{y}} = \begin{bmatrix} \tilde{y}_{[1]} \\ \tilde{y}_{[2]} \\ \vdots \\ \tilde{y}_{[N]} \end{bmatrix},$$

$$\mathbf{B}(t) = \text{diag}\left(B_i(t)\right),$$

$$\mathbf{D}(t) = \text{diag}\left(D_i(t)\right),$$

$$\mathbf{C} = \text{diag}\left(C_i\right),$$

$$\mathbf{A}(t) = \begin{bmatrix} A_{11}(t) & A_{12}(t) & \dots & A_{1N}(t) \\ A_{21}(t) & A_{22}(t) & \dots & A_{2N}(t) \\ \vdots & \vdots & \ddots & \vdots \\ A_{N1}(t) & A_{N2}(t) & \dots & A_{NN}(t) \end{bmatrix}$$

The matrices B(t), D(t), C(t), and A(t) are block diagonal, representing the local dynamics of each DER unit. The system matrix A(t) includes the DER's internal dynamics and the coupling between different DER units.

3 Model Predictive Control for DC-DC Converter

Developing a discrete-time model for the DC converter is essential to implement MPC. The circuit diagram of the step-up boost converter is presented in Figure 4. The output voltage of this step-up DC converter is regulated by adjusting the duty cycle of the pulse width modulation (PWM) signal. A significant limitation of MPC is its variable switching frequency, which can present challenges in specific applications. Where S_1 is a controllable switch, R_1 is the damping resistance, and current through inductor L is i_{L1} and the voltage across the capacitor C_1 is v_{C1}. V_{in} represents the input voltage of the DC source. A second-order low-pass filter is utilized to reduce high-frequency components in the signal. Equation (8) describes the inductive behaviour, while Equation (9) explains the capacitive nature of the system:

$$\frac{di_{Ll}(t)}{d(t)} = -\frac{R_1}{L_1} i_{Ll}(t) - \frac{V_{cl}(t)}{L_1} + \frac{V_{cI}(t)}{L_1} u(t) + \frac{V_{\text{in}}}{L_1} \quad (8)$$

$$\frac{dV_{cl}(t)}{d(t)} = \frac{1}{C_1} i_{L_1}(t) - \frac{1}{C_1} i_{L_1}(t) u(t) - \frac{1}{R_1 C_1} V_{cl}(t) \quad (9)$$

The function u(t) defines the switch states as presented in Equation (10). When the switch S_1 is equal to 1 and is in the ON state, whereas if S_1= 0, it is deemed to be in the OFF state.

$$u(t) = \begin{cases} 0 & S_1 = 0 \\ 1 & S_1 = 1 \end{cases} \quad (10)$$

The discrete-time model of the DC converter is presented in Equation (11-12). These equations are formulated to predict the future behavior of voltage and current, and they are derived from Equations (6-7) & (11-12).

$$i_{l1}(k+1) = \left(\frac{TR_1}{L_1} - 1\right) i_{L1}(k) + (u(k) - 1)\frac{T}{L_1} V_{cl}(k) \quad (11)$$

$$V_{c1}(k+1) = \frac{T}{C_1} i_{Ll}(k) + \left(1 - \frac{T}{C_1 R}\right) V_{c1}(k) - \frac{T}{C_1} i_{L1}(k) u(k) \quad (12)$$

Where the next (coming) instant is demonstrated by the term (k+1), the T represents the sampling time.

The development of model predictive control critically involves formulation of the cost function, which is determined by the positive value of the error between the reference and the predicted state parameter value. In this study, the single objective CF is chosen and expressed in Equation (13).

$$J(k+1) = \left(V_c^*(k)^2 - V_{c1}(k+1)\right)^2 \quad (13)$$

The execution of the MPC algorithm to acquire the dataset is as follows:

- At the beginning of the switching instant, the converter's current and voltage are measured using sensors.
- Equations (11-12) are utilized to predict the state parameter at the next instant for all possible switching states, and then the CF is calculated using Equation (13) for each possible state.
- The state in which the CF attains its minimum value is selected to determine the switch position of the converter in the upcoming instant.

The data set acquired from the MPVC for the DC/DC converter is used to train the ANN.

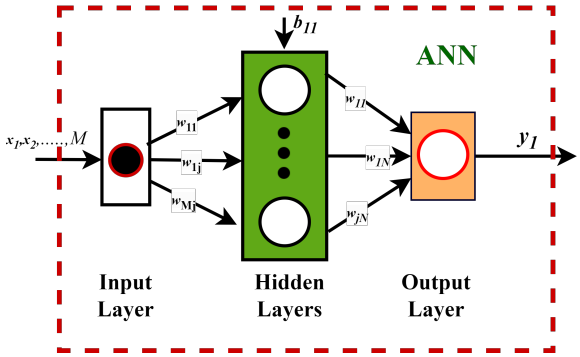

Fig. 5: Overview of multi-layer ANN with multi inputs and single output.

4 Implementation of Artificial Neural Network

Implementing linear control, such as PI, is easy and cost-effective. However, it cannot capture all the power system dynamics, especially when integrating renewable energy and complex loads such as CPL and impedance loads. These additions bring more uncertainties and non-linearities in modern power systems. Consequently, there is a need for more intelligent control schemes that provide robust performance across a wide range of operating conditions and are capable of managing and addressing the issues mentioned above. In this context, artificial intelligence and machine learning offer promising solutions. These advanced techniques can adapt to complex system behaviours and understand dynamics from data patterns. By leveraging AI, modern control approaches can achieve resilience, efficiency and greater flexibility as required by the modern power system. An artificial neural network (ANN) is a computational model inspired by the structure and function of human neural networks. It is a key technique within the broader field of machine learning and is designed to model complex relationships between inputs and outputs (targets). ANN models use learning algorithms to identify patterns in historical data, enabling them to make intelligent decisions and predictions. Figure 5 depicts the basic structure of multi-input and single output ANN. where M represents the input features ($\forall_m = \{1, ..., M\}$) and y is single output. It consists of several interconnected layers of artificial neurons, also referred to as nodes. The typical structure of ANN is divided into three

layers, i.e. input layer, hidden layer, and output layer. The input layer corresponds to features or raw data sets. In the input layer, the neuron represents each feature. Each input x_m is multiplied by the weighting factor $w_m(\forall_j = \{1, ..., j\})$ and added to the hidden layer. Hidden layers are responsible for processing and transforming information from the input layer by defining weights and activation functions to learn the complex patterns between inputs and outputs. The number of hidden layers depends upon the complexity of the problems. The output layer gives output or predictions based on previous knowledge. The ANN-based PV monitoring system is proposed in [43]. An ANN-based algorithm has been developed to detect cyber attacks in [44]. In [25], authors proposed MPC-aided ANN-based voltage control for 2-level VSC to attain better performance and lower THD. Furthermore, ANN-based MPC for a three-level flying capacitor converter is studied in [41] to prove the reduction of MPC computation burden using ANN. The ANN is considered a power tool for forecast and estimation in different power applications. This study aims to illustrate the implementation of ANN-based voltage control for DER unit in a DC microgrid with a reduced number of sensors and its effectiveness over a wide range of operations. In order to implement the ANN, The MPC-based voltage control is implemented for a step-up DC-DC converter to collect the error data between measured and reference voltage and output switching states having other characteristics such as load shift, change in input voltages, etc. By choosing these parameters, the single input and single output feed-forward ANN is developed

In this study, the single input and single output feed-forward ANN is implemented to reduce the computational burden and complexity and achieve better results while preserving all characteristics of the parent technique.

The output of a single neuron is mathematically expressed as:

$$y = \text{Act}\left(b + \sum_{i=1}^{M} x_i w_i\right), \tag{14}$$

Where $Act(.)$, w_i, b, and M are the activation function, weights of each input x_i, bias or correction factor, and the number of input elements (or neurons) where the input features $x = \{x_1, x_2, \ldots, x_M\}$, respectively. The most commonly used types of activation functions are hyperbolic tangent, softmax, linear, and sigmoid) [45]. An FF-ANN layer is developed by joining the multiple neurons into a single layer. The general equation used to compute the output of the multi-input single-output FF-ANN can be expressed as:

$$\begin{aligned} y_1 &= Act\left(\sum_{j=1}^{J} {}^{2}w_{j1} h_j + {}^{2}b_1\right), \\ h_j &= Act\left(\sum_{m=1}^{M} {}^{1}w_{mj} x_m + {}^{1}b_j\right), \quad \forall j = \{1, \ldots, J\}, \end{aligned} \tag{15}$$

where y_1 is the output of the ANN, represents the weights of the hidden and output layers, J is the number of hidden layers, M represents the number of input neurons, and refers to the biases of the hidden and output layers, respectively.

4.1 Training of ANN

This subsection outlines the steps involved in training the ANN. The training of ANN is divided into two phases: Offline and online. In the offline phase, MPVC is formulated, developed, and tested using Matlab/Simulink simulations. The data extraction process begins by collecting the inputs and outputs of the implemented control technique. Various tests, such as step changes in load, voltage references, and supply voltages, are conducted to characterize the parent control approach comprehensively. After gathering the raw data, the selection of inputs and targets for training the ANN is based on a hit-and-trial method. The error between the output and reference voltage is ultimately chosen as the primary input feature, while the converter's switching action serves as the output feature in this study.The dataset selected for the offline training of the ANN consists of randomly sampled data from different reference voltage levels, including 90V, 95V, 100V, and 105V. The dataset is then randomly split into three subsets: training (70%), validation (15%), and testing (15%). The network is designed with ten hidden neurons, and training is performed using the Bayesian regularization technique, utilizing the "trainbr" function in MATLAB.

The confusion matrix visualizes and summarizes the performance of the trained ANN, as shown in Figure 6, which assesses the performance based on the network's output. In our case, the ANN outputs either 0 or 1, representing the pulse for the switch S1.The dataset comprises 180,006 samples in total. The acquired dataset consists of 78.78% samples from output class 1 and 21.22% from output class 0. The proposed controller successfully predicts the output class for random samples with an overall accuracy of 97.2% and a precision of 100 % as expressed in Table 2. Table 3 compares the various control techniques, showcasing the number of sensors required for implementation. The MPC and multi-input ANN require two sensors to implement the methods. The proposed ANN technique only needs output voltage measurement, which makes it easy to implement and reduces hardware complexity.

The trained ANN replaces MPC for real-time voltage control in the test phase. The trained ANN model is exported to Simulink to test its performance under the original scenario. To sum up, the complete procedure of the learning-based control strategy is illustrated in Fig.8, highlighting the key steps of the training and test phases. Additionally, Figure 7 visually represents the entire process. It is essential to mention that MPC accuracy relies on the system's mathematical modeling. However, the proposed control scheme does not require the system's model but a training dataset. It directly maps the raw input features to the desired outputs. Therefore, the performance of the ANN does not depend upon the system model or its parameters.

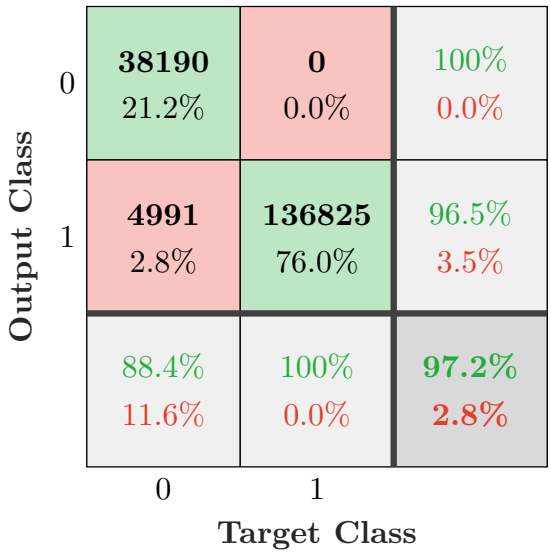

Fig. 6: Confusion matrix of the trained ANN based on the overall training data, where the correct and incorrect observations are highlighted in green and red, respectively.

4.2 Stability Analysis using Lyapunov's Method

Data-driven controls such as MPC-aided ANN have gained significant attention in control applications due to their ability to

Table 2 Performance Metrics of the Model

Metric	Value
Accuracy	97.2%
Precision (Class 1)	100%
Recall (Class 1)	96.5%
Specificity (Class 0)	100%
F1 Score (Class 1)	98.2%

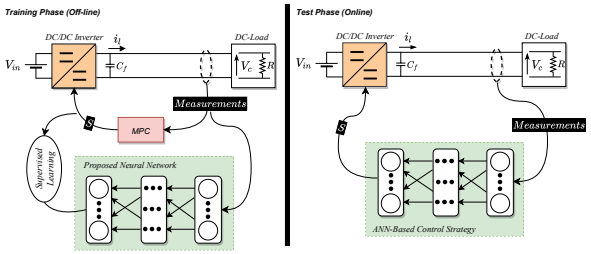

Fig. 7: Graphical overview of whole training process [26].

Table 3 Comparison of sensor requirements for different control approaches.

Control Technique	Features Used	Inputs	Outputs
MPC	Vin, Vout, Iout	3	1
Multi-Input ANN [26]	Vin, Vout, Iout	3	1
SISO ANN (Proposed)	Vout	1	1

approximate complex nonlinear functions and comprehensively understand the system dynamics. The stability of control systems is a fundamental requirement to ensure predictable and reliable performance, unlike traditional control systems, where stability can be ensured through Lyapunov-based methods and recursive feasibility. ANNs present significant challenges due to their inherent nonlinearity, high-dimensionality, and data-driven nature, making formal stability proofs more complex. In [46], the authors propose a data-driven MPC scheme that ensures stability using Lyapunov analysis and recursive feasibility, using Hankel matrix representations for linear time-invariant (LTI) systems. However, applying similar stability guarantees to ANNs is challenging due to their non-convex optimization space, lack of explicit state-space models, and dynamic parameter updates via gradient descent. In [47], the authors analyze the robust stability of a data-driven MPC scheme without terminal constraints, proving practical exponential stability with a sufficiently long prediction horizon, even under noisy measurements. However, applying similar stability guarantees to ANNs is difficult due to their nonlinear activation functions, high-dimensional weight matrices, and stochastic updates, which complicate continuity and stability analysis. This study analyzes the controller's stability using Lyapunov's direct method. To validate the robustness of the ANN controller, we employ Lyapunov stability analysis and evaluate the system's convergence behavior through numerical simulations, as it is challenging to prove the mathematical stability of data-driven control techniques. A nonlinear system is considered Lyapunov stable if there exists a continuously differentiable Lyapunov function $V(x)$ satisfying:

- Positive definiteness: $V(x) > 0$ for all $x \neq 0$ and $V(0) = 0$, ensuring that the function measures system energy.

- Negative semi-definiteness: The time derivative $\dot{V}(x)$ satisfies $\dot{V}(x) \leq 0$, indicating that the energy of the system does not increase.

- Asymptotic stability: If $\dot{V}(x) < 0$, then $x \to 0$ as $t \to \infty$, ensuring that the system error vanishes over time.

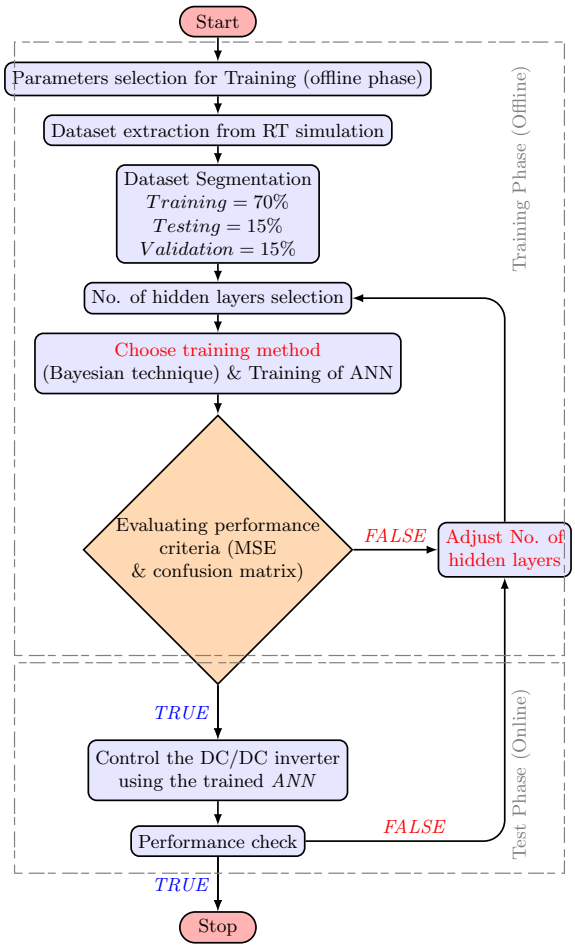

Fig. 8: Main steps in deploying the ANN-based control strategy for the DC/DC converter.

The ANN controller's stability is evaluated by defining a quadratic Lyapunov function:

$$V(x) = \frac{1}{2} V_{\text{error}}^2 \tag{16}$$

where

$$V_{\text{error}} = V_{\text{ref}} - V_{\text{actual}} \tag{17}$$

Figure 9 shows the Lyapunov stability verification plots based on simulation data. Figure 9 (a) presents the Lyapunov function $V(x)$ vs time plot. It can be observed from the figure that the Lyapunov function achieves the zero value in a short time, which means that the system stabilizes quickly. The controller effectively drives the state toward equilibrium. consequently, the controller fulfills the key criteria and is considered asymptotic stable. Figure 9 (b) demonstrates that the derivative of the Lyapunov function is also negative and decreases over time towards zero. We conclude that:

$$\frac{dV}{dt} \leq 0. \tag{18}$$

Since $\frac{dV}{dt} \leq 0$, the system satisfies the conditions for Lyapunov stability. Moreover, as $V_{\text{error}}(t) \to 0$ over time, the system is asymptotically stable.

4.3 Discrete-Time Lyapunov Stability Analysis

The quadratic Lyapunov function in the discrete domain can be defined as:

$$L(k) = \frac{1}{2} V_{\text{err}}(k)^T V_{\text{err}}(k) \tag{19}$$

where $V_{\text{err}}(k) = V_{\text{ref}}(k) - V_{\text{actual}}(k)$. This function satisfies the following properties:

- Positive definite: $L(k) > 0$ for all $V_{\text{err}}(k) \neq 0$
- Zero at equilibrium: $L(k) = 0$ if and only if $V_{\text{err}}(k) = 0$

The change in the Lyapunov function between two discrete sampling instants is:

$$\Delta L(k) = L(k+1) - L(k) \tag{20}$$

$$\Delta L(k) = \frac{1}{2} V_{\text{err}}(k+1)^T V_{\text{err}}(k+1) - \frac{1}{2} V_{\text{err}}(k)^T V_{\text{err}}(k) \tag{21}$$

Assuming that V_{ref} remains constant due to small sampling time:

$$V_{\text{err}}(k+1) = V_{\text{ref}}(k) - V_{\text{actual}}(k+1) \tag{22}$$

The controller affects V_{actual} through the ANN model:

$$V_{\text{actual}}(k+1) = f\left(V_{\text{actual}}(k), \text{ANN}\left(V_{\text{err}}(k), i_L(k), V_{\text{in}}(k)\right)\right) \tag{23}$$

The change in output voltage due to the controller can be approximated as:

$$V_{\text{actual}}(k+1) - V_{\text{actual}}(k) = \alpha \cdot V_{\text{err}}(k) \tag{24}$$

where $0 < \alpha < 1$ is a convergence factor.

Substituting into the error expression:

$$\begin{aligned} V_{\text{err}}(k+1) &= V_{\text{ref}}(k) - V_{\text{actual}}(k+1) && (25)\\ &= V_{\text{ref}}(k) - \left(V_{\text{actual}}(k) + \alpha \cdot V_{\text{err}}(k)\right) && (26)\\ &= (1-\alpha) \cdot V_{\text{err}}(k) && (27) \end{aligned}$$

Substituting into the Lyapunov difference:

$$\begin{aligned} \Delta L(k) &= \frac{1}{2}\left[(1-\alpha)^2 V_{\text{err}}(k)^T V_{\text{err}}(k) - V_{\text{err}}(k)^T V_{\text{err}}(k)\right] && (28)\\ &= -\alpha(2-\alpha) \cdot \frac{1}{2} V_{\text{err}}(k)^T V_{\text{err}}(k) && (29) \end{aligned}$$

Since $0 < \alpha < 1$, it follows that:

- $\Delta L(k) < 0$ for all $V_{\text{err}}(k) \neq 0$
- $\Delta L(k) = 0$ if and only if $V_{\text{err}}(k) = 0$

The quadratic Lyapunov function $L(k)$ represents the "energy" of the voltage error. The negative definite nature of $\Delta L(k)$ proves that this error energy decreases monotonically with each time step, eventually converging to zero. Furthermore, the controller's effectiveness is characterized by the convergence factor α, which determines the rate at which the system approaches the reference voltage.

5 Results

Figure 10 illustrates the graphical implementation of the proposed reduced-sensor control technique for a single-step-up DC/DC converter. This technique requires only a voltage sensor to effectively regulate the output voltage at the PCC, eliminating the need for additional sensors and reducing overall system complexity and cost. Figure 13 depicts the hardware-in-the-loop (HIL) testing setup used to validate the proposed control technique. The setup includes an

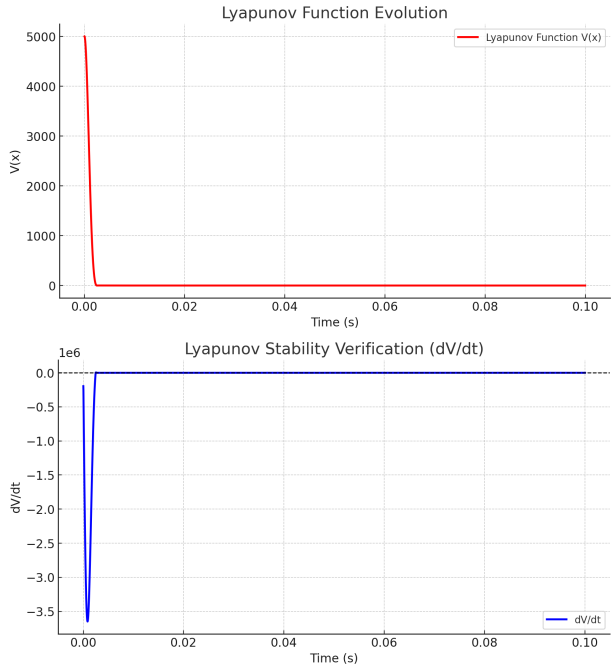

Fig. 9: Lyapunov stability verification Plots (a) Lyapunov function evolution (b) Lyapunov stability verification

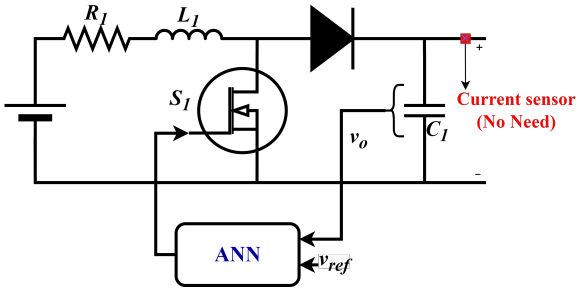

Fig. 10: Block diagram of proposed ANN controller implementation for single DER unit.

OPAL-RT 4510 real-time simulator, a graphical user interface (GUI) desktop, and a Keysight EXR058A 8-channel oscilloscope. The HIL platform operates in a hardware-synchronized mode, where analog inputs and outputs of the simulator are enabled and carefully configured for optimal performance. In this setup, each DER unit's output voltages and currents are measured using a simulator analog output measurement board. These signals are fed back into the simulator via an analog input board using wired connections. This approach ensures that critical real-world factors—such as system time delays, electrical noise, and signal interference—are accurately incorporated into the testing environment. Such fidelity allows for rigorous evaluation of the controller's performance under realistic operating conditions. The simulation parameters of the DC MG are given in Table 4. The performance comparison of different controllers in terms of overshoot and settling time is presented in Table 5. Figure 11 illustrates the performance of three different control techniques applied to step up DC-DC converter, comparing their output voltage and current responses. As shown in Figure 11, PI-based voltage control exhibits a relatively fast transient response but suffers from significant overshoot, which may lead to stability issues or stress on the system. The MPC-based voltage strategy improves with a more controlled rise and less overshoot, indicating better predictive

adjustments and system stability. However, the proposed artificial neural network control with reduced sensor outperforms both PI and MPC by achieving a rapid and precise rise to the desired levels with minimal overshoot and almost no fluctuation, displaying superior performance in maintaining consistent output. This quick settling time and the steady-state accuracy of the ANN suggest that it can better handle complex, dynamic conditions within the DC-DC converter's operation. The comparison between PI, MPC, and proposed ANN is carried out using MATLAB/SIMULINK.

Table 4 Simulation Parameters.

Parameter	Value
DC Input V_{in}	80 [V]
Inductor value L	4×10^{-5} [H]
Resistance Value R	10×10^{-3} [Ω]
Capacitor C_f	600 [μF]
Line parameters Z_{12}	R =0.51 [Ω], L =10 [μH]
Line parameters Z_{13}	R =2 [Ω], L =70 [μH]
Line parameters Z_{24}	R =0.51 [Ω], L =12.1 [μH]
Line parameters Z_{43}	R =4 [Ω], L =60 [μH]
DC output V_{out}	100 [V]
PI Parameters	$K_p = 0.00547$, $K_i = 7$

Table 5 Controller performance comparison

Controller	Settling Time	Overshoot
PI	19.9 mSec	180%
MPC	124 μSec	0.445%
Proposed ANN	**99 μSec**	**0.325%**

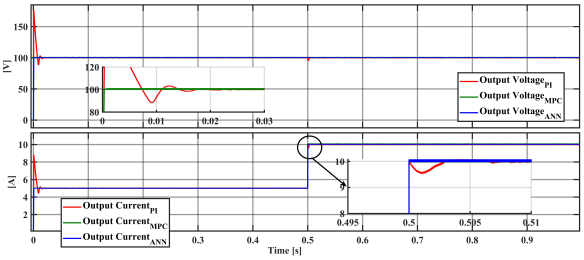

Fig. 11: Performance evaluation of PI and MPC and ANN-based voltage control.

5.1 *Voltage Tracking*

In this case, we investigate and test the controller's performance and transient response while tracking the voltage reference. The controller performance is tested in an interconnected DC MG system, as presented in Figure 12. The test system consists of 4 DER units interconnected via transmission lines with their impedance. The DC test bench system is working in autonomous mode. Initially, the voltage of all DER units is set as per values expressed in Table 4.

As per the guidelines outlined in IEEE 1159-2019, the controller must ensure stability, achieve the intended transient and steady-state performance, and zero steady-state error in a closed-loop DC microgrid. The transient response of the proposed controller while tracking the voltage reference is shown in Figure 14. The observed waveform indicates that the studied controller effectively stabilizes the voltages of DER units according to their respective reference values without showing any undershooting or overshooting behavior.

Figure 15 illustrates the response of the proposed control regarding the change in voltage reference from 100V to 102V and 100V to 98V for DER_1 and DER_4 accordingly at t = 1 s. The response of the

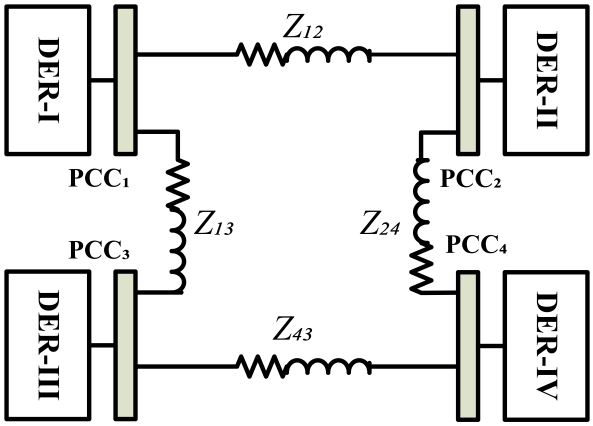

Fig. 12: The layout of the DC MG test bench system has four DER units connected in the ring structure.

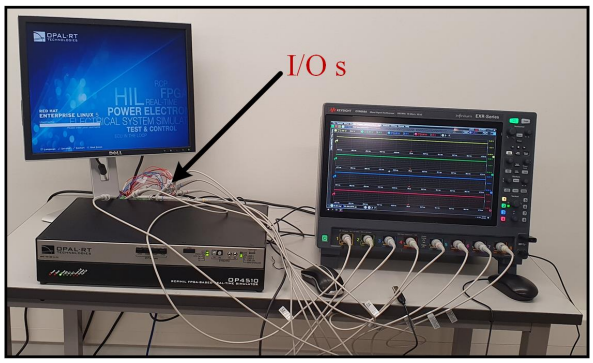

Fig. 13: Demonstration of HIL testing setup used to implement the DC MG.

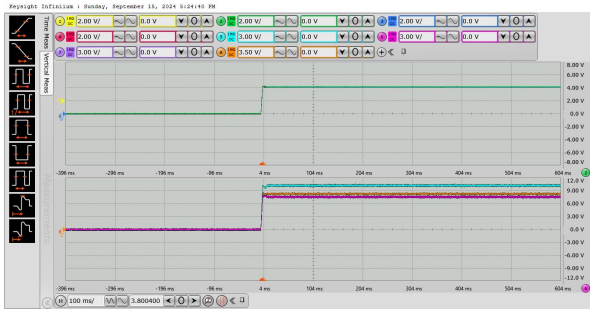

Fig. 14: The transient response evaluation of the proposed controller in DC MG test system.

output voltage of DER_1 and DER_4 under the change of reference voltage is shown in Figure 15 (a). It can be observed from Figure 15 that the proposed controller remains stable against voltage reference change, attains the new reference without any transient and steady-state error, and follows the IEEE standards guideline. Furthermore, the output voltage of the neighbouring DGs of DER_1 and DER_4 remains stable and adjusts their current accordingly to meet the load connected to their respective PCC. It follows the reference without taking into account the disturbance and system impedance, as shown in Figure 15. So, the robustness and stability of the proposed controller are confirmed in these results against the change in reference voltage.

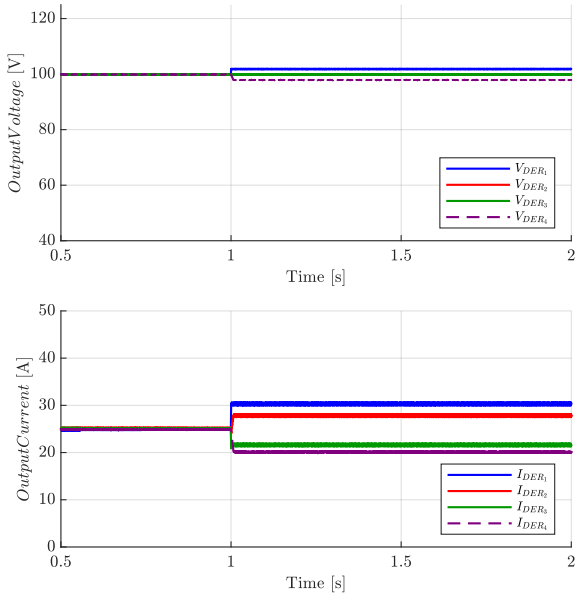

Fig. 15: Response of the DC microgrid to a reference voltage change for DER_1 and DER_4 at 1 second, with DER_1 adjusted from 100V to 102V and DER_4 from 100V to 98V. (a) Output voltage of all four DERs, (b) Output current of all DER Units connected in ring structure.

5.2 PnP Functionality of DER Units

The plug-and-play capability of the DER units in MG is one of the essential requirements for the control system due to the intermittent nature of renewable energy. This test is validated rigorously in the real-time environment using the OPAL-RT Opal 4510 real-time simulator. The results are captured using a key sight EXR058A 8-channel oscilloscope. In this scenario, we investigate the performance of the proposed controller under the PnP functionality of the DERs. DER_4, connected to DER_2 and DER_3, is removed from the system at t= 1 sec and is again connected back into the microgrid at t=1.5 sec. However, the load at PCC4 remains connected all the time. This operation affected the adjacent DG units. The voltage and output current of all DERs are depicted in Figure 16. As shown in Figure 16, the DER_4 output current becomes zero. In contrast, the output current of the DER_2 and DER_3 increases to meet the load demand according to their capacity. At the same time, the voltage of all DGs remains stable without any disturbance and follows the reference with zero steady-state error. These results prove the robust performance of the proposed controller and the PnP capability in DC MG.

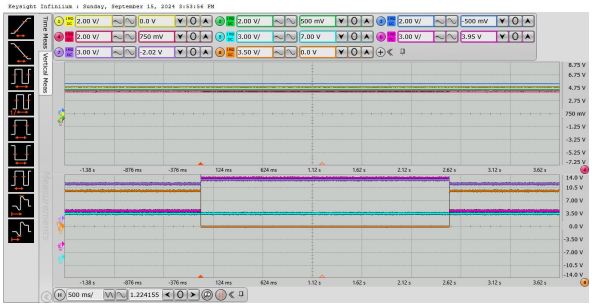

Fig. 16: Response of the DC microgrid following the removal of DER_4 from the system.

5.3 Microgrid Topology Reconfiguration

This test case is performed to validate the stability and resilience of the proposed control system under different distribution network configurations. Initially, the configuration of the MG is in a ring-type distribution network. However, the line Z_{43} between DER_3 and DER_4 is disconnected, transforming the DC MG to a radial-type distribution network, as illustrated in Figure 17. Figure 18 presents the output voltages of all four DG at their PCCs. It is worth mentioning that the voltage of DERs remains stable and shows no fluctuation. The findings of this case depict the optimal performance of the designed controllers in response to the variations resulting from uncertainties that affect the MG configurations.

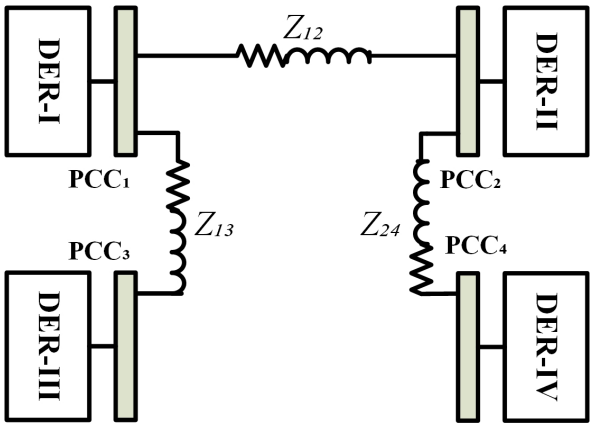

Fig. 17: DC microgrid layout after changing from the ring to radial distribution topology.

Fig. 18: Output voltage of DER units against DC MG reconfiguration.

5.4 Adaptability to unknown load variations

In this case, we investigate the performance of the developed controller against the load uncertainties. In addition, the system transient response and overshoot under varying load conditions are also studied. In the beginning, the loads mentioned in the table are connected at PCC3. At t= 1 sec, the load is reduced to 1.25 kW at PCC3 as manifested in Figure 19. The 1st graph of the scope illustrates the output voltage of DER_1 and DER_4. The 2nd window of the oscilloscope shows the output voltage of DER_3, where the load is decreased, and the 3rd scope exhibits the output current of DER_3. It can be seen that with the decrease in load, the output current also decreases, but the voltage at all PCCs remains stable without any disturbance. Hence, the proposed controller shows robust behavior against unknown load variations.

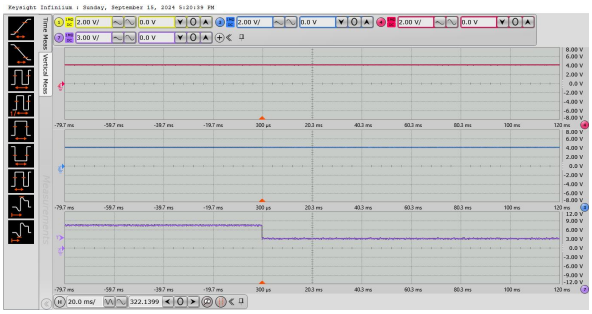

Fig. 19: Output voltage and current response of DER units under unknown load variation test.

5.5 Controller response to parametric variation

In this test, the sensitivity analysis of the proposed controller in a DC microgrid (MG) is conducted to demonstrate its stability against parametric variations. To evaluate the controller's robustness, the DC MG impedance is reduced by 20%, and the response of the DER units is analyzed. Figure 20 illustrates the output voltage and current of all four DER units, confirming that the controller maintains stability despite parametric variations.

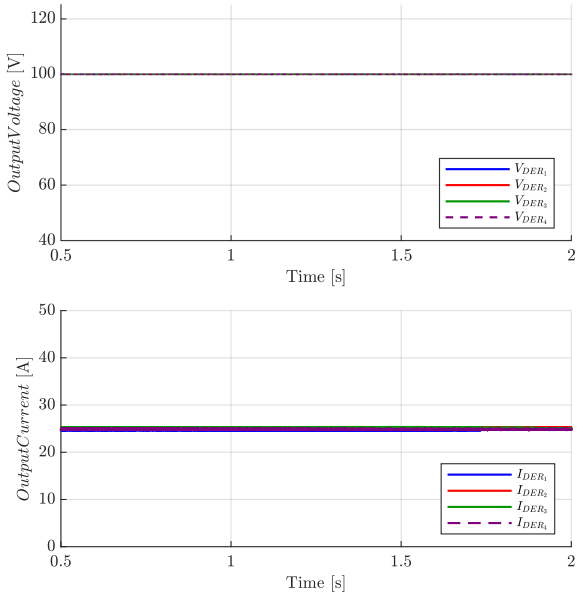

Fig. 20: Voltage and current response of DER units in a ring configuration under a 20% reduction in line impedance compared to values in Table 4.

6 Conclusion

Due to the high variations in loads and nonlinear dynamics of the power system, regulating the DC-DC converter is a significant problem. This article presents a reduced sensor ANN-based voltage control approach for a DC-DC step-up converter as a DG. Initially, the model predictive voltage control is implemented as an expert to extract the data set for the ANN training. After the ANN has been trained on different parameters and loading conditions, The finely tuned reduced sensor ANN is implemented to control the DC-DC converter. The proposed control technique performs better in various aspects, such as DERs' plug-and-play (PnP) operation, parameter variation, topology reconfiguration, and load fluctuations. Lyapunov stability analysis is also carried out to demonstrate the stability of the system via numerical simulation. It is important to mention that the ANN is trained and tuned using data from a single converter. However, it has been applied to four-bus systems that incorporate line parameters to assess its effectiveness. The results indicate that the proposed controller performs well in all scenarios compared to the classical PI controller. The real-time hardware-in-loop results also validate the robust performance of the proposed control approach under different cases.

Author Contributions

Hussain Sarwar Khan: conceptualization, investigation, methodology, software, validation, writing – original draft **Kimmo Kauhaniemi:** supervision, writing – review and editing

Acknowledgment

This work is carried out in a project titled Smart Grid 2.0 with the financial support provided by Business Finland under Grant No. 1386/31/2022. The financial support provided by the funding organisation is highly acknowledged.

Conflicts of Interest

The authors declare no conflicts of interest.

Data Availability Statement

The data that support the findings of this study are available from the corresponding author upon reasonable request.

7 References

1 A. Anand, A. Ranjan, S. Devassy, B.K. Verma, S.K. Ram, and A.K. Dhakar. Review of hierarchical control strategies for dc microgrid. *IET Renewable Power Generation*, 14(10):1631–1640, 2020.
2 Mahdi Zolfaghari, Gevork B Gharehpetian, Miadreza Shafie-khah, and Joao PS Catalao. Comprehensive review on the strategies for controlling the interconnection of ac and dc microgrids. *International Journal of Electrical Power & Energy Systems*, 136:107742, 2022.
3 M. Mosayebi, M. Gheisarnejad, and M.H. Khooban. An intelligent sliding mode control for stabilization of parallel converters feeding cpls in dc-microgrid. *IET Power Electronics*, 15(14):1596–1606, 2022.
4 F. Ibanez, J. Echeverria, and L. Fontan. Master–slave dc droop control for paralleling auxiliary dc/dc converters in electric bus applications. *IET Power Electronics*, 10(10):1156–116, 2017.
5 Y. Mi, J. Guo, S. Yu, P. Cai, L. Ji, Y. Wang, D. Yue, Y. Fu, and C. Jin. A power sharing strategy for islanded dc microgrid with unmatched line impedance and local load. *Electric Power Systems Research*, 192:106983, 2021.
6 Nabil Mohammed, Leonardo Callegaro, Mihai Ciobotaru, and Josep M Guerrero. Accurate power sharing for islanded dc microgrids considering mismatched feeder resistances. *Applied Energy*, 340:121060, 2023.
7 M. Saleh, Y. Esa, and A.A. Mohamed. Communication-based control for dc microgrids. *IEEE Transactions on Smart Grid*, 10(2):2180–2195, 2018.
8 Pasquale Montegiglio, Giuseppe Acciani, Maria Dicorato, Giuseppe Forte, and Francesca Marasciuolo. A decentralized power and bus voltage regulation approach for dc microgrids. *IEEE Transactions on Industry Applications*, 59(4):4773–4785, 2023.
9 R Jeyasenthil, Tarakanath Kobaku, Bidyadhar Subudhi, Subham Sahoo, and Tomislav Dragicevic. Design and experimental validation of robust pid control for a power converter in a dc microgrid application. In *Microgrid Cyberphysical Systems*, pages 89–114. Elsevier, 2022.
10 C.-F. Hsu, I.-F. Chung, C.-M. Lin, and C.-Y. Hsu. Self-regulating fuzzy control for forward dc–dc converters using an 8-bit microcontroller. *IET Power Electronics*, 2(1):1–13, 2009.
11 T.-F. Wu, C.-H. Chang, and Y.-H. Chen. A fuzzy-logic-controlled single-stage converter for pv-powered lighting system applications. *IEEE Transactions on Industrial Electronics*, 47(2):287–296, 2000.
12 T. Gupta, R.R. Boudreaux, R.M. Nelms, and J.Y. Hung. Implementation of a fuzzy controller for dc-dc converters using an inexpensive 8-b microcontroller. *IEEE Transactions on Industrial Electronics*, 44(5):661–669, 1997.

13 Zainab Ameer Al-Dabbagh and Salam Waley Shneen. Neuro-fuzzy controller for a non-linear power electronic dc-dc boost converters. *Journal of Robotics and Control (JRC)*, 5(5):1479–1491, 2024.

14 S. Oucheriah and L. Guo. Pwm-based adaptive sliding-mode control for boost dc–dc converters. *IEEE Transactions on Industrial Electronics*, 60(8):3291–3294, 2012.

15 H.S. Khan, K.S. Fuad, M. Karimi, and K. Kauhaniemi. Fault current level analysis of future microgrids with high penetration level of power electronic-based generation. In *2021 IEEE 9th International Conference on Smart Energy Grid Engineering (SEGE)*, pages 48–53, 2021.

16 L. Cheng, P. Acuna, R.P. Aguilera, J. Jiang, S. Wei, J.E. Fletcher, and D.D.C. Lu. Model predictive control for dc–dc boost converters with reduced-prediction horizon and constant switching frequency. *IEEE Transactions on Power Electronics*, 33(10):9064–9075, 2017.

17 S.R. Mohapatra and V. Agarwal. An advanced voltage support scheme considering the impact of zero-sequence voltage under microgrid faults using model predictive control. *IEEE Transactions on Industrial Electronics*, 67(10):8957–8968, 2020.

18 Y. Shan, J. Hu, K.W. Chan, Q. Fu, and J.M. Guerrero. Model predictive control of bidirectional dc–dc converters and ac/dc interlinking converters—a new control method for pv-wind-battery microgrids. *IEEE Transactions on Sustainable Energy*, 10(4):1823–1833, 2018.

19 Z. Karami, Q. Shafiee, Y. Khayat, M. Yaribeygi, T. Dragicevic, and H. Bevrani. Decentralized model predictive control of dc microgrids with constant power load. *IEEE Journal of Emerging and Selected Topics in Power Electronics*, 2019.

20 L. Chen, F. Gao, K. Shen, Z. Wang, L. Tarisciotti, P. Wheeler, and T. Dragićević. Predictive control based dc microgrid stabilization with the dual active bridge converter. *IEEE Transactions on Industrial Electronics*, 67(10):8944–8956, 2020.

21 H.U.R. Habib, S. Wang, M.R. Elkadeem, and M.F. Elmorshedy. Design optimization and model predictive control of a standalone hybrid renewable energy system: A case study on a small residential load in pakistan. *IEEE Access*, 7:117369–117390, 2019.

22 Muhammed Cavus, Adib Allahham, Kabita Adhikari, and Damian Giaouris. A hybrid method based on logic predictive controller for flexible hybrid microgrid with plug-and-play capabilities. *Applied Energy*, 359:122752, 2024.

23 N. Jin, S. Hu, C. Gan, and Z. Ling. Finite states model predictive control for fault-tolerant operation of a three-phase bidirectional ac/dc converter under unbalanced grid voltages. *IEEE Transactions on Industrial Electronics*, 65(1):819–829, 2017.

24 B.-R. Lin. Power converter control based on neural and fuzzy methods. *Electric Power Systems Research*, 35(3):193–206, 1995.

25 I.S. Mohamed, S. Rovetta, T.D. Do, T. Dragicević, and A.A.Z. Diab. A neural-network-based model predictive control of three-phase inverter with an output lc filter. *IEEE Access*, 7:124737–124749, 2019.

26 H. S. Khan, I. S. Mohamed, K. Kauhaniemi, and L. Liu. Artificial neural network-based voltage control of dc/dc converter for dc microgrid applications. In *2021 6th IEEE Workshop on the Electronic Grid (eGRID)*, pages 1–6, 2021.

27 S. Saadatmand, P. Shamsi, and M. Ferdowsi. The voltage regulation of a buck converter using a neural network predictive controller. In *2020 IEEE Texas Power and Energy Conference (TPEC)*, pages 1–6, 2020.

28 S. Saadatmand, M.S.S. Nia, P. Shamsi, M. Ferdowsi, and D.C. Wunsch. Neural network predictive controller for grid-connected virtual synchronous generator. In *2019 North American Power Symposium (NAPS)*, pages 1–6, 2019.

29 A.N. Akpolat, M.R. Habibi, E. Dursun, A.E. Kuzucuoğlu, Y. Yang, T. Dragičević, and F. Blaabjerg. Sensorless control of dc microgrid based on artificial intelligence. *IEEE Transactions on Energy Conversion*, 36(3):2319–2329, 2020.

30 M. Ahmed, A. Vahidnia, M. Datta, and L. Meegahapola. An adaptive power oscillation damping controller for a hybrid ac/dc microgrid. *IEEE Access*, 8:69482–69495, 2020.

31 Sidra Kanwal, Muhammad Qasim Rauf, Bilal Khan, and Geev Mokryani. Artificial neural network assisted robust droop control of autonomous microgrid. *IET Renewable Power Generation*, 18(7):1346–1369, 2024.

32 Aimin Wang, Minrui Fei, Dajun Du, Chen Peng, and Kang Li. Scalable neural network control for nonlinear dc microgrids under plug-and-play operations. *IEEE Transactions on Industrial Informatics*, 2025.

33 Hussain Sarwar Khan and Kimmo Kauhaniemi. Fpga validated advanced learning-based voltage control of dc/dc converter feeding cpl in dc microgrid applications. In *2023 IEEE 32nd International Symposium on Industrial Electronics (ISIE)*, pages 1–6. IEEE, 2023.

34 S. Zhao, F. Blaabjerg, and H. Wang. An overview of artificial intelligence applications for power electronics. *IEEE Transactions on Power Electronics*, 2020.

35 A.N. Akpolat, E. Dursun, and A.E. Kuzucuoğlu. Deep learning-aided sensorless control approach for pv converters in dc nanogrids. *IEEE Access*, 9:106641–106654, 2021.

36 A.H. EL-Ebiary, M.I. Marei, M.A. Attia, and M. Mokhtar. A sensorless cyber-attacks mitigation technique based on braided lyapunov state observer. *Electric Power Systems Research*, 235:110881, 2024.

37 N. Obeidi, M. Kermadi, B. Belmadani, A. Allag, L. Achour, and S. Mekhilef. A current sensorless control of buck-boost converter for maximum power point tracking in photovoltaic applications. *Energies*, 15(20):7811, 2022.

38 M. Tavan, K. Sabahi, M. Shahparasti, A. Hajizadeh, M. Soltani, and M. Savaghebi. Sensorless control of a single-phase ac–dc boost converter without measuring input voltage and current. *IEEE Access*, 11:59059–59070, 2023.

39 S.K. Kim and C.K. Ahn. Proportional-derivative voltage control with active damping for dc/dc boost converters via current sensorless approach. *IEEE Transactions on Circuits and Systems II: Express Briefs*, 68(2):737–741, 2020.

40 M. Tucci, S. Riverso, J.C. Vasquez, J.M. Guerrero, and G. Ferrari-Trecate. A decentralized scalable approach to voltage control of dc islanded microgrids. *IEEE Transactions on Control Systems Technology*, 24(6):1965–1979, 2016.

41 D. Wang, Z.J. Shen, X. Yin, S. Tang, X. Liu, C. Zhang, J. Wang, J. Rodriguez, and M. Norambuena. Model predictive control using artificial neural network for power converters. *IEEE Transactions on Industrial Electronics*, 69(4):3689–3699, 2021.

42 M.S. Sadabadi, Q. Shafiee, and A. Karimi. Plug-and-play robust voltage control of dc microgrids. *IEEE Transactions on Smart Grid*, 9(6):6886–6896, 2017.

43 L. Chen and X. Wang. Enhanced mppt method based on ann-assisted sequential monte–carlo and quickest change detection. *IET Smart Grid*, 2(4):635–644, 2019.

44 M.R. Habibi, H.R. Baghaee, F. Blaabjerg, and T. Dragićević. Secure mpc/ann-based false data injection cyber-attack detection and mitigation in dc microgrids. *IEEE Systems Journal*, 16(1):1487–1498, 2021.

45 K. Hornik. Approximation capabilities of multilayer feedforward networks. *Neural Networks*, 4(2):251–257, 1991.

46 Julian Berberich, Johannes Köhler, Matthias A Müller, and Frank Allgöwer. Data-driven model predictive control with stability and robustness guarantees. *IEEE Transactions on Automatic Control*, 66(4):1702–1717, 2021.

47 Joscha Bongard, Julian Berberich, Johannes Köhler, and Frank Allgöwer. Robust stability analysis of a simple data-driven model predictive control approach. *IEEE Transactions on Automatic Control*, 68(5):2625–2637, 2023.